Impact of fillers on physical and mechanical properties of an epoxy matrix, and the effect of surface modification using a silane coupling agent

Jenny Natalie Anvik Torkildsen

Master thesis in
Materials, Energy and Nanotechnology
60 Credits

Department of Chemistry
Faculty of Mathematics and Natural Sciences

UNIVERSITY OF OSLO

May 2018

2018

Impact of fillers on physical and mechanical properties of an epoxy matrix, and the effect of surface modification using a silane coupling agent

Jenny Natalie Anvik Torkildsen

http://duo.uio.no/

Print: Reprosentralen, University of Oslo

Acknowledgement

This thesis has been a cooperation between the University of Oslo (UiO) and Jotun AS under the supervision of Professor Harald Walderhaug and Thor Håkon Krane Thvedt, PhD. The thesis is a part of the master's degree in Materials, energy and nanotechnology, and has been carried out in 2017-2018 at the department of chemistry (UiO), and Jotun's research and development center in Sandefjord. The contents of the thesis were determined by Jotun AS, and have been interesting to work with.

I would like to thank my supervisors, Professor Harald Walderhaug and Thor Håkon Krane Thvedt, PhD, for their support and help, for trusting and allowing me to learn and develop. I would also like to thank the Specialty group at Jotun for their interest in my work and help with practical issues, Samuel Akogyeram, PhD, for the help with DMA, Matthew Read, PhD, for the help with UTM and surface modification, Hieu Trung Mai for the pretreated wollastonite powder and valuable conversations, Heng Li, PhD, for the help with FT-IR and SEM, Spyridon Diplas, Sissel Jørgensen and Martin Sunding for helping me collecting and interpreting the XPS results and Endre Torkildsen for helping me create illustrative figures.

Last, but not at least, I would like to thank my family, friends and fiancé Håkon for always supporting me and listening to all my thoughts and ideas during the work with this thesis.

Oslo, May, 2018

Jenny N. A. Torkildsen

Abstract

Fillers are used in coating and composite materials to enhance or introduce new properties. Deterioration of certain properties have been explained by a lack of interactions between the polymer and the filler. The interactions between a diepoxy-diamine matrix and four different fillers have been investigated in this work. The physical and mechanical properties of the epoxy matrix/filler materials have also been tested, mainly as free films, using a filler loading of 10 % of the CPVC of the fillers.

Barium sulfate ($BaSO_4$), mica ($KAl_2(AlSi_3O_{10})(OH)_2$), aramid (Kevlar fibers) and wollastonite ($CaSiO_3$) were the four fillers tested. XPS and FT-IR analysis were used to detect the possible interactions between the epoxy matrix and the filler particles. New peaks or chemical shifts were not observed, indicating lack of interactions. The surface of the filler particles was modified by a silane coupling agent, 3- aminopropyltriethoxysilane, to obtain a chemical bond between the epoxy matrix and the filler particles. The surface modified filler particles were examined with XPS and a successful surface modification was observed by presence of carbon, silicon and nitrogen (amine groups and protonated amine groups) on the surface of the fillers. Neither XPS nor FT-IR analysis revealed indications of interactions after surface modification. By using SEM for analysis of fractured surfaces of the epoxy/filler films it was observed that the surface modified filler particles were slightly more attached to the epoxy matrix than the unmodified filler particles.

The stiffness and the T_g of the samples were analyzed using DMA and showed that all fillers increased the stiffness of the epoxy matrix, however, the addition of filler particles did not change the T_g. The strength and toughness of the epoxy/filler samples were tested with tensile and flexural tests using an UTM. The strength and toughness of the epoxy matrix decreased by the addition of all the four various fillers. This circumstance was explained by the filler particles acting as mechanical hinders for the elongation of the epoxy matrix. The permeability of water vapor was tested with Payne permeability cups and were found to decrease slightly by addition of fillers. The strength, toughness and permeability properties were improved by surface modification of the filler particles (stated with its exceptions). The differences observed in the physical and mechanical properties between the epoxy/filler samples (with unmodified and modified particles) were explained to be influenced the most by the size, shape and rigidity of the filler particles since differences in the interactions or main chemistry of the epoxy/filler samples (epoxy/$BaSO_4$, epoxy/mica, epoxy/aramid and epoxy/wollastonite) were not observed.

Abbreviations

Λ – Lambda

δ - Phase lag

σ - Stress

ε - Strain

%Area – Percentage area

A – Absorbance

at.% - Percentage atomic concentration

BSE – Back-scattered electrons

CPS – Counts per second

CPVC – Critical pigment volume concentration

DGEBA – Diglycidyl ether of bisphenol A

E – Modulus

E' – Storage modulus

E'' – Loss modulus

Epoxy/filler – Samples composed of an epoxy matrix and filler particles

Epoxy/m-filler – Samples composed of an epoxy matrix and surface modified filler particles

DMA – Dynamical mechanical analysis

FT-IR – Fourier transform infrared spectroscopy

LVR – Linear viscoelastic region

OA/Oil abs. – Oil absorption

PVC – Pigment volume concentration

SE – Secondary electrons

SEM – Scanning electron microscope

T_g – Glass transition (temperature)

UTM – Universal testing machine

Wollastonite-fs – Wollastonite from supplier

XPS – X-ray photoelectron spectroscopy

Table of contents

1 Introduction

Today, paint and coatings are used in a range of markets, for instance as a protector in electrical circuits, as a corrosion inhibitor and antifouling agent on ships or for decoration and protection on houses and buildings. Paint has existed for a long time, with the earliest documented found back to the 16th century BC, in France, Spain and South Africa [1]. The paint used at that time was made by adding mineral pigments like iron oxide or manganese dioxide into animal fat. By the many years in-between the 16th century BC and today, the paint has developed, and it now consists of a number of different components, which all contribute with various functions to optimize the final film [2]. Paint was originally made by natural occurring products found in the nature like in the example above, but when the marked for paint applications expanded, the need for more rapid-drying binders and improved application methods appeared. Rapid-drying binders were developed, and volatile organic solvents were added to the binders to keep them in liquid phase while storing and applying [1].

The increased use of volatile organic solvents was given focus in the late 1960s, due to challenges with environmental pollution [1]. The focus on environmental protection influenced the development of paints and led to new and more environmentally friendly paints such as waterborne coatings, low-solvent coatings and solvent free powder coatings, but also new application methods with a higher material transfer efficiency [1].

All types of paints are designed to have specific functions, and the performance of the paint film is decided by the components in the paint. Depending on which surface to be coated, a number of varying properties are required. To obtain a highly functional and protective coating, the chemical composition of the coating is therefore important [3]. Every component, the binder, solvent, pigment, filler and additive should therefore be taken into consideration regarding how it contributes to the performance properties of the coating.

In this thesis, the influence of fillers on one specific binding system have been investigated. The influence of fillers in coatings and composites has been widely covered in the literature for many kinds of fillers and polymers. Fillers have shown good effects on several properties, and dependent on application area, properties like permeability, strength, scratch resistance or stiffness are reported to be enhanced by filler particles in polymer/filler systems.

The addition of fillers to polymer systems may enhance certain properties on the behalf of other properties. For instance, epoxy/filler systems with hard fillers show high abrasion resistance and anti-corrosive properties, but low flexibility and impact resistance [2]. Decrease in strength as a consequence of increased stiffness has also been observed for several polymer/filler systems [4,5,6,7,8].

Already in the mid-1930s to 1940s, surface modification of filler particles was suggested and tested to solve the problem with decrease in properties as strength and toughness [9]. Surface modification can be accomplished for different types of surfaces with different types of modification agents and/or methods. Surface modification of glass surfaces with silanes has been widely studied [10,11,12,13] since silanes have shown promising results and can be used for several types of fillers and in combination with various types of polymers.

The distribution of the filler particles in polymer matrixes and the orientation of fillers particles are highly important to investigate since poor distribution may deteriorate the mechanical properties, and orientation may increase or decrease properties [14].

A thorough study of the influence of four different types of fillers on an epoxy-amine system are presented in this thesis, both with and without surface modification. Storage modulus, T_g, strength, toughness and permeability have been tested, and the results for the four epoxy/filler systems have been explained based on investigation of epoxy/filler interactions and fractography. The importance of the distribution of the filler particles in the epoxy matrix and the influence of possible orientation of the filler particles have been poorly covered in the literature and have been given focus in this work.

2 Theory and background

2.1 Paint and coatings

In order to understand the performance of paint and coatings, the role of each of the components in the formulations and the process from turning a liquid paint into a solid film is crucial to know. In this section, the general composition of a paint formulation will first be explained, followed by a description of the film formation process.

A coating is a material that when applied to a substrate, creates a solid film on the surface of the substrate, mainly to protect or decorate the surface. The term coating is used in general for a material that is applied to a surface, and the term paint is used for a material with pigment, which is applied to a surface [1].

There are many ways to categorize types of paint and coatings, for example classing them by type of binder, type of curing method or by its properties. Paint systems can for instance simply be divided into four main groups; Solvent borne paints, water borne paints, powder coatings and other paints [15]. These four main groups can be further divided into a great number of different paints where well-written literature is available [15].

Generally, paint consists of five components; binder, solvent, pigments, fillers and additives [16]. The binder forms the basic structure of the film, defines the main properties of the coating and often determines the method of application [1]. Binders are macromolecules with a molecular mass that varies from 500 – 30 000 Daltons, and form networks with molecular masses of millions when the coating film is cured [1]. By varying the molecular mass of a binder, film properties like elasticity, viscosity, adhesion and hardness may change [1]. Most types of macromolecules used are highly viscous polymers, often called resins, and exist both as natural and synthetic. Epoxy, acryl and alkyd resins have been widely used as binders, with both volatile organic compounds and water as solvents [17]. In order to store the paint over time, and to be able to spread it as well as possible, many coating materials need added solvent.

Pigments are used in paint to obtain decorative effects and/or weather resistance and must be added to the binder in certain amounts to obtain a uniform spreading of the particles and avoid flocculation [16]. Pigments are normally added in amounts of 10-80 vol.% of the paint, dependent on desired physical appearance [16]. Fillers, also called extenders, are used in paint and coatings to increase the volume of the paint, and/or to obtain new or improved properties, which is further described in Section 2.3 [16]. Fillers are normally added in amounts of 20-90 vol.% [18]. Type of fillers and the effect on the performance of the cured films are described in Section 2.3. Additives are substances added to modify or obtain specific properties of the coating material, and can for instance be defoamers, rheology additives, or wetting and dispersing agents. Additives are added in amount of 0.01 – 1 vol.% [16].

2.1.1 Film formation

The formation of a solid film is a crucial step in the coating process and should be well understood to obtain a high-performance coating. The film formation is the step where the coating material goes from having a liquid form to a solid film. The conditions needed for the full curing process to occur, such as time and temperature, are important for the performance of the film or for instance for how quickly the coating surface can be over-coated, stored or handled in other ways.

To understand the film formation process, considering the glass transition temperature (T_g) for the coating material/polymer is a good place to start. The T_g of a polymer is the temperature of which the polymer changes from a glassy (amorphous) state to a rubbery state [36]. The value of the T_g of a material strongly impact the flow properties, and when the temperature decreases below the binder's T_g in a coating material, the binder exists in the solid state, which prevents the macroscopic flow of the material [19]. The T_g of the coating material must increase during the film formation process to exist in the glassy state after being applied. There are two ways to increase the T_g: solvent evaporation or a chemical reaction [19]. Solvent evaporation and chemical reactions are normally called physical and chemical curing, respectively, and film formation often consist of a combination of both methods [1].

Evaporation of volatile organic solvents from solvent borne paints, and water from water borne paints are physical film curing. This curing mechanism mainly works

in coatings with high molecular weight binders [1]. The evaporation of solvent results in an increase in T_g, and the film gradually enters the solid state, and has a higher T_g. Powder coatings can also cure through physically curing by cooling of polymer melts [1].

Chemical curing is based on functional and reactive groups of low molecular weight polymers that copolymerize, forming a cross-linked network [19]. There are two main types of cross-linking reactions, called chain-growth and step-growth, or polyaddition and polycondensation, respectively [19]. The film formation process by the step-growth polymerization will be explained in further detail due to the binding system used in this thesis.

The step-growth polymerization can occur for a binding system consisting of two types of low molecular weight monomers/polymers with reactive groups, referred to here as monomer A and cross-linker B. The functional monomers A and B will copolymerize through the reactive groups and results in a structure with a high molecular weight as illustrated in Figure 2.1 [19]. Depending on the functional groups, a small molecule can be released as a result of the condensation reaction between A and B, but this is not the case for all types of step-growth polymerizing binding systems. The epoxy-amine system used in this thesis cross-links by step-growth but does not release a small molecule in the cross-linking reaction. The more cross-links that are formed, the higher will the cross-link density of the final film be. It will be gradually more and more difficult for the free reactive groups in monomer A to find a reactive group on a cross-linker B as the T_g of the film increases, and a maximum limit of conversion is therefore often observed. For instance, diepoxy-diamine systems have a maximum limit of conversion in films at 90-95% [19].

During film formation, the evaporation or cross-linking processes makes the molecular structure less free to move, and the film tends to shrink. Further evaporation or adhesion to the substrate after the first stages of film formation can introduce stresses, resulting in a fragile film. It is therefore important to understand the film formation process in order to avoid formation of internal stresses and to design the desired end properties of the film due to e.g. crosslink density or amount of water/solvent present [19].

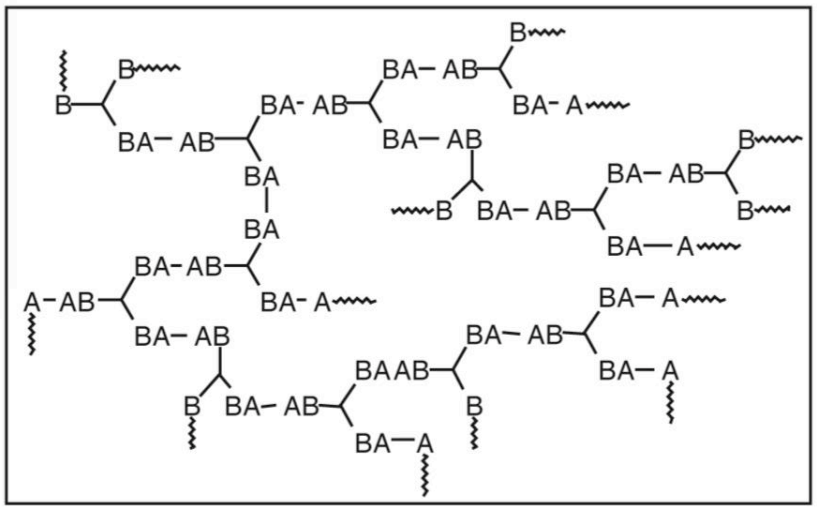

Figure 2.1: Illustration of a crosslinked polymer network with a difunctional monomer A and trifunctional crosslinker B [19].

2.1.2 Application methods

Paint and coatings can be applied with various methods depending on type of nature, shape and size of the substrate, type of paint, environmental considerations, cost and the speed of the application [2]. The application can be performed manually with brushes, drawdown applicators or rollers, or by mechanical methods, such as dipping or spraying. [1]. The different techniques have their difficulties associated with them. Paint applied by rollers can be prone to air bubbles and spattering and during spraying the solvents can evaporate faster than desired, resulting in poor film appearance [2]. In this work, the paint will only be applied manually with drawdown applicators, as described in Section 3.4.

2.2 The epoxy system

Epoxy resins are polymers with one or more epoxy groups (epoxy/epoxide/oxirane, see Figure 2.2), but the term is also used for cross-linked epoxy systems, even though the cured systems contain no or only a small number of epoxy groups [20].

Cured epoxy resins are amorphous thermosets, and are known for high mechanical strength and toughness, excellent chemical and corrosion resistance and good electrical, adhesive and thermal properties [20]. Due to the mentioned mechanical and chemical properties, epoxy resins are used in a wide range of applications as protective coatings, structural applications such as electrical laminates and semiconductor encapsulants, flooring and adhesives [20].

Since epoxy resins were commercially available in the late 1940s, the number of various epoxy resins have increased. Epoxy resins differ in the functionality and type of backbone, from e.g. aliphatic, cycloaliphatic to aromatic. The most used epoxy resins are prepared by coupling of compounds with two active hydrogen atoms and epichlorohydrin, followed by dehydrohalogenation. The epoxy resins produced from epichlorohydrin are called glycidyl-based resins [20]. There exist a wide range of epoxy resins, and it would be beyond the scope of this thesis to describe all these types. A well written review of epoxy resins is available in [20].

Liquid epoxy resins are a class of resins produced from the coupling of epichlorohydrin with bisphenol A. They have the structure shown in the top of Figure 2.2 and are called diglycidyl ether of bisphenol A (DGEBA). The polymerization rate for liquid epoxy resins is rather low ($n \approx 0.2$) [20], resulting in highly cross-linked networks in the presence of a curing agent. For cured DGEBA structures, the bisphenol A moiety contributes with toughness, rigidity and elevated temperature performance, the ether linkages contribute with chemical resistance, and the hydroxyl and epoxy groups contribute with adhesive properties if the DGEBA is applied to a substrate [20].

Almost all epoxy resins are converted into solid materials through reaction with the epoxy or hydroxyl groups using a curing agent acting catalytically or coreactively [20]. The catalytic curing agent acts as an initiator for homopolymerization between the epoxy resin monomers, while the coreactive curing agent acts as a comonomer in the polymerization process. Depending on desired properties, various curing agents can be used, and the coreactive agents most used are primary or secondary amines, phenols or carboxylic acids [20].

Selecting a curing agent, the chemistry of the epoxy resin and the curing agent must be matched, and the epoxy resin/curing agent should be mixed based on a stoichiometric ratio. A suitable curing time and temperature must also be developed for the individual epoxy resin/curing agent systems. These factors, among others, can decide the final epoxy solids mechanical and chemical performance, by developing an epoxy system with the desired cross-link density, tightness of the network and chemical structure [20].

In this work, the DGEBA epoxy resin has been used with a polyamine curing agent, and the cross-linking reaction is illustrated in Figure 2.2. The cross-linking reaction is a step-growth process, where the epoxide ring is opened by the amine and a chemical bond is formed between the carbon-atom in the epoxide ring and the nitrogen atom in the amine. The full structure of the curing agent is not open information. The polyamine is an epoxy adduct dissolved in benzylalcohol. The ratio of epoxy resin to curing agent and the curing time and temperature are developed by Jotun and are shown in Section 3.1 and 3.4.

To improve or change specific properties, modifying agent as for instance fillers, solvents or additives are normally added to the epoxy system. Especially liquid epoxy resins with tight and highly cross-linked networks might show low flexibility and toughness at the expense of other properties such as elevated temperature performance, chemical resistance and rigidity [20].

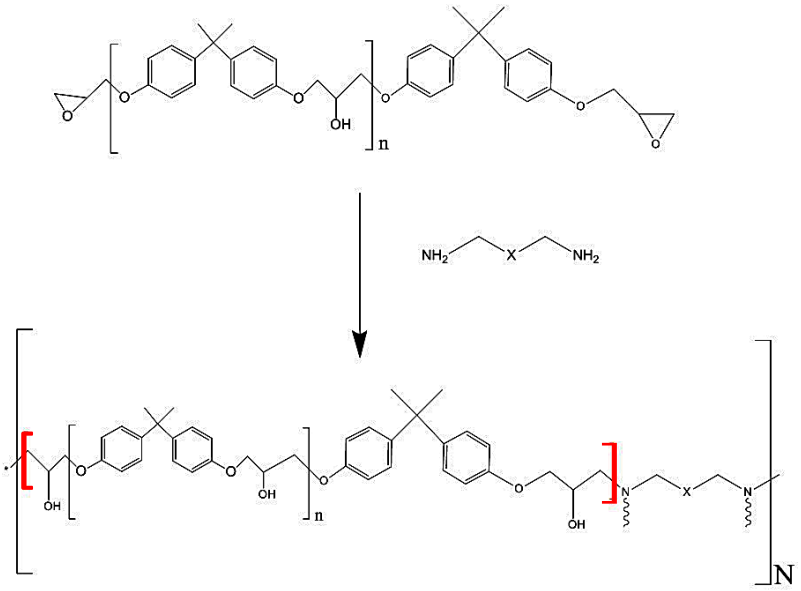

Figure 2.2: Crosslinking-process between the epoxy resin and curing agent (polyamine) used in this work. The red brackets define the structure that is repeated inside the black brackets as the wavy bond, and the black brackets define the overall structure that is repeated.

2.3 Fillers

Systematically use of fillers in paints have history back to the ancient Egyptians, where the minerals $CaCO_3$ and $CaSO_4$ were frequently used [18]. Despite the early history, a remarkable increase in filler production were not seen until the industrial revolution in the 18th century [18]. During the last two centuries, the use and function of fillers in paints have developed from being incorporated in paint to increase the volume and reduce the cost, to contribute with enhanced properties of the paint [16,18]. In the 1970s, the plastic industry also increased the use of fillers as a result of increased requirements on the plastics like higher strength, modulus or lower thermal expansion coefficient [14].

Fillers are used in many types of paint and coatings to obtain the desired performance of the paint film. For instance, fillers contribute to strength and anti-corrosive protection, minimizing the degradation due to UV, water or temperature, give tailored thermal properties like reduce transfer of heat to keep interior cold by infrared radiation reflecting properties, or maximizing transfer of heat to heat water in solar panels with infrared radiation absorbing properties [2]. There exists a number of fillers which can contribute to different properties as the ones previously mentioned, and it is very useful to know the characteristics of different types of fillers and the possible applications. Fillers are mainly minerals like oxides, salts or silicates, but may also be fibers or coal [14]. Various shapes of the filler particles include spheres, cubes, blocks, flakes and fibers, and the properties listed in Table 2.1 are the most used properties of a filler [14].

Table 2.1: List of important properties when selecting a filler [14]

Particle shape, particle distribution, surface area
Chemical composition
Optical, thermal, physical, conductive properties

The particle shape, size distribution and surface area decide the packing efficiency of the filler in a polymer/filler system. These properties in turn affect e.g. the rheology or mechanical properties of the system. The chemical composition of the filler is of importance for all properties due to the fact that the bulk chemistry and especially chemistry of the surface of the fillers decides the possibilities

for interaction between the filler and the polymer. A thorough review of fillers for use in paint/plastics is available in [18,14], respectively.

Four fillers with various shapes have been used in this work, and Table 2.2 lists some of the characteristics of these fillers. Barium sulfate is a salt consisting of small nodular/block-like shaped particles, mica is a potassium aluminium silicate consisting of plate-like particles, aramid is a polyamide with a fibrous shape and wollastonite is a calcium silicate consisting of needle-like shaped particles. The fillers were chosen based on the different shapes. All fillers have received attention in research, where for instance barium sulfate particles have increased the modulus and toughness in polypropylene composites [21], mica has increased the tensile strength and modulus of polyetheretherketone [22], aramid has increased the interlaminar shear strength and T-peel strength (see Section 2.4.2) of epoxy composites [23], and wollastonite has increased the scratch resistance of ethylene-propylene composites [6].

Common for many of the systems studied in the published articles on polymer/filler systems is the lack of an interaction between the filler and the polymer, resulting in weaker strength and toughness compared to a situation where an interaction is present. Surface modification of fillers has therefore been introduced in this work and is described in Section 2.3.2.

Table 2.2: The characteristics of the fillers tested in this work. The values were collected from the technical data sheet of the filler, which is available in Appendix B.

	Barium Sulfate	**Mica**	**Aramid**	**Wollastonite**
Chemical composition	$BaSO_4$	$KAl_2(AlSi_3O_{10})(OH)_2$	Polyamide*	$CaSiO_3$
Shape	Block	Plate-like	Chopped fibers	Needle/fiber
Mean particle diameter/size (μm)	3.4	8-12	< 125	12
Surface area (m^2/g)	1.5	8.3	8 – 12	1.3
Density (g/cm^3)	4.4	2.8	1.4	2.9
Linseed oil Absorption (g/100g)	13.0	49-53	366.0	22
CPVC (vol.%)	61.9	39.3	15.0	59.8

* Polyamide structure: $[-NH-C_6H_6-NH-CO-C_6H_6-CO-]_n$

2.3.1 Filler concentration

The relationship of filler to binder in paints is described by a value called the pigment volume concentration (PVC), as given by Equation 2.1 [2]:

$$PVC\ [\%] = \frac{Volume\ of\ Pigment\ and\ Filler}{Volume\ of\ Pigment\ and\ filler + Volume\ of\ Binders} x\ 100 \qquad (2.1)$$

The two extremes are 0 % PVC which would be a film of pure binder, or 100% PVC which would be a film of only pigment/filler. The critical pigment volume concentration (CPVC) is the value at which the paint has just enough binder to fully wet all the pigment/filler particles and the voids between them, as shown in Figure 2.3. The binder/polymer is referred to as a polymer matrix, and the filler particles are distributed in this matrix. Properties of polymer/filler systems such as strength, water absorption, opacity and stiffness may change abruptly above the CPVC, and it is therefore important to determine the CPVC. The oil absorption value is the amount of oil needed to completely wet 100 grams of filler powder, and the CPVC can be determined by this value as given by Equation 2.2 [2]. OA is the oil absorption and ρ_{filler} and ρ_{oil} is the density of the filler and oil, respectively. The oil absorption of linseed oil is in general used but will only give an estimate of the real CPVC for the individual binding systems [2].

The size, size distribution, shape and surface area of the fillers affect the CPVC [16]. As the properties of the polymer/filler systems such as stiffness, strength and permeability are mainly determined by the binder, these properties can be altered by fillers. The CPVC of fillers varies, and consequently the filler loading of the polymer/filler systems varies. For instance, epoxy/ graphene-oxide and epoxy/carbon black had filler loadings of 0.1-0.6 and 0-2 wt.%, respectively [24,25], and polypropylene/barium sulfate, polyetheretherketone/mica and polyetherketone/wollastonite had filler loadings of 24, 20 and 10-40 wt.%, respectively [21,22, 26]. All these systems showed enhanced modulus (storage/Youngs/bending) and/or strength (tensile/flexural) at the specific filler loadings used.

The ratio of the PVC used in the paint to the CPVC of the filler used is called Λ, lambda, and is defined in Equation 2.3 [18] (the reference uses the letter Q instead of Λ). Lambda is an important

value to consider when comparing different type of fillers, as this value indicates at which extent the filler is added relative to the specific filler's CPVC.

$$CPVC = \frac{1}{1 + \frac{OA * \rho_{filler}}{\rho_{oil}}} \tag{2.2}$$

$$\Lambda = \frac{PVC}{CPVC} \tag{2.3}$$

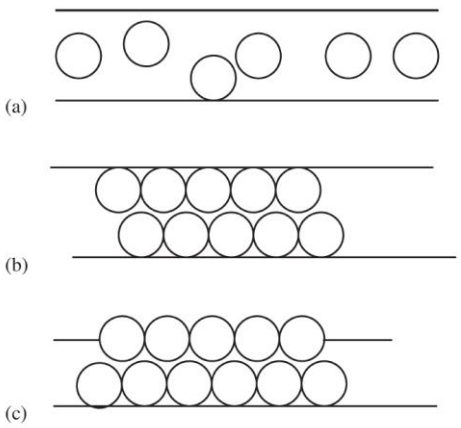

Figure 2.3: Illustration of films with pigment/filler amounts a) below CPVC, b) at the CPVC and c) above CPVC [2].

2.3.2 Surface modification of fillers

The surfaces of most fillers are hydrophilic, which can be disadvantageous for the polymer/filler interaction for some binder systems. Modifying the surface with a coating material can result in a filler surface with modified properties such as lower surface energy or changed hydrophilicity/hydrophobicity. Functional groups may have been added, dependent on the surface modifying substance.

Dependent on type of filler and binding system, various surface modification agents can be used as e.g. stearic acid, organofunctional silane, siloxane, silicane and titanate [18]. Plasma treatment has also been used as a surface modification technique for e.g. aramid fibers, where new functional groups are introduced on the fiber surface by the plasma treatment [23,27,28].

In chemical surface modification (silanes, titanates, etc.), the surface modifier is coupled to the mineral surface by chemisorption, which can be ionic or covalent in nature, by various treatment techniques like for instance direct application, addition to the polymer or solvent/surface modifier solution mixed with filler [14]. The surface modified filler is then able to interact with the binder/polymer through molecular entanglement (chain length and chemistry of modifier must be matched with binder), van der Waals forces (dispersion, dipole), hydrogen bonding or covalent bonds (e.g. cross-linking), dependent on the surface modifier and the binder [14].

Surface modification can contribute to various properties dependent on the surface modifier. Short functional coupling agents normally binds the matrix near to the filler surface, increasing the rigidity, and possibly reducing the elongation, but it increases the strength. Long chain coupling agents might, however, act as plasticizers and reinforce through chain entanglement [14].

Organofunctional silanes have been used on many different fillers and have the general formula R-Si-X_3, where R is an organofunctional group which can react with the binder. The X is a hydrolysable group such as methoxy or ethoxy [14]. The modification process of filler surfaces by silanes are based on a condensation reaction between the hydrolysed X-groups of the silane and hydroxyl groups on the filler surface [14], as shown in Figure 2.4. The filler surfaces can be hydroxylated prior to the modification process in order to have a large number of hydroxyl groups present on the filler surface [12,29,30].

The surface modification agent used in this work was 3-aminopropyltriethoxysilane, called ameo and is displayed in the illustration in Figure 2.4. The hydrolysed form of ameo can form covalent bonds with the –OH groups of the mineral surface as M-O-Si, where M-O is the mineral-oxide group, and the Si atom is the silicon atom of the silane. Hydrogen bonds between hydroxyl groups and amine-groups of the silane have also been observed earlier and been used as proof for an interaction between the mineral and the silane [11,12,13,14,31].

The organofunctional R group of the ameo is an aminopropyl group with $–NH_2$ as the functional part available for covalent bonding with the binder system, as illustrated in Figure 2.4 [32].

X-ray photoelectron spectroscopy and/or Fourier transform infrared spectroscopy, see Section 2.5.2 and 2.5.3, have been used to investigate surface modification of for instance glass surfaces [11,12,13], TiO_2 particles [31], $BaSO_4$ particles [33] and aluminum surfaces [34]. These two techniques have also been used in this work.

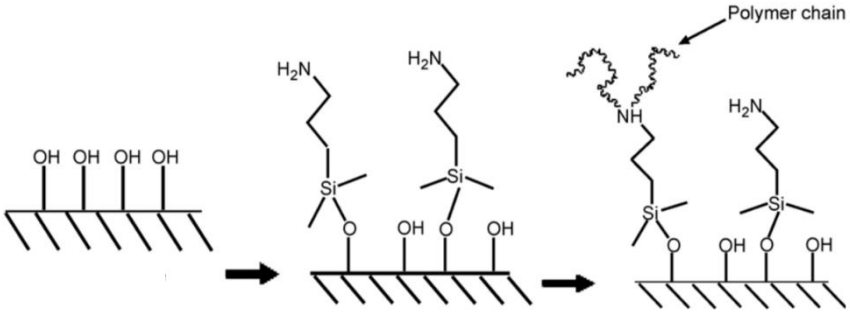

Figure 2.4: Illustration of the surface modification process of a filler surface with –OH groups and the ameo surface modification agent [32].

2.4 Physical and mechanical properties

The physical and mechanical properties of polymer/filler materials are mainly determined by the polymer matrix but can be influenced by filler particles. For thermosetting polymer systems, the curing process is crucial in order to achieve the desired polymer structure. The physical and mechanical properties investigated in this thesis will be introduced in this section. Mechanical properties may be considered as a subgroup of physical properties, but the term has been used in this work for the physical properties measured by applying a force to the material.

2.4.1 Modulus and glass transition

When a material is exposed for a stress, it will be deformed, and the study of applied stress and resulted deformation is called rheology [35]. The stress (force/area) can be applied in several ways, for instance, stretch, compression and/or shear. When stress has been applied, the material can respond by returning back to the original form (elastic material), being deformed (liquid) or something in between elastic and deformed, i.e. a viscoelastic material. Paint films often show viscoelastic behavior.

The applied stress and resulted deformation, called strain, is often presented as a stress-strain curve as shown in Figure 2.5. Equation 2.4 described the relation between stress, σ, and strain, ε, and E, Youngs modulus [35]. The relation between stress and strain is also included, where F is the force applied to the area A of the material, and ΔL is the change in length due to the stress. L_0 is the original length. Equation 2.4 is based on Hooke's law, and is valid for the linear part of the stress-strain curve [35]. The stiffness of a material is represented by the slope of the stress-strain curve, i.e. the modulus [36]. Dependent on type of stress applied to a material, the modulus, E, in Equation 2.3 may be expressed due to the applied stress, e.g. Youngs modulus from uniaxial tensile stress (see page 32-33), storage modulus from dynamical mechanical tests (see page 31-32) or bending modulus from flexural stress (see page 32-33). Ideally, the modulus of a material should be the same from all tests, but differences in the applied stress, especially for viscoelastic materials, may result in various values for the different modulus values.

$$E = \frac{\sigma}{\varepsilon} = \frac{\frac{F}{A}}{\frac{\Delta L}{L_0}} \tag{2.4}$$

The area where the stress-strain curve increases linearly is the area where the material acts elastically, and the modulus can be calculated. This area is called the linear viscoelastic region (LVR) for viscoelastic materials. By further increase in stress, the material will deform plastically, and at some point, fractures [35]. Addition of fillers to a polymer matrix will enhance the modulus as the fillers normally has a higher modulus than the polymer matrix [14]. The enhanced modulus gives the polymer/filler material a greater resistance to deformation than the pure polymer matrix. The hardness and rigidity of the fillers affects the efficiency of the modulus enhancement as harder and more rigid fillers will contribute to a stiffer matrix, but the size and shape of the fillers are also reported to have a large influence on the modulus. For instance, considering the shape of fillers, the modulus will be most influenced in the order rods > plates > spheres [4].

The stress-strain behavior and modulus of materials can be determined by a tensile test, a flexural test or a dynamical mechanical analysis (DMA), which all are described in Section 2.5.5, 2.5.5 and 2.5.4, respectively.

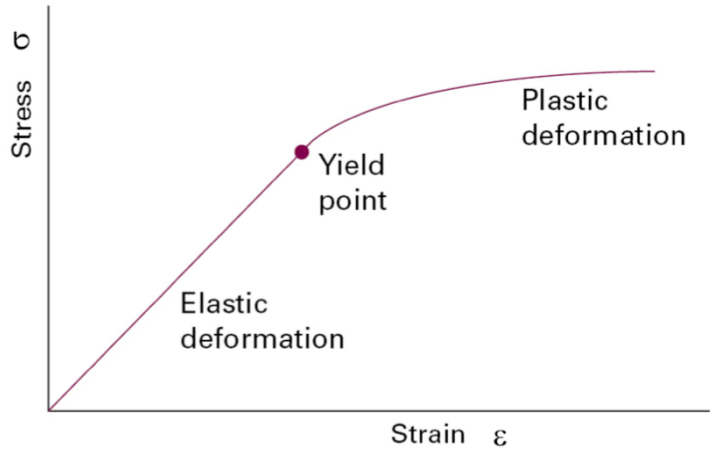

Figure 2.5: A typical stress-strain curve [35].

Dynamical mechanical analysis is one among several experiments where the modulus of a material is recorded simultaneously as the temperature is changed and this analysis technique is explained in Section 2.5.4. These experiments are normally conducted to investigate the temperature response of the material and possible transitions in the material. The result is presented as a modulus-temperature curve as illustrated in Figure 2.6. The modulus can also be dependent on time or frequency, but this will not be a topic in this work. In Figure 2.6, the temperature dependent modulus E' is illustrated, which is the elastic (storage) modulus, and will be described in Section

2.5.4. These experiments are often performed on polymer materials, as the properties of polymer materials can change drastically with temperature. At low temperatures, polymers may have a high modulus and be stiff, and exist in the glassy state. By increasing the temperature, the polymer structure will be freer to move, and the materials often go through the glass transition (T_g), where movement of large polymer segments occur. The material following enters the rubbery state, where the material has a low modulus, and is soft [37]. Figure 2.6 illustrates the temperature dependent behavior of various types of polymers, where some polymers enters the state of viscous flow after the rubbery plateau, while others, e.g. chemical cross-linked polymers remains at the rubbery state due to the covalent bonds. The binding system used in this thesis is chemically cross-linked and goes from the glassy state to the rubbery region/plateau at the glass transition.

The glass transition of polymeric materials is highly dependent on type of polymer but can also be affected by fillers. The effect of fillers varies, and addition of one type of filler can increase the T_g, while addition of another filler may decrease the T_g. For instance, whereas carbon black nanoparticles increase the T_g of epoxy composites [25], silica particles decrease the T_g of epoxy composites [38]. Addition of barium sulfate particles does, however, not change the T_g of epoxy-based powder coatings [39]. The amount of filler in the polymer matrix, distribution of the filler particles, the polymer-filler interaction and the size/shape/chemistry of the fillers will decide to what extent the filler affects the T_g of the sample [25,40,41].

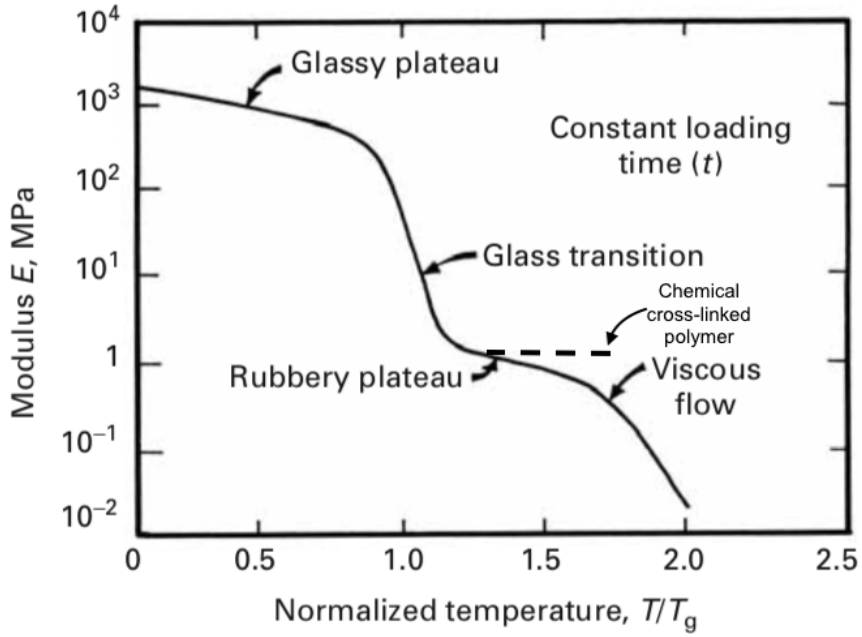

Figure 2.6: Illustration of modulus-dependence of temperature for polymers. The illustration is borrowed from [42], and the behavior above the T_g for chemical cross-linked polymers is added. The modulus in this illustration is the elastic storage modulus, and the temperature is normalized with respect to the T_g.

2.4.2 Strength and toughness

A measure of the strength and toughness of a material can be found using the stress-strain curve of the material at interest. Test conditions like temperature and rate of deformation are important since stress/strain properties of viscoelastic materials are both temperature and time dependent. Tests that apply stress beyond the linear viscoelastic region of the material can reveal the strength and toughness of the material. Tensile and flexural tests, explained in Section 2.5.5, stretch out and pushes down materials until they break, respectively. The results are shown as stress-strain curves, illustrated in Figure 2.7 [42].

The strength of materials is defined as the maximum load the material can sustain [36], and the toughness is often defined as the amount of energy the sample can absorb before it breaks [36]. Referring to the stress-strain curve, the strength is the stress at break and/or the highest point on the curve, and the toughness is defined as the area under the stress-strain curve [36]. A material with high strength must have a structure with chemical/physical bonds strong enough to withstand high stress, and for the material to show high toughness, the applied stress must be absorbed by e.g. plastic deformation. From Figure 2.7 the brittle polymer has high strength, but low toughness, as the sample do not elongate much before it breaks. The more ductile polymer shows lower strength, but higher toughness, as the sample is able to absorb more energy.

The strength and toughness of polymer materials is affected by fillers and the increase or decrease in strength/toughness is dependent on both polymer and filler type. For the binding systems similar to the one used in this thesis, addition of coarse wollastonite has decreased the flexural strength [7], while addition of plasma treated aramid fibers has increased the interlaminar shear strength [23] of an epoxy system. Interlaminar shear strength and T-peel strength is properties often reported for polymer/filler systems. Interlaminar shear strength is measure by a flexural test (see page 33), where the span between the bars is small compared to the thickness of the sample. This will induce a high shear stress in the sample during bending, and gives a measure of the interlaminar resistance, reported as the interlaminar shear strength [42]. The T-peel test is an adhesion test, where the coating and substrate (the samples are coatings applied to a substrate) is pulled apart, and the force needed to pull is measure [43]. The test gives a measure of the adhesional strength between the coating and the substrate. These properties have not been examined in this work but is described due to referring of these properties of other polymer/filler systems.

With addition of fillers, the filler distribution, size and shape of the filler and especially the interfacial interaction between filler and polymer are important factors to consider, since all these factors contributes to the strength and toughness of the polymer/filler systems. An even distribution of filler particles is important in order for the material to be able to distribute the applied stress through the polymer matrix without stress concentration in e.g. filler agglomerates [14]. Poor particle distribution will result in a mix of major and minor regions of polymer matrix, and the minor polymer matrix regions will weaken the material. An even distribution of filler particles will give even sizes of polymer matrix regions, and a higher strength [14]. When the material deforms plastically, the polymer matrix must be able to stretch around the filler particles in order to elongate and hold a high toughness. The shape, size and packing of the filler particles are therefore important when examining properties of polymer/filler materials [14]. Orientation of filler particles can also affect the possibility of the polymer matrix to stretch around the particles, and influence of orientation on the physical and mechanical properties of polymer/filler systems are discussed in Section 2.4.4.

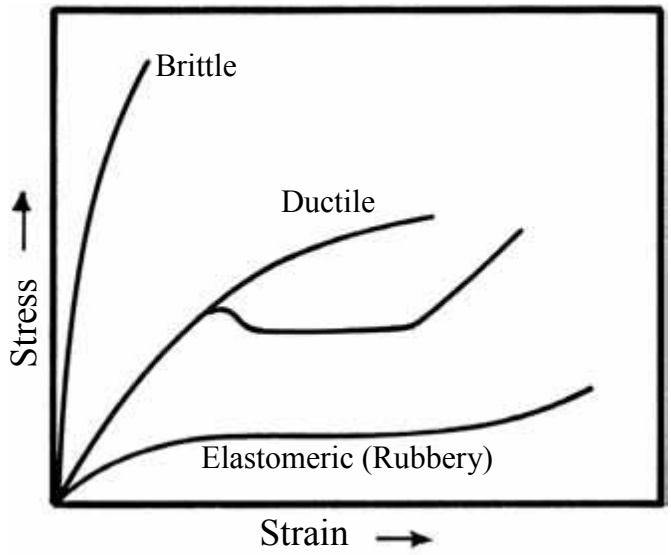

Figure 2.7: Typical stress-strain curves for brittle, ductile and elastomeric polymer materials [42].

2.4.3 Permeability

There exist many definitions of permeability, depending on area of science. In this work, the permeability is defined as the diffusion of a gas/vapor or liquid through a solid material [43]. The gas or liquid which passes through the material is called the permeant, and can be e.g. water vapor, O_2, HCl or SO_2 [43,44]. The solid material in this thesis is a thin paint/coating film, and the permeability of polymers will be introduced below.

Permeability is an important issue in several applications of polymer films as for instance protection of metals from corrosion or where total isolation of a surface from the environment is wanted. For wood surfaces, where no liquid water should be able to pass, but water vapor needs to pass through the polymer film, the water permeability properties of the film is crucial [44]. Organic polymer coatings are used for protection against corrosion of metals. Deep understanding of the corrosion process and the possible protection mechanisms is beyond the scope of this thesis, but the three main protection mechanisms are 1) The electrochemical mechanism, 2) The physiochemical mechanism and 3) The adhesional mechanism [43]. For corrosion protection, the permeants O_2 and H_2O (liquid or vapor) are most often of interest [43].

The exact permeation process will vary depending on the polymer material and permeant, but a general model used to understand the process is presented in Figure 2.8, with description of the steps 1. - 5. in the figure. This model is based on Thomas Grahams solution-diffusion theory from 1866 (postulated that the permeation of a permeant was dependent on dissolution in the material, followed by transmission of the dissolved permeant through the material), Fick's first law and Henry's law [43]. Fick's first law describes that the flux of matter diffusing (parallel to one axis) is proportional to the first derivative of the concentration [35], and Henry's law states that [43]: *At a constant temperature, the amount of a given gas dissolved in a given type and volume of liquid is directly proportional to the partial pressure of that gas in equilibrium with that liquid.*

The physiochemical corrosion protection mechanism is the diffusion and permeation of gases/liquids. Coatings based on this mechanism are often called barrier coatings. These coatings are designed to slow down or block the permeation of e.g. O_2 and H_2O by a blocking effect as shown in Figure 2.9 [43]. As the polymer matrix has been the same for all fillers in this thesis, the influence of polymer structure and curing history have not been dealt with here. However, the blocking effect of the fillers has been studied. Various results on the permeability of water vapor or liquid water though the same polymer film have been reported. Some systems show difference in

water vapor and liquid water permeability, while other systems show the same vapor and liquid permeability [44].

The permeation of water vapor has been tested in the thesis, and the most common test method for vapor permeation is the cup method [43], which is described in Section 2.5.6.

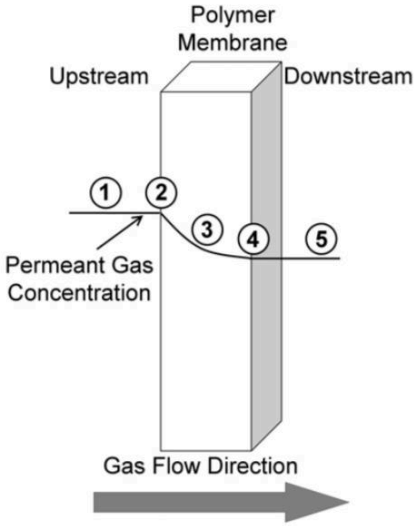

1. Diffusion of permeant molecule to polymer surface.
2. Adsorption of permeant molecule on the polymer/upstream atmosphere interface.
3. Diffusion of permeant through the polymer film.
4. Desorption of the permeant molecule on the polymer/downstream atmosphere interface.
5. Diffusion of permeant molecule from the polymer surface to the downstream atmosphere

Figure 2.8: A permeation model based on Grahams solution-diffusion model and Fick's and Henry's laws [43].

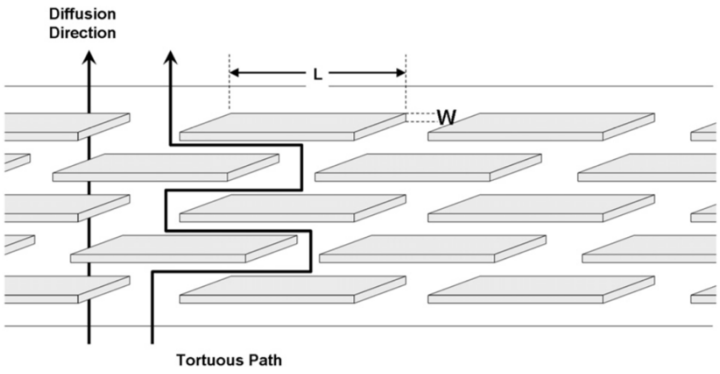

Figure 2.9: Illustration of the barrier enhancement by filler particles in polymer matrixes [43].

2.4.4 Orientation of filler particles

The aspect ratio of a shape is the ratio of the shapes longer side to the shorter side. Filler particles with large differences in the different dimensions, e.g. length vs. width, are called high aspect ratio particles. Fillers with high aspect ratio shapes can align in a specific direction in coatings. The orientation of the filler particles can affect the physical and mechanical properties such as strength, toughness and permeability.

The direction of the applied stress in tensile and flexural tests are illustrated in figures 2.10 and 2.11. For the tensile test, the elongation will occur in the same directions as given by the arrows in Figure 2.10. A polymer/filler sample with high-aspect ratio filler particles aligning with the longest side parallel with the stress direction may be able to elongate longer than a polymer/filler sample with orientation of the high-aspect ratio filler particles with the longest side aligned perpendicular to the stress direction. Consequently, it will also show a higher toughness [14]. This behavior is expected because it is easier for the polymer to stretch around the thinnest side of the filler particle under elongation. From Figure 2.11 it is seen that in flexural tests, the sample will be exposed to compression on the upper side and tensile stress on the lower side of the sample [36]. The same reasoning as for the tensile test and orientation will be valid for the flexural test sample.

As shown by Figure 2.9, an orientation of filler particles where the particles cover as much of the surface as possible in the direction perpendicular to the thickness of the gives rise to the lowest permeability of these polymer/filler samples [43]. Also, other properties like strength and modulus can be changed by a dominant or preferred orientation of the filler particles [14]. For instance, it has been found that the stiffness of epoxy/carbon fiber composites increased significantly from an anisotropic to a quasiisotropic orientation of the carbon fibers [41].

The orientation of filler particles has been investigated by observing the horizontal and vertical cross-section of paint films with SEM by observing number of particles aligned in each direction. Only the filler particles with high aspect ratio were investigated for orientation.

Under tensile and flexural test, the samples are elongated as a result of the applied stress. For polymer/filler samples, the pure part of the matrix will elongate until the applied stress overcomes the bond strength in the polymer structure. In the regions of polymer and filler, the polymer matrix will be restricted in the ability to stretch by the filler particles as explained previously. The interfacial bond between the polymer and the filler will then be important and decide if voids are created between the polymer matrix and the filler under elongation [14]. A microscopy study of

fracture surfaces is therefore a technique to observe fracture mechanics [36,42] and to get an indication of the polymer-filler interactions [14]. This approach has been used in this study and is referred to as fractography [45].

Figure 2.10: Illustration of the stress directions applied to a sample in a tensile test

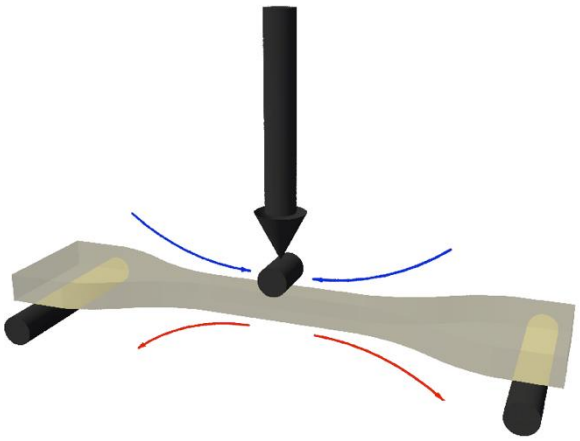

Figure 2.11: Illustration of the stress directions applied to a sample in a flexural test during bending.

2.5 Analysis instruments

To explain how filler particles impact a polymer matrix, several instruments should be used in order to investigate the chemical and mechanical properties of the samples. The dispersion, orientation and possible epoxy-filler interactions have been investigated using Scanning electron microscope (SEM), X-ray photoelectron spectroscopy (XPS) and Fourier transform infrared spectroscopy (FT-IR). The mechanical and physical tests have been conducted using a Dynamical mechanical analysis instrument (DMA), a Universal testing machine (UTM) and Payne permeability cups. Surface modification was investigated by XPS. The following sections describe these analysis instruments.

2.5.1 Scanning electron microscope

A scanning electron microscope is an electron microscope that produces images of both topography and composition of the sample. Utilizing an energy dispersive spectrometer, it can perform chemical analysis of the sample.

An electron beam scans over the sample, and the electrons from the beam (called primary electrons) interact with the sample. These interactions lead to secondary electrons, backscattered electrons and characteristic X-rays, which are the signals normally detected in a SEM.

The secondary electrons (SE) are created by inelastic scattering by the primary electrons, and SE signals will only arrive from the surface of the sample (5-50 nm), as the SE created further into the sample does not have enough energy to escape. SE signals will therefore give images of the topography of the sample. Back-scattered electrons (BSE) are produced when primary electrons are elastically scattered by the nucleus of an atom. The BSE signals arrive from 50-300 nm in depth from the sample surface and will give information on the composition of the sample, as illustrated in Figure 2.12.

X-rays are created when a primary electron knocks out a SE and leaves a hole in an inner shell. An outer shell electron falls down and emits an X-ray. All elements will emit characteristic X-rays that give information on the chemistry of the sample. Energy dispersive spectrometers are used for analysis of the X-rays.

A SEM consists of an electron gun and electromagnetic and objective lenses, focusing the electron beam in a straight line above sample, as shown in Figure 2.13. The electron beam

scans over the sample and interacts with it as described above. The SE and X-ray detectors are normally placed on the sides of the sample chamber, and the BSE detector normally above the sample (Figure 2.13 only show one type of setup for detectors). The electron beam scans over the sample, and the intensity of electrons/photons from each spot is detected by the detector, which makes up the SEM image as a collection of different intensities [46].

There exist several types of SEM instruments. Typical for insulating samples as the ones investigated in this thesis is to use SEM instruments which have the possibility to introduce a low pressure in the sample chamber, i.e. so called environmental or variable pressure SEM [46].

In this work, SEM was used to examine the dispersion and orientation of the fillers particles, as these characteristics can change the physical and mechanical properties of the samples (see above). Fractography is the study of fracture surfaces by a microscope. SEM is used for fractography in this study. The effect of surface modification of mica in polyetheretherketone composites [22] and the effect of surface modification of barium sulfate in polypropylene composites [21] have been illustrated by fractography using SEM.

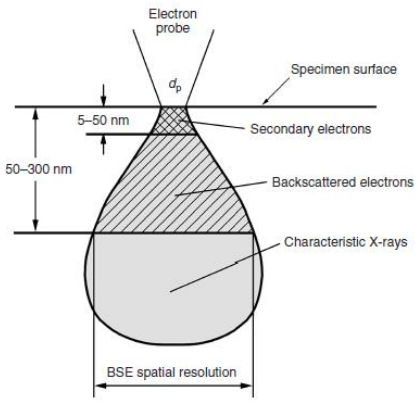

Figure 2.12: Interactions occurring when an electron beam hits the surface of a material and illustration of the depth the interactions happen. [46].

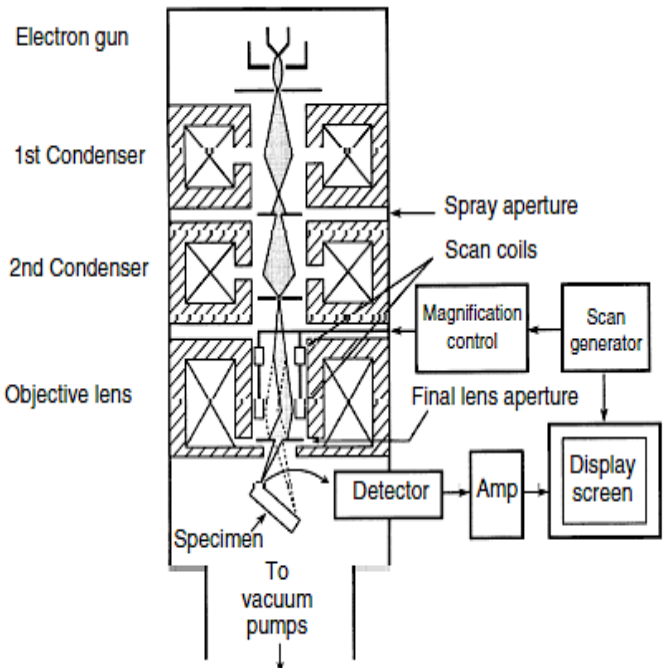

Figure 2.13: Schematic illustration of the instrumental setup in a SEM [46].
The X-ray and BSE detector are not included in this illustration.

2.5.2 X-ray photoelectron spectroscopy

X-ray photoelectron spectroscopy (XPS), also called electron spectroscopy for chemical analysis is a spectroscopy technique designed for the study of surfaces due to the analyzing depth normally being between 0-10 nm [46]. The XPS method is based on the photoelectric effect, where the sample is bombarded with X-rays with a given energy. As the X-rays hit the sample surface, electrons in the uppermost layer will be liberated. As the electrons only can escape from a certain depth in the sample surface (0-10 nm), the signal will only arrive from the surface. This is why XPS is called a surface sensitive technique.

If an X-ray hits a core inner shell electron, this electron will leave the atom as shown in Figure 2.14, and this electron is called a photoelectron. This leaves a vacancy in the inner shell, which is filled by an electron from an outer shell. The process can knock out a new electron, called an Auger electron, or a photon may be emitted. The auger electrons and photoelectrons are detected, and the detector measures the kinetic energy of the electrons, which by Equation 2.5 can give the binding energy, where $E_{binding}$ is the binding energy of the electron, E_{photon} is the energy of the X-rays, $E_{kinetic}$ is the measured kinetic energy of the electron and ϕ is an instrument and material dependent work function.

$$E_{binding} = E_{photon} - (E_{kinetic} + \phi) \tag{2.5}$$

A XPS instrument is an ultrahigh vacuum system that avoids gas contamination on the surface of the sample and avoids scattering of the photoelectrons by the gas molecules on its way from the sample to the detector [46]. The instrumentation of the XPS instrument used in this work is shown in Figure 2.15. The instrument consists of a sample chamber under ultrahigh vacuum, an X-ray source and monochromator for the X-rays, an electron analyzer and an electron energy detector. As the X-rays liberate electrons as described above, the electrons enter the electron analyzer (there exist several types, concentric hemispherical analyzer given as example here), where the electrons are focused and retarded to a certain energy (pass-energy) before they are sent through the hemisphere and finally are detected in the end of the hemisphere as illustrated in Figure 2.15.

The results of a XPS-analysis are spectra displaying intensity versus binding energy of the photoelectrons which have been knocked out by the X-rays. As described above, the instrument calculates the binding energy of the electrons arriving from the sample surface.

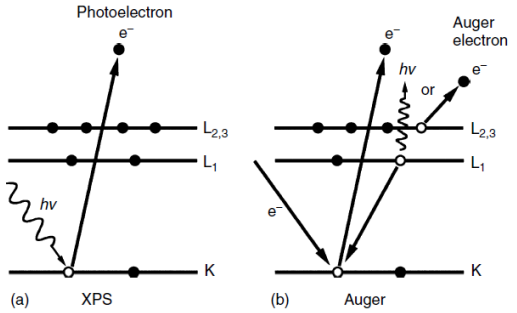

Figure 2.14: Illustration of an X-ray kicking out a photoelectron (left) and the following process of an electron falling down one shell, kicking out an Auger electron [46].

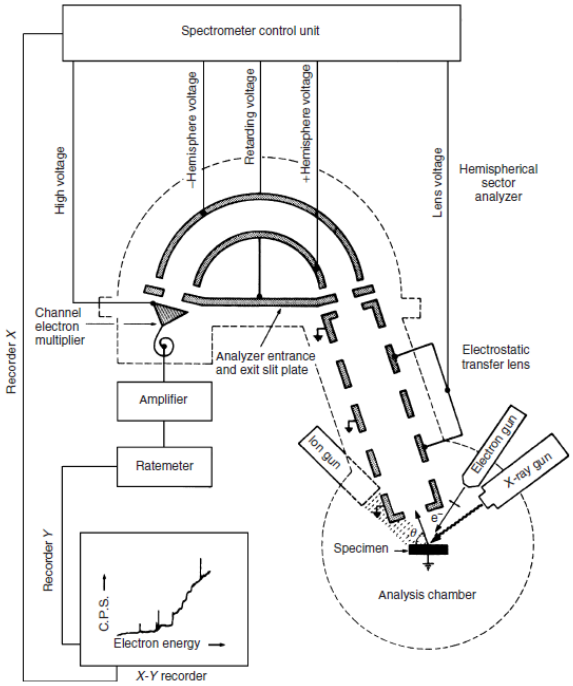

Figure 2.15: Sketch of the instrumentation of a typical XPS instrument, here with a concentric hemispherical electron analyzer [46].

Each element will have electrons emitted with a specific energy corresponding to the binding energy of an electron in an inner-shell of the element [46]. For instance, if there is carbon in the sample, a binding energy of ~284-289 eV will be detected, as this corresponds to the binding energy of electrons in the 1s orbital of carbon. All elements have specific energy ranges corresponding to the binding electron of the electrons which are likely to be knocked out. For instance, oxygen is represented by electrons arriving from the 1s orbital, and the oxygen signal is therefore referred to as the O1s peak, and silicon has electrons arriving from the 2p orbital and is referred to as the Si2p peak. The intensity of electrons detected at a given binding energy is often measured as counts per second. The intensity given as counts per second for the various elements will therefore be a value proportional to the number of atoms of the specific elements present on the sample surface. Percentage atomic concentration of the sample may therefore be calculated based on the intensities in the XPS spectra.

In a XPS-analysis, one may collect signal from a wide range of energies, often called a survey spectrum, in order to get a view of all the elements in the sample. If the sample composition is known, high-resolution spectra can be collected, which are spectra with higher resolution, over a narrower energy range, typically covering the energy range of one elements signal. An element may exist in several states in a sample, for instance carbon in the form of C-C, C-O and C=O bonds. All these chemical states will contribute with a signal to the peak observed in the spectra. The XPS-data are often interpreted by the use of a software program to find the possible contributions to the signals observed in the XPS-spectrum. This procedure is known as peak fitting, and often based on referring to the literature for already reported binding energies for the various chemical states. Based on the peak fitting procedure for a high-resolution spectrum, percentage area (%Area) of the various binding states (peak fitted to compose the main signal) may also be calculated. The %Area represent to which extent each binding state contributes to the specific elements signal.

The resolution of a XPS-spectrum can be adjusted with the so-called pass energy and step size. The pass energy determines which energy the incoming photoelectrons from the sample must have in order to enter the electron analyzer and determines the resolution of the XPS spectrum [46]. The step size determines the distance between each data point in the XPS spectrum. High pass energy and high step size will result in spectra with low resolution, while low pass energy and low step size will result in spectra with high resolution.

As XPS is a surface sensitive technique, it has been used to examine the effect of surface modification of fillers as mentioned earlier. Examples include the detection of the silane groups on mica surfaces [47] and detection of silane groups after silane treatment or new chemical groups on the surface after plasma treatment of aramid fibers [48]. XPS may possibly reveal if there is a chemical bond between a polymer and a filler surface. These effects may be related to by chemical shifts or new peaks in the spectra. Chemical shifts may arise from that a changed charge of an ion gives it a different electron binding energy than the electrons from a neutral version of the atom, or a change in the chemical environment of the element. For instance, Bolouri et al. concluded that there may exist a chemical bond between an epoxy resin and aluminum oxide surface, by observing protonated amino groups interacting with hydroxyl groups attached to aluminum oxide [49].

2.5.3 Fourier transform infrared spectroscopy

Infrared spectroscopy is the study of interactions between infrared radiation and matter. Infrared radiation is a part of the electromagnetic spectrum and has longer wavelength than visible light. In infrared spectroscopy, the wavelengths corresponding to the vibrational frequencies of molecules are in interest, which typically are between 2.5 μm and 25 μm [50]. The terms wavelength, frequency and wavenumber are all used in infrared radiation spectroscopy and are measures of energy. The relation between wavelength, λ, frequency, ν, and wavenumber, $\bar{\nu}$, are shown in Equation 2.6 (c is the speed of light) [50].

$$\nu\ (Hz) = \ \bar{\nu}\ (cm^{-1}) \cdot c = \frac{c\ (cm/sec)}{\lambda\ (cm)} \tag{2.6}$$

The covalent/ionic bonds in molecules vibrate and can absorb energy corresponding to the frequency of the vibrational modes (stretching and bending) of the chemical bonds [50]. Further introduction to vibrational modes will not be described here but is available in [50]. Each chemical bond will have specific vibrational modes with specific frequencies, which makes it possible to expose a sample for infrared radiation with specific wavelengths and detected which wavelengths which were absorbed or transmitted. A sample may be exposed for a range of infrared radiation frequencies and the detecting of all the absorbed frequencies makes up what is called an infrared radiation spectrum of a sample. The infrared spectrum is displayed as percentage absorbance (or transmittance) of infrared radiation as a function of wavenumber.

The infrared spectrum of a compound is often referred to as a fingerprint for the compound. Since all bonds have different vibrational frequencies, and the environment of the bond might affect the vibrational frequency, comparing infrared spectra of potentially similar compounds can reveal if there are differences between them [50].

Instruments determining the absorption spectrum of a sample is named infrared spectrometers, and a Fourier transform infrared spectroscopy instrument (FT-IR) has been used in this work. The working principle in a typical FT-IR instruments is illustrated in Figure 2.16. Infrared radiation is sent to a mirror which (ideally) spreads the radiation 50/50 towards a stationary mirror and a movable mirror. The radiation is following reflected back from the two mirrors and half of each radiation/waves (ideally) will combine, and hit the sample. As one of the movable mirror change position, the combined waves will be in and out of phase, constructing an interferogram. This interferogram contains all the frequencies of the infrared spectrum. As the waves pass through the

sample and are detected, the signal will only contain the transmitted frequencies, and the absorbance by the sample may be found. The signal is detected as a plot of intensity versus time, and a Fourier transform process of the plot transforms the data to a plot of intensity versus frequency [50]. This spectrum is for convenience further displayed as a transmittance or absorbance versus wavenumber plot and is called a FT-IR spectrum. Tables of known wavenumbers corresponding to absorption by specific chemical groups may be used to interpret the FT-IR spectra.

From FT-IR analysis one detects which chemical groups that is present in a sample. Since the vibrational frequency of a bond may be influenced by the environment, interactions between compounds can be observed. For instance, Hammer *et al.* reported an interaction between carboxylic carbonyl group and Ba^{2+} by shift in wavenumber of 3 cm^{-1} of the carbonyl signal [33], and Pathak *et al.* observed a decrease in wavenumber of ~53 cm^{-1} of the carbonyl signal due to a hydrogen bond between a carboxylic carbonyl and hydroxyl group of an epoxy molecule [24]. FT-IR has also been used to show the existence of silane groups on filler surfaces after surface modification of TiO_2 particles [31].

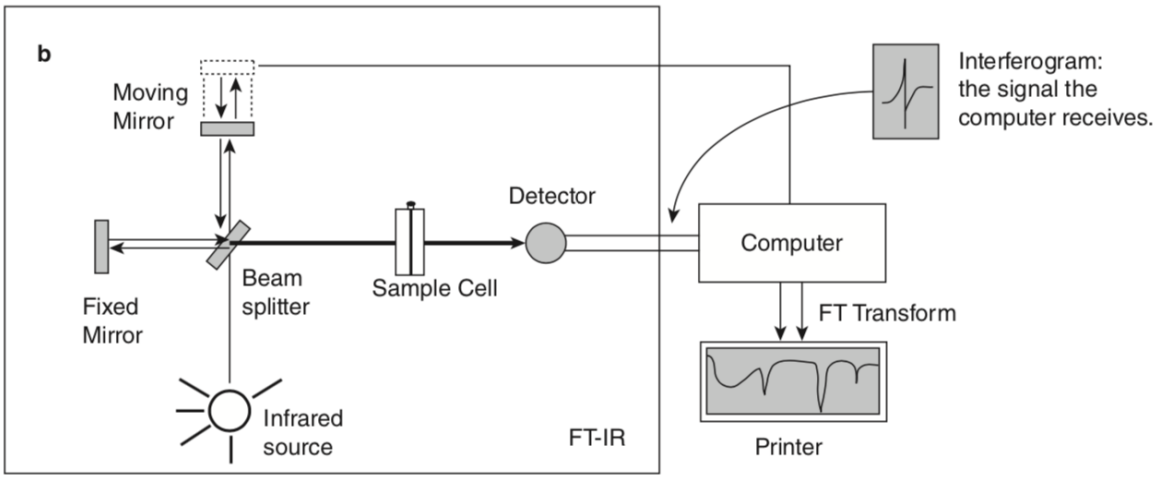

Figure 2.16: Illustration of the instrument setup of a Fourier transform infrared spectrometer [50].

2.5.4 Dynamical mechanical analysis

Dynamical mechanical analysis (DMA) is an analyzing technique used to observe mechanical properties of materials. A small oscillating force is applied to the sample as a function of time, temperature or frequency, and the materials response is measured.

When a force is applied to a material with a known geometry, with a given frequency ω, it introduces a stress (σ). A corresponding deformation can be observed for the material, often called strain (ε). For a purely elastic material, the applied stress and corresponding strain would be in phase, but for a purely viscous material, the resulting strain would be 90° out of phase compared to the applied stress [42]. Viscoelastic materials will have a phase lag, given as δ, in between 0° and 90°, as shown in Figure 2.17. The results are displayed using the complex modulus, E*, which is given in Equation 2.7, and is the ratio between the stress amplitude (σ_A) and the strain amplitude (ε_A). E* can also be written according to equations 2.8 and 2.9, where E' is the storage modulus and E'' is the loss modulus, i.e. the materials elastic and viscous response, respectively [37]. All DMA-tests are performed in the linear viscoelastic region of the samples, where the frequency of the stress and strain is equal [37]. The ratio between the elastic and viscous response is presented as tan δ, as expressed by Equation 2.10.

The storage modulus represents the stiffness of the sample, the loss modulus represents the energy dissipated during one cycle, and tan δ is a measure of the mechanical damping, or energy lost at the given test conditions [37].

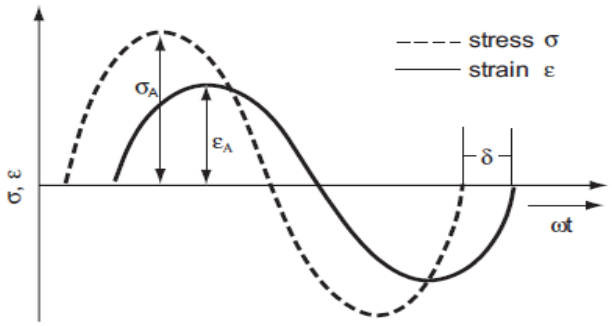

Figure 2.17: The stress and strain signals as a function of frequency/time [37].

$$|E*| = \frac{\sigma_A}{\varepsilon_A} = \sqrt{[E'(\omega)]^2 + [E''(\omega)]^2} \qquad (2.7)$$

$$E'(\omega) = |E*| \cdot \cos\delta \qquad (2.8)$$

$$E''(\omega) = |E*| \cdot \sin\delta \qquad (2.9)$$

$$\tan\delta = \frac{E''(\omega)}{E'(\omega)} \qquad (2.10)$$

Two types of DMA-measurements are normally used, deformation-controlled tests (applies a sinusoidal deformation, and the needed stress is measured) or force-controlled tests (applies a sinusoidal stress, and the deformation is measured) [37]. In the coating and composite science, DMA measurements are frequent used to give information on the effect of fillers, based on the stiffness and glass transition temperature characteristics of the samples [22,38,51].

2.5.5 Universal testing machine

A universal testing machine (UTM), also called a material testing machine, has gained the name due to the ability of performing a range of tests with the same machine. Tensile test, flexural bend test, compression test, shear test, etc. [42]. The tests conducted in this work have been the tensile test and the flexural test.

A universal testing machine is a machine which may extend or compress materials. A typical UTM is constructed of a load frame, which is two supports for the cross-head part. The cross-head is the part of which can be moved up or down, dependent on the test conducted, and is normally moved with a constant rate determined in the test setup. The load cell is an electrical device measuring the force needed to move down or up the cross-head, i.e. measuring the force applied to the sample. For measuring the elongation or deformation of a sample, a clip-on extensometer is often used (a device which measures the length of an object). The extensometer is clipped on to the sample and records the elongation/deformation of the sample. Where an extensometer is not practically possible, the elongation or deformation is measured by the distance the cross-head is moved up or down. Various sample holders are available for all the different tests possible to conduct on the UTM. The recorded data (stress/strain) is saved on a computer, and the results are normally presented as stress-strain curves.

In tensile tests, the samples normally have one dimension significantly larger than the two others, and films are often prepared as “dog bone samples” (see Section 3.9, page 46). The sample is mounted in the stationary and movable sample holder, with the long side between the two clamps, as illustrated in Figure 2.18. The tensile test basically consists of extending the sample uniaxial by applying a uniaxial tensile stress to the sample (see Figure 2.10, page 23), and recording the force needed to extend the sample at a given rate and the elongation of the sample [42]. The elongation of the sample is measured by an extensometer. The result of the test is presented as a stress-strain curve, where properties such as Young’s modulus, tensile strength and tensile toughness of the sample can be determined.

For the flexural test, also called the three-point bending test, the samples are also normally prepared to have one dimension significantly larger than the two others. The sample is placed on two holders/bars on each side of the length of the sample, and the load may be applied in the center of the two holders, as shown in Figure 2.18. The load is applied with a given speed rate and when the sample is bended between the two bars, it is exposed for compression stress on the upper side (the side in contact with the load), and tension stress on the lower side [42], as shown in Figure 2.11 (page 23). The result of the test is presented as a stress-strain curve, where properties such as bending modulus, flexural strength and flexural toughness of the sample can be determined.

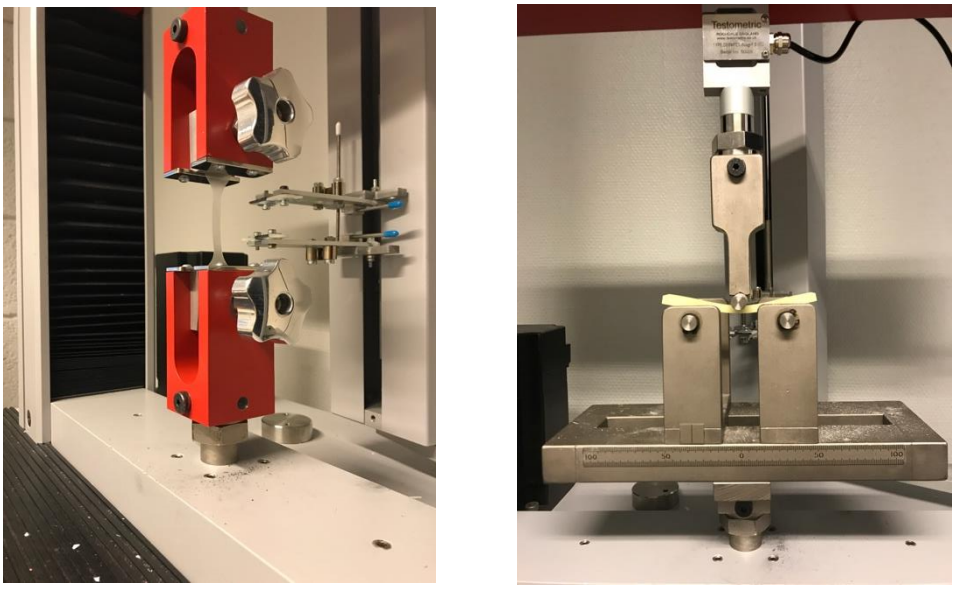

Figure 2.18: To the left, a «dog bone sample» mounted in the sample holders for tensile test, and to the right, a thicker “dog bone sample” is placed on the two bars in each side, with the crosshead pushing the sample a bit down in a flexural test.

2.5.6 Payne permeability cups

Payne permeability cups are among one of the methods used to measure the permeability of water vapor through paint films/coatings. The Payne permeability cups are based on a simple idea; a liquid (the permeate) or desiccant is placed in the permeability cup, and the sample in interest is placed on top of the cup and sealed with a sealing ring and clamps (Figure 2.19). The permeability cup is then placed in the desired test conditions, and any loss (liquid in cup) or gain (desiccant in cup) in weight after the experiment will be due to a transfer of the permeant through the sample [43]. The assembly is weighed through the time of the test, and the temperature and pressure are logged.

The water vapor permeability may be calculated from Equation 2.11 [44], where the flux is the amount of permeant which has diffused though the film at a given time, the thickness is the thickness of the film and Δpressure is the pressure difference below and above the film. The flux was found by a plot of weight loss versus time, divided by the film area. The thickness of the film was measured prior to the film by a digital caliper. The difference in pressure was calculated as given in Equation 2.12 [52], with %RH being the percentage relative humidity. The permeability value had the unit of g/m·day·Pa.

$$Permeability = \frac{flux \cdot thickness}{\Delta pressure} = \frac{\frac{amount\ of\ permeant}{film\ area\ \cdot time} \cdot thickness}{\Delta pressure} \tag{2.11}$$

$$\Delta pressure = \frac{\text{Difference in \%RH}}{100} \cdot (\text{Saturation Vapor Pressure}) \tag{2.12}$$

Figure 2.19: An Elcometer Payne permeability cup.

3 Materials and Methods

3.1 Sample composition

In order to observe how the fillers impacted the properties of the paint films, and minimize and avoid other contributing factors, a simplified paint formulation was used as sample composition in this study. The paint formulation consisted of a binding system (resin+curing agent) and filler particles.

The binding system was composed of a liquid epoxy and a curing agent. The liquid epoxy was produced from bisphenol A and epichlorohydrin and Epikote Resin 828EL from Momentive was used. The epoxy resin has been named the liquid epoxy for convenience in this work. The structure of the liquid epoxy is illustrated in Figure 2.2. The curing agent used, Noramine V15 from Jotun was a polyamine epoxy adduct in benzylalcohol, and the structure is shown in Figure 2.2. The liquid epoxy and polyamine were used in the weight mixing ratio 100:52 (epoxy:curing agent). As introduced in Section 2.3, four different fillers with unlike shape and chemistry were used in this work. Images of the fillers are shown in Figure 3.2. All raw materials were used as received from supplier without further purification, and a list of all chemicals used in this work is available in Appendix A.

The filler powder and liquid epoxy were mixed in a Speedmixer (DAC 600.1 FVZ), shown in Figure 3.1 [53], for 3-10 minutes (dependent on volume) at 1600-2000 rpm in order to obtain a well-mixed dispersion of the filler particles in the liquid epoxy. The concentration of filler in the paint formulation is presented in the next section. The speedmixer works as a dual asymmetric centrifuge by rotating the sample around the main axis in the middle of the sample chamber, and around its own vertical axis, but in the opposite direction.

Figure 3.1: The speedmixer (DAC 600.1 FVZ), used to mix the liquid epoxy resin, filler particles and curing agent [53].

If agglomeration of filler particles was observed, the liquid epoxy and filler were mixed additionally at a high speedrate (2300 rpm) until a surface temperature of the mixture up to 50°C was achieved (the solution might be heated as a result of the shear forces acting on the particles in the solution). The curing agent was mixed with the liquid epoxy (+filler) by the speedmixer, at 1600 rpm for 30 seconds to 1 minute dependent on volume. The paint mixture was then applied to a surface, within 15 minutes after mixing with the curing agent.

The samples consisting of liquid epoxy, filler particles and curing agent in their cured form have been referred to as epoxy/filler. For instance, the sample containing $BaSO_4$ particles has been named epoxy/$BaSO_4$.

3.2 Filler concentration

As described in Section 2.3.1, CPVC is an important parameter, dependent on the linseed oil absorption value. The oil absorption value can also be found for other resins and was tested with the liquid epoxy (Epikote Resin 828EL) in this work. The method and results can be found in Appendix C, and the oil absorption values from the epoxy test differed with a factor of approximately 2 from the linseed oil-abs. values, resulting in lower CPVC values if the epoxy oil-abs. values were used. Even though these changes in oil-abs. were found, the paint formulations were made based on the linseed oil-abs. values due to the fact that linseed oil absorption values are the common values usually used in the polymer/composite science.

Approximately the same percentage of the CPVC were used for all fillers in order to compare systems where the same amount of epoxy is contributing to wetting of filler particles, as explained in Section 2.3.1. Due to the different CPCV value of the fillers (see Table 3.1), a low lambda needed to be used. 10 % of the CPVC value was used, giving lambda = 0.1 (see Equation 2.3). A calculation error in the beginning of the work resulted in slightly different values for lambda, as shown in Table 3.1. The difference in lambda should not pose difficulties when comparing the samples but were kept in mind during interpretation of the results.

Two forms of aramid fibers, pulp and powder were used. The only difference between the pulp and the powder was the length of the fibers, which was ~1 mm and ~100 μm, respectively. The aramid fibers in pulp form was first used but later changed to powder form as it was difficult to obtain a well dispersed solution with the liquid epoxy resin. All results presented are for the short aramid fibers unless otherwise stated.

Table 3.1: List of PVC and weight percent values used for the filler in the epoxy paint films, together with linseed CPVC values and the lambda number.

Filler	CPVC (linseed oil) (vol.%)	PVC (vol.%)	Lambda ≈ 0.1 (PVC/CPVC)	Weight percent wt.%
Barium Sulfate	62.0	3.60	0.06	12.4
Mica	39.4	3.40	0.09	7.9
Aramid fibers	15.1	2.40	0.16	3.0
Wollastonite	59.4	5.20	0.09	11.9

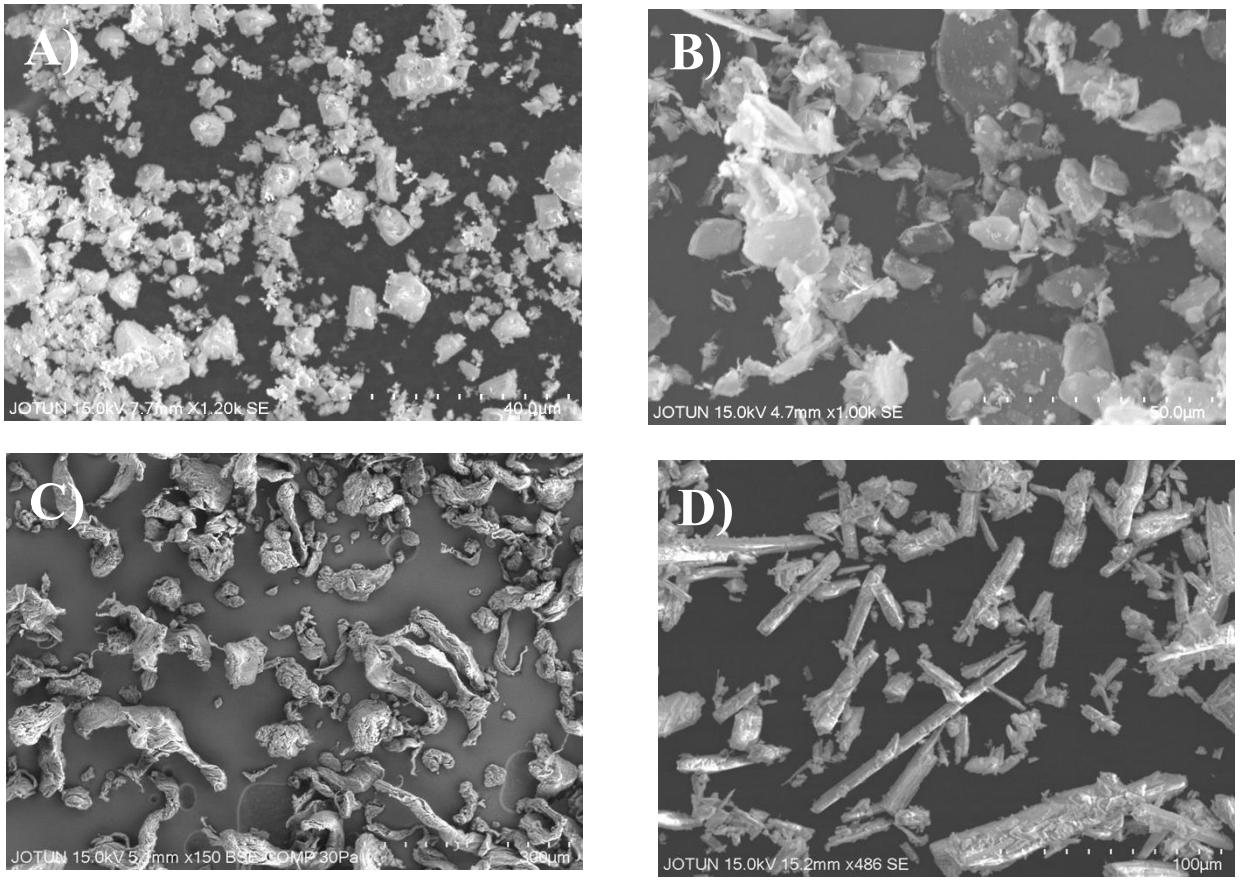

Figure 3.2: SEM images of the fillers. The filler powders were spread on carbon tape (the black background on the images). A) barium sulfate, B) mica, C) aramid fibres and D) wollastonite.

3.3 Surface modification of fillers

The surface of the fillers can be modified with various methods and/or substances. Silanes have already shown effect for all fillers investigated in this work [7,8,47,54], and were therefore also used in this work. The aramid fibers were also exposed to plasma to achieve new functional chemical groups at the surface, but due to shortcomings with the procedure and a lack of change in results compared to the unmodified aramid fibers, the plasma treatment was only briefly tested. The results are available in Appendix I. For quality comparison, a wollastonite powder pretreated with the same silane coupling agent as in this work was also tested. The pretreated wollastonite powder was delivered by The Quarzwerke Group and has been abbreviated wollastonite-fs/wolla-fs (i.e. wollastonite from supplier). The sample composition with surface modified fillers was prepared in the same way as described above for the unmodified fillers. The samples are referred to as epoxy/filler when the unmodified fillers are used and epoxy/m-filler when the surface modified fillers are used. The surface modified filler particles are referred to as m-filler, for instance, m-$BaSO_4$ for surface modified $BaSO_4$ particles.

The silane used was 3-Aminopropyl-triethoxysilane from Momentive, called Ameo, and the structure is presented in Figure 3.3. The fillers were treated with silane by a solution method [10,12,14,38] where ethanol and water were mixed in a 9:1 ratio, and the ethanol/water solution was mixed with the silane in a 5:1 ratio (ethanol/water:silane). The silane/solvent solution was added to the filler powder after 10-15 minutes, and the mixture was speed mixed at 2350 rpm until the surface of the mixture reached a temperature of 70-90^{o}C. 1 wt.% of silane was added relative to the amount of filler. For instance, if 100 grams of filler was to be modified, 1 gram of silane was mixed with 5 grams of ethanol/water (left to hydrolyse in 10-15 min) and was then added to the filler. The modified filler powder was dried at 100^{o}C ± 5^{o}C for 24 hours. The treated $BaSO_4$ powder was difficult to distribute uniformly in the liquid epoxy, and agglomeration of particles was observed and could not be avoided.

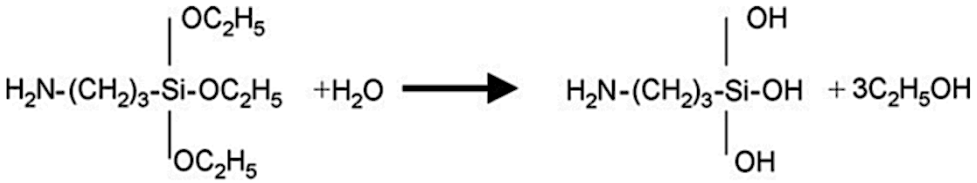

Figure 3.3: The structure of the ameo-silane used in this thesis, and the hydrolysis reaction of the silane to silanol [32].

3.4 Preparation of free films

For almost all tests done in this work, the four epoxy/filler compositions were applied to a Mylar film (Polyester film), while still in liquid state, by drawdown applicators with various openings, giving varying thicknesses of the films, as illustrated in Figure 3.4 [55]. After curing, the films could be removed from the Mylar film, resulting in free films. For physical and mechanical testing, it was important that the films were fully cured, in order to compare the films under the same conditions. A curing procedure developed by Jotun was used, which consisted of 1 day in room temperature, 5 days in 60°C and 1 day in room temperature. Details on the development of the curing and mixing procedure are given in Appendix D.

Figure 3.4: Illustration of the use of an applicator to make a paint film with a specific wet-thickness that is dependent on the applicator opening [55].

3.5 Scanning electron microscope

SEM was used to determine how the fillers spread in the epoxy-matrix, if there was any orientation tendency and for fracture analysis. The SEM used in this work was a Hitachi SU3500, often called a variable pressure-SEM. The SEM, equipment shown in Figure 3.5, had a wolfram electron source, and three detectors, i.e. a back-scattered electron detector, a secondary electron detector and a X-ray detector. Depending on the electric conductivity of the sample and the depth of interest (topography/composition), an accelerating voltage between 7-20 kV was used. The sample chamber was kept under vacuum when analyzing, or, a pressure of 10-40 Pa was kept in the sample chamber for the insulating samples. Magnification and other settings for each image obtained are shown in the image or displayed in the figure text.

For analysis of distribution and orientation of the filler particles, films of applied wet-thickness 200, 400, 600, 800, 1000 and 1200 µm were cut into smaller parts and embedded in an epoxy-matrix (same type of epoxy as in the paint films) containing electrically conductive Nickel (se Figure 3.6) to avoid charging problems during analysis in the SEM. Charging problem may cause focusing difficulties and undesired bright images. Samples of both the horizontal and the vertical cross-section of the films were prepared for analysis (horizontal/vertical direction is illustrated in Figure 3.12). The samples were polished with a Beta grinder-polisher from Buehler at 300 rpm with silicon-carbide grinding paper (P240 (52 µm), P1200 (14 µm), P4000 (5 µm)) to achieve a smooth surface for analysis. For fracture analysis, the fractured samples were molded into an epoxy-matrix, and then coated with platinum (3 nm layer with a Cressington 308R Coating system) as shown in Figure 3.6.

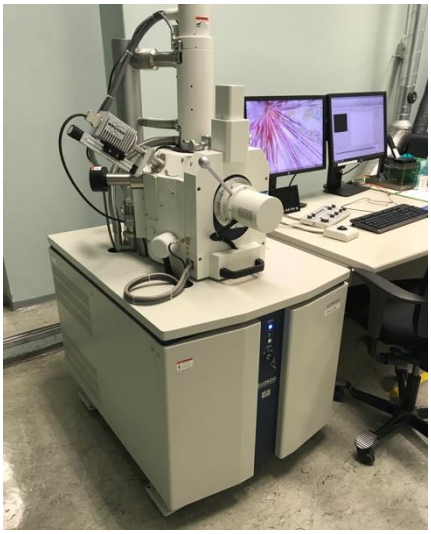

Figure 3.5: The Hitachi SU3500 used in this work.

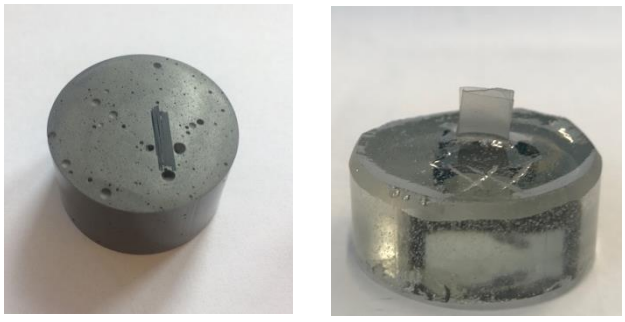

Figure 3.6: SEM-samples. To the left, six films (applied thickness 200 – 1200 µm) are embedded in an epoxy-matrix containing nickel. To the right, fracture samples points out, coated with Pt, giving it a greyish color.

3.6 X-ray photoelectron spectroscopy

A Kratos Axis Ultra DLD instrument shown in Figure 3.7 with a monochromatic Al anode (Photon energy=1486.69 eV) was used to examine the fillers in powder form (before/after surface modification) and cross-sections of the films. The XPS-instrument was operated by Spyridon Diplas (Research manager, Sustainable energy technology department, Sintef) and/or Martin F. Sunding (Research Scientist, Sustainable energy technology department, Sintef).

For all samples, both survey scans and high-resolution spectra were collected. The survey scans were collected with pass energy of 160 eV and a step size of 1.0 eV, and the high-resolution spectra were collected with pass energy of 20 eV and step size of 0.1 eV. As the samples were electrically insulating, charge neutralization was used. Charge neutralization is a process were a small amount of low energy electrons is sent continuously to the sample surface to compensate for the positive charge created due to the emission of photoelectrons during the experiment [46].

The spectra were further analyzed using a Casa XPS software. The Casa XPS software is a processing tool designed for XPS spectra and is used for e.g. peak fitting. All epoxy/(m-)filler spectra were calibrated to have the C-C peak at 284.8 eV, and the filler powder spectra were calibrated to one of the elements in the filler. The height of the peaks was normalized relative to each other when comparing, by defining a binding energy value at which all spectra had the same value at the y-axis (counts per seconds). The peaks were deconvoluted empirically, based on procedures found in literature (references given in the results and discussion) and knowledge about the expected sample composition. The peak deconvolution was especially based on the database of Beamson and Briggs [56] and articles over similar topics as the ones covered in this thesis.

XPS requires sample preparation to successfully detect the interaction between the filler and the epoxy-matrix. Samples of the fillers in powder form (unmodified and modified) and cross-sections of the film samples (epoxy/filler and epoxy/m-filler) were analyzed. The fillers were placed in a holder on the sample holder or directly to carbon tape, and a flat surface of the powders were prepared before analyzing to avoid charging and focus problems. The epoxy/filler paint films were made by applying paint with a wet thickness of 1200 μm to a Mylar-film, which was cured at room temperature (~22°C) in three weeks before further sample preparation. The free films were broken into smaller pieces by hand to avoid contamination from any cutting equipment in the cross-section area. The dry film thickness varied from 690-700 μm for the paint films. For the paint film with aramid fiber as filler, the film pieces were glued together by a mix of the liquid epoxy and curing

agent used in the film, see Figure 3.9. This mix was used in order to avoid use of glue that could influence the results. For the epoxy/m-filler paint film cross-sections, the fracture surfaces from flexural testing were analyzed. The epoxy/m-filler samples were cured with one day at bench and five days in 60°C, in addition to one day bench procedure. They were considered to be fully cured when analyzed.

Figure 3.7: The Kratos Axis Ultra DLD used in this work.

Figure 3.8: Samples for XPS analysis attached to the sample holder. From the left: Aramid pulp, paint film with aramid (two paint films glued together with epoxy), paint film with wollastonite, paint film with mica, paint film with barium sulphate, reference paint film, mica powder, wollastonite powder and barium sulfate.

3.7 Fourier transform infrared spectroscopy

A PerkinElmer Spectrum 100 - Fourier transform infrared spectrometer (Figure 3.9) with a reflectance accessory (Quest from Specac, Figure 3.9) was used for the measurements. Since a reflectance accessory was used, the samples were placed on top of a crystal, and sample preparation was hardly necessary.

The crystal was washed with ethanol prior to and in between each experiment, and a preview spectrum was collected prior to the background spectrum to assure that there was no contamination on the crystal. When the crystal was clean, the background was collected, and the baseline was checked to be in between 99-100 % Transmittance. The sample was placed on top of the crystal, and the spectrum was collected using 12 scans in the wavenumber region from 4000 to 400 cm^{-1}, and a resolution of 4 cm^{-1}. All samples were tested three times in room temperature.

For the FT-IR analysis, spectra were collected for the liquid epoxy, the (un)modified fillers, and liquid epoxy/(m-)filler mixtures. For the fillers, 1 g of powder was dissolved/mixed in 2-3 mL ethanol and drop of the mixture was placed on top of the crystal. The ethanol was evaporated before the measurement was started. The liquid epoxy/(m-)filler formulations were mixed with a speedmixer, and a drop of the epoxy/(m-)filler mix was deposited directly on the crystal. The epoxy/(m-)filler spectra were normalized to have 0.3 in absorbance at the $–CH_3$ peak at ~2966 cm^{-1}, and the baseline was set to be zero for all spectra at 3990 cm^{-1}. For the investigation of the surface modification of the filler powders, the normalization was normally done using the most intensive in the filler spectra.

Figure 3.9: To the left, the PerkinElmer Spectrum 100 - Fourier-Transform infrared spectrometer used in this work. To the right, the reflectance accessory (Quest) used for the samples is shown.

3.8 Dynamical mechanical analysis

A Q800 DMA instrument, shown in Figure 3.10, from TA instruments was used for all samples. The load can be applied to a sample in several ways in the instrument, e.g. tensile mode, compression mode or three-point bending mode. Tensile mode, illustrated in Figure 3.11, were used on all samples in this study. In tensile mode, the sample is placed between a fixed clamp and a movable clamp, allowing for sinusoidal deformation of the sample, and an applied tension stress.

To find the linear viscoelastic region for the neat epoxy-matrix, a force-controlled test that applies a sinusoidal stress and measures the deformation/strain was performed on an epoxy reference sample. The stress-strain curve (see Figure H.1 in Appendix H) showed that an amplitude of 5 μm could be used as the oscillating strain. As all the samples consisted of the same epoxy-matrix, the same amplitude was used for all samples. Deformation controlled experiments, where a sinusoidal deformation is applied to the sample and the stress is measured, were performed on all samples as a function of temperature. A number of tests were conducted in the temperature range -80°C to 200°C, but this temperature range was reduced to -50°C to 200°C since no characteristic material transitions were observed in the low temperature region. The frequency of the sinusoidal deformation was set to 1 Hz, and 5°C /min was chosen as heating rate. Heating rate at 2°C /min was also tested on a sample in order to see if the behavior of the sample was dependent on the heating rate (available in Appendix H).

The free films were obtained from application on a Mylar film as described above and had a wet thickness of 600 μm (200 μm < dry film thickness < 450 μm for all samples). The curing conditions (time, temperature) for the paint films are crucial for the curing process and the mechanical properties and modulus curves were therefore collected as simultaneously as possible. The samples were prepared by cutting out a rectangular piece of the paint film with a length and width of ~20 mm and ~0.5 mm, respectively. The samples were cut from the film after the whole curing process were finished, which may have led to small cracks, giving slightly different results in each repetition. If the samples had clear irregularities, fine sand paper was used to adjust the sides, to make the geometry as correct as possible. The exact width and thickness of the samples were measured by a digital caliper after the sample preparation was finished. The length was measured by the instrument as the distance between the two clamps the sample were placed between.

To investigate if there were direction dependent properties due to orientation of the filler particles, the films were cut both horizontally and vertically, as illustrated in Figure 3.12. Reference films of neat epoxy were also tested. The curing process ultimately used was not fully developed when these tests were conducted. The tested films were cured in room temperature in 2.5 – 3 weeks and were therefore not fully cured.

Figure 3.10: The Q800 dynamical mechanical analysis instrument used in this work.

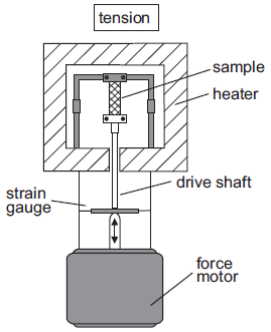

Figure 3.11: Illustration of tensile mode for deformation [37].

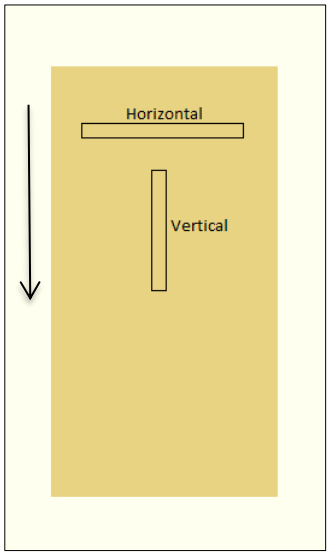

Figure 3.12: Illustration of a horizontal and vertical cut of a film (light brown) applied to a Mylar film (light yellow). The arrow illustrates the application direction.

3.9 Universal testing machine

A M500-25CT Universal testing machine (UTM) from Testometric was used for test of mechanical properties and is displayed in Figure 3.13 [57]. Tensile and flexural tests were conducted using the UTM. Both types of test were performed at room temperature. Minimum ten samples were tested using the tensile test and minimum eight samples were tested using the flexural test for each epoxy/filler composition. The geometry for each individual sample was measured by a digital caliper prior to the test. The thickness and width of the middle (thin) part of the dog bone samples (see Figure 3.13) were measured.

In the tensile test, a thin film (dry film thickness~100 -200 μm) was stretched until it broke and the force needed to stretch the film and the elongation of the film were measured. The film was stretched at a rate of 1 mm/min and was preloaded with a force of 1 Newton in order to stretch the film in the beginning of the test. The elongation/strain was measured by an extensometer (see page 32). The free films were made by application on a Mylar film as described in Section 3.4, and the "dog bone" samples (see Figure 3.13) were cut the first day in the curing process by a so called "Dog bone cutter". In the flexural test (three-point bending test), the sample was placed on two bars in each end of the sample. The crosshead which bends the sample during the experiment was placed above the sample in a start position. The samples were preloaded with a force of 1 Newton prior to the test and then pushed down by a rate of 2 mm/min. The crosshead pushed down and bended the sample until it broke. For the flexural tests, 6 mm thick samples were made by pouring paint into sample molds, which were left to cure for one day at the bench. They were then taken out of the mold and the curing procedure was continued. The samples were polished with a grinding machine, a drum sander. In the drum sander, the samples were placed on an abrasive belt and moved under a moving grinding belt which polished the surface of the samples. By moving the samples through the drum sander, the samples obtained the same thickness.

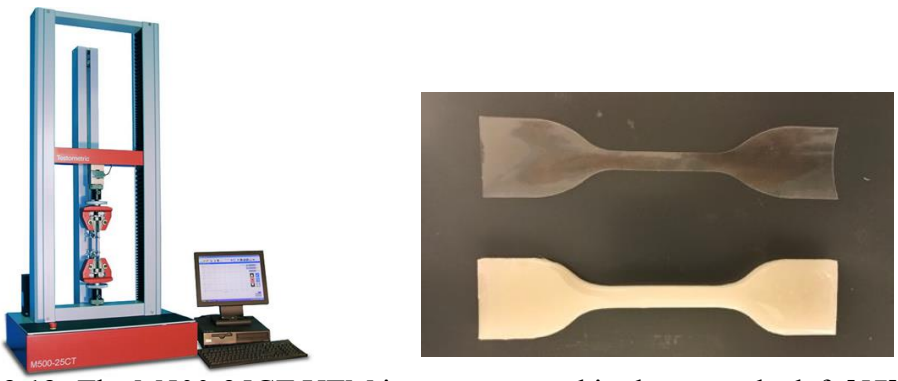

Figure 3.13: The M500-25CT UTM instrument used is shown to the left [57], and samples for tensile and flexural testing are displayed to the right.

3.10 Payne permeability cups

The water vapor permeability of the films were measured using Elcometer 5100 Payne permeability cups (Figure 3.15) at 40°C. The films used in the tests were thin, and both the dry film thickness and the weight of the films were measured before the test. A temperature of 40°C was chosen since it was below the T_g of the paint films, somewhat higher than room temperature, and represents a reasonable temperature that paint/coatings may experience in its applications.

Films of thickness 100-200 μm (from application to Mylar film) were prepared, and samples fitting the Payne permeability cup were cut the first day in the curing process (one day in room temperature) to avoid cracks. 10.0 gram of distilled water was added to the Payne permeability cup before the film sample was placed between the cup and the sealing ring/ rubber gasket. The clamps were fastened tightly. The assembly was weighed using a precision of 0.001 g before the test started. The permeability cups were kept in an oven at 40°C and weighed 1- 4 times (or more) until a linear behavior in the mass loss versus time graph was observed (normally within 48 h). The weighing during the test were performed on a 0.01 digits precision weight, and may not have given precise results, but the assembly was weighed on a weight with 0.001 digits after the test was finished.

In order to calculate the permeability of the samples, the relative humidity in both the Payne permeability cup and in the oven needed to be logged. The relative humidity in the test cup was considered to be ~100 vapor % humidity since the evaporation of water occurs in this limited space. The pressure/relative humidity in the oven was logged by a TQC HM9000 Data Logger (small temperature and humidity logging USB device placed in the oven during the experiments) under each experiment. The average relative humidity during the test-time was used in the calculations described in Section 2.5.6.

Figure 3.14: A paint film placed in the Payne permeability cup.

4 Results and discussion

The results obtained for the epoxy/filler samples and the discussion of these results are first presented. The epoxy-filler interaction, distribution and orientation of the filler particles and the physical and mechanical properties are discussed in detail. The effects of surface modification are presented in Section 4.5. Since physical and mechanical properties of the epoxy/filler films were easily influenced by changes in polymer matrix, temperature, time and impurities/deformations, all measurements were conducted with several repetitions and are presented with a standard deviation of the results. The method used for standard deviation is given in Appendix A.

4.1 Chemical composition and epoxy/filler interactions

The chemical composition of the epoxy/filler films were investigated using X-ray photoelectron spectroscopy (XPS) and Fourier transform infrared spectroscopy (FT-IR). These techniques yield information on the chemistry of the samples, on the basis of the binding energy and vibrational modes of the elements/chemical groups in the samples, respectively.

XPS is a surface sensitive technique, where the results relate to the first 0-10 nm from the surface of the sample. Bolouri *et al*. showed the existence of chemical bonds between an epoxy resin and an aluminum surface using XPS by observation of a reduction of the number of hydroxyl groups due to a reaction between epoxy-hydroxyl groups and aluminum surface hydroxyl groups. A new signal from amine groups hydrogen bonded with the surface also appeared [49]. These kinds of observations were kept in focus through the interpretation of the results in this work.

To investigate the bulk epoxy/filler composition, the cross-section of the films was analyzed. For all epoxy/filler films tested, signals from the filler particles were observed, showing that the area investigated contained both filler particles and epoxy-matrix. The survey spectra of the epoxy/filler films are found in Appendix E.

Deconvolution of the peaks in the high-resolution spectra were performed in order to find the chemical states of the element contributing to the peaks. Difference in width and shape of the peaks originating from the same element in different samples indicated if different chemical groups contributed to the peaks. The epoxy/filler samples examined using XPS were cured in room temperature for 3.5 weeks, and DMA-results (see Appendix D) from films cured under those curing

conditions revealed that the films were not fully cured. The interpretation of the epoxy/filler XPS results was therefore based on the chemical shifts in the high-resolution spectra and comparing the chemical state of the filler in the epoxy film versus the chemical state of the filler in powder form. Since the films were not fully cured, it was difficult to compare the results in more detail as for instance comparing quantification of specific chemical bonds like C-C, C-OH and C-O-C.

The epoxy matrix consisted of carbon, nitrogen and oxygen, and a comparison of chemical shifts inside these peaks were thought to give an indication of a possible interaction between the epoxy matrix and the filler particles. The chemical shifts in the C1s peak, see figures 4.1 and 4.2, were used to investigate possible filler/epoxy interactions since the carbon signal only originated from the epoxy-matrix. It is relatively simple to make a peak fit of the C1s peak as the chemical states (C-C, C-OH, etc.) appears at binding energies distinct from each other.

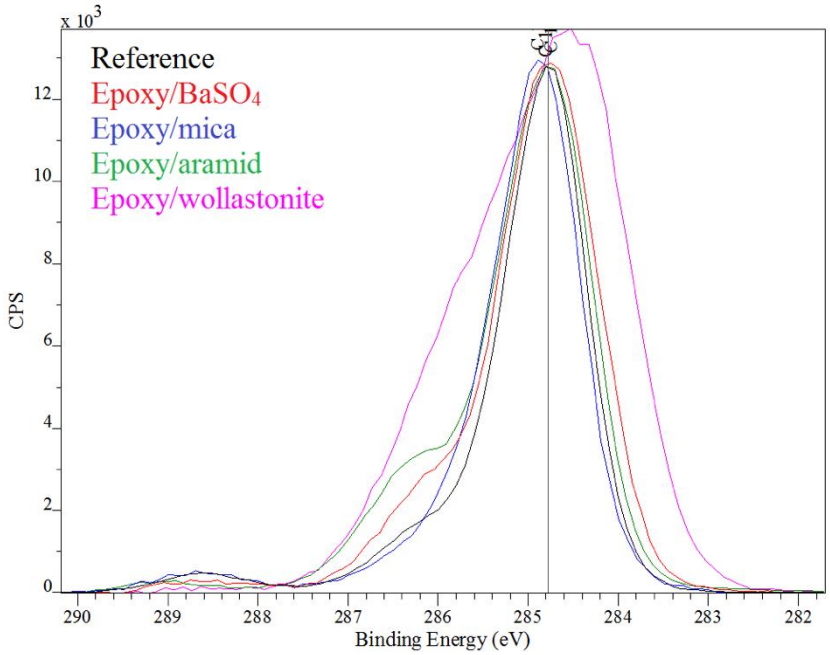

Figure 4.1: High-resolution C1s spectra of the epoxy/filler samples. The spectra are normalized at the value given by the vertical line.

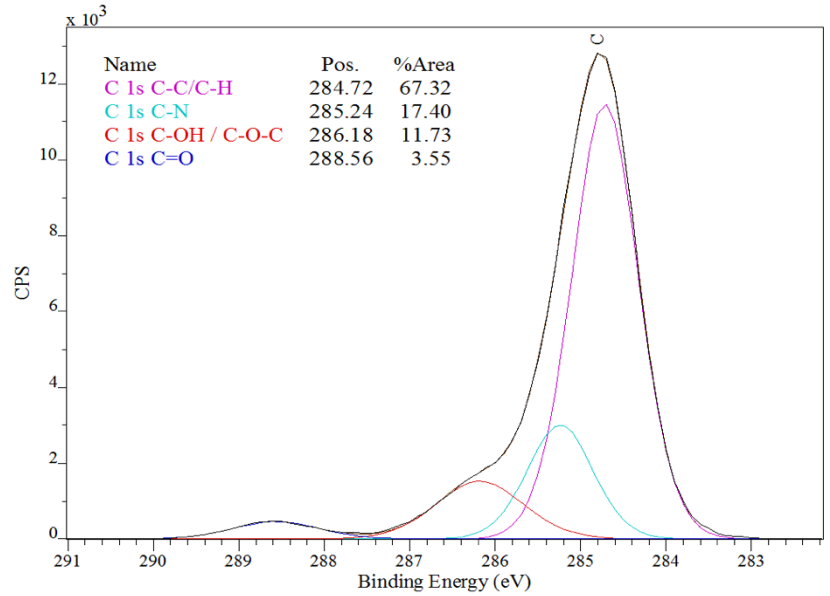

Figure 4.2: High-resolution C1s spectra for the reference neat epoxy sample. A curve fitting procedure has been applied to the spectrum as described in Section 3.6.

The O1s peak will have contributions from the oxygen in the filler particles as well and is rather complicated to make a peak fit for since the binding energies of the various chemical states (C-O, C=O, Si-O, etc.) tend to overlap. After surface modification, and in all cases for the epoxy/aramid samples, the C1s peak contained signals from the filler particles. This circumstance complicated the interpretation. The N1s signal was weak and overlapped with each other for all samples. The C1s spectra for all epoxy/filler films are shown in Figure 4.1, and the O1s and N1s spectra are displayed in Appendix E. In Figure 4.2, the peak fitted C1s spectrum for the neat epoxy sample is shown to illustrate where the various binding state signals were located.

The shoulders on the left side of the peaks indicate a higher number of C-OH and C-O-C (ether and/or epoxide) groups in the epoxy/aramid and epoxy/$BaSO_4$ samples compared to the reference film and epoxy/mica film but will not be further discussed due to the films not being fully cured. The epoxy/wollastonite peak was broad, making it difficult to compare it to the other peaks. Broad peaks are observed if charging occurs during the experiment, which is likely to have been the case for the epoxy/wollastonite sample [46].

The position of the peaks in a XPS spectrum is dependent on the binding energy of the electrons and the local chemical and physical environment of the electrons. A change in the position of a peak is called a chemical shift (see Section 2.5.2, page 28). The chemical shifts found for the C1s peaks is presented in Table 4.1 together with the literature values of the chemical shifts investigated, from the XPS polymer database of Beamson and Briggs [56]. The database made by Beamson and Briggs is a collection of peak fitted XPS-spectra for various polymers, thereby providing a minimum and maximum binding energy normal to observe for the different chemical bonds, dependent on the various polymer systems. The C-C/C-H peak was set to be at 0 eV, and the change in energy to the next peak within the C1s signal was reported as the chemical shift. There was no clear trend with a change in the chemical shifts between the neat epoxy film and epoxy/filler films, and all shift values observed were between the minimum and maximum values previously observed for these binding-states.

Table 4.1: Chemical shifts tabulated in units of eV, observed in the high-resolution C1s spectra of the epoxy/filler samples.

Chemical bond	Reference (eV)	Epoxy/ $BaSO_4$ (eV)	Epoxy/ mica (eV)	Epoxy/ aramid (eV)	Epoxy/ wollast. (eV)	Chemical shift from Beamson and Briggs [56]
C-C / C-H	0	0	0	0	0	0
C-N	0.5	0.47	0.44	0.53	0.69	0.56 – 1.41
C-OH / C-O-C	1.5	1.48	1.19	1.57	1.52	1.13-1.75
C=O/ C-O-C*=O	3.9	3.96	3.85	4.32	-	2.81-2.97/3.64-4.23

A comparison of the chemical state of the filler elements in unmodified/modified form and when incorporated in the epoxy film can also give an indication if there is an interaction. Xu *et al.* reported a chemical bond between a silane modification agent and TiO_2 particles by a shift of the Ti2p peak of 0.2 eV together with a new signal due to protonated amine groups [31].

Figure 4.3 shows the barium (Ba3d) and sulphur (S2p) peaks for the unmodified $BaSO_4$ powder (blue spectra) and the epoxy/$BaSO_4$ sample (black spectra). The signals mainly overlapped, and the overlapping spectra means that the chemical state of the filler particles were not affected by the epoxy matrix. The noisy signal from the epoxy/$BaSO_4$ sample was due to a low amount of $BaSO_4$ particles in the sample surface.

The chemical state of the elements in mica, aramid and wollastonite did not show an indication of being changed when incorporated in the epoxy matrix. The high-resolution XPS spectra of the elements (Al 2p, Si 2p for mica, Ca 2p and Si 2p for wollastonite and C1s, N1s and O1s for aramid) in powder form overlapped with the spectra from the same elements from the epoxy/filler samples. The spectra illustrating this overlapping are displayed in figures E.6 and E.8 in Appendix E.

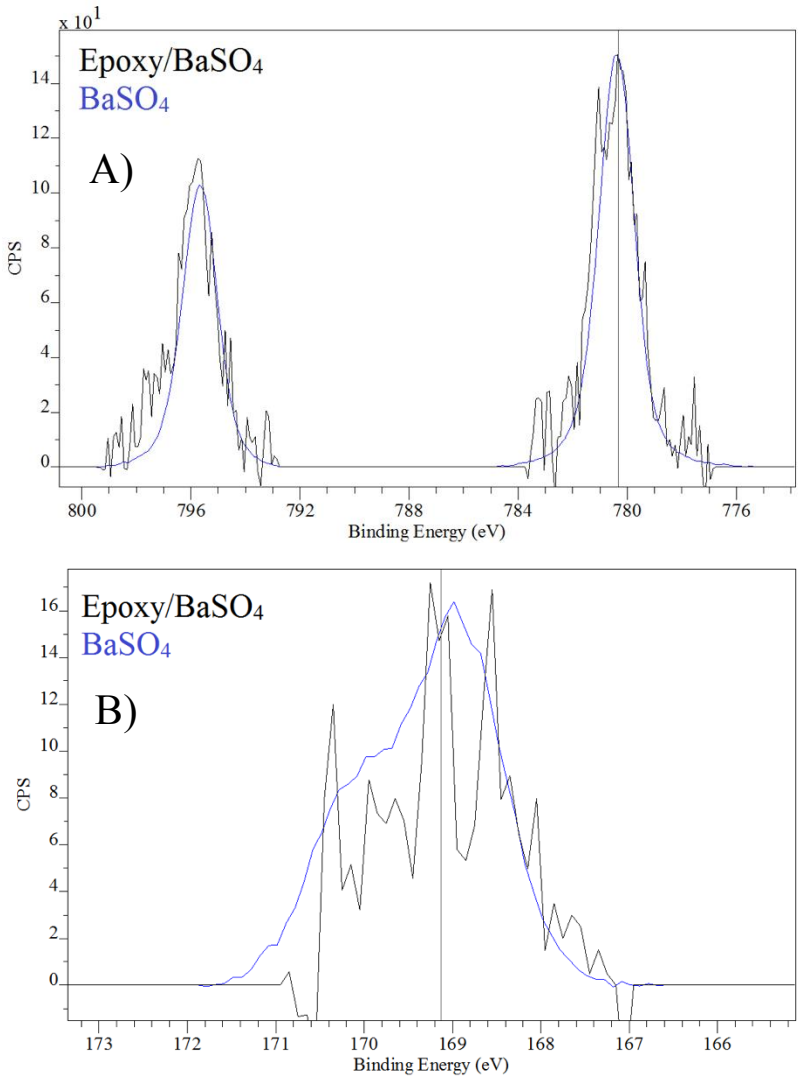

Figure 4.3: High-resolution spectrum of barium (A) and sulphur (B). The black signal was obtained from the epoxy/$BaSO_4$ sample, and the blue signal was obtained from the unmodified $BaSO_4$ powder. The vertical black line is the value at which the normalization was performed.

In Figure 4.4, the high-resolution spectra of carbon of the aramid pulp (unmodified filler) and a part of the high-resolution spectra of all the epoxy/filler samples are presented. The signal at high binding energy in the carbon peak is presented for the epoxy/filler samples in Figure 4.4. B). Since the aramid structure has C-C, C-N and C=O carbon-bonds, the appearance of these signals was as expected. The C=O peak is a characteristic small peak to the left for the main C1s peak at ~288 eV [27,48]. The peak at 288.6 eV for the reference and some of the epoxy/filler samples (see Figure 4.1 and Table 4.1) is shown in Figure 4.4 and can be explained by the presence of an ester group according to Beamson and Briggs [56]. The C=O/ester peak was not expected to be found in the spectra of the epoxy/filler samples. Carbonyl and ester groups have been observed in photodegradation of epoxy surfaces earlier [58,59], and the ester signal observed in this work have therefore been believed to be caused by an oxidation process of the surface [3].

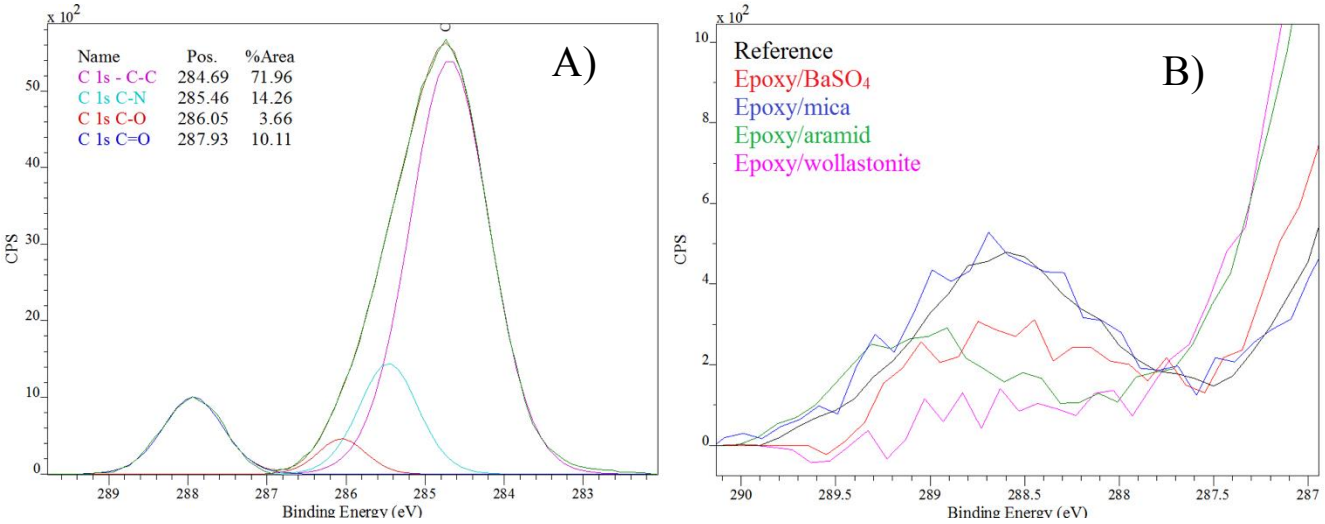

Figure 4.4: High-resolution C1s XPS spectra of the A) aramid fibers and B) all epoxy/filler films, zoomed in to show the C=O peak.

The FT-IR results revealed what molecular groups that were present in the samples and were used to investigate any possible interaction between the fillers and the liquid epoxy.

A clear difference in intensity or peak position in the liquid epoxy/filler spectra indicated if the chemical and/or physical surroundings were changed for the molecular groups as compared to the situation in the neat liquid epoxy. For instance, Hammer *et al.* have shown an interaction between Ba^{2+} (in $BaSO_4$) and carboxyl carbonyl groups in polymer blends by a shift in wavenumber (vibrational frequency) of the carboxyl carbonyl signal by 3 cm^{-1} in a FT-IR spectrum of a polymer/$BaSO_4$ blend [33].

Three spectra were collected for all samples in order to assure quality of the results. A liquid epoxy/filler mixture was tested without any curing agent present, since the -OH peak from the epoxy and the -NH group from the curing agent could overlap and complicate the interpretation. The results could therefore only show a possible interaction between the liquid epoxy and the filler.

Figure 4.5 displays the spectra for the neat liquid epoxy and liquid epoxy/filler mixtures. The liquid epoxy and filler powder were mixed with lambda=0.1 (see Section 3.2, page 36) for the fillers in the mixture. A clear change in peak position or intensity for the chemical groups were not observed for any of the mixtures, and the difference in signal visible in the 1300-400 cm^{-1} was due to signal from the filler powders. All filler powders had absorbance in the wavenumber region of ~1500-400 cm^{-1}, and presence of the filler powders in the liquid

epoxy/filler mixtures therefore increased the signal in this region. Very small changes (±0.5 cm^{-1}) in the position of the ether peaks (C_{phenyl}-O and $C_{aliphatic}$-O) were observed in the liquid epoxy/mica and liquid epoxy/$BaSO_4$ mixtures. These small changes were not large enough to verify a clear interaction [24,60], and smaller than the resolution of the spectra (4 cm^{-1}). The spectra showing the small differences are available in figures F.10-F.11 in Appendix F.

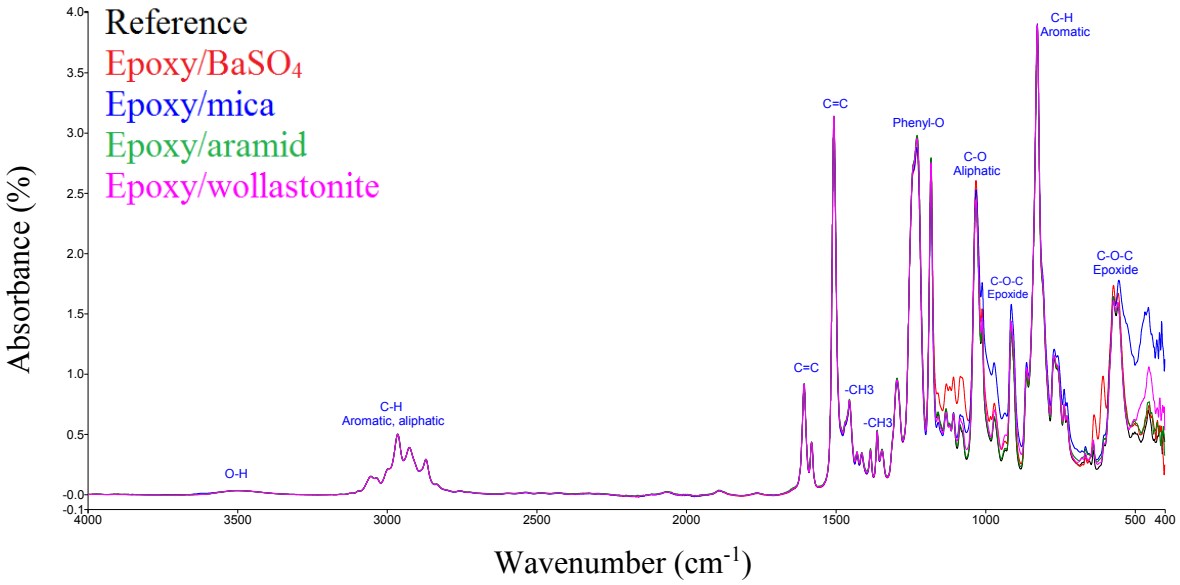

Figure 4.5: FT-IR spectra for liquid epoxy-filler mixtures, obtained with a resolution of 4 cm^{-1} and 12 scans at room temperature.

4.1.1 Characterization of the surface of the fillers

The surfaces of all filler powders were analyzed using XPS to investigate what chemical groups were present on the surface of the fillers. The purity of the fillers was also determined in this analysis. For the surface modified fillers, the XPS results might reveal to what extent the surface modification was successful, and the results are discussed in Section 4.5.1. The surface chemistry of the fillers was not studied in detail since this would be beyond the scope of this thesis. An overview of possible contamination or clear changes in chemical composition are discussed below.

It is difficult to make a good peak fit the high-resolution O1s spectra since they included oxygen signals from the filler and contamination species, and the various signals often overlaps. The survey spectra of all filler powders are displayed in Figure 4.6.

The theoretical bulk percentage atomic concentration (at.%) of each element in the fillers were compared to the percentage atomic concentration of the elements in the surface of the filler powders, and the results are presented in tables E.1 – E.4 in Appendix E.

The aramid fibers gave signals from all the expected chemical groups, and the elemental composition of the aramid fibers from the XPS survey spectrum gave atomic percentages with 11, 11 and 78 at.% for nitrogen, oxygen and carbon, respectively. This result was expected based on the chemical structure of the fibers.

Even though the composition of the aramid fibers were found as theoretically expected, the high-resolution C1s and O1s spectra showed signal from both single- and double-bond oxygen atoms (see C1s spectrum in Figure 4.7 and O1s spectrum in Figure E.10 in Appendix E). This indicates that there were single bond oxygen groups on the surface of the aramid fibers [27,48]. The theoretical aramid structure only has one type of bond involving oxygen, i.e. the C=O bond, and the single bonded oxygen has been believed to be caused by contamination species, or resonance between the C=O and C-N-H, and C-O-H and C=N bonds in the aramid structure.

$BaSO_4$, mica and wollastonite had a lower at.% of oxygen than theoretical expected (see tables E.1, E.2 and E.4, Appendix E). Oxygen is likely to have been replaced/covered by the carbon detected in the surface [61]. Despite these carbon impurities, the $BaSO_4$ and mica powders showed high purity [61,62], respectively. The wollastonite powder also showed

signal from carbon impurities, but as seen in Figure 4.7, the C1s spectrum of wollastonite showed an additional peak at 289.4 eV. Wollastonite surfaces react may with CO_2, resulting in $CaCO_3$ groups in the surface [63]. The additional peak at 289.4 eV is likely to be due to these $CaCO_3$ groups.

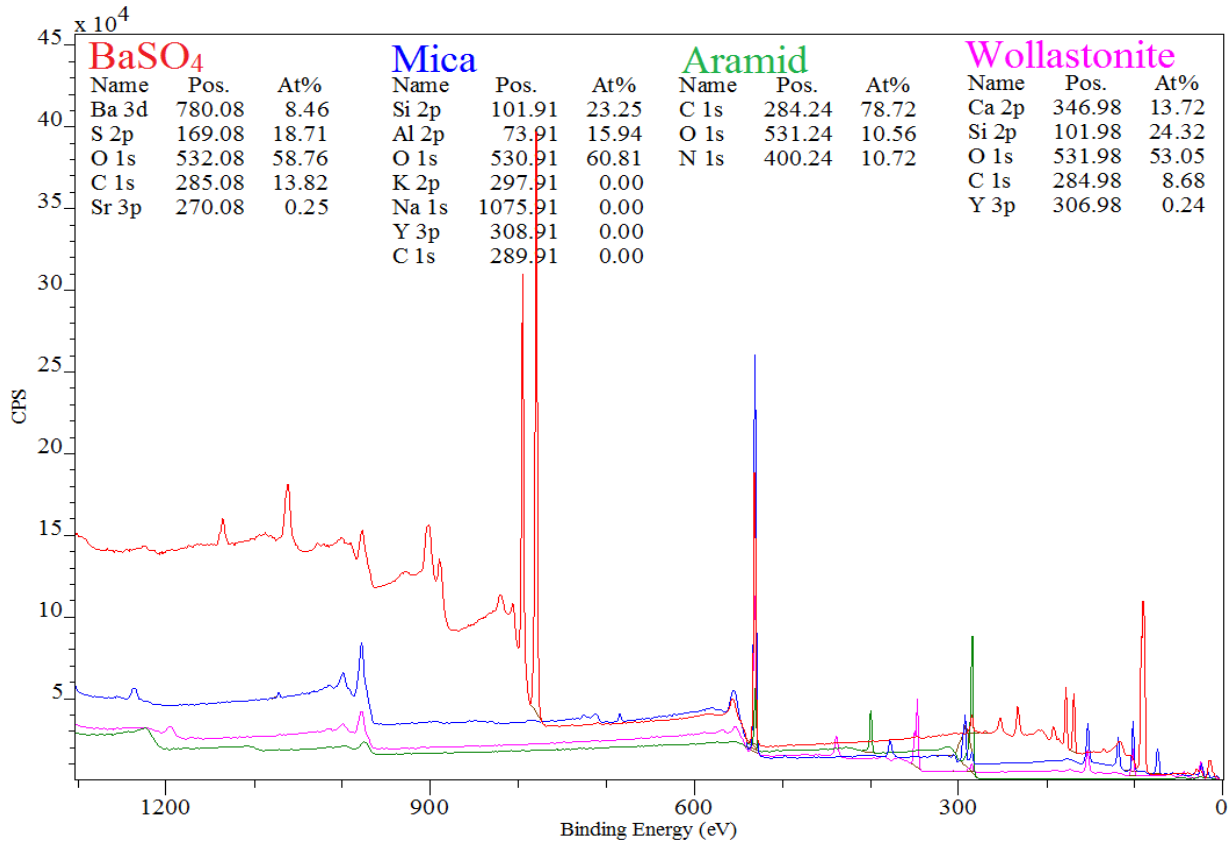

Figure 4.6: XPS survey spectra of the filler powders; $BaSO_4$ with red spectra, mica with blue spectra, aramid with green spectra and wollastonite with pink spectra.

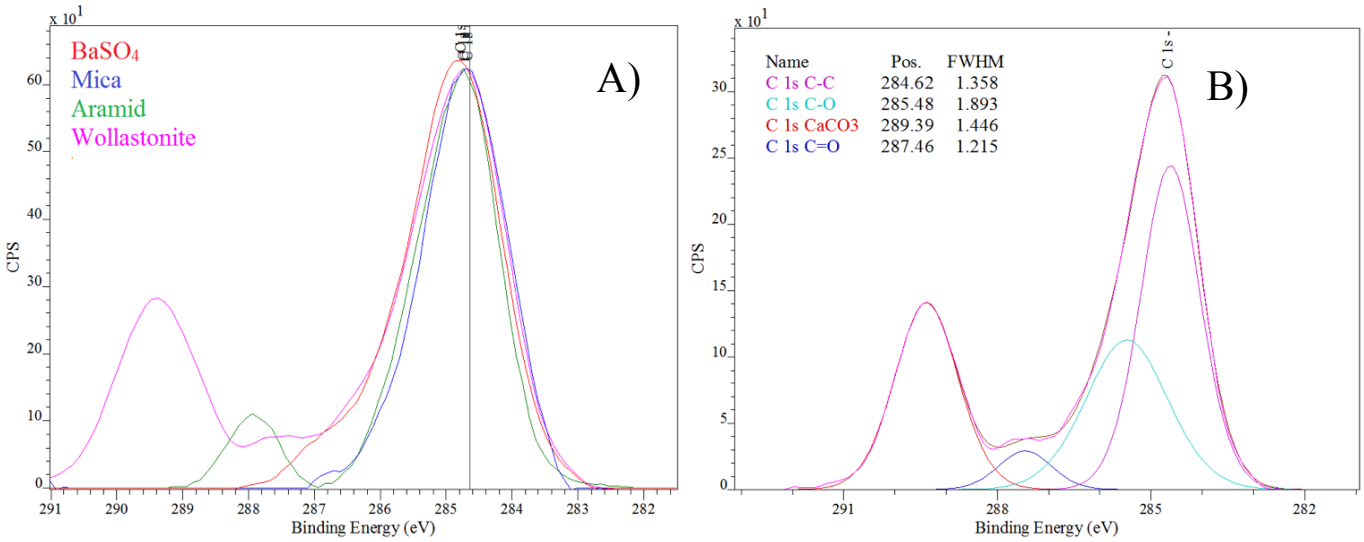

Figure 4.7: High-resolution XPS C1s spectra of A) all filler powders and B) of the wollastonite powder, peak fitted.

4.1.2 Distribution of the filler particles

In order for the filler particles to positively influence the overall properties of the epoxy-matrix, it is important that the filler particles are well distributed, as e.g. agglomeration can give an inhibitory effect [4,38].

Agglomerates may contain voids and air, which lower the modulus since the modulus of air/voids can be considered to be zero [4,14]. On the other hand, hard agglomerates without any voids or air trapped in between the particles could result in a higher modulus compared to a sample without agglomerates [4]. Zhuang *et al*. observed a decrease in tensile and flexural strength at higher filler loadings (above 30 vol.%) due to agglomerates in phenolphthalein polyetherketone/wollastonite composites [26]. The agglomerates were considered to be the initiation of the fracture and lower the interfacial area between the filler particles and the polymer matrix. Xian *et al.* also observed decrease in flexural stress and strain at break due to agglomeration in epoxy/wollastonite composites at filler loadings above 10 vol.% of wollastonite particles [7].

The explanation behind the decrease in strength and elongation due to agglomerates may be explained by an agglomerate being a large obstacle for the polymer matrix during elongation compared to single filler particles uniformly distributed. The polymer matrix may not be able to stretch around the agglomerate, and the polymer/filler sample will fracture where the agglomerate is present, or, voids will be created.

The particle distribution was investigated using SEM. All fillers particles were well distributed in the paint films (however, see note about aramid fibers below), independent of the paint film thickness. Images of a selection of the films for all fillers are shown in Figure 4.8, illustrating the distribution. The light spots are the filler particles and the grey background is the epoxy-matrix. The aramid fibers in the epoxy/aramid films showed a tendency to be bent. A significant number of air bubbles was also observed in the epoxy/aramid films, see left side on image in Figure 4.8 C, and Figure 4.13 A), which may have been present due to air trapped in the bent fibers during the film formation/sample preparation.

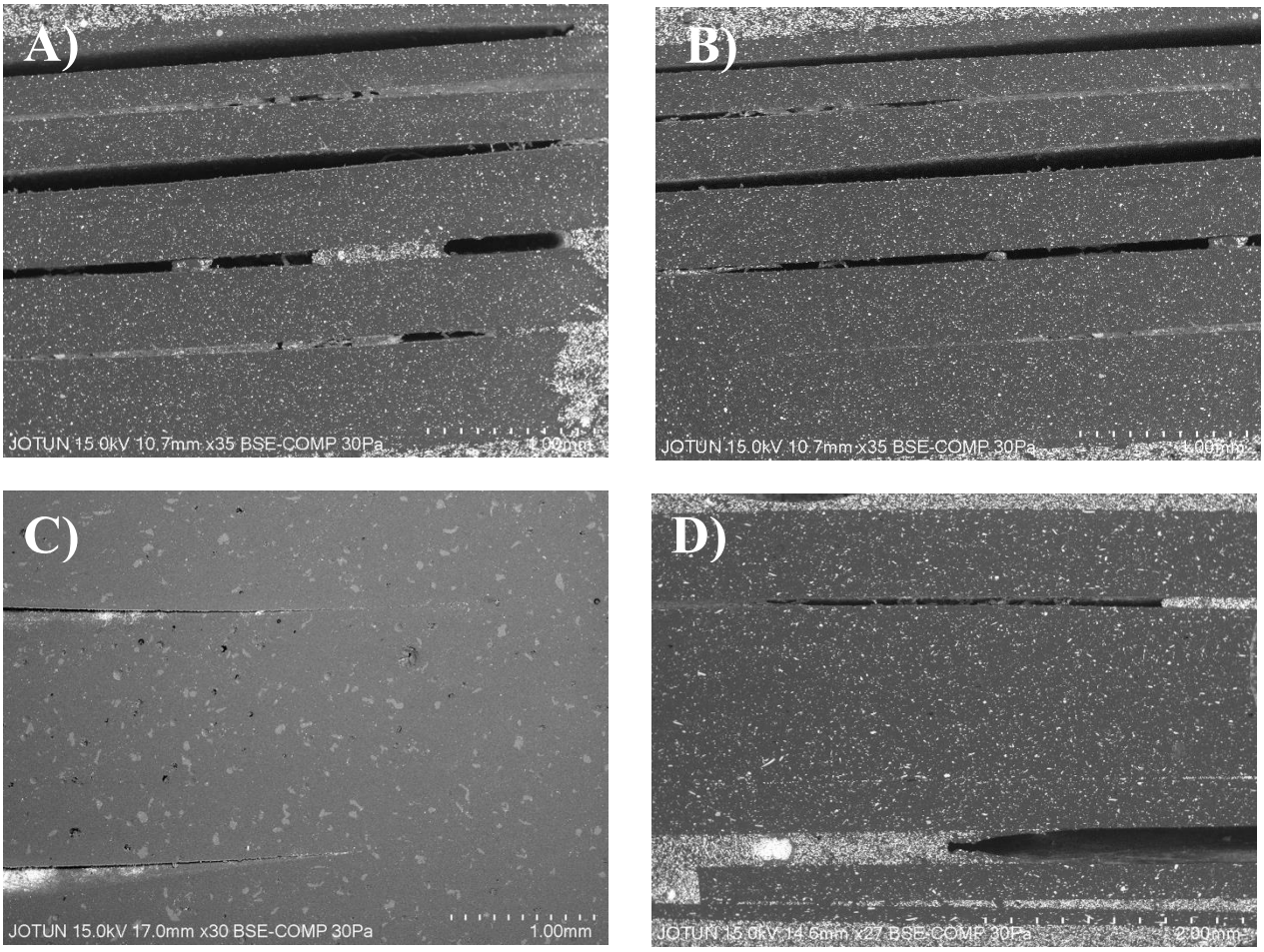

Figure 4.8: Image of the horizontal or vertical cross-section of films with various thickness. A) barium sulfate, vertical, B) mica, horizontal, C) aramid fiber, horizontal, D) wollastonite, vertical. All images were obtained using SEM.

4.1.3 Orientation of the filler particles

The orientation of the filler particles was investigated as it may influence the chemical and physical properties of paint films. Possible preferential orientation of the filler particles was examined by observing the horizontal and vertical cross-sections of the paint films with thickness ranging from 200 to 1200 μm using SEM (horizontal and vertical directions are illustrated in Figure 3.12 in Section 3.8). All films in this work were made by drawdown applicators as illustrated in Figure 3.4, and it is important to note that the results are only valid for this film preparation method, and not e.g. spraying. Images of the horizontal and vertical cross-section of one film thickness are shown in Figure 4.10 - 4.13 for all epoxy/filler films, and the direction of the cross-section is given above the images. The barium sulfate particles were nodular/blocks, as shown in Figure 3.2A), page 37, and did not show any special orientation. However, the mica, aramid and wollastonite particles had a high aspect ratio and were plate-like, fibrous and needle-like, respectively. An orientation tendency was seen if there was a significant number of filler particles aligned in a specific direction in the horizontal and vertical cross-section of the film. Random areas in the cross-section of the films were chosen, and the number of particles with a clear horizontal/"laying" or vertical/"standing" orientation was counted. Particles with a slanted orientation were not counted. Minimum two areas in all film thicknesses were examined. The ratio of horizontally versus vertically aligned particles of all film thicknesses are displayed in Table G.1 in Appendix G, and the average ratios of all thicknesses are presented in Table 4.2. No clear thickness dependent orientation was observed, and the ratio of both the vertical and horizontal cross-section of the film were similar, indicating the same orientation tendency in both directions.

The results indicated that the mica particles were aligned with the plate-like surface horizontally in both the horizontal and vertical cross-sections of the films, as shown in Figure 4.11, and given by Table 4.2. In Figure 4.12 one may see that the wollastonite particles varied in size, and that the horizontal and vertical cross-sections appeared as similar. The ratio of horizontally versus vertically aligned particles were also similar for the horizontal and vertical cross-sections, resulting in the same orientation tendency as seen for the mica particles. The orientation of the mica and wollastonite particles is illustrated in Figure 4.9. The orientation of the high-aspect ratio fillers was the same in the horizontal and vertical cross-sections of the free films and differed in the direction of the thickness of the films.

The aramid fibers were flexible, and the other filler particles investigated were hard/stiff. The flexibility of the aramid fibers made the fibers to align rather randomly in the films. As shown in Figure 4.13, the fibers were not stiff, and the same fiber could align in various directions dependent on what cross-section that were investigated. It is therefore believed that the aramid fibers were too flexible to obtain a specific orientation in the films, and no ratio of horizontal/vertical alignment is given in Table 4.2 for the aramid fibers. The orientation was investigated in detail on samples with the same weight percent of filler in the paint formulation (≈0.12 wt.%) for all epoxy/filler films, and the same orientation tendency was observed when lambda = 0.1 (see Equation 2.3 page 12) for the epoxy/filler films.

Table 4.2: Average orientation observed in horizontal and vertical cross-section in the paint films with applied thickness of 200, 400, 600, 800, 1000 and 1200 µm. Presented as ratio between number of particles aligned horizontal versus vertical.

	Epoxy/mica Ratio, horiz./verti.		**Epoxy/wollastonite** Ratio, horiz./verti.	
Cross-section	Horizontal	Vertical	Horizontal	Vertical
Average ratio value of all film thicknesses examined	**2.9 ± 0.5**	**3.7 ± 1.5**	**3.4 ± 1.2**	**4.2 ± 1.9**

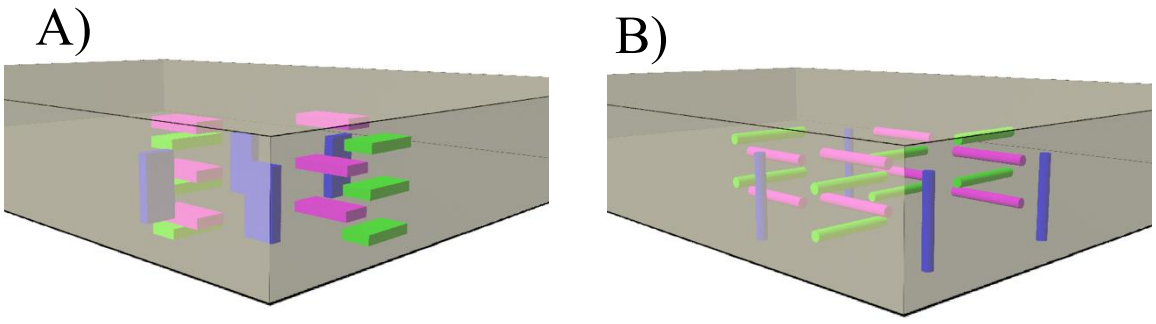

Figure 4.9: Illustration of the orientation of the A) plate-like mica particles and B) the needle-like wollastonite particles in the epoxy-matrix (grey). The green and pink particles illustrate horizontally aligned/laying particles and the blue particles illustrate the vertically aligned/standing particles. Particles with a slanted orientation were not considered.

Horizontal

Vertical

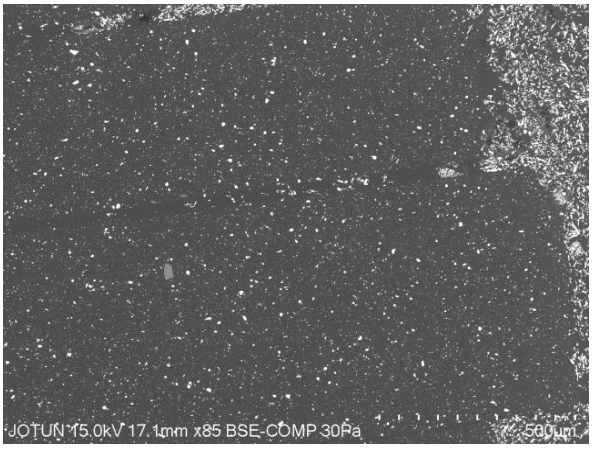

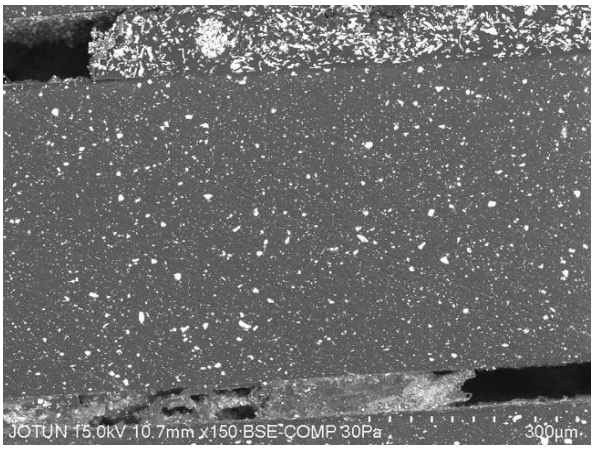

Figure 4.10: Images obtained with SEM of the horizontal and vertical cross-sections of **epoxy/$BaSO_4$** films with applied thickness of 1000 µm. The horizontal cross-section shows two films with applied thickness of 800 and 1000 µm.

Horizontal

Vertical

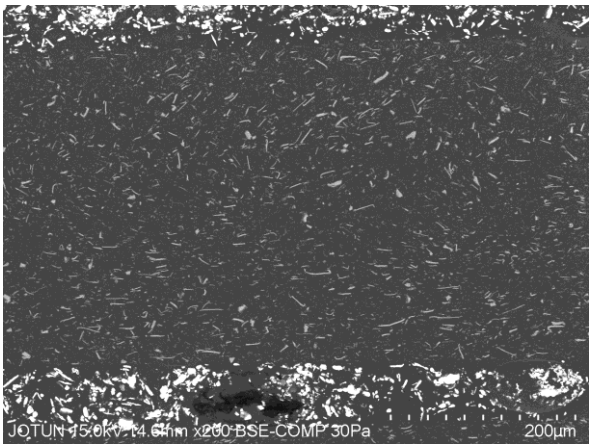

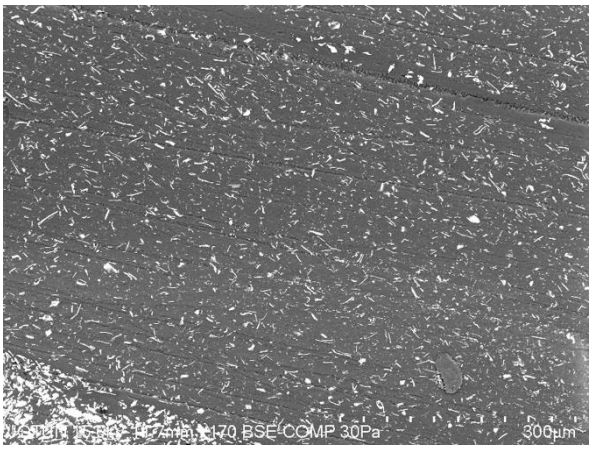

Figure 4.11: Images obtained with SEM of the horizontal and vertical cross-sections of **epoxy/mica** films with applied thickness of 600 µm.

Horizontal

Vertical

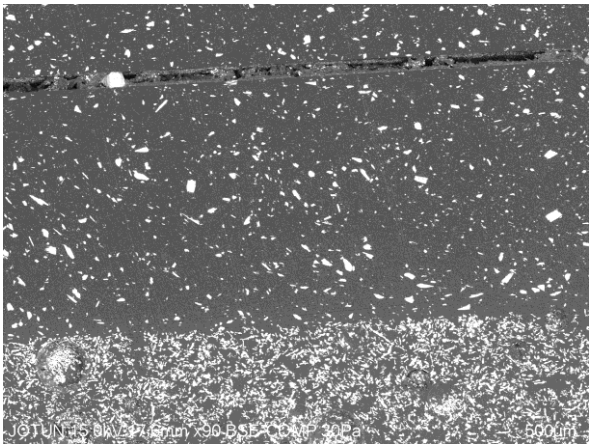

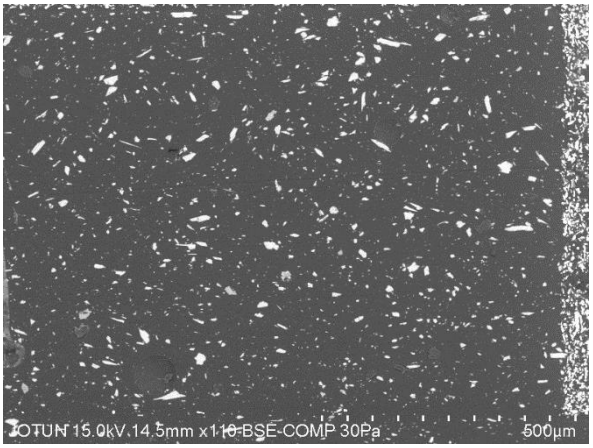

Figure 4.12: Images obtained with SEM of the horizontal and vertical cross-sections of **epoxy/wollastonite** films with applied thickness of 1000 µm.

Horizontal

Vertical

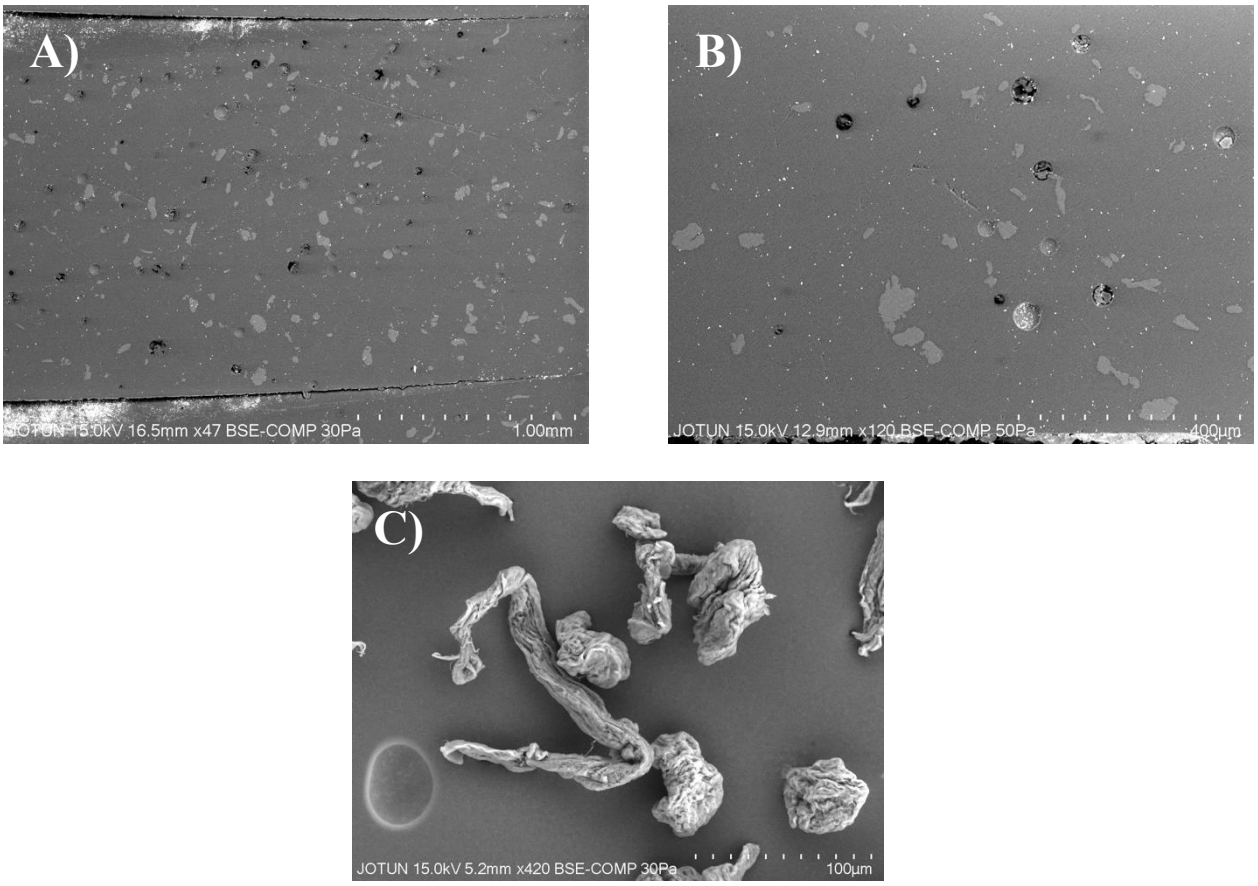

Figure 4.13: Images obtained using SEM of A) the horizontal and B) vertical cross-sections of **epoxy/aramid** films with wet thickness of 800 µm, and at various magnifications. Image C) shows how some of the fibers were bent and not fully stretched out.

4.2 Mechanical properties

The mechanical properties of the paint films have been examined using deformation-controlled tests under a temperature gradient utilizing dynamical mechanical analysis (DMA), and tensile and flexural tests with a universal testing machine (UTM). The fracture surfaces from tensile and flexural testing have also been analyzed to understand the fracture mechanism.

4.2.1 Development of the curing and mixing procedure

The curing and mixing procedure used in the sample preparation strongly affected the test results. The curing procedure involves the time and the temperature under which the polymer film is left to cross-link before any testing is conducted, and the mixing method is the method used to mix the liquid epoxy, filler particles and the curing agent. As reported in the literature, addition of filler can affect the curing [64,65], but as curing behavior not is the focus in this work, all mechanical testing were done using fully cured films. Three curing procedures and two mixing procedures were tested in order to find a method which gave homogenous and fully cured films. Tests on the dynamical mechanical analysis instrument revealed whether the films were fully cured and gave an indication of the reproducibility of the DMA-experiments [19,64]. Several adjustments were made, and the sequence and explanation of the adjustments are given in detail in Appendix D.

Air bubbles, inhomogeneous distribution of filler particles, micro cracks and voids are expected to make problems to a certain degree in paint films and were observed in this work as well. This kind of irregularities will affect the results, and all results from DMA presented are based on minimum two repetitions from two different batches, and tensile and flexural tests were conducted with minimum four repetitions from two different batches.

4.2.2 Impact of filler particles on the mechanical properties

The mechanical properties of polymer/filler systems have been widely studied and the enhancement or deterioration of properties have been predominately explained on the basis of three mechanisms in the literature:

1. **Interfacial constrain**
   The polymer molecules arranged around the filler particles are more constrained than the molecules located further away from a filler particle as a result of mechanical hindrance [14,25,26,40].
2. **Free volume increase**
   Addition of filler can increase/decrease the free volume and/or cross-link density of the polymer matrix [25,64,65].
3. **Interfacial bonding**
   Interfacial bonding between the filler and the polymer matrix transfers the applied stress from the matrix to the filler, resulting in a film that can resist more and reinforces the film [5,8,21,23].

The chemical and physical properties of the filler particles, like the chemical composition, size, shape, and surface area, decide which of the above-mentioned mechanisms (1-3) that dominates. A combination of the various mechanisms is often seen, and thus expected for the fillers investigated in this work as well. The three mechanisms listed above have been used below to explain the results obtained in this work. Fillers used in pure form in polymer coatings/composites are normally known to be inert, and lack chemically active groups on their surface [16,26,54]. In order to achieve bonding between the filler and the polymer matrix surface modification of the filler particles with a coupling agent is normally applied [7,8,47,54]. All four fillers used through this work were tested for surface modification in order to illustrate the effect, and the results are presented and discussed in Section 4.5.

The fillers tested are all reported not to form interfacial bonds of significance with pure polymers in composites [21,22,26,64], and no chemical interactions were detected for the epoxy/filler samples in this work, as discussed in Section 4.1.

4.2.3 Moduli

Dynamical mechanical analysis measurements were conducted on the paint films to observe the mechanical behavior at various temperatures. The storage modulus (E') of all epoxy/filler samples are displayed in Figure 4.14, and the curves chosen were based on four repetitions. All curves showed approximately the same decrease in the storage modulus around 100-140°C, followed by a plateau at higher temperatures, which is characteristic for a cross-linked system. A higher value of the storage modulus means, according to Equation 2.7, Section 2.5.4, that a larger stress was applied to the film in order to acquire the same strain. The higher the value of the modulus the stiffer was the sample. A lower modulus value can, to the contrary, indicate a more flexible film.

The Youngs and bending moduli values of the epoxy/filler samples from the tensile test and flexural test are compared to the storage modulus of the epoxy/filler samples in Figure 4.15. To evaluate change in stiffness after adding fillers to the epoxy matrix, the various epoxy/filler samples modulus values shown in Figure 4.15 have been compared. The standard deviation was rather large for the tensile test results (Youngs modulus), which probably was a result of uneven film thickness and difficulty in aligning the samples correct in the UTM.

The values of the moduli are a measure of the response of the films and will only show the impact of the fillers on the epoxy matrix in the linear viscoelastic region. From all three tests, the values of the modulus increased by adding the rigid fillers mica and wollastonite, while the change in modulus by adding $BaSO_4$ or aramid fibers were not obvious.

Increase in storage/Youngs/bending modulus by addition of fillers has been reported earlier [14,4], and can be explained by the fact that the rigid filler particles restrict the movement of the molecular groups in the epoxy matrix and makes the film stiffer (mechanism 1 above). Hence, a greater stress was necessary in order to obtain the same displacement/amplitude.

The effect of the filler particles was more obvious at higher temperatures, because above the T_g, the molecular mobility of the epoxy matrix was high, and the restriction effect of the filler particles to the movement of the epoxy segments was more marked [26,66]. Addition of aramid fibers did not reinforce the epoxy-matrix significantly above the T_g, possibly due to the shape and softness of the aramid fibers, in combination with the presence of air bubbles, observed in the epoxy/aramid films (see page 57) [14]. The size and shape of the aramid fibers have been shown earlier to have a trapping effect on the liquid epoxy and curing agent during curing, resulting in regions of unreacted

epoxide and amino groups, and a lower cross-link density. This circumstance leads to a lower storage modulus compared to the storage modulus of the neat epoxy (mechanism 2, page 64) [64].

Barium sulfate has been reported to give rise to a weak interaction in both polypropylene and epoxy composites, respectively [21,39]. This interaction has been related to the change in mechanical properties compared to the pure polymer material. Since the $BaSO_4$ particles did not show an obvious indication of a binding or chemical interaction with the epoxy in this work, the reinforcement of the epoxy-matrix by the $BaSO_4$ particles must be explained by interfacial constrain of the epoxy segments by the particles (mechanism 1, see above).

No epoxy/filler combinations showed a clear indication of strong interfacial interactions between the epoxy-matrix and the filler surface in this work. Wollastonite and mica has also been reported to show restriction on the molecular mobility in polymer matrixes in composites [22,26,51], and the changes in moduli values and stiffness observed for all epoxy/filler samples are therefore believed to be mainly caused by mechanism 1, interfacial constrain.

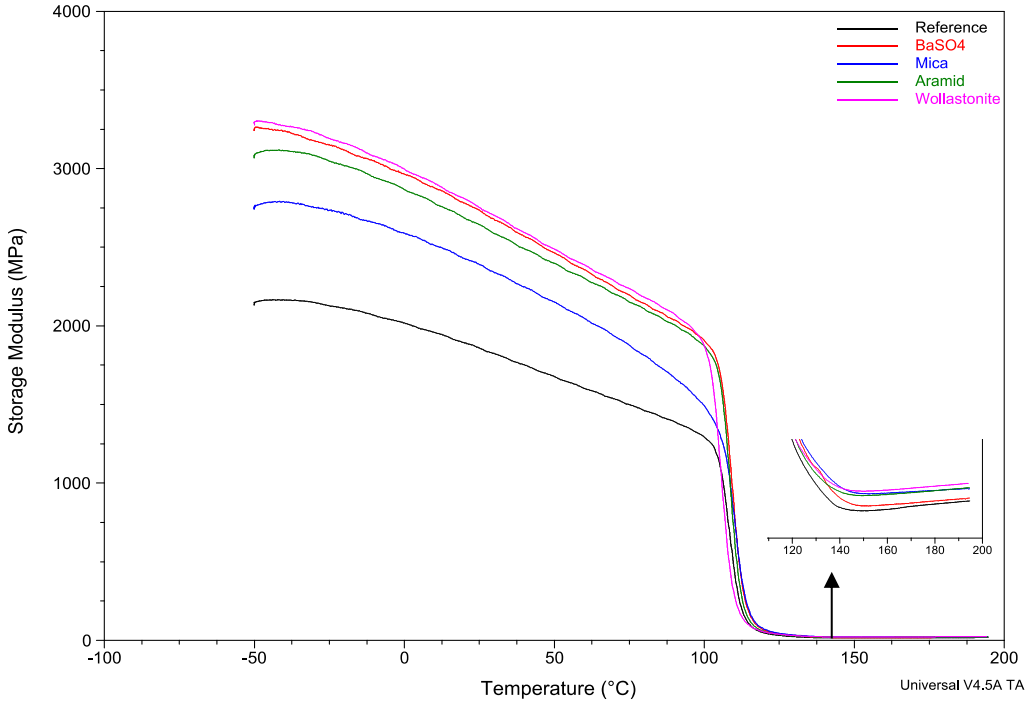

Figure 4.14: The storage modulus obtained from DMA measurements of epoxy/filler samples. The insert view shows the storage modulus curves in logarithmic scale at high temperature.

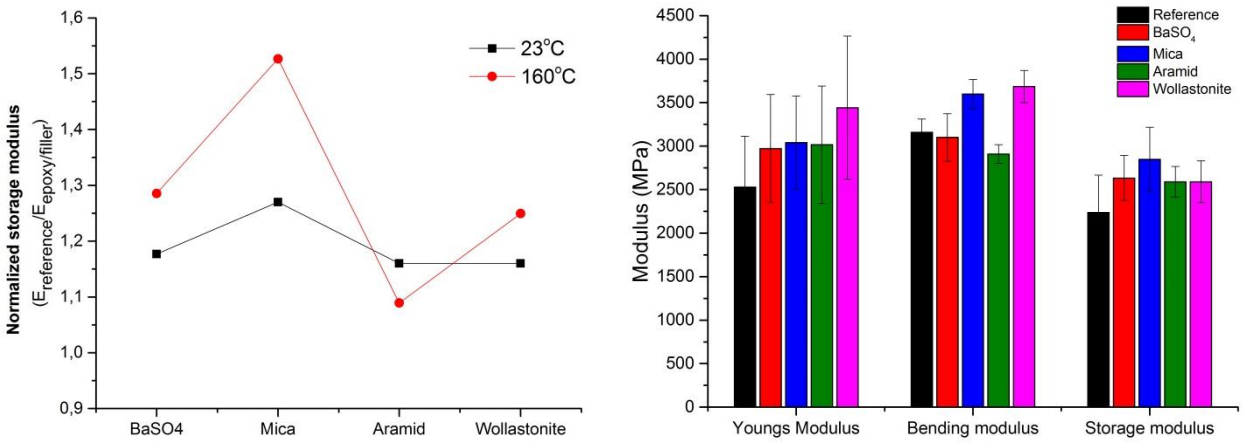

Figure 4.15: To the left, normalized storage modulus at temperatures below (black,■) and above (red,●) the T_g, and to the right, the modulus values obtained using the tensile test, flexural test and DMA test, respectively.

4.2.4 Glass transition - T_g

The glass transition temperatures were found based on the DMA results. The tan δ values are calculated by dividing the loss modulus by the storage modulus (Equation 2.10, page 32) and reflect if the elastic or viscous part of the rheological properties of the samples dominates. The values have been plotted as a function of temperature, see Figure 4.16. A peak in the tan δ peak vs temperature curve indicates viscous movement in the material, and a typical example is the glass transition. Additional peaks in the curve will indicate if there is a movement of molecular groups at the temperature where the peak is observed. The height of the peak reflects the number of molecular segments that is in movement, and the width of the peak reflects the temperature range where the movement occurs [38]. The glass transition of a polymer material occurs when large segments of the polymer-matrix are free to move. Examples of factors that influence the T_g are polymerization-degree, additional substances in the polymer-matrix (e.g. fillers), their orientation and the thermal conductivity of the polymer [41]. Fillers with various shapes and sizes may give rise to different free volumes in the polymer structure. If the free volume is small, the segments will not be able to move easily, and a higher temperature is necessary to reach the T_g.

The tan δ curves (see Equation 2.10, page 32) constructed are displayed in Figure 4.16. The curves had a low value (<0.1) up to around 100°C, indicating that the films had mainly elastic response up to this temperature. At around 100°C, the glass transition occurred in the films. The broad tan δ peak indicated that the glass transition occurred over a temperature range rather than a specific temperature. The T_g temperatures presented in Figure 4.17 represents the temperature the curves passed through the maximum. As the glass transition temperature depends on the degree of

polymerization of the matrix, it can be verified that as the films were more fully cured by changing the curing process, the T_g increased as shown in Figure D.1 – D.4 in Appendix D. The height of the tan δ peak decreased when the films were more fully cured. This indicates that fewer segments contributed to the glass transition, in agreement with the fact that the network had a higher cross-link density.

The change in T_g upon adding filler particles in composites has been reported to increase [25,26,51], decrease [5,38,64], or not be significantly changed [22,39,66]. The decrease in T_g has been attributed to a lower cross-link density, which may result in shorter chain segments and a quicker viscous response [64]. An increase in T_g after addition of filler has been attributed to interfacial constrains in combination with interfacial interactions [25].

The glass transition temperatures for the epoxy/filler samples are presented in Figure 4.17. The T_g increased ca 2°C for the epoxy/filler samples compared to the neat epoxy-matrix (reference). This was within the standard deviation of the observed T_g temperatures for the samples. The small change in T_g indicates that the polymer structure of the epoxy-matrix was not changed by the addition of any of the fillers particles. An increase in filler concentration could possibly affect the structure to a larger extent, but this possibility has not been investigated in this work.

Even though the epoxy structure was not changed to an extent where it affected the glass transition, valuable information can be obtained by observing the height and width of the tan δ peak. The

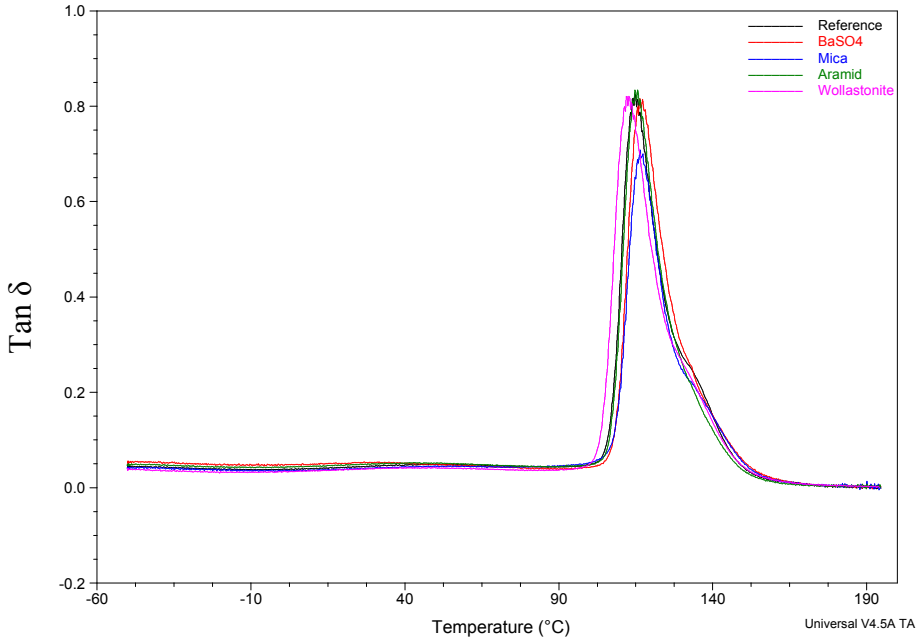

Figure 4.16: Tan δ curves from DMA measurement at a frequency of 1 Hz, an amplitude of 5 μm and temperature ramp of 5°C/min.

width reflects the temperature range of which the segmental motion occurs, and the height reflects the number of moving segments [38].

The height and width of the tan δ peaks are displayed in Figure 4.18. The height of the tan δ peaks were defined as the maximum value of the tan δ peak, and the width was defined as the length (measured in °C) of a horizontal line between the onset and offset of the peak. The height of the tan δ peaks was different for the various epoxy/filler samples and all epoxy/filler samples had a lower tan δ peak compared to the reference (neat epoxy sample). The height was compared to the width of the tan δ peak, which is also presented in Figure 4.18. The general trend observed was an increase in width and decrease in height, indicating that the glass transition occurred over a wider temperature region and with a lower number of molecular groups contributing to the glass transition after addition of fillers [38]. The reference sample was expected to have a higher tan δ peak, since the sample consisted of ~100% cross-linked polymer, while the epoxy/filler samples had 3-12 wt.% of filler [38].

The difference in width was small when comparing the different epoxy/filler samples, but the difference in height was somewhat larger. The change in height was believed to be caused by mechanical constrain of polymer segmental movement by the fillers (see mechanism 1, page 64) [26]. The height could be arranged from highest to lowest in the order reference > epoxy/wollastonite ≈ epoxy/aramid ≈ epoxy/$BaSO_4$ > epoxy/mica. The small difference in vol.% of filler loading in the epoxy/filler samples was not likely to be the explanation, due to the fact that the epoxy/wollastonite sample had the highest vol.% and the epoxy/aramid sample had the lowest

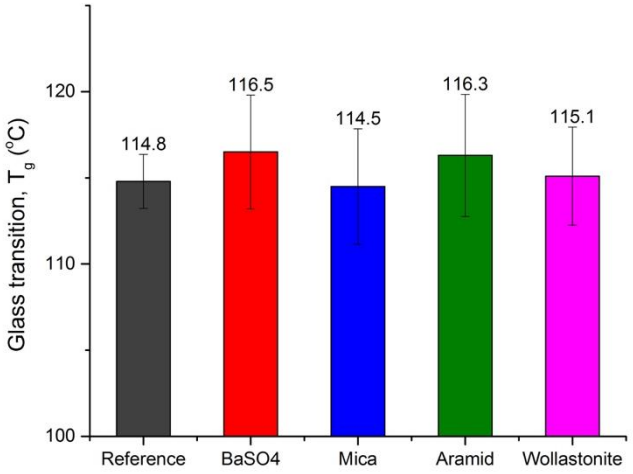

Figure 4.17: T_g values of the epoxy/filler samples. The T_g was defined as the temperature where the tan δ curve passed through a maximum.

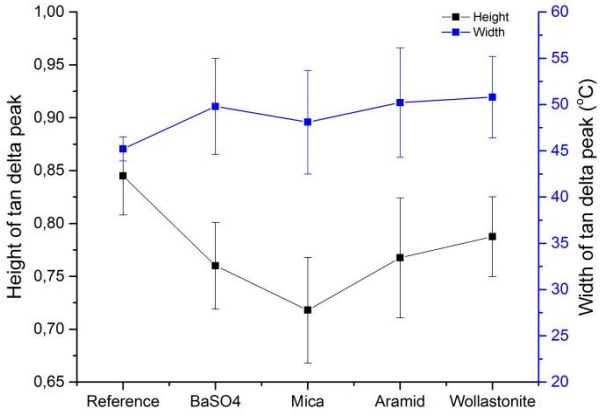

Figure 4.18: Height and width of the tan δ peaks.

vol.% and both these samples had the highest height of the epoxy/filler samples. The change in height was rather believed to be caused by the size, shape or chemistry of the fillers.

The standard deviations of the reported height and width were large. Even though seven DMA measurements were conducted on the reference epoxy samples and four repetitions for the epoxy/filler samples were performed, the standard deviations were still large. This circumstance was probably observed due to small differences in cross-linking and local epoxy/amine structure in the various film, and/or air bubbles and small deformations in the films.

The storage modulus values for the epoxy/filler samples displayed in Figure 4.15 showed that the increase in modulus had the reversed order as the change in height of the tan δ peak, when comparing the various epoxy/filler samples. As discussed above, the rigid fillers restricted the movement of the epoxy segments (see mechanism 1, page 64), giving the samples a higher modulus, and fewer segments contributing to the glass transition. This was shown by the decrease in height of the tan δ peak [4,51,66]. Considering the standard deviation for the height of the tan δ peak curves, the epoxy/$BaSO_4$, epoxy/wollastonite and epoxy/ aramid samples had the same height within experimental uncertainty. The epoxy/mica samples had a slightly lower tan δ peak, a fact that could be explained referring to the shape of the filler particles. When the epoxy/filler samples were sinusoidally deformed in the DMA-measurements, the epoxy-matrix were sinusoidally stretched in order to reach the set deformation. The mica-flakes had a high aspect ratio (flake shape) and probably represented the most difficult obstacles for the epoxy segments, inhibiting the stretching of the epoxy matrix during deformation, resulting in fewer segments contributing to the glass transition, and a lower tan δ peak.

For several curves a small irregularity was seen after the main glass transition (see Figure H.3 versus H.4 in Appendix H). This is often called a tailing peak and is explained in the literature as a second T_g for the polymer chains experiencing molecular mobility constrains by filler particles [40, 67]. The second T_g's reported in the literature are more marked than the irregularity observed in this work and have been reported to occur at significantly higher temperatures than the first T_g. The size and position of the second tan δ peak have been reported to be dependent on the fraction of polymer chains constrained and the thickness of the constrained polymer layer on the filler surface [67]. Due to the fact that the irregularity was observed for both the reference samples and epoxy/filler samples, the irregularity cannot be explained as a clear second T_g for constrained polymer chains by filler particles, but could be a result of micro cracks, air bubbles or bad sample placing under the experiment.

4.2.5 Stress-strain curves

The tensile and flexural test results are presented as stress-strain curves and are presented in Figure 4.19. The tensile and flexural tests showed the same tendency, but as previously mentioned, the standard deviation from the tensile test results was high, due to presence of air bubbles, micro cracks, and problematic sample positioning in the instrument. The mechanical properties such as strength and toughness of the samples have therefore been based on the flexural test results.

The shape of the stress-strain curves for the epoxy/filler samples is typical for brittle samples, which can withstand high stress but do not elongate much before they break. The reference sample showed a more ductile behavior, and this sample was deformed more before it broke. When the tensile and flexural tests were conducted, the samples were stretched and bended, respectively. As the samples were stretched, the epoxy matrix started to undergo plastic deformation and the fillers could either be stretched together with the epoxy matrix, or act as mechanical hinders, concentrating the stress, which possibly could have resulted in voids around the fillers [14].

The size and shape of the fillers are important for the mechanical properties of the epoxy/filler samples. The $BaSO_4$ particles which were smallest in size and have the lowest aspect ratio compared to the various filler particles tested, showed the highest stress and strain at break of the tested fillers of the epoxy/filler samples. The other fillers were in contrast larger, and had a much higher aspect ratio, which made it difficult for the epoxy matrix to stretch around the particles under elongation [14].

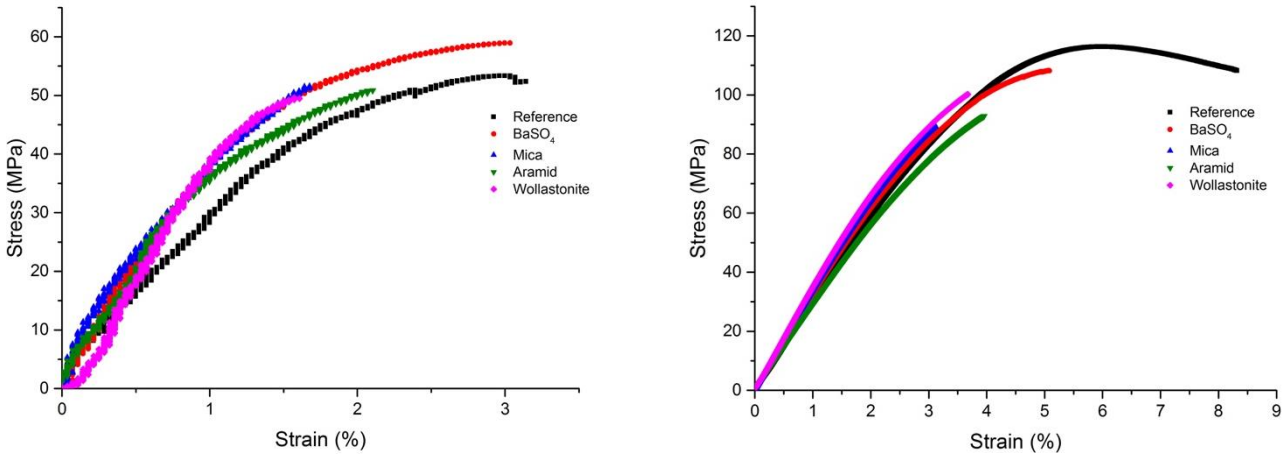

Figure 4.19: Stress/strain curves from tensile (left) and flexural (right) tests using UTM at room temperature.

Larger filler particles with high aspect ratio will consequently result in stress concentration and mechanical hindrance for the epoxy matrix. This circumstance could have led to a lower strain at break.

The strength of materials is defined as the maximum load the material can sustain [36]. For all epoxy/filler samples, the strength is presented as stress at break from the flexural test results in Figure 4.20, and the strength discussed in this work is therefore flexural strength. For the neat epoxy samples, an additional value called flexural strength have also been included, since the neat epoxy matrix underwent plastic deformation and had a lower stress at break than the maximum stress possible to overcome for the sample. As seen in Figure 4.20, the strength decreased by addition of filler, and decreased to the lowest degree by addition of $BaSO_4$ particles. This might have been a result of a more uniform stress distribution through the matrix material, since the $BaSO_4$ particles were the smallest particles tested and had the lowest aspect ratio [14].

The toughness of materials is a measure of the amount of energy they can absorb before they break and is normally defined as the area under the stress strain curve [42]. From the data presented in Figure 4.19 it is clear that the toughness decreased by the addition of filler, and the toughness could be ranked as reference > epoxy/$BaSO_4$ > epoxy/wollastonite ≈ epoxy/aramid ≈ epoxy/mica, taking the experimental uncertainty into consideration. The same explanation as given for the decrease in strength can be used for the decrease in toughness. When the materials are exposed to increasing stress, this stress must be distributed and absorbed, resulting in elongation of the material. By addition of fillers, the samples did not elongate as much as the neat epoxy matrix due to mechanical hindrance by the filler particles, and stress were likely concentrated around the particles. The epoxy/mica samples showed the lowest strain and stress at break, which may be compared with the correspondingly DMA-results, where the epoxy/mica samples also showed the lowest tan δ peak height. These results may be explained by mechanism 1 (page 64), i.e. the mechanical restriction effect of the filler particles on the epoxy segments.

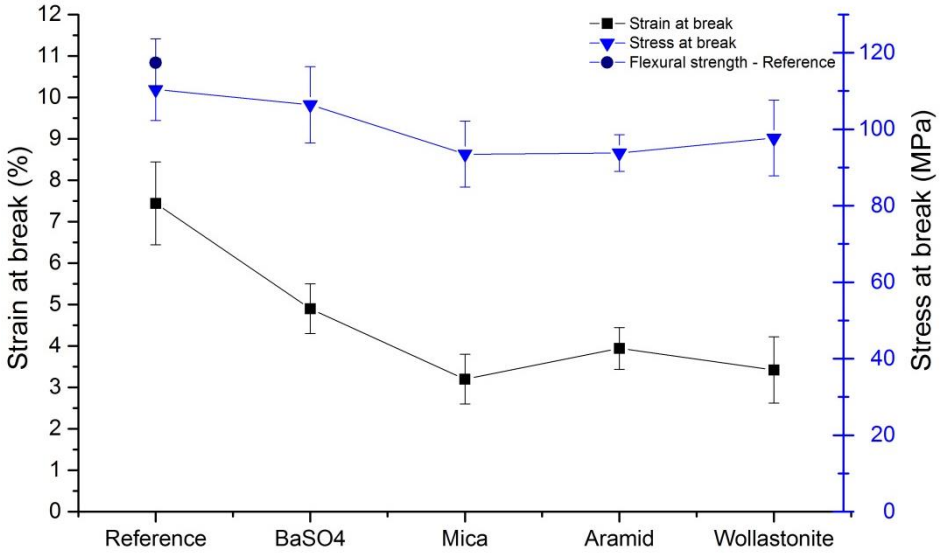

Figure 4.20: Stress and strain at break for the epoxy/filler samples from flexural tests conducted at room temperature.

4.2.6 Directional dependence of mechanical properties

The directional dependence of the mechanical properties determined using the dynamical mechanical analysis are first presented and discussed, followed by a discussion of the directional dependence of the mechanical properties determined using tensile and flexural tests.

By testing films that were cut both horizontally and vertically (see page 45 for direction illustration), any directional dependence on the dynamical mechanical properties could be detected. As explained in the Materials and Methods section (Section 3.7), the chosen curing process and sample preparation method were not used for the study of directional dependence of the results obtained from the DMA-measurements. No additional results obtained using the updated curing process are presented since the same orientation of the filler particles was observed in both the horizontal and vertical cross-sections of the free films. Figure 4.21 displays the storage modulus and tan δ curves for samples of epoxy/mica cut horizontally and vertically (the curves for the rest of the epoxy/filler sampled are available in Figure H.5 – H.7 in Appendix H). No clear difference in the samples cut horizontally or vertically was observed, and a possible small difference was believed to be caused by different curing percentage of the films from the two batches. Hence, no directional dependence of the dynamical mechanical properties was observed by the DMA-tests. This finding corresponded well with that the orientation of filler particles were the same in both the horizontal and the vertical cross sections of the films.

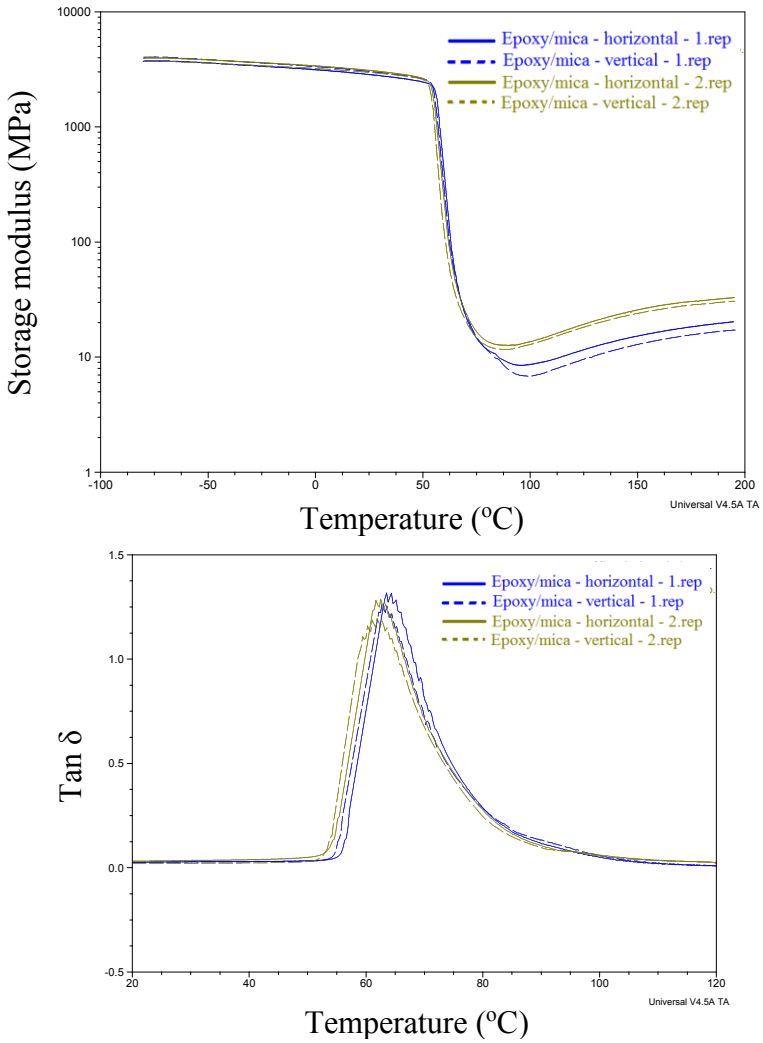

Figure 4.21: Storage modulus (left) and tan δ curve (right) for epoxy/mica samples cut horizontally and vertically, cured in room temperature for 2-3 weeks. The curves are results obtained from two repetitions on two batches.

The orientation of the filler particles might have influenced the strength and toughness of the epoxy/filler samples. When the epoxy matrix is stretched, it will elongate as shown by the results for the neat epoxy sample. An orientation of the filler particles where the largest area of the particles aligns parallel with the elongation direction will give the highest strength and toughness, as this orientation would give the epoxy matrix the smallest obstacle to stretch around.

The tensile and flexural tests cause stress in the samples in various directions as shown in the theory section (page 23). During the tensile test, the sample was elongated parallel to the horizontal/vertical cross-section of the film, dependent on sample preparation. For the flexural test, the sample was compressed at the top and experienced tension in the lower part where it was elongated [36]. The orientation of the particles were the same in the horizontal and vertical cross-section of the film for the epoxy/mica (plate-like) and epoxy/wollastonite

(needle shape) samples, and independent of which cross-section the samples were taken from for the tensile test, the results were therefore the same.

For the flexural tests, the samples were prepared with the use of molds, and the horizontal and the vertical directions earlier introduced (page 45) could not be referred to with these samples. The orientation of the filler particles in the epoxy matrix for the tensile test sample were the same as for the free films presented above and is illustrated in Figure 4.22. The mica and wollastonite particles mainly had the same orientation as shown in Figure 4.22 in the flexural test samples as well but the sample preparation also led to parts where the particles had slightly more mixed orientations.

For the epoxy/wollastonite samples, a majority of needles orientating horizontally/"laying" in both the horizontal and vertical direction were observed (see page 59), as illustrated in Figure 4.22. When the epoxy/wollastonite samples were stretched, the wollastonite particles with the orientation of the longest side parallel with the stress direction should have been the easiest obstacle for the matrix, while the particles orientating perpendicular to the stress direction or vertically/"standing" in the films should have been the largest obstacle. The epoxy/wollastonite samples would, based on these conclusions, obtain the largest stress and strain at break values when all the wollastonite particles were aligned horizontally in the film and parallel to the direction of the applied stress. For the epoxy/mica samples, a majority of mica particles aligning with the big plate-surface horizontally in the film were observed. This orientation of the mica particles gives the epoxy matrix the smallest/thinnest side of the particles to stretch around under elongation. The mica particles make up the smallest possible obstacle with this orientation, compared to e.g. an orientation of only vertically aligned mica particles, which would give the epoxy matrix the largest possible obstacle under elongation. Based on these conclusions, the observed orientation of the mica particles should have given the highest possible strength and toughness for the epoxy/mica samples.

The aramid fibers did not show a special orientation, and the size and flexible behavior observed for the aramid fibers in the epoxy/aramid films was believed to decrease the strength and toughness of the samples. If the aramid fibers were fully stretched out, and aligned horizontally in the films, the films could possibly have achieved a higher strength and toughness.

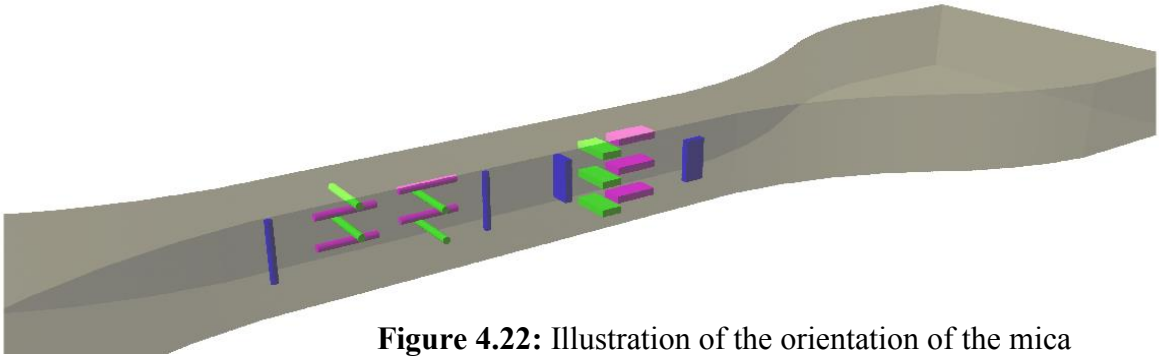

Figure 4.22: Illustration of the orientation of the mica particles (plate-like, right side) and the wollastonite particles (needle-like, left side) in the dog bone samples. Particles with a slanted orientation were not considered.

4.3 Fractography

Analysis of the fractured surfaces resulting from mechanical tests are called fractography and the analysis can yield information on how and where the samples failure [45]. Test samples from tensile and flexural tests using UTM were analyzed using SEM and a selection of the fractured samples are shown in figures 4.23 and 4.24. In image A) in Figure 4.23, only the upper film is the fractured film. For images B)-E), only one surface is visible, i.e. the fractured surface.

As seen in Figure 4.24, the filler particles pointed out of the fracture, and were not covered by any epoxy, indicating a lack of epoxy-filler interactions. $BaSO_4$ was the only filler which partly showed any coverage by the epoxy matrix. The $BaSO_4$ powder consisted of the smallest particles tested in this work and these particles were believed to (as discussed above) not disturb the movement of the epoxy matrix as much as the other fillers. This could be the explanation behind the observed fracture surface, where the epoxy matrix managed to stretch around the filler particles.

When the dog bone sample (see page 46) was pulled in opposite directions during the tensile test, there should ideally had been an interaction between the filler and the matrix in order for the overall film to hold together at higher stresses and not fracture. The fracture surfaces in Figure 4.23 indicate that the fracture surfaces of the epoxy/filler samples showed many small cracks, and not a smooth/flat fracture like the reference sample (Figure 23 A). This indicates that the samples failed around the filler particles. This process is called “dewetting” of the fillers and decreased the strength of the samples [14].

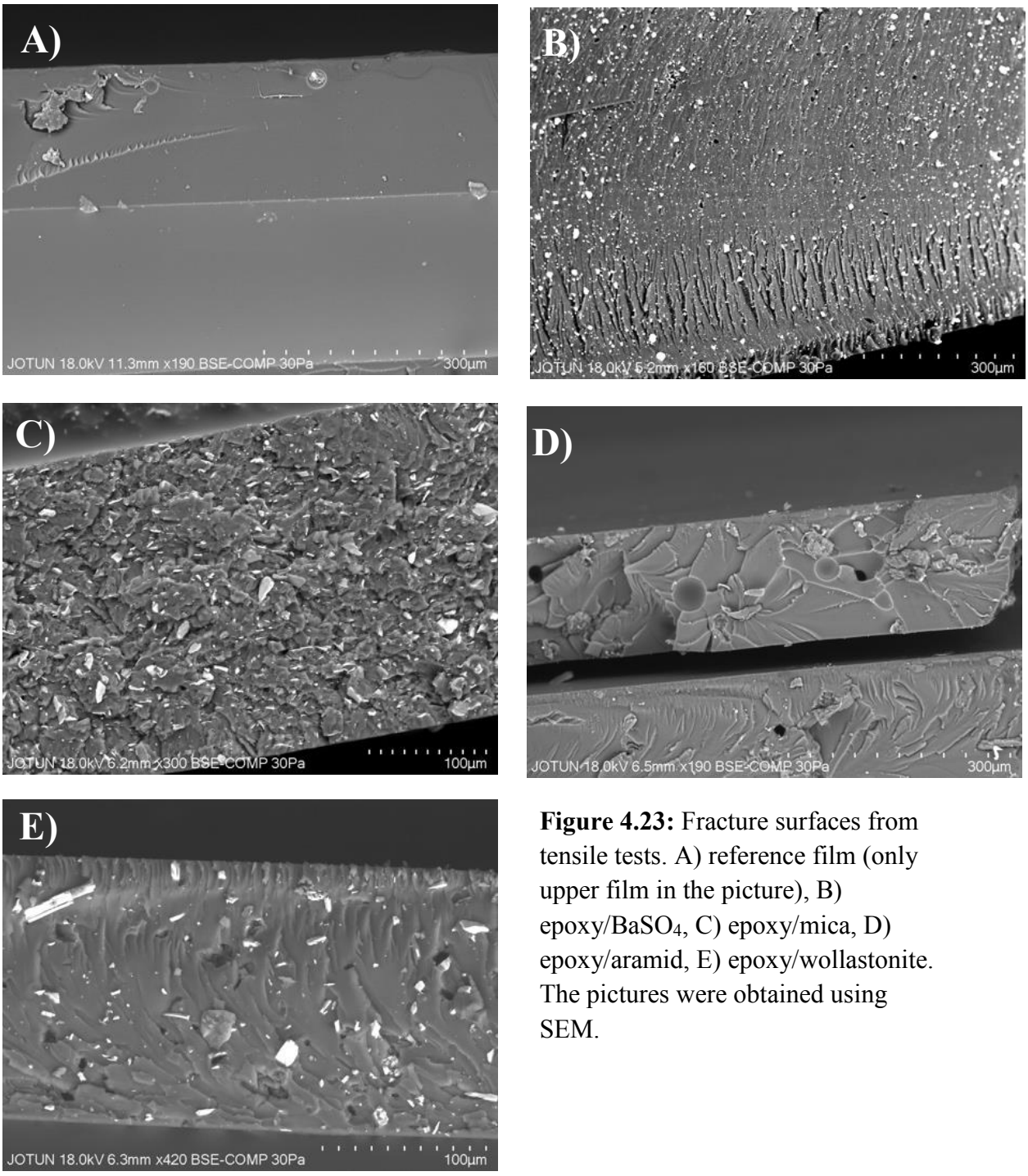

Figure 4.23: Fracture surfaces from tensile tests. A) reference film (only upper film in the picture), B) epoxy/$BaSO_4$, C) epoxy/mica, D) epoxy/aramid, E) epoxy/wollastonite. The pictures were obtained using SEM.

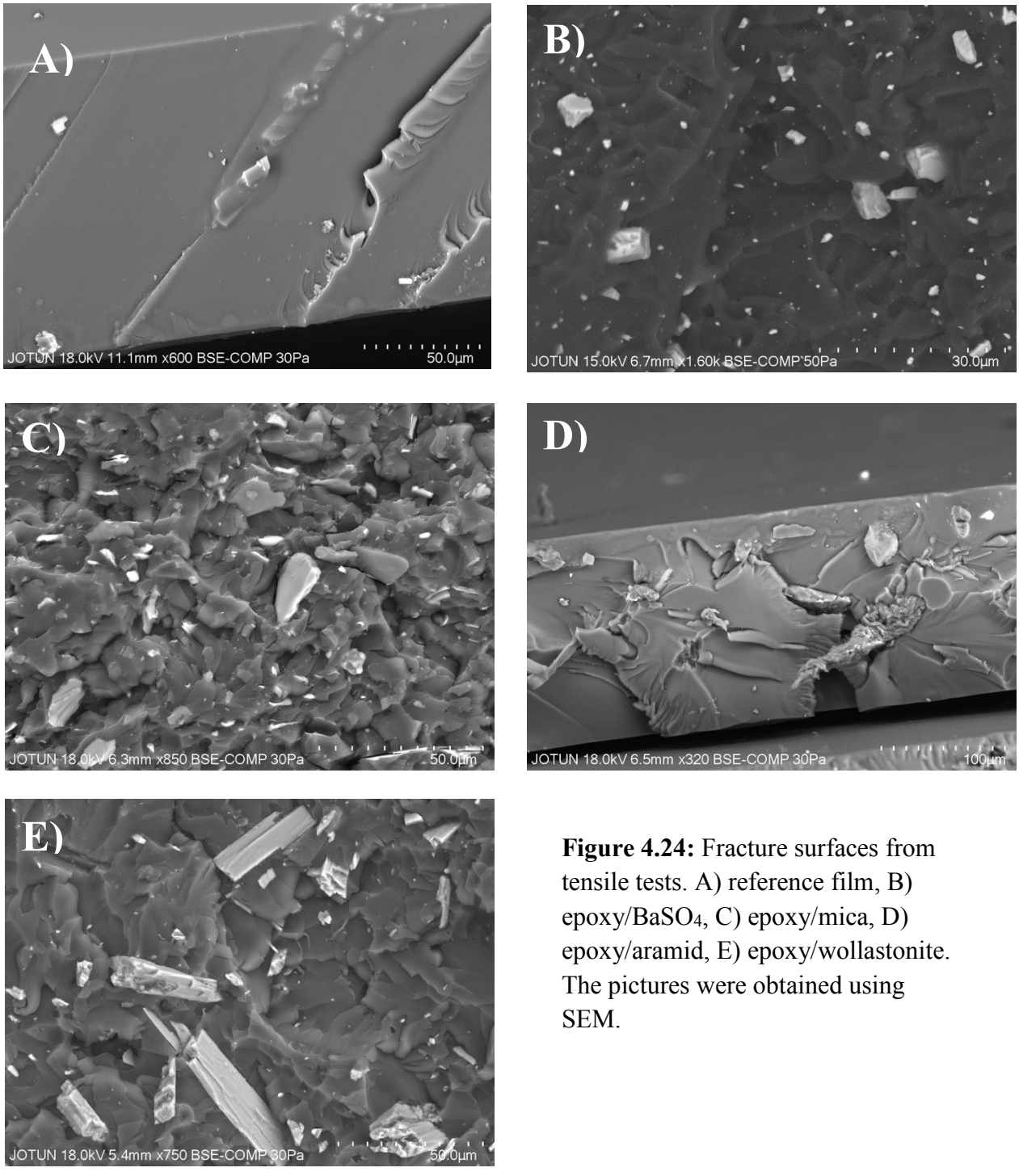

Figure 4.24: Fracture surfaces from tensile tests. A) reference film, B) epoxy/$BaSO_4$, C) epoxy/mica, D) epoxy/aramid, E) epoxy/wollastonite. The pictures were obtained using SEM.

4.4 Permeability of water vapor

The permeability testing in this work was conducted using films with thickness in the range 50-200 μm, over a period of two-four days, at a temperature of 40°C. The permeability may differ over time since absorbed water may change the epoxy matrix structure [44]. The time dependence of the permeability has not been investigated in this work. The water vapor may easily permeate through voids and air bubbles, and it is therefore important to obtain an even distribution of the filler particles and avoid cracks in the film during the sample preparation.

For a molecule to diffuse through a polymer film is must first be adsorbed on the polymer surface, diffuse through the polymer and desorb on the other side of the polymer film [43,44]. Since the polymer matrix was the same for all the samples in this work, and the overall epoxy structure seemed to be unchanged by the addition of the filler particles (referring to the XPS, FT-IR and DMA-results), the difference in permeability observed was expected to be caused by the presence of the filler particles.

Inorganic fillers normally reduce the permeability of water vapor through paint films, forcing the water molecules to go around the filler particle [14], as shown in Figure 2.9. The permeability results from the epoxy/filler samples are presented in Figure 4.25. Considering the experimental uncertainty, the permeability of the epoxy-matrix films did not change significantly by the addition of filler particles. However, the slight decrease in permeability observed for the epoxy films containing inorganic fillers ($BaSO_4$, mica, and wollastonite) is likely due to a blocking effect [43].

The amount of filler in the samples (see Table 3.1, page 37), size and orientation of the particles may have influenced the blocking effect. The amount of filler in each epoxy/filler sample varied in order to keep lambda=0.1, as shown in Table 3.1. The size of the various filler particles was also different, as previously discussed, and can be ranked in the order $BaSO_4$ < mica < wollastonite < aramid. The samples that contained mica and wollastonite had a lower permeability than the samples that contained $BaSO_4$, in agreement with the guess that mica and wollastonite should show a higher blocking effect due to the larger filler particles in this case. The high aspect ratio of the mica and wollastonite particles may also have enhanced the blocking effect since the largest side of the high aspect ratio shape were orientated perpendicular to the direction of the thickness of the films.

The small difference in filler concentration might have influenced on the blocking effect, but the aramid fibers, which had the highest lambda and smallest concentration compared to the other

epoxy/filler samples (see Table 3.1, page 37) had an even higher permeability than the neat epoxy matrix, and this result was not believed to be caused by the concentration difference. The higher permeability to water vapor for the epoxy/aramid films is likely due to the air bubbles which were observed in epoxy/aramid films (see page 57) [32]. The permeability of the epoxy/aramid films is reported with a large standard deviation, even though seven repetitions of the permeability test were conducted. The variation between each epoxy/aramid film, due to a difference in distribution of filler particles, air bubbles and voids, is probably the reason. The permeability results presented for the other epoxy/filler films is a result of minimum four repetitions, and showed a higher reproducibility, and consequently lower standard deviation.

The orientation of the filler particles might have influenced on the permeability results, and for mica and wollastonite, for which there were observed a preferred orientation, the filler particles orientated with the biggest area horizontal in the films, resulting in a high blocking effect.

It could have been interesting to see the effect of fillers on the permeability above the T_g as well, but since the T_g is above 100°C, it is difficult to successfully accomplish the test without any water vapor escaping in the possible void between the Payne cup and the film.

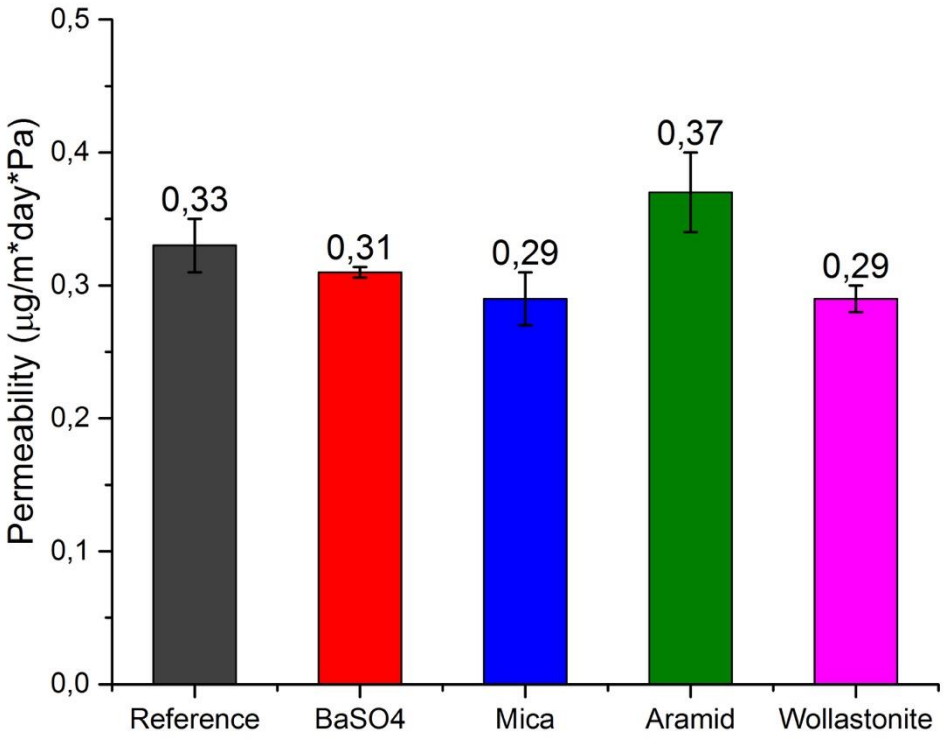

Figure 4.25: Permeability measured for the epoxy/filler films at 40°C using Payne Permeability cups.

4.5 Surface modification

Surface modification of the fillers were performed using a silane coupling agent and the silane was chosen based on the possibilities for cross-linking with the epoxy binding system. The silane used on the fillers consisted of a part which could be hydrolysed and following a reaction with the mineral surface, and a functional group that could react with the binding system. The hydrolysable groups in the silane used in this work were ethoxy groups, and the functional group was a $-NH_2$ group. The quality of the surface modification was examined using XPS and FT-IR. A pretreated wollastonite powder from The Quarzwerke Group treated with the same silane coupling agent (ameo) as in this work and was tested to compare with the results of the surface modification made in this work. The pretreated wollastonite powder have been abbreviated wollastonite-fs/wolla-fs (wollastonite from supplier).

The same mechanical and physical tests presented previously were also conducted on the epoxy/modified-filler samples (abbreviated epoxy/m-filler, see page 38). It was expected that the silane treatment might give rise to stronger interactions between the epoxy and the filler, resulting in stronger and tougher samples with lower permeability. The distribution and orientation of the filler particles were also investigated since the distribution and orientation can influence the physical and mechanical properties (see page 22).

The wollastonite-fs powder had an average particle size of 3.5 μm, which was smaller than the wollastonite powder used in this work, as shown in Figure 4.26. The change in size of the particles might have affect the toughness and strength of the epoxy/wolla-fs samples compared to the original (un)modified wollastonite particles.

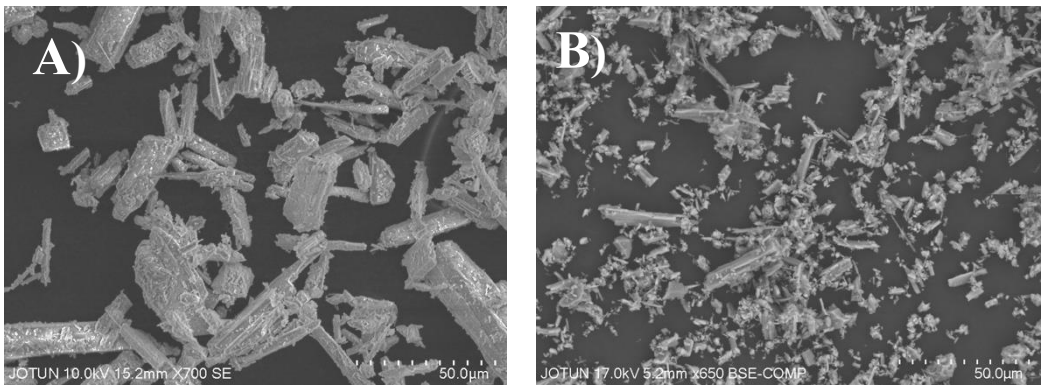

Figure 4.26: A) The original wollastonite particles used in the study, and B) the pretreated wollastonite-fs particles.

4.5.1 Surface analysis

To verify if the fillers had been successfully surface modified, the modified fillers were analyzed using both FT-IR and XPS after surface modification.

For the FT-IR analysis, the fillers were mixed in proportion of 1:1 with ethanol and placed on the reflectance crystal to dry before the FT-IR spectra were collected. Figure 4.27 show the FT-IR spectra for the unmodified wollastonite powder, the modified wollastonite powder and the ameo coupling agent. The FT-IR spectra of the other modified filler powders are available in Figure F.1-F.4 in Appendix F.

FT-IR has previously been used to verify surface modification [11,13,31], but did not reveal any signal from the silane coupling agent in this work. A weak change in wavenumber (vibrational frequency) were observed, which might have been due to the washing and drying of the filler powder in the surface modification process (i.e. addition of silane-solution, speedmixing and drying). The same procedure was conducted on the fillers without the silane present (water/ethanol was mixed with filler, then dried). The FT-IR spectrum of the unmodified filler powders (after washing and drying) also showed a small shift in wavenumber, which is illustrated by in Figure F.5 in Appendix F, for unmodified mica, modified mica and washed unmodified mica.

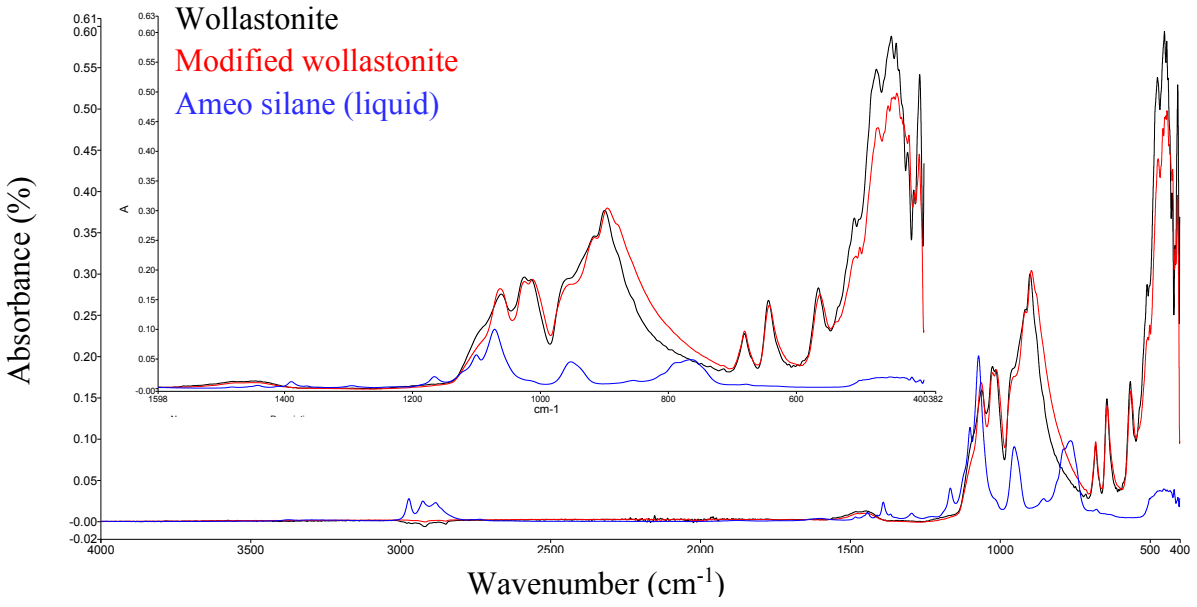

Figure 4.27: FT-IR spectra of wollastonite powder (black), modified wollastonite powder (red) and ameo silane in liquid form (blue). The insert displays the signal from 1500 – 400 cm^{-1} in more detail, and the intensity of the ameo have been lowered due to the other spectra. The spectra were collected with 12 scans and a resolution of 4 cm^{-1} at room temperature.

As the FT-IR signals were obtained from the first 1-2 μm of the sample [68], the signals of the specific surface groups might not have been visible. The analysis of the surface modification process was therefore based on the XPS results. The surface modified fillers were examined using XPS to compare the surface of the fillers prior to and after the modification.

Ideally, the treated filler powders should have been washed prior to the XPS analysis, in order to remove any physiosorbed silane. Since the treated filler powders were tested with XPS without being washed, some of the Si, C and/or N signal might have originated from the physiosorbed silane. It was therefore important to locate the chemical bond between the mineral and the silane or any physical adsorption. The chemical bond might have been a Si-O-M bond where M was either Si, Ca, K, C or another element in the fillers [14].

Table 4.3 displays the percentage atomic concertation of silicon, carbon and nitrogen found on the surface of the surface modified filler powders. The survey spectra of unmodified and modified filler powders are available in figures E.11 – E.15 in Appendix E. All fillers gave rise to signals from silicon, nitrogen and carbon on the surface. Carbon contamination was observed on all unmodified filler surfaces, and the amounts of silicon and nitrogen have therefore been used as an indication of the presence of ameo silane. Signals from both the filler and the ameo silane indicate that the spectra reflect the chemistry of the filler, the ameo silane and the interface between them.

Figure 4.28 displays the high-resolution N1s XPS spectra for all the fillers. The N1s signals were peak fitted as shown in Figure 4.28B), with the C-N and N-H signal at binding energy of ~399.7 eV, and N+ (i.e. protonated amine groups) signal at binding energy of 401.8 eV. The protonated nitrogen groups have previously been observed after surface modification, and their presence has been explained as a result of a reaction between the amine group on the surface modifier and a hydroxyl group on the surface of the substrate or a hydroxyl group on a silanol monomer [11,12,13,31]. The reaction between the amine and the hydroxyl groups has resulted in a strong hydrogen bond and has been considered as a chemisorption of the modification agent to the substrate [12]. The observation of protonated amino groups on m-$BaSO_4$, m-mica, m-wollastonite and wolla-fs (see explanation for abbreviation on page 38) were therefore considered as proof for the existence of an ameo network on the filler surfaces with possible chemisorption through hydrogen bonds between the ameo amine groups and

surface hydroxyl groups. Figure 4.29 illustrates an ameo network on a surface modified filler surface [13]. The specific M-O-Si bond were not observed since they might possibly have overlapped with the other present signals. For instance, the chemical bond between ameo and the wollastonite or mica surface would be Si-O-Ca, Si-O-Si or Si-O-Al. All these bonds are already present in the filler composition, and the signal from a possible Si-O-M bond would be merged with the signal from the filler.

The modified aramid fibers contained minor amounts of silicon and somewhat more nitrogen on the surface, as shown in Table 4.3 (and Figure E.13 in Appendix E). Ai *et al.* [54] successfully modified the surface of kevlar fibers with an alkoxysilane, where the amount of silicon on the surface was 1.8 at.%, which is considerably higher than 0.71 at.% which were observed in this work. Since no hydrogen bonding between the surface and the amine group was observed, and only a small amount of silicon existed on the surface, the surface modification of the aramid fibers seems to have occurred to a minor extent.

During the surface modification process, there is a competing process between the polymerizing involving silanol monomers, and the condensation reaction between the silanol and the mineral surface [14]. The silanol monomers may polymerize outside the filler particles as well as directly on the mineral surface, resulting in a filler particle wrapped in a siloxane-network that can cross-link with the epoxy matrix [13]. The competing polymerization reaction between the silanol monomers may result in “islands” of silanol, which has been observed for ameo silane and polyamides on glass surfaces [12,13]. The “islands” observed for the ameo and polyamide disappeared after a washing procedure of the treated surface after modification. It is therefore believed that a part of the silane signal observed in the XPS results in this work originates from ameo-islands.

The pretreated wollastonite particles (wollastonite-fs) from The Quarzwerke Group were included in the work to compare with the surface modification done in this work. The calcium and silicon spectra were similar for m-wollastonite and wollastonite-fs, indicating the same chemical state of the wollastonite particles in both powders. The chemical state of the amino groups was the only visible difference between m-wollastonite and wollastonite-fs, without considering impurities in the powders. The wolla-fs particles had a higher number of protonated amino groups than the m-wollastonite particles. The ratio of protonated amino groups versus the neutral amino groups is visible as the height difference between the left versus right side of the high-resolution N1s peak in Figure 4.28. The m-mica particles seemed

to have the highest amount of protonated amino groups of all the surface modified powders. This may have indicated that the ameo network were stronger on the m-mica and wollastonite-fs particles than the other m-fillers due to a higher number of hydrogen bonds between the filler/silane-network or silanol/silane-network groups.

Table 4.3: Percentage atomic concentration of silicon, carbon and nitrogen observed on the surface of the modified filler powders. The at.% are collected from the XPS survey spectra.

Element	**m-$BaSO_4$ (at.%)**	**m-mica (at.%)**	**m-aramid (at.%)**	**m-wolla. (at.%)**	**wolla-fs (at.%)**
Silicon	3.98	19.75	0.71	22.40	21.78
Carbon	21.39	8.81	77.57	16.89	10.17
Nitrogen	5.13	1.61	11.06	3.45	1.68

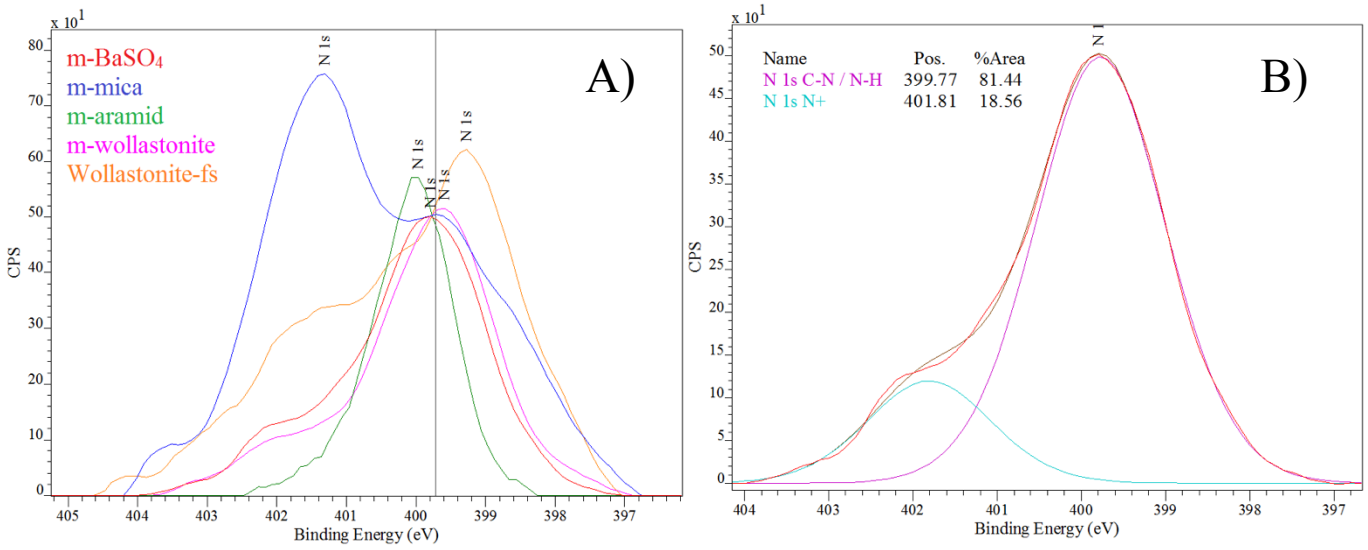

Figure 4.28: A) XPS high-resolution N1s spectra of m- $BaSO_4$, m-mica, m-aramid, m-wollastonite and wolla-fs, and B) peak fitted N1s spectra for m- $BaSO_4$.

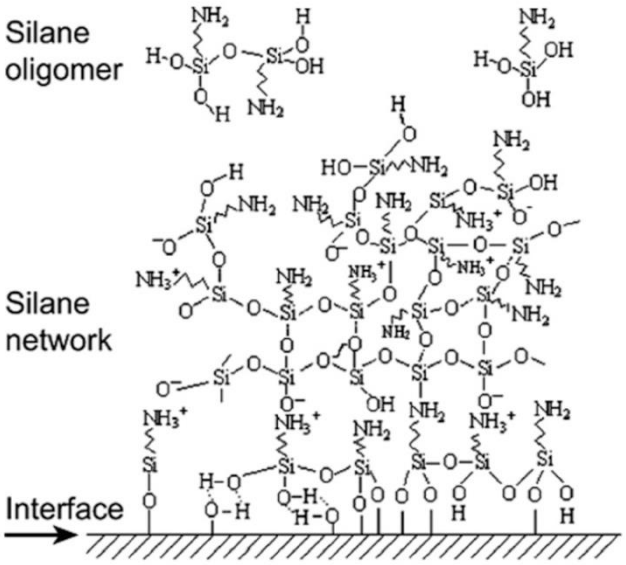

Figure 4.29: Illustration of a possible created ameo network on a surface [13].

4.5.2 Epoxy matrix/filler interaction

The epoxy-filler interaction was expected to be more significant after surface modification, using the ameo silane. All fillers showed signal from silicon and nitrogen using XPS, and all fillers except the aramid fibers had the characteristic protonated amine groups originating from a hydrogen bond with filler-hydroxyl groups or silanol hydroxyl groups (see figures 4.28 and 4.29), indicating the presence of the an ameo silane network.

For the FT-IR analysis, the modified filler was mixed with liquid epoxy in a 1:1 weight ratio. The liquid epoxy/m-filler spectra were compared with the modified filler powder spectra and epoxy/filler spectra in order to observe any new peaks or clear shifts in wavenumber. As seen in Figure 4.30, no additional peaks or shifts was observed for the liquid epoxy/m-wollastonite. The spectra for the other liquid epoxy/m-filler mixtures are available in figure F.6 – F.9 in Appendix F (m-aramid was not tested due to poor modification, as observed using XPS (page 83-85) and mechanical tests (Section 4.5.4, page 93).

The liquid epoxy/m-filler spectra were also compared to the pure liquid epoxy spectra and epoxy/filler spectra. The FT-IR spectra of liquid epoxy/m-$BaSO_4$ and liquid epoxy/m-wolla mixtures did not reveal chemical shifts for any chemical groups. The corresponding spectrum of liquid epoxy/m-mica mixture revealed a change in wavenumber for the ether groups and a chemical shift change for the aromatic rings with reference to the epoxy/mica sample. The total shift in wavenumber from the pure liquid epoxy was +0.64 cm^{-1} for the C=C signal,

+2.54 cm^{-1} for the C_{phenyl}-O signal and -4.03 cm^{-1} for the $C_{aliphatic}$-O signal. The spectrum of the epoxy/wolla-fs mixture also showed a significant change in wavenumber for the ether groups and the aromatic rings with reference to the pure liquid epoxy: +0.36 cm^{-1} for the C=C signal, +1.59 cm^{-1} for the C_{phenyl}-O signal and -1.72 cm^{-1} for the $C_{aliphatic}$-O signal. The spectra displaying the shifts are available in figures F.11 and F.12 in Appendix F. The enhanced shift of wavenumber was closer to the shift that Hammer *et al.* observed for the interaction between Ba^{2+} (from $BaSO_4$) and carboxyl carbonyl, which was 3 cm^{-1} [33].

The observed wavenumber/frequency shift for the liquid epoxy/m-mica and liquid epoxy/wolla-fs samples could not in themselves prove the existence of an interaction since the shift also might have been present as a result of increased filler concentration in the mixture. The XPS results are therefore also included to further investigate possible interaction.

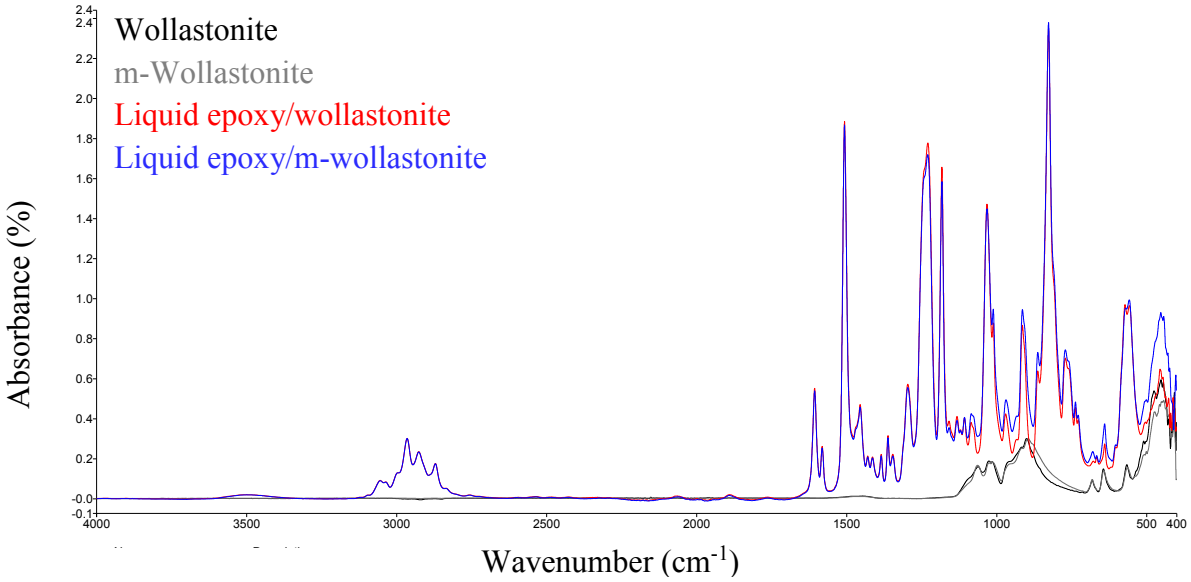

Figure 4.30: FT-IR spectra of unmodified wollastonite powder (black), modified wollastonite powder (grey), a liquid epoxy/wollastonite mixture (red) and a liquid epoxy/m-wollastonite mixture (blue).

To analyze the epoxy-filler interaction using XPS, the fractured surfaces from flexural testing were analyzed since the fractured surface contained both the epoxy matrix, the filler surface and the interface between them (was observed using fractography, see page 100). In Section 4.1, where the epoxy-filler interaction of the epoxy/filler samples were discussed, the XPS analysis was conducted on the cross-section of non-fully cured films, while the epoxy/m-filler samples presented in this section were fully cured. The fracture surface of the pure epoxy was also examined as a reference

using XPS. The spectra of the reference sample presented in Section 4.5.6 and the reference fracture surface are compared in figures 4.31 and 4.32. The high-resolution C1s spectra overlapped, except for an additional peak in the fracture surface sample at 286.9 eV, attributed to epoxide groups based on the binding energy [56]. Increased number of epoxide groups in the fracture surface may have indicated that the samples fractured where the free epoxide groups were present, in contrary to the cross-section samples where the samples were fractured breaking the films by hand with a higher speed and stress. The N1s spectrum of the fracture surface was slightly shifted compared to the cross-section sample, indicating a greater number of N-H bonds. An additional signal at 400.6 eV probably results from the curing agent.

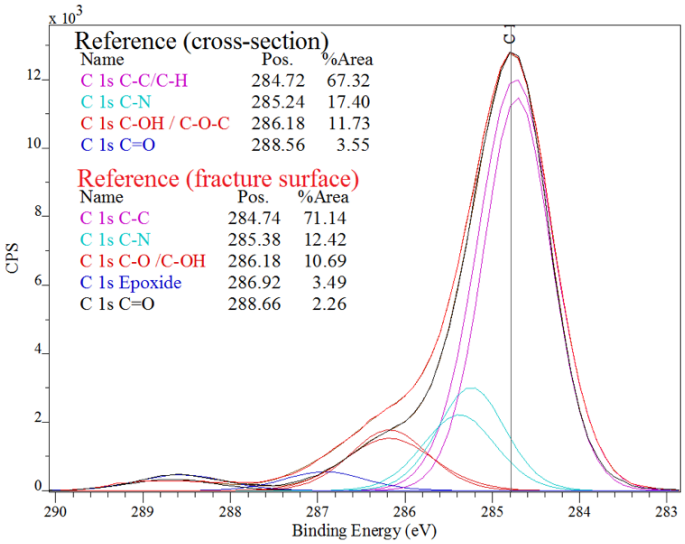

Figure 4.31: The high-resolution C1s spectra of the reference cross-section (black line) and fracture surface (red line) samples.

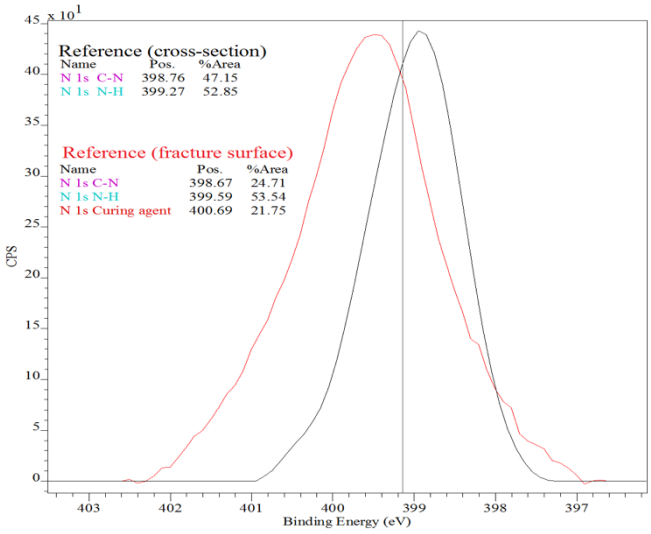

Figure 4.32: The high-resolution N1s spectra of the reference cross-section (black line) and fracture surface (red line) samples.

All the epoxy/m-filler samples yielded signal from filler particles, but the epoxy/wolla-fs sample only had a low signal from wolla-fs particles in the fracture sample (shown in the survey spectra, Figure E.16 in Appendix E). The chemical shifts in the C1s peaks are presented in Table 4.4 and were determined as described at page 50 for the epoxy/filler samples. The C-C, C-N, and C-OH/C-O-C signals appeared at roughly the same binding energies as in the epoxy/filler samples and these bonds are consequently not considered to have been altered by the modified fillers. New bonds or interactions were expected to be visible as new peaks or larger shifts binding energy. The C1s spectra of the fractured surfaces, see Figure 4.33, appeared with an additional peak due to epoxide groups, which not were present in the cross-section samples in the epoxy/filler films. Since the epoxide peak was observed for the fracture surface of the reference sample as well, the more intense epoxide

signal in the epoxy/filler films, have been explained by the fact that the filler particles were hinders for uncured epoxide groups meeting amine groups during the film formation. Uncured epoxide groups were probably observed in the reference film as well since the chain mobility decreases during film formation as explained in the Theory and background section (see page 4-5). The percent area determined using peak fitting of the C1s peak for the epoxy/m-filler films is presented in Table 4.5 (peak fitting and percentage area determination explained in page 28). The reference film had the smallest %Area of epoxide groups, and the concentration of epoxide groups increased (based on %Area) in the order reference < epoxy/m-wolla < epoxy/m-mica < epoxy/m-$BaSO_4$ < epoxy/wolla-fs < epoxy/m-aramid. Aramid fibers have earlier shown a trapping effect on epoxide groups [64], resulting in regions with unreacted epoxide groups. This behavior may have explained the high number of epoxide groups observed in this work. The increased number of uncured epoxide groups in the epoxy/filler films probably contributed to the lowered strength of the samples.

The epoxy/m-$BaSO_4$, epoxy/m-mica, epoxy/m-aramid and epoxy/m-wolla samples gave rise to a new shake-up satellite peak compared to the observation for the epoxy/filler samples, as illustrated by the epoxy/m-$BaSO_4$ C1s spectrum in Figure 4.33. Shake-up satellites are additional peaks observed that occur from an interaction between an outgoing photoelectron and a valence electron [46]. The photoelectron will lose some of its kinetic energy and appear in the XPS spectrum at a higher binding energy than it originally had. In polymers, shake-up satellites tend to originate from interaction between a photoelectron and a delocalized electron in an aromatic ring [46]. The new/increased signal from the shake-up satellite might have indicated that the aromatic rings are more concentrated in the facture surfaces in the samples, giving rise to the shake-up satellites.

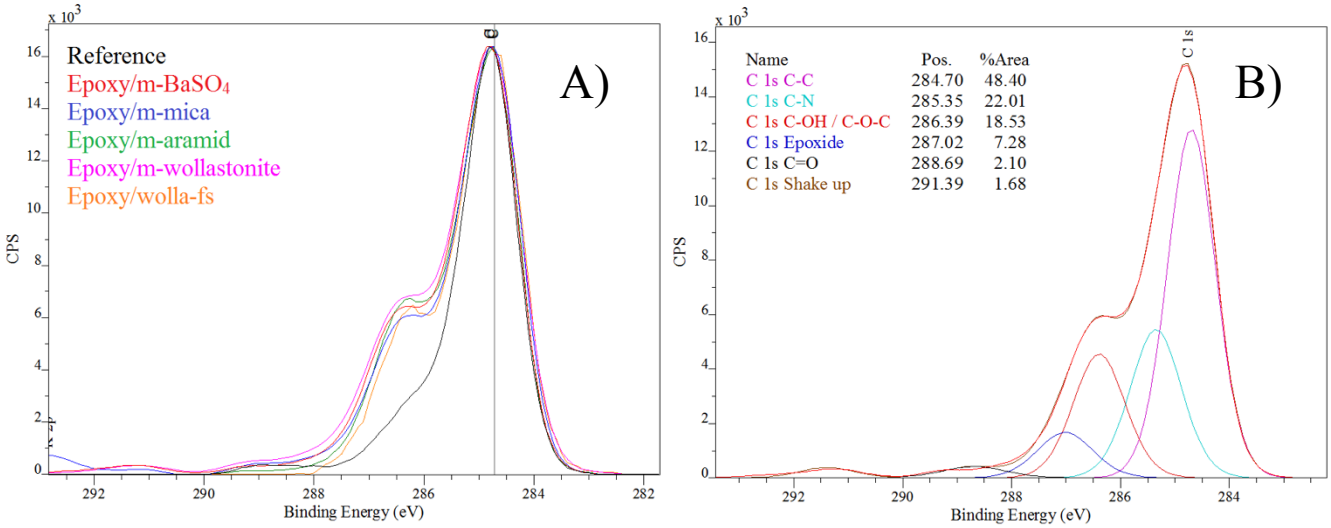

Figure 4.33: A) high-resolution C1s spectra of the epoxy/m-filler samples and B) high-resolution peak fitted C1s spectra of the epoxy/m-$BaSO_4$ sample for illustration of the peak contribution.

Table 4.4: Chemical shifts observed in the C1s peaks for the epoxy/filler and epoxy/m-filler samples. For explanation to the chemical shifts from Beamson and Briggs, see page 50.

Chemical bond	Reference Reference -fracture	BaSO4 m-$BaSO_4$	Mica m-Mica	Aramid m-Aramid	Wollast. m-Wolla. Wolla-FS	Chemical shift from Beamson and Briggs [56]
C-C / C-H	0 0	0 0	0 0	0 0	0 0 0	0
C-N	0.5 0.7	0.5 0.7	0.4 0.6	0.5 0.6	0.7 0.7 0.6	0.56 – 1.41
C-OH / C-O-C	1.5 1.5	1.6 1.7	1.2 1.7	1.5 1.7	1.5 1.8 1.7	1.13-1.75
C-O-C Epoxide	- 2.2	- 2.3	- 2.4	- 2.0	- 2.5 2.1	2.02
C=O/ C-O-C*=O	3.9 4.0	4.3 4.0	3.9 4.1	4.0 4.0	- 4.0 -	2.81-2.97/ 3.64-4.23

Table 4.5: Percent area (%Area) determined by deconvolution of C1s signal of epoxy/m-filler samples.

Chemical bond	Reference	Epoxy/m-$BaSO_4$	Epoxy/m-Mica	Epoxy/m-Aramid	Epoxy/m-wollastonite Epoxy/wolla-fs
C-C	71.1	48.4	42.2	44.7	47.9 46.3
C-N	12.4	22.0	24.8	24.7	21.1 30.9
C-OH / C-O-C	10.7	18.5	20.7	17.6	21.0 13.5
Epoxide	3.5	7.3	5.7	12.2	5.3 9.31
C=O	2.3	2.1	2.0	0.83	3.12 -

The XPS high-resolution N1s spectra of the epoxy/m-filler samples are presented in Figure 4.34. The peak fitted N1s peak for the epoxy/m-mica sample are also displayed in Figure 4.34 to illustrate the chemical bonds that contributed to the peak. The protonated amine groups on m-$BaSO_4$, m-mica, m-wolla and wolla-fs particles were also observed in the high-resolution N1s spectra of the epoxy/m-filler samples for epoxy/m-$BaSO_4$, epoxy/m-mica and epoxy/m-wolla samples. This observation indicates that the ameo network still was present on the filler surfaces after the fracture had occurred. This finding indicated that if there was a filler-ameo-epoxy bond, the fracture was likely to happen between the ameo and the epoxy, and not between the filler and the silane. For the reference, epoxy/m-aramid and epoxy/wolla-fs samples, no signal from the protonated amine groups was observed due to absence of silane (reference), a poor modification process (aramid fibers), and low signal from the filler particles in the epoxy/wolla-fs sample, respectively.

The chemical state of the elements in the filler particles were observed through the high-resolution XPS spectra of the elements. As in Section 4.1 (see page 51), the high-resolution spectra of the various elements in the fillers were compared between the filler particles in powder form and when incorporated in the epoxy matrix. Neither new peaks nor chemical shifts were observed when comparing the high-resolution spectra of the elements in the fillers, for any of the fillers. The spectra are displayed in figures E.4 to E.8 in Appendix E.

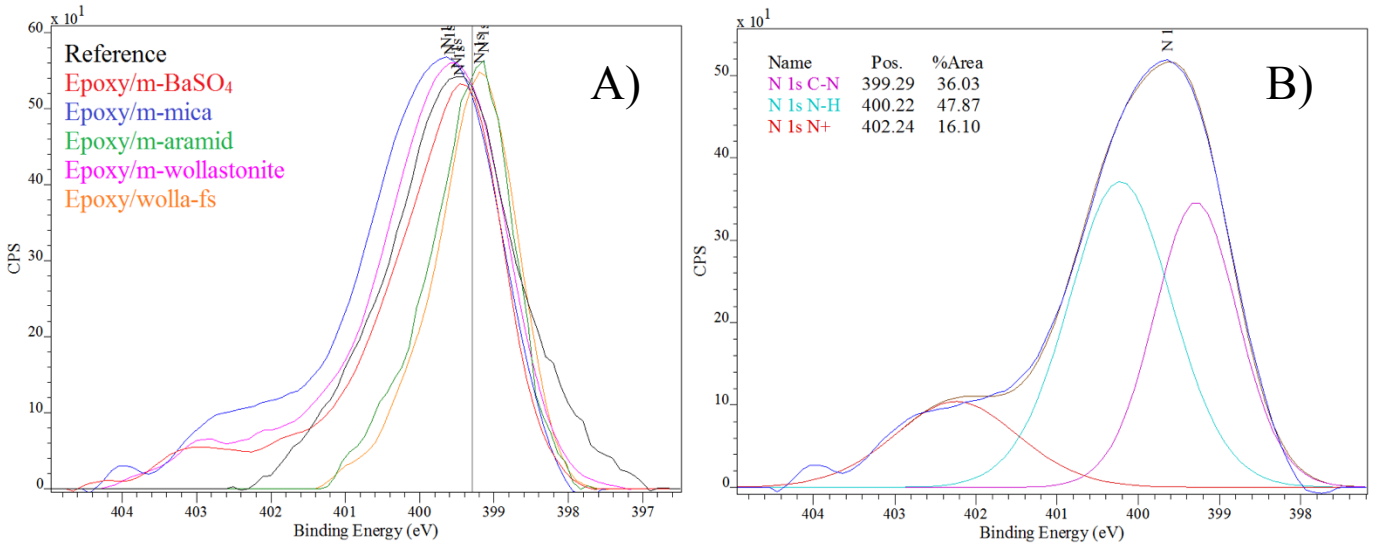

Figure 4.34: A) high-resolution N1s spectra of the epoxy/m-filler samples and B) high-resolution peak fitted N1s spectra of the epoxy/m-mica sample to illustrate the peak contribution.

4.5.3 Distribution and orientation

Well distributed filler particles are needed to ensure wanted physical and mechanical properties of polymer/filler materials (see page 57). The distribution of filler particles in the epoxy/m-filler samples was examined in the same way as for the epoxy/filler samples (page 40 and 57). All epoxy/m-filler films, with wet thickness in the range 200-1200 μm, showed a good distribution, and images of several film with various thickness are available in Appendix G.

Agglomeration of filler particles may lead to a decrease in strength and toughness since stress concentration may occur and the silane effect may decrease. Agglomeration was observed during the speedmixing between the liquid epoxy and modified $BaSO_4$ and modified wollastonite powders. Improvement of the mill base and increasing mixing time were tested with little success, especially for the epoxy/m-$BaSO_4$ mixture. Figure 4.35 shows the agglomerates observed in the epoxy/m-$BaSO_4$ films where some agglomerates are marked with red circles. In addition, a close-up image of a m-$BaSO_4$ agglomerate is shown. Figure 4.36 shows a close-up image of a m-wollastonite-agglomerate, where it is demonstrated that several small particles have flocculated. During the surface modification process, the silanol groups may react with the mineral surface or to another silanol molecules. In this way, particles can be bound together with a siloxane-network (see Figure 4.29, page 86). It will then be hard to distribute the agglomerates.

For m-mica and m-wollastonite, the same orientation of particles as for the epoxy/filler samples was observed. The orientation of the wollastonite-fs in the epoxy/wolla-fs films was investigated and the same tendency as the epoxy/(m-)wolla films was observed. The orientation was not studied in as great detail as in Section 4.1.3 for the epoxy/wollastonite films, but images of horizontal and vertical cross-sections are shown in Figure G.5 in Appendix G.

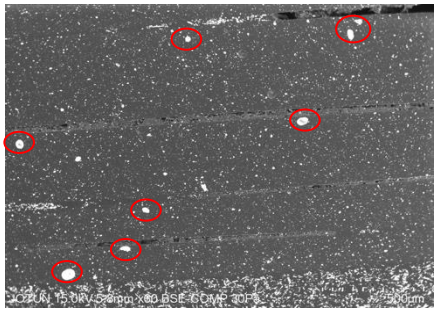

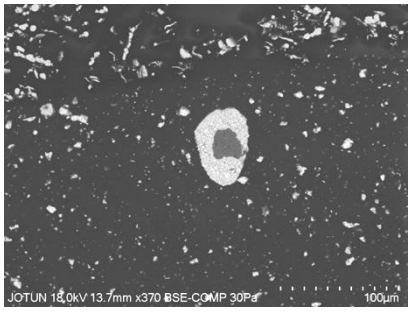

Figure 4.35: Epoxy/m-$BaSO_4$ films with agglomerates (left image) and close-up image of a m-$BaSO_4$ agglomerate (right image).

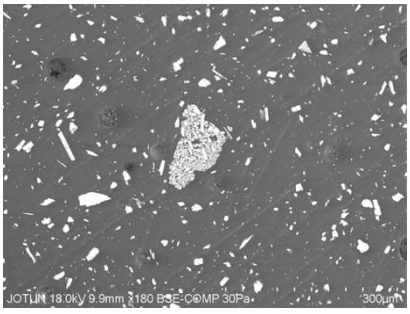

Figure 4.36: Image of a m-wollastonite agglomerate

4.5.4 Mechanical properties

The effect of surface modification of filler particles in coatings/plastics depends on the surface modifying agent used. Common for functional surface modifiers which have the ability to cross-link to the polymer is an increase in rigidity and strength. The surface modifier then couples the filler and the polymer, yielding a more rigid structure, with higher strength, but possibly the same or a smaller elongation ability [14].

The flexural test results are presented in Figure 4.37, where the epoxy/filler results are marked using bold lines, and the epoxy/m-filler results are represented by the thin lines. Figure 4.38 presents the stress and strain at break from flexural testing on both epoxy/filler and epoxy/m-filler samples. Surface treatment of mica and wollastonite yielded increased strength at the same elongation, as compared to the samples containing the unmodified particles. The epoxy/wolla-fs samples had high strength and toughness. As discussed above, the wolla-fs powder consisted of smaller particles than m-wollastonite, might explained the increased strength. The epoxy/wolla-fs samples had almost the same stress at break as the ultimate stress for the pure epoxy reference samples, and increased stress at break as compared to the reference sample. The size of the wolla-fs particles made it possible for the epoxy-matrix to stretch around the particles. The high strength was likely to be caused by the surface modification, where the silane was a coupling agent between the wollastonite-fs

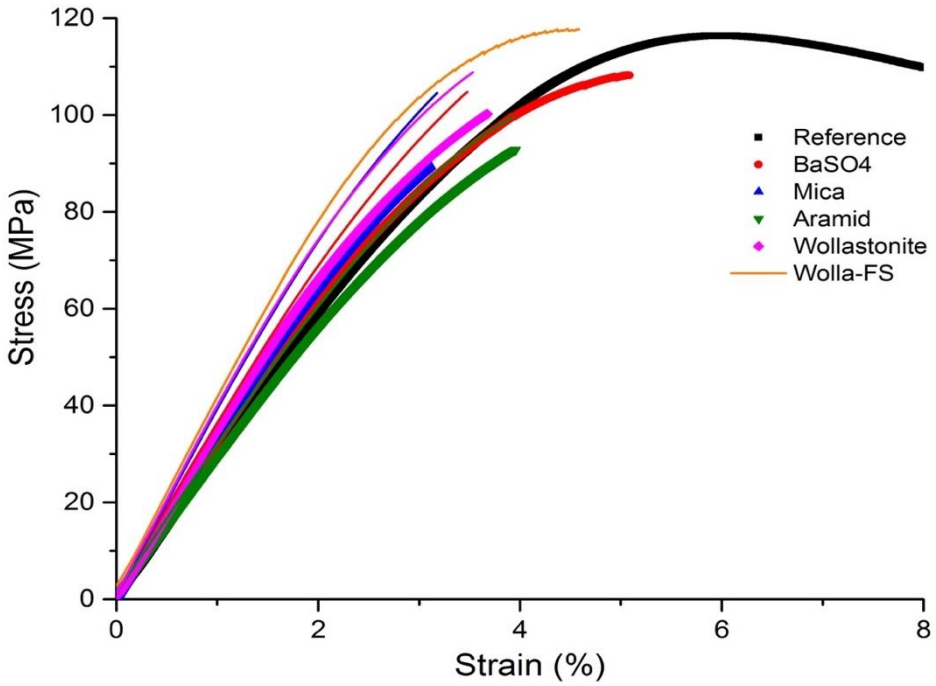

Figure 4.37: Stress-strain curves from flexural tests of epoxy/filler samples (bold lines) and epoxy/m-filler samples (thin lines). The tests are conducted at room temperature using UTM.

particle and the epoxy-structure. The elongation of the epoxy/m-$BaSO_4$ samples were less than for the epoxy/$BaSO_4$ samples, which could be explained by the observed agglomeration of particles, or the fact that the epoxy matrix now was coupled to fillers by the silane coupling agent. A stretching of epoxy matrix around the $BaSO_4$ particles might therefore have been constricted. The strength, displayed as stress at break, did not change as a result of surface treatment. This could indicate that the decrease in elongation due to agglomeration or hindered stretching (as a result of a chemical bond between the silane and the epoxy-matrix) were compensated by the increased strength by the silane coupling agent. This might have caused the same at break for the epoxy/$BaSO_4$ and epoxy/m-$BaSO_4$ samples. The m-$BaSO_4$ and wolla-fs particles were of the same size but had different chemistry and probably not the same concentration of silane on the surface. The results from the epoxy/$BaSO_4$ and epoxy/wolla-fs were compared to see correlations due to the size of the particles, and to avoid contribution to the results from the agglomeration of the m-$BaSO_4$ particles. From Figure 4.38, one may see that the epoxy/wolla-fs samples had approximately the same strain at break as the epoxy/$BaSO_4$ samples and the stress at break were higher for the epoxy/wolla-fs compared to the epoxy/ $BaSO_4$. The chemistry of the m-wollastonite and wollastonite-fs particles were the same and the only clear difference between the particles was the size,

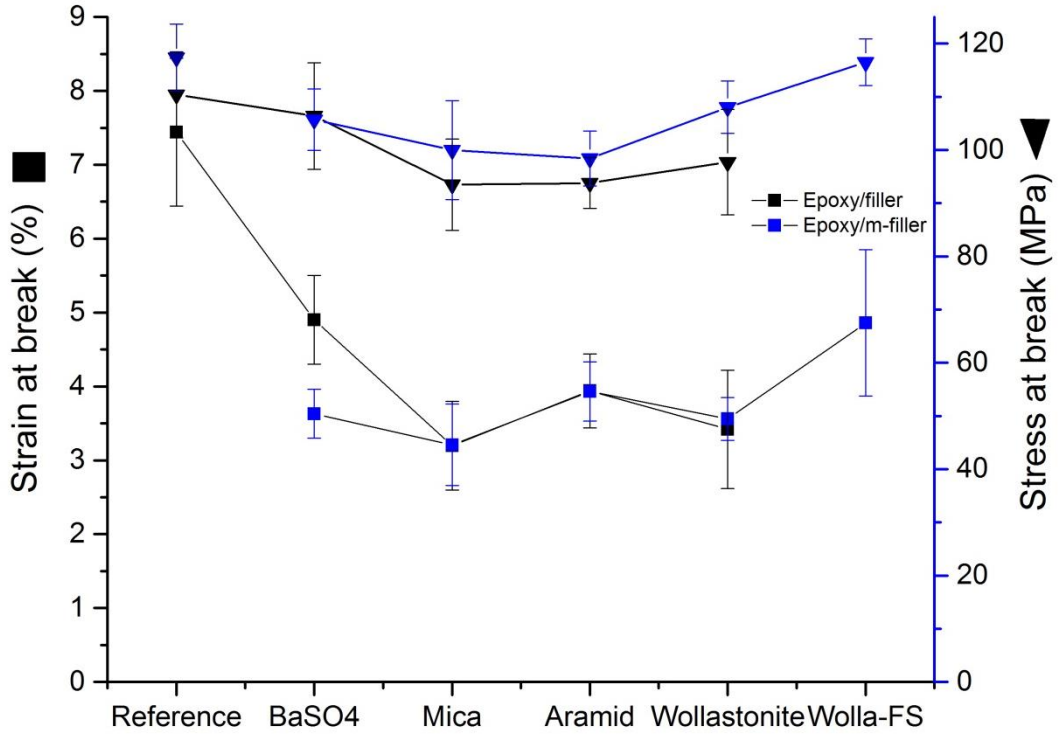

Figure 4.38: Stress and strain at break values from flexural test conducted at room temperature for epoxy/filler (black points) and epoxy/m-filler (blue points) samples.

where the m-wollastonite particles had an average particle size of 12 μm and the wollastonite-fs of 3.5 μm. The strain and stress at break were higher for the epoxy/wolla-fs samples compared to the epoxy/m-wollastonite samples. The comparison between the results of the epoxy/wolla-fs samples to the epoxy/$BaSO_4$ and epoxy/m-wollastonite samples indicated that if considering elongation properties of the epoxy/filler samples, the size of the particle may be of bigger influence than for instance the chemistry and shape of the filler particles. However, if considering the strength properties of the samples, the chemistry and shape of the filler particles may have a larger influence.

The epoxy/m-aramid samples had the same strain at break and a slightly larger stress at break in the flexural test results, as compared to that of the epoxy/aramid samples. Considering the standard deviation, the increase in strength was almost negligible, but a larger difference after surface modification as compared to the epoxy/m-$BaSO_4$ sample was obvious (see Figure 4.38). In Figure 4.37, the stress/strain curve for the epoxy/m-aramid sample follows the epoxy/$BaSO_4$ curve and is displayed as the thin green line. The stress/strain curve revealed slightly higher strength and toughness of the epoxy/m-aramid sample, as a result of the surface modification of the filler particles. As discussed in Section 4.5.1, the surface modification of the aramid fibers was problematic, and this circumstance might have explained that the stress-strain behavior was similar to that of the epoxy/aramid samples.

The tensile test results should ideally have showed the same trend as the flexural test results. As discussed above, the experimental uncertainty in the tensile test was high for the brittle samples tested in this work. The epoxy/m-filler samples were also tested with the tensile test

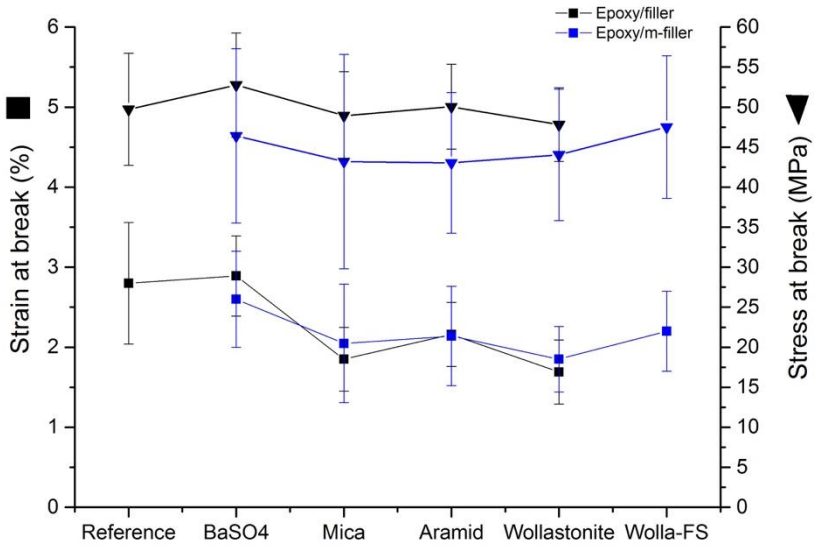

Figure 4.39: Strain (■) and stress (▼) at break from tensile tests of epoxy/filler (black points) and epoxy/m-filler (blue points) samples.

and the results are presented in Figure 4.39. The strain at break were identical for the epoxy/filler and epoxy/m-filler samples, and considering the experimental uncertainty, the stress at break were also similar. These results were not considered to be able to illustrate the effect of surface modification of the filler particles, due to the high experimental uncertainty.

The DMA results are presented in figures 4.40-4.42. The storage modulus and tan δ curves are presented in Figure 4.40. The storage modulus curves were similar to that of the epoxy/filler samples, indicating that the silane groups did not change the epoxy matrix to such an extent that they changed the mechanical properties tested using the DMA. The position and shape of the tan δ peak representing the glass transition did not change for the epoxy/m-filler samples either, if considering the experimental uncertainty.

The width and height of the tan δ peaks are presented in Figure 4.42 (see definition for height and width at page 69). They were roughly unchanged and within the experimental uncertainty for all samples, except for the epoxy/m-mica sample. The height of the peak increased after surface modification of mica, which may be explained by the hypothesis that it was easier for the epoxy segments to move around/beside the mica flakes when the silane coupling agent was present. This indicates that the silane acted as a bridge between the mica-flake and the epoxy structure. The other epoxy/m-filler samples did not display differences, likely due to easier movement of the epoxy segments around the fillers particles, independent of silane treatment.

The glass transition temperatures of the various epoxy samples are presented in Figure 4.41. Within experimental uncertainty (the standard deviations are shown as error bars in the figure), the T_g's were the same for all samples, with the possible exception for the epoxy/m-$BaSO_4$ sample, where the T_g decreased by approximately 4°C. This decrease in T_g was probably a result of agglomeration of the m-$BaSO_4$ particles, as the agglomerates probably gave rise to regions of epoxy matrix with a lower cross-link density.

Based on expected increased interactions between the filler particles and the epoxy matrix after surface modification, the T_g was expected to have increased, since the polymer network was believed to be more cross-linked [51]. The addition of the ameo-silane containing a primary amine functional group was also expected to increase the cross-link density as the amine was thought to cross-link with the epoxy-network. A possible explanation to the lack of such positive results could be that the mechanical properties tested in the DMA-measurements were within the linear viscoelastic region (LVR). Movement of the epoxy segments were not large enough to see a clear

manifestation of the silane coupling agent. The results of the flexural test, which tests the material outside the LVR as well, clearly showed the effect of the silane by a larger difference in the results of the reference and the epoxy/(m-)filler samples (e.g. difference in stress/strain at break).

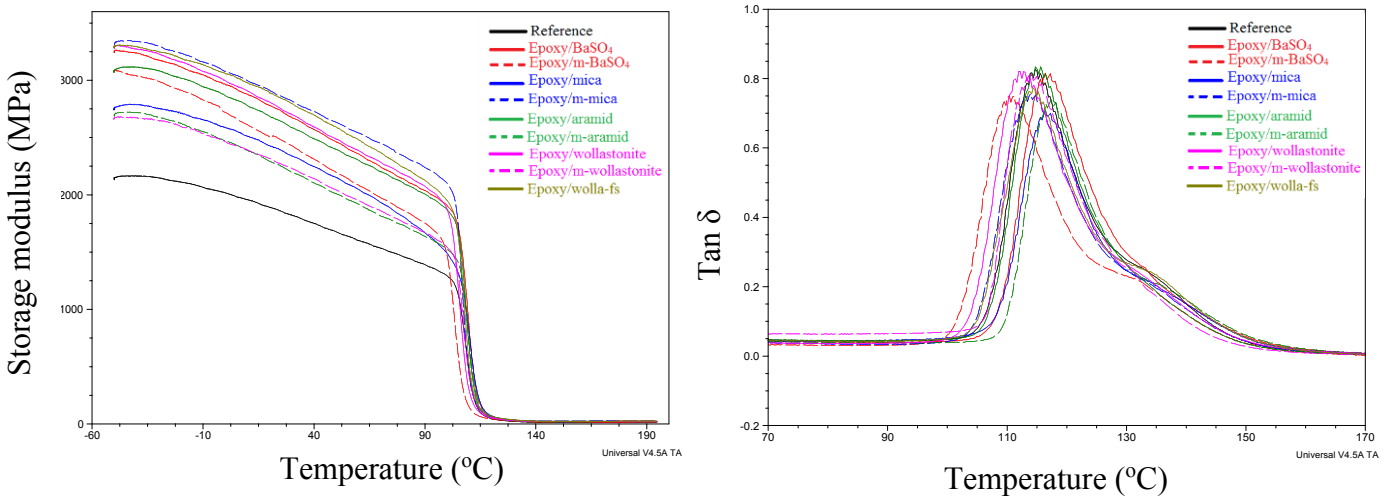

Figure 4.40: The storage modulus curves (left) and tan δ curves (right) for the epoxy/filler and epoxy/m-filler samples from DMA-measurements at a frequency of 1 Hz, an amplitude of 5µm and temperature ramp of 5°C/min.

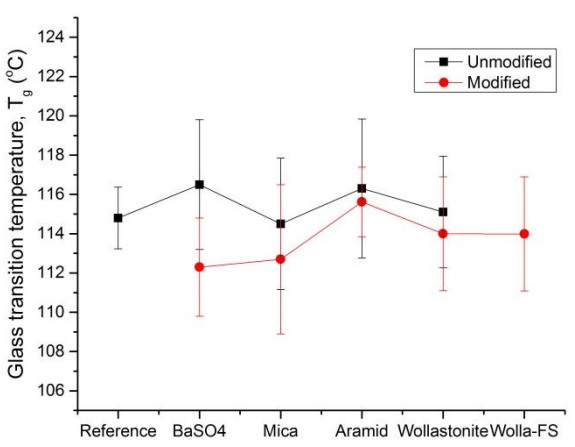

Figure 4.41: The glass transition temperatures defined as the temperature at the peak of the tan δ curve (see Figure 4.40) for the epoxy/m-filler and epoxy/filler samples.

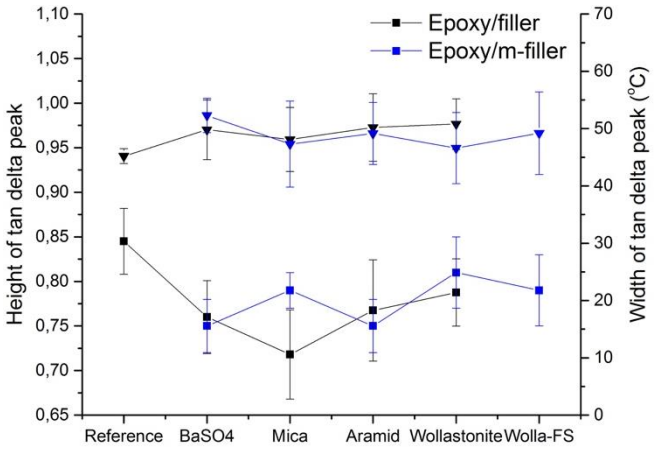

Figure 4.42: The height (■) and width (▼) of the tan δ peaks for the epoxy/m-filler (blue points) and epoxy/filler (black points) samples.

The values of various moduli of the epoxy/m-filler samples are presented in Figure 4.43 and compared to the corresponding values of the epoxy/filler samples. The results of the samples with and without the silane varied due to type of test (Youngs modulus from tensile test, bending modulus from flexural test and storage modulus from DMA-measurements). As values of the moduli are determined in the linear viscoelastic region, these values should ideally show the same trend in all tests. Considering all test results, one may conclude that the moduli values did not change significantly, in agreement with the small differences seen for the DMA-results. The epoxy/m-filler samples revealed the same influence on the modulus at high temperature (160°C), as shown in Figure 4.43 D).

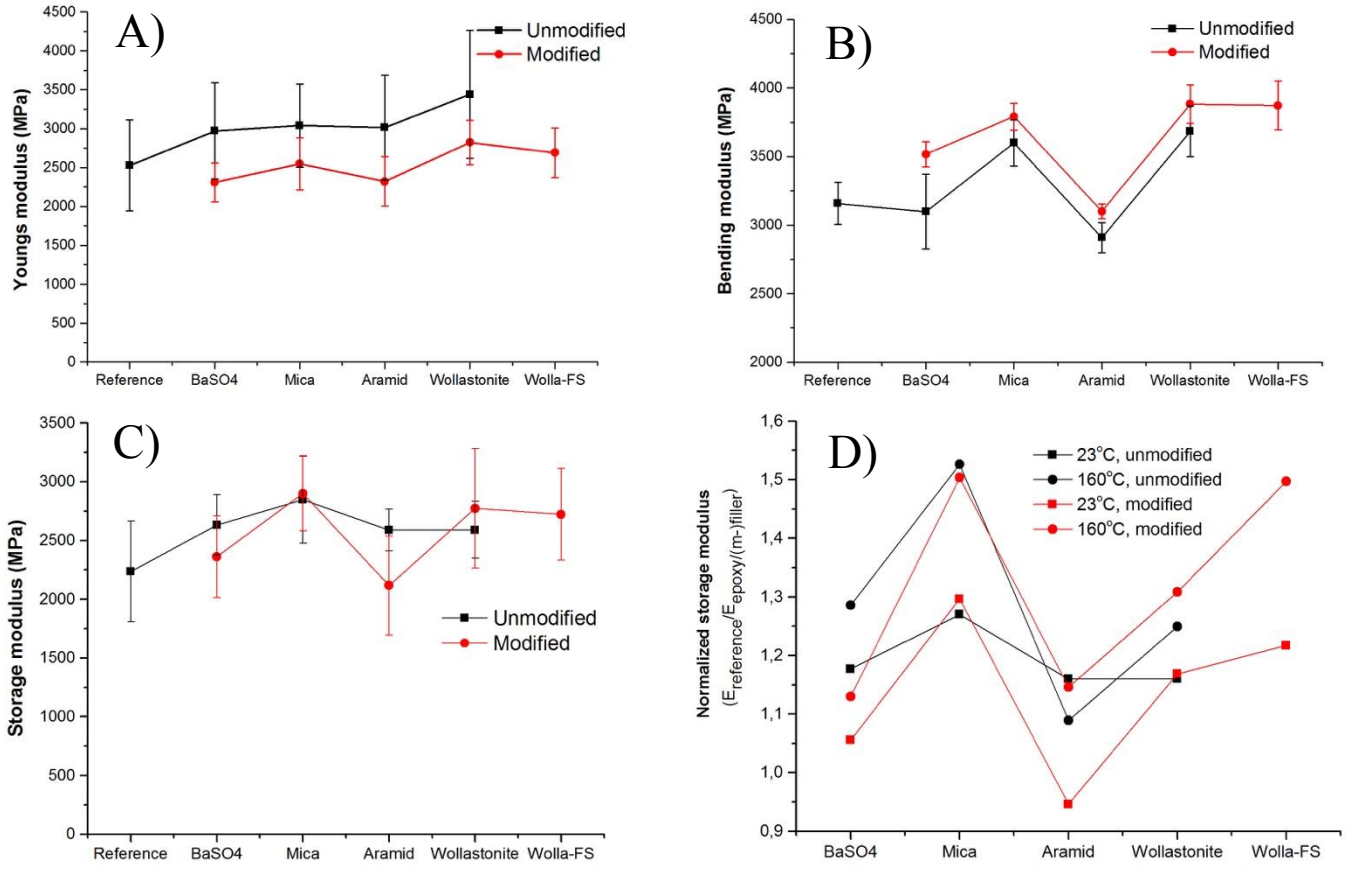

Figure 4.43: A) Youngs modulus, B) bending modulus and C) storage modulus of epoxy/filler and epoxy/m-filler samples, measured at room temperature using tensile test, flexural test and DMA, respectively. D) shows the normalized storage modulus at 23°C and 160°C for the epoxy/filler and epoxy/m-filler samples.

4.5.5 Permeability of water vapor

The XPS results from the fractured surfaces of the epoxy/m-filler samples showed signal from protonated amine groups, which indicated that the silane network was present on the filler particles pointing out of the fracture. Based on these results, the permeability of water vapor of the epoxy/m-filler samples was expected to have decreased since the polymer network was expected to be denser with the silane network possibly filling the voids between the epoxy matrix and the filler particles.

The permeability of water vapor of the epoxy/m-filler samples is presented in Figure 4.44. A decrease in permeability as compared to the epoxy/filler samples is demonstrated. Considering the experimental uncertainty, the epoxy/m-aramid and possibly the epoxy/m-$BaSO_4$ and epoxy/m-wollastonite samples showed a distinct difference in permeability. After surface modification of the fillers, using ameo, the desired result was a tighter network with a chemical bond between the filler, the ameo and the epoxy. The observed decrease in permeability was therefore believed to be caused by an increased filler-silane-epoxy interaction and/or less voids between the filler particles and the epoxy matrix. The effect of the modification of the fillers was most marked for the aramid fibers. The epoxy/aramid samples contained a number of air bubbles in the films. Air bubbles were also seen in the films with the surface modified aramid fibers, as shown in Figure 4.45. The decrease in permeability has therefore been explained by a decrease in voids between the aramid fibers and the epoxy, due to the presence of the silane. Ismail *et al*. also observed reduction in the permeability of various gases by a reduction in the voids between the organic/inorganic phases in a polymeric material by the use of the ameo coupling agent [32].

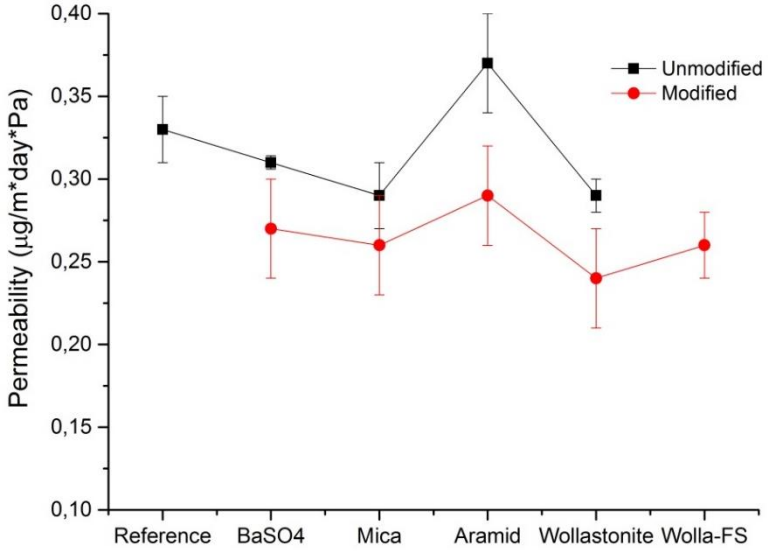

Figure 4.44: Measured permeability for the epoxy/filler (black points) and epoxy/m-filler (red points) samples with Payne Permeability cups at 40ºC.

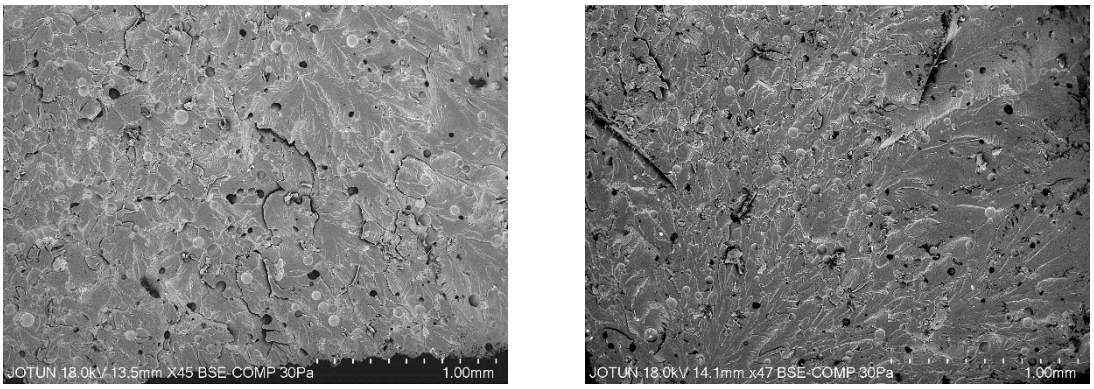

Figure 4.45: Fracture surfaces from flexural tests of epoxy/aramid (left) and epoxy/m-aramid (right), illustrating air bubbles observed in the samples.

4.5.6 Fractography

The fracture surfaces had the same rough surface structure after surface modification of the fillers. Figure 4.46 show the corresponding fracture surfaces of the flexural samples, where the epoxy/m-filler samples appeared smoother than the reference sample surface, but by increasing the magnification one sees a rough surface in Figure 4.47. The images in this figure were taken using the samples from the tensile test and show how the filler particles were left in the fractures. The roughness of the samples indicated that the samples still fractured near the fillers. However, more force was necessary to achieve fracture.

The fracture surface of the epoxy/m-$BaSO_4$ did not change, in compliance with the small and unchanged mechanical properties observed compared to the samples containing unmodified $BaSO_4$. As seen from Figure 4. 47, image E) and F), the aramid fibers in the epoxy/m-aramid sample seemed to be more covered of epoxy than the unmodified aramid fibers in the epoxy/aramid samples. The conditions used on the SEM in order to obtain the two pictures, E) and F), were about the same, and the color difference between the fibers in the two images were thought to be explained by a layer of epoxy on the aramid fibers in the epoxy/m-aramid sample, giving the fiber a slightly darker grey appearance.

The fracture surface of epoxy/m-mica showed that the m-mica particles were slightly tighter attached to the epoxy matrix than the uncoated mica particles, as seen in Figure 4.47 C) and D). The difference between the samples containing coated and uncoated mica particles was smaller than expected, referring to the observed increase in flexural strength.

The surface modification of wollastonite yielded increased strength of the epoxy/m-wolla samples compared to the epoxy/wolla samples (Figure 4.38, page 94). This was also visible in fractography analysis as shown in in Figure 4.47 G) and H), where the m-wollastonite particles seemed to be attached to the epoxy to a larger degree than for the unmodified particles. The wolla-fs particles were clearly attached to the epoxy-matrix, indicating an interaction between the filler particles and the epoxy matrix. It was difficult to observe a differences in the covering of the filler particles between m-wollastonite and wollastonite-fs to the epoxy matrix since the size of the particles differed.

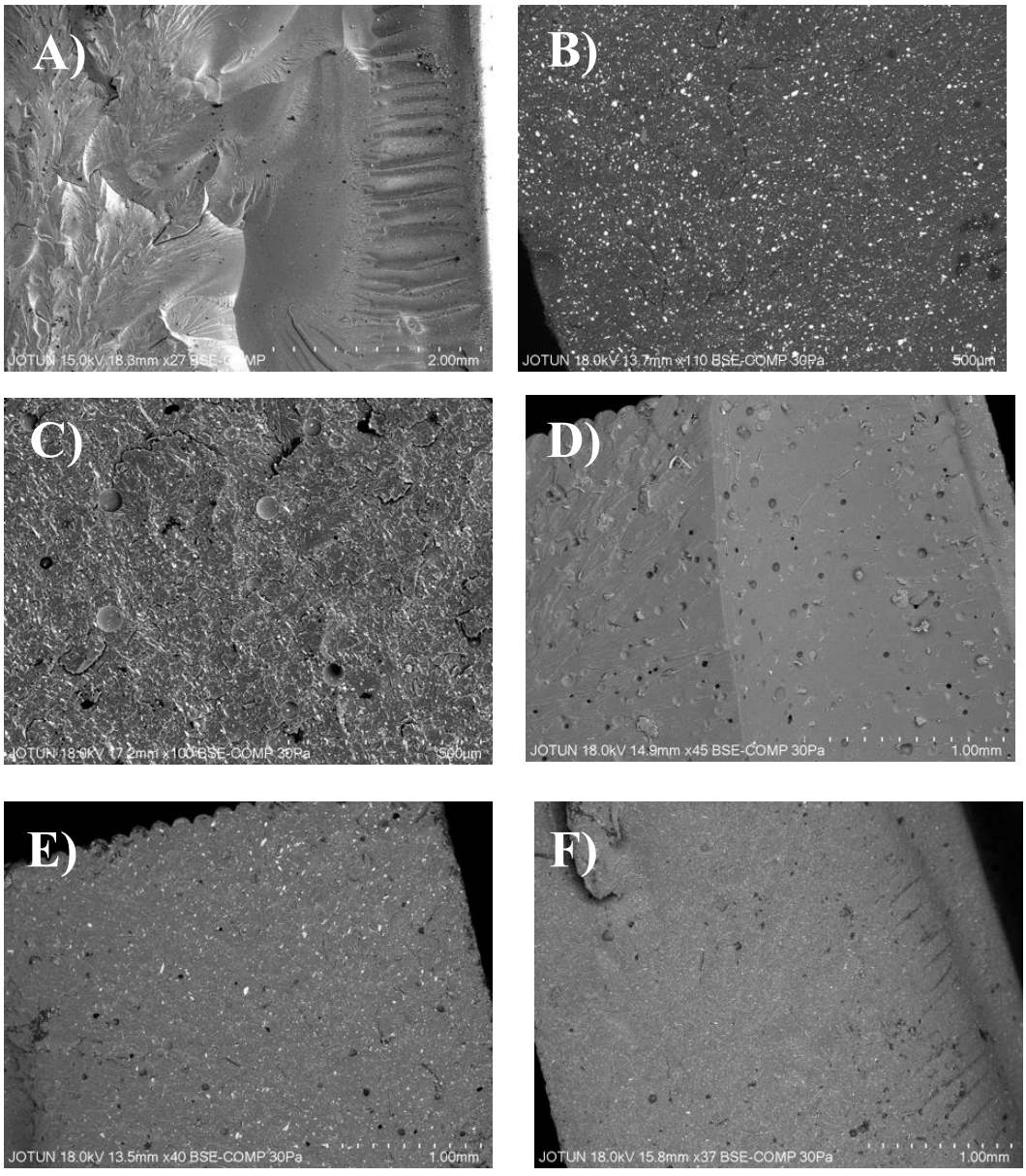

Figure 4.46: Flexural test fracture surfaces of A) reference, B) epoxy/m-$BaSO_4$, C) epoxy/m-mica, D) epoxy/m-aramid, E) epoxy/m-wolla and F) epoxy/wolla-fs.

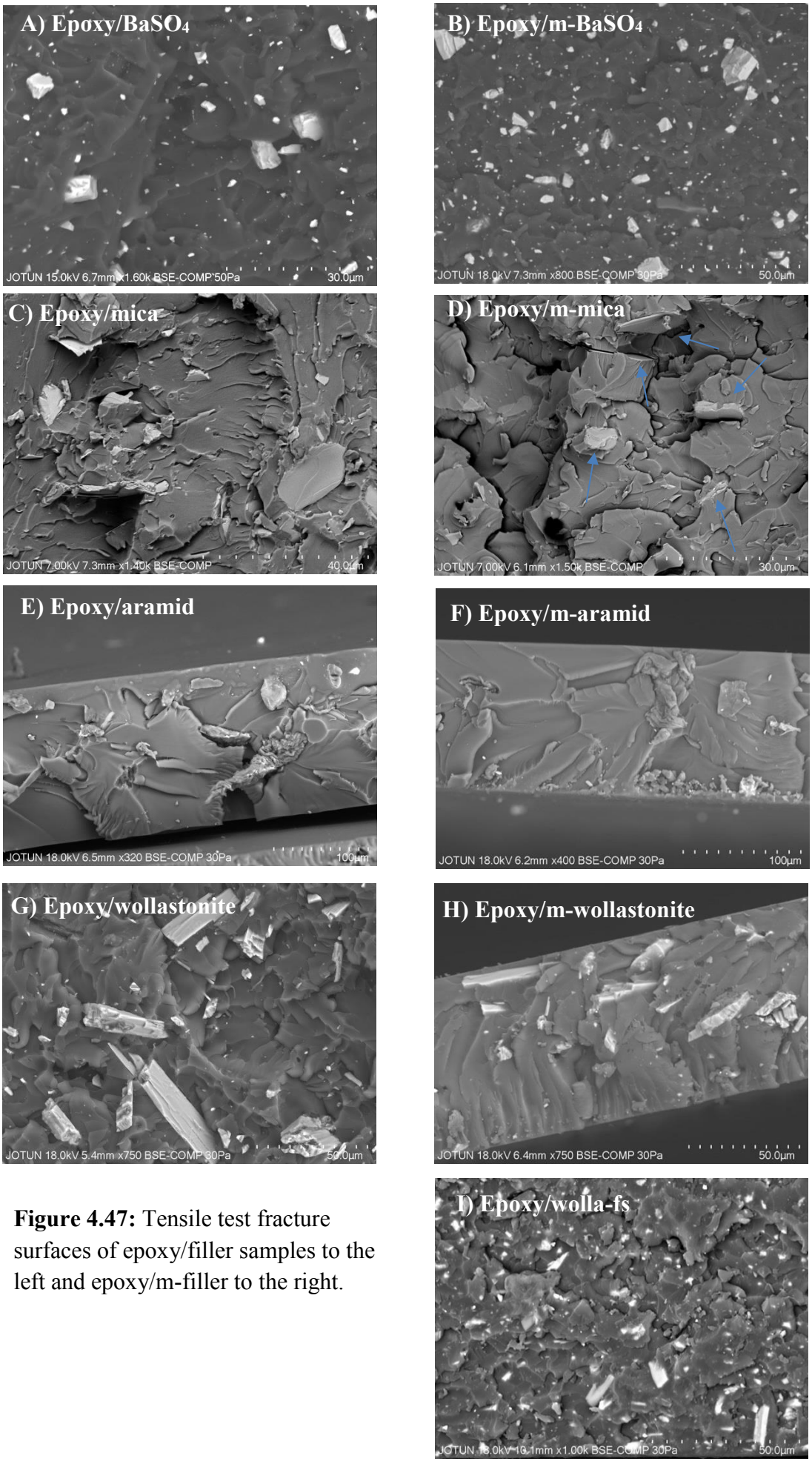

Figure 4.47: Tensile test fracture surfaces of epoxy/filler samples to the left and epoxy/m-filler to the right.

5 Conclusions

A thorough study of the influence of four different fillers on a diepoxy-diamine system have been reported. The various moduli values increased for all epoxy/filler samples compared to the pure epoxy matrix, while the T_g was not influenced by addition of any of the fillers. The flexural strength and toughness decreased for all epoxy/filler samples compared to the pure epoxy matrix. This circumstance was explained by the filler particles acting as mechanical hinders for the epoxy segments during elongation. The permeability was lowered to a small extent by incorporation of the mineral fillers and increased by the incorporation of the aramid fibers, the latter probably due to the presence of a high number of air bubbles in these films.

The distribution of filler particles was uniform in all epoxy/filler samples. Orientation were observed in the epoxy/mica and epoxy/wollastonite films, but none of the tests in this work revealed directional dependent properties in the horizontal and vertical direction of the free films.

Indications of interaction between the epoxy matrix and the filler particles were not observed by using FT-IR and XPS. The chemistry of all epoxy/filler films seemed similar, indicating that the main part of the chemistry not was affected by the incorporation of filler particles. Study of the fracture surfaces from tensile and flexural tests displayed a circumstance known as dewetting, indicating a rather weak interaction between the matrix and the filler particles.

The filler particles were coated with the silane coupling agent “ameo” to enhance the interaction possibilities. XPS analysis revealed a successful modification process by the presence of carbon, silicon and nitrogen on all filler surfaces.

New or enhanced interactions between the epoxy matrix and the filler particles after the surface modification were not observed using FT-IR and XPS. However, the fractography analysis showed that the surface modified filler particles were slightly more attached to the epoxy matrix compared to the situation in the epoxy/filler samples. The distribution of the surface modified filler particles was uniform for all epoxy/m-filler samples, except for the epoxy/m-$BaSO_4$ film due to m-$BaSO_4$ agglomerates. The physical and mechanical properties of the epoxy/m-$BaSO_4$ samples were influenced by the m-$BaSO_4$ agglomerates. The stiffness and T_g of the epoxy/m-filler samples did not change significantly, while a weak increase in

strength and toughness and a small decrease in permeability were observed compared to the epoxy/filler samples (stated with its exceptions).

Addition of filler particles to the diepoxy-diamine system in this work resulted in stiffer films with a slightly lower permeability to water vapor and decreased strength and toughness. Surface modification enhanced the strength, toughness and resistance to water vapor to a small extent, while the other physical and mechanical properties in main were unchanged. The distribution of filler particles influenced the mechanical properties, where agglomeration of filler particles lowered the toughness. Possible chemical interactions between the epoxy matrix and the filler particles were not observed for the unmodified or modified filler particles. Fractography revealed that the filler particles were slightly more attached to the epoxy matrix in the fracture surfaces after surface modification. Due to a lack of observed interactions between the epoxy matrix and the filler particles, the size, shape and rigidity of the filler particles were considered to influence the properties of the epoxy matrix the most.

6 Future Work

It took time to familiarize with this area of science and the knowledge and experience with paint, composite materials and physical and mechanical testing developed during the work. Hence, there is a list of things that would be interesting to investigate more, and a few of these is listed below.

- It would be interesting to see the effect of an increased filler loading. Differences between the various fillers may be enhanced at a higher filler loading. The aramid fibers, however, will be problematic to add with a higher loading due to the high oil absorption. Another filler with a fibrous shape and a lower oil absorption would be to prefer in this case.

- As the size of the filler particles seemed to affect the strength and toughness of the matrix/filler films, it would be interesting to study the influence of samples with the same filler but with various sizes. For instance, samples with filler particles with the sizes ~5μm, ~30μm, ~50μm and ~100μm.

- A thorough XPS-study of fracture surfaces from tensile or flexural tests may reveal detailed information about where and how the materials failure and could lead to a deeper understanding of the observed mechanical properties.

- It would be interesting to test a wollastonite powder with particles of sizes comparable to the wollastonite-fs particles, in order to examine if the size of the particles is of the biggest influence, or if the surface modification in this work not were as successful as thought.

- Since the orientation of the high-aspect ratio fillers was the same in the horizontal and vertical cross-sections of the free films and differed in the direction of the thickness of the films, it would be interesting to conduct tests where the properties of the samples could be tested in both the direction of the thickness of the materials and in the horizontal and vertical direction (both perpendicular to the thickness direction).

7 References

[1] D. Stoye, B. Marwald, W. Plehn. “Ullmann’s encyclopedia of industrial chemistry – Paint and coatings, 1. Introduction”, *Wiley-VCH Verlag GmbH & Co, 25,* **2012,** 647-659

[2] A. Guy. “ The chemistry and physics of coatings: Edition 2, The science and art of paint formulation”, *Royal Society of Chemistry,* **2004,** 317-346

[3] A. B. Port, C. Cameron. “The chemistry and physics of coatings: Edition 2, Performance properties of coatings”, *Royal Society of Chemistry,* **2004,** 64-95

[4] L. E. Nielsen. “Mechanical properties of particulate-filled systems”, *Journal of composite materials, 1,* **1967**, 100-119

[5] M. Sudheer. “Thermomechanical properties of epoxy/PTW composites”, *Journal of mechanical engineering and automation, 6,* **2016**, 18-21

[6] A. Dasari, R. D. Misra. “Scratch deformation characteristics of micrometric wollastonite-reinforced ethylene-propylene copolymer composites”, *Polymer engineering and science, 44(9)*, **2004**, 1738-1748

[7] G. Xian, R. Walter, F. Haupert. “Comparative study of the mechanical and wear performance of short carbon fibers and mineral particles (wollastonite, $CaSiO_3$) filled epoxy composite”, *Journal of polymer science: Part B: Polymer physics, 44,* **2006**, 854-863

[8] K. Wang, J. Wu, L. Ye, H. Zeng. “Mechanical properties and toughening mechanisms of polypropylene/barium sulfate composites”, *Composites: Part A, 34,* **2003,** 1199-1205

[9] S. Sterman, J. G. Marsden. «Silane coupling agents», *Industrial & Engineering Chemistry, 58(3),* **1966**, 33-37

[10] F. M. Fowkes, D. W. Dwight, D. A. Cole. “Acid-base properties of glass surfaces”, *Journal of Non-Crystalline Solids, North-Holland, 120,* **1990**, 47-60

[11] P. S. Arora, J. G. Matisons, A. Provatas, R. St. C. Smart. “Aminohydroxysiloxanes on E-glass fibers”, *Langmuir*, *11*, **1995**, 2009-2017

[12] E. Metwalli, D. Haines, O. Becker, S. Conzone, C. G. Pantano. “Surface characterizations of mono-, di-, and tri-aminosilane treated glass substrates”, *Journal of colloid and Interface Science, 298,* **2006,** 825-831

[13] X. Liu, J. L. Thomason, F. R. Jones. “XPS and AFM study of interaction of organosilane and sizing with E-Glass fibre surface”, *The Journal of adhesion, 84(4),* **2008,** 322-338

[14] H. S. Katz, J. V. Milewski, “Handbook of fillers for plastics”, *Van Nostrand Reinhold Company Inc.,* **1987**, 3-76

[15] H-J. Streitberger, E. Urbano, R. Laible, B. D. Meyer, E. Bagda, F. A. Waite, M. Philips. “Ullmann’s encyclopedia of industrial chemistry – Paint and Coatings, 3. Paint systems”, *Wiley-VCH Verlag GmbH & Co, 26,* **2012,** 1-29

[16] K. Köhler, P. Simmendinger, W. Roelle, W. Scholz, A. Valet, M. Slongo. “Ullmann’s encyclopedia of industrial chemistry – Paint and coatings, 4. Pigments, Extenders and Additives”, *Wiley-VCH Verlag GmbH & Co, 26,* **2012,** 31-51

[17] A. R. Marrion. “The chemistry and physics of coatings: Edition 2, Chapter 6: Binders for Convential Coatings”, *Royal Society of Chemistry,* **2004,** 96-151

[18] D. Gysau. “Fillers for paints – 2nd Revised edition”, *Hanover: Vincentz Network, European Coatings tech files,* **2011**, 13-18, 57-58, 144-152

[19] A.B. Port, C. Cameron. “The chemistry and physics of coatings: Edition 2, Chapter 4: Film formation”, *Royal Society of Chemistry,* **2004,** 46-63

[20] H.Q. Pham, M. J. Marks. “Ullmann’s encyclopedia of industrial chemistry – Epoxy Resins”, *Wiley-VCH Verlag GmbH & Co, 13*, **2012,** 156-244

[21] K. Wang, J. Wu, H. Zeng. ”Microstructure and fracture behaviour of polypropylene/barium sulfate composites”, *Journal of applied polymer science, 99,* **2006**, 1207-1213

[22] M. Rahail Parvaiz, P. A. Mahanwar. ”Effect of coupling agent on the mechanical, thermal, electrical, rheological and morphological properties of polyetheretherketone composites reinforced with surface-modified mica”, *Polymer-plastics technology and engineering, 49,* **2010**, 827-835

[23] S.R. Wu, G.S.Sheu, S.S. Shyu. “Kevlar fiber-Epoxy Adhesion and its effect on composite mechanical and fracture properties by plasma and chemical treatment”, *Journal of applied polymer science, 62,* **1996**, 1347-1360

[24] A. K. Pathak, M. Borah, A. Gupta, T. Yokozeki, S. R. Dhakate. “Improved mechanical properties of carbon fiber/graphene oxide-epoxy hybrid composites”, *Composites Science and Technology, 135,* **2016**, 28-38

[25] T. V. Kosmidou, A. S. Vatalis, C. G. Delides, E. Logakis, P. Pissis, G.C. Papanicolaou. ”Structural, mechanical and electrical characterization of epoxy-amine/carbon black nanocompoites”, *eXPRESS Polymer Letters, 2,* **2008**, 364-372

[26] G. Zhuang, Y. Yang, B. Li. ”Reinforced effect of wollastonite on Phenolphthalein Poly(ether ketone)”, *Journal of applied polymer science, 65,* **1997**, 649-653

[27] P. J. de Lange, P. G. Akker. ”Adhesion activation of twaron aramid fibers for application in rubber: Plasma versus chemical treatment”, *Journal of adhesion science and technology, 26,* **2012**, 827-839

[28] M. Su, A. Gu, G. Liang, L. Yuan. ”The effect of oxygen-plasma treatment on Kevlar fibers and the properties of Kevlar fibers/bismaleimide composites”, *Applied surface science, 257,* **2011**, 3158-3167

[29] Z. Yuan, J. Yu, B. Rao, H. Bai, N. Jiang, J. Gao, S. Lu. “Enhanced thermal properties of epoxy composites by using hyperbranched aromatic polyamide grafted silicon carbide whiskers”, *Macromolecular research, 22(4),* **2014**, 405-411

[30] Y. Fan, G. Wang, X. Huang, J. Bu, X. Sun, P. Jiang. “Molecular structures of (3-aminopropyl)trialkoxysilane on hydroxylated barium titante nanoparticle surfaces induced by different solvents and their effect on electrical properties of barium titante based polymer nanocomposites”, *Applied surface science, 364*, **2016**, 798-807

[31] X. Xu, L. Wang, S. Guo, L. Lei, T. Tang. “Surface chemical study on the covalent attatchment og hydroxypropyltrimethyl ammonium chloride chitosan to titanium surfaces”, *Applied surface science, 257,* **2001**, 10520-10528

[32] A. F. Ismail, T. D. Kusworo, A. Mustafa. “Enhanced gas permeation performance of polyethersulfone mixed matrix hollow fiber membranes using novel Dynasylan Ameo silane agent”, *Journal of Membrane Science, 319,* **2008**, 306-312

[33] C. O. Hammer, F. H. J. Maurer. “Polymer-filler interaction and control of structure inbarium sulphate-filled blends of polypropylene”, *Composite interfaces, 5(3),* **1997**, 241-256

[34] L. Forget, F. Wilwers, J. Delhalle, Z. Mekhalif. “Surface modification of aluminium by *n*-pentanephosphonic acid: XPS and electrochemical evaluation”, *Applied surface science, 205*, **2003**, 44-55

[35] P. Atkins, J. de Paula. “Atkins’ PHYSICAL CHEMISTRY, 10th Edition”, *Oxford University Press,* **2014,** 710-713, 762-764 and 791

[36] R. J. D. Tilley. “Understanding Solids – The science of materials, Second Edition”, *John Wiley & Sons Ltd,* **2013**, 281-305

[37] G. W. Ehrenstein, P. Trawiel, G. Riedel. “Thermal analysis of plastics: Theory and practice, Chapter 6”, *Hanser Publications,* **2004**, 236-252

[38] D. Olmos, J. Baselga, I. Mondragon, J. González-Benito. “The effect of surface modification of silica microfillers in an epoxy matrix on the thermomechanical properties”, *Journal of adhesion science and technology, 22,* **2008**, 1443-1459

[39] D. Piazza, N. P. Lorandi, C. I. Pasqual, L. C. Scienza, A. J. Zattera. ”Influence of a microcomposite and a nanocomposite on the properties of epoxy-based powder coating”, *Materials science and engineering, 528,* **2011**, 6769-6775

[40] G. Tsagaropoulos, A. Eisenberg. “Dynamic Mechanical study of factor affecting the two glass transition behavior of filled polymers. Similarities and differences with random ionomers”, *Macromolecules, 28,* **1995**, 6067-6077

[41] J. Wolfrum, G. W. Ehrenstein. “Dynamical mechanical thermo analysis of high performance composites – influences and problems”, *Journal of composite materials, 43(21),* **2000,** 1788-1806

[42] M. A. Meyers, K. K. Chawla. “Mechanical Behavior of Materials”, *Cambridge university press*, **2009**, 56, 79, 110-119, 124-125, 188-190, 540-547 and 507-515

[43] L. W. Mckeen. «Permeability properties of plastics and elastomers, 3rd edition», *William Andrew, an imprint of Elsevier,* **2012**, 1-37

[44] N. S. Sangaj, V.C. Malshe. «Permeability of polymers in protective organic coatings”, *Progress in organic coatings, 50*, **2004**, 28-39

[45] T. Jollivet, E. Greenhalgh. “Fractography, a powerful tool for identifying and understanding fatigue in composite materials”, *Procerdia Engineering, 133,* **2015,** 171-178

[46] Y. Leng “Materials Characterization – Introduction to microscopic and spectroscopic methods”, *Wiley – VCH Verlag GmbH & Co,* **2013,** 127-129, 135-137, 221-250

[47] Y. Nakamura, T. Usa, T. Gotoh, N. Yokouchi, T. Iida, K. Nagata. “AFM observations of silane coupling agent layers having a vinyl group deposited on a mica surface”, *Jorunal of adhesion science and technology, 20(11),* **2006**, 1199-1213

[48] Z. Zhang, H. Liang, X. Hou, Y. Yu. ”Plasma surface modification of poly(m-aramide) fabric for adhesion improvment to fluorosilicone rubber”, *Jorunal of adhesion science and technology, 15,* **2001,** 809-822

[49] H. Bolouri, R. A. Pethrick, S. Affrossman. “Bonding of a simulated epoxy resinto aluminium surfaces studied by XPS”, *Applications of surface science, 17*, **1983**, 231-240

[50] D. L. Pavia, G. M. Lampman, G. S. Kriz and J. R. Vyvyan. “Introduction to spectroscopy, Fifth Edition”, *Cengage Learning,* **2015**, 14-106

[51] Q. Zhang, D. Li, D. Lai, Y. You, B. Ou. “Preparation, Microstructure, mechanical, and thermal properties of In situ polymerized polyimide/organically modified sericite mica composites”, *Polymer composites, 37,* **2016**, 2243-2251

[52] C. Roberts. “Laboratory testing of coating permeance”, *KTA University,* http://www.paintsquare.com/education/branding_images/Laboratory%20Testing%20of%20Coating%20Permeance-KAT1.pptx , 12.04.18

[53] SpeedMixers, Dac 600.1 FVC, *FlackTek Inc SpeedMixer*, http://speedmixer.com/products/speedmixers/medium-mix-up-to-1000g/dac-600-1-fvz/ , 12.04.18

[54] T. Ai, R. Wang, W. Zhou. “Effect of grafting alkoxysilane on the surface properties of Kevlar fiber”, *Polymer composites, 28(3),* **2007**, 412-416

[55] Paul N. Gardner Co. Inc. “Paul N. Gardner Releases three paint and coating testing applicators”, https://www.qualitydigest.com/inside/metrology-news/paul-n-gardner-releases-three-paint-and-coating-testing-applicators.html, 03.04.18

[56] G. Beamson, D. Briggs. “High resolution XPS of Organic polymers, The scienta ESCA300 Database”, *John Wiley & Sons,* **1992**

[57] Testometric, 25KN Machines, https://www.testometric.co.uk/25kn/ , 13.04.18

[58] S. Scierka and A. Forster. “An XPS study on the effect of pigment on the UV degradation of an epoxy system”, *Federation of societies for coating technology,* **2003**

[59] B. De’Nève, M. Delamar, T. T. Nguyen, M.E.R. Shanahan. “Failure mode and ageing of steel/epoxy joints”, *Applied surface science, 134,* **1998**, 202-212

[60] W. Guang-Heng, Z. An-ning, H. Xiao-Bing, ”Effect of coal filler on the properties of soy protein plastics”, *Journal of applied polymer science*, *102*, **2006**, 3134-3143

[61] C. Elmi, S. Guggenheim, R. Gieré. “Surface crystal chemistry of phyllosilicates using X-Ray Photoelectron Spectroscopy: A review”, *Clays and minerals, 64(5),* **2016***,* 537-551

[62] Peter J. Schmitz. “Characterization of the surface of $BaSO_4$ powder by XPS”, *Surface Science Spectra, 8,* **2001**, 195-199

[63] R. C. Longo, K. Cho, P. Brüner, A. Welle, A. Gerdes, P. Thissen. “Carbonation of wollastonite(001) Competing hydration: Microscopic insights from Ion Spectroscopy and Density functional theory”, *Applied Materials and Interfaces, 7,* **2015**, 4706-4712

[64] J. J. Suay Antòn, M. Monleòn Pradas, J. L. Gomez Ribelles. “The effect of kevlar Reinforcement on the curing, termal and dynamical-mechanical properties of an epoxy/anhydride system”, *Polymer engeneering and science, 40,* **2000**, 1725-1735

[65] P. Bajaj, N. K. Jha, R. Ananda Kumar. “Effect of mica on the curing behavior of an amine-cured epoxy system: Differential scanning calorimetric studies», *Journal of applied polymer science, 40,* **1990**, 203-212

[66] M. Poletto, M. Zeni, A. J. Zattera. «Dynamic mechanical analysis of recycled polystyrene composites reinforced with wood flour», *Journal of applied polymer science, 125*, **2012**, 935-942

[67] G. Tsagaropoulos, A. Eisenberg. "Direct observation of two glass transitions in silica-filled polymers. Implications for the morphology of random ionomers", *Macromolecules, 28,* **1995**, 396-398

[68] Specac, Products, FTIR Accessories, Reflextance, ATR, "How the ATR accessory work",

https://www.specac.com/en/documents/application-notes/how-atr-works and, 16.04.18

Appendix A. Chemicals used in the work and standard deviation method

A.1 Chemicals used in the work

Table A.1: List of all chemicals used in this work and the purpose with them

Chemical	Supplier	Purpose
Barium Sulfate $BaSO_4$	Portaryte	Filler
Mica, Muscovite $KAl_2(AlSi_3O_{10})(OH)_2$	Norwegian Talc AS	Filler
Aramid, polyparap-henyleneter-ephthalamide, $[-NH-C_6H_6-NH-CO-C_6H_6-CO-]_n$	Teijin	Filler
Wollastonite $CaSiO_3$	Nyco minerals	Filler
Tremin 283 600 "Silane treated wollastonite" Silan-$CaSiO_3$	The Quarzwerke Group	Filler (check surface modification characteristics)
Epikote Resin 828EL Diglycidyl ether of bisphenol A	Momentive	Binder in the paint formulation
Noramine V15 Polyamine epoxy adduct	Jotun AS	Epoxy curing agent
Thinner 17 Xylene/butanol	Jotun AS	Used for cleaning
Ethanol C_2H_6O	Arcus AS	Used for cleaning Used for surface modification Used for filler-slurry samples for FT-IR
Ion exchanged water/distilled water	Jotun AS	Cleaning Surface modification Permeability
Conductive filler Ni	Buehler	Conducting filler in epoxy formulation used in SEM sample-preparation

Silquest A 1100 “Ameo” 3-aminopropyltriethoxysilane	Momentive	Surface modification of filler surfaces

* Formula is not given due to company security for Jotun.

A.2 Standard deviation method used in the work

With all tests where several repetitions were conducted, the results have been presented with a standard deviation. This is important due to display the experimental uncertainty.

All standard deviations were calculated with the use of the “STDEV.S” function in Excel (Microsoft, Office), and represent how widely the results are spread from the average value. This is the “Sample standard deviation” function, and this standard deviation method were chosen due to the results acquired in this work only representing the properties of these samples under the exactly chosen curing process and often includes some deformations and faults (air bubbles, non-uniform distribution of filler particles and/or liquid epoxy and curing agent, etc.).

The STDEV formula calculates the standard deviation value based on formula A.1, where $\bar{x}$ is the average value of all the results, x is the various test results and n is the number of values in the set[1].

$$STDEV = \sqrt{\frac{\sum(x - \bar{x})^2}{(n-1)}} \qquad (A.1)$$

[1] Microsoft, Office, STDEV function. https://support.office.com/en-us/article/stdev-function-51fecaaa-231e-4bbb-9230-33650a72c9b0 , 13.04.18

Appendix B. Technical data sheet for the fillers and binding system components

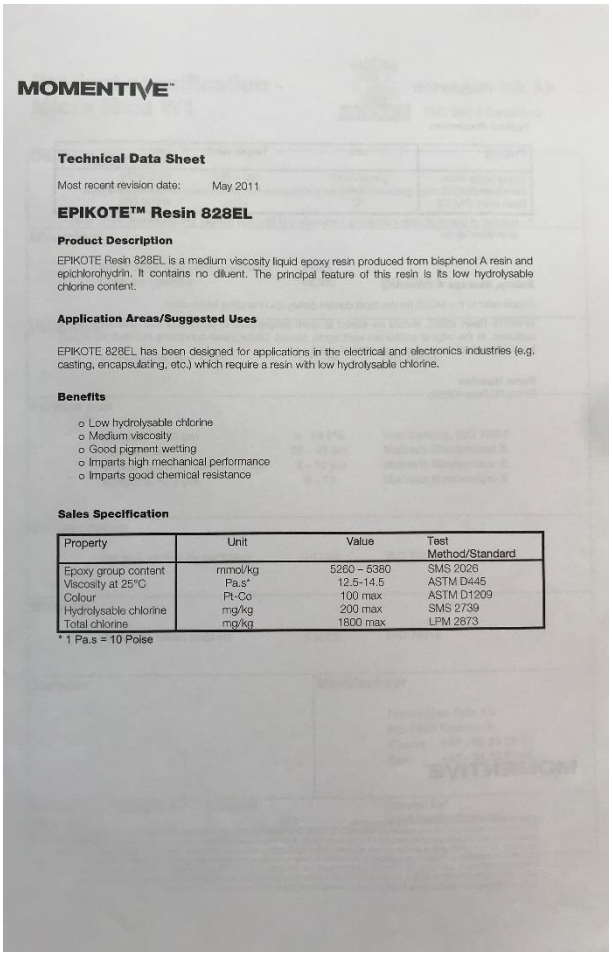

MOMENTIVE

Technical Data Sheet

Most recent revision date: May 2011

EPIKOTE™ Resin 828EL

Product Description

EPIKOTE Resin 828EL is a medium viscosity liquid epoxy resin produced from bisphenol A resin and epichlorohydrin. It contains no diluent. The principal feature of this resin is its low hydrolysable chlorine content.

Application Areas/Suggested Uses

EPIKOTE 828EL has been designed for applications in the electrical and electronics industries (e.g. casting, encapsulating, etc.) which require a resin with low hydrolysable chlorine.

Benefits

- Low hydrolysable chlorine
- Medium viscosity
- Good pigment wetting
- Imparts high mechanical performance
- Imparts good chemical resistance

Sales Specification

Property	Unit	Value	Test Method/Standard
Epoxy group content	mmol/kg	5260 – 5380	SMS 2026
Viscosity at 25°C	Pa.s*	12.5-14.5	ASTM D445
Colour	Pt-Co	100 max	ASTM D1209
Hydrolysable chlorine	mg/kg	200 max	SMS 2739
Total chlorine	mg/kg	1800 max	LPM 2873

* 1 Pa.s = 10 Poise

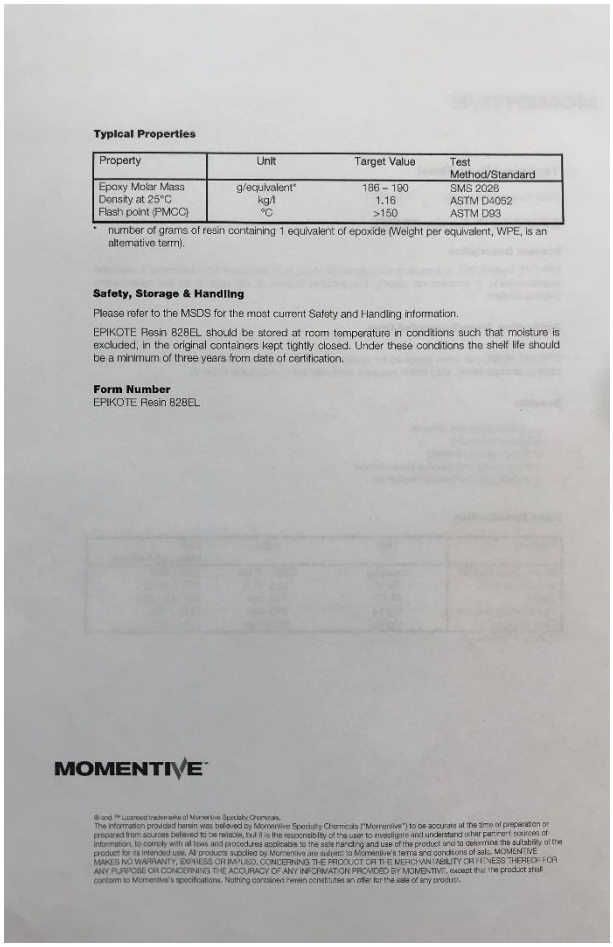

Typical Properties

Property	Unit	Target Value	Test Method/Standard
Epoxy Molar Mass	g/equivalent*	186 – 190	SMS 2026
Density at 25°C	kg/l	1.16	ASTM D4052
Flash point (PMCC)	°C	>150	ASTM D93

* number of grams of resin containing 1 equivalent of epoxide (Weight per equivalent, WPE, is an alternative term).

Safety, Storage & Handling

Please refer to the MSDS for the most current Safety and Handling information.

EPIKOTE Resin 828EL should be stored at room temperature in conditions such that moisture is excluded, in the original containers kept tightly closed. Under these conditions the shelf life should be a minimum of three years from date of certification.

Form Number
EPIKOTE Resin 828EL

MOMENTIVE

Figure B.1: Technical data sheet for the liquid epoxy used in this work.

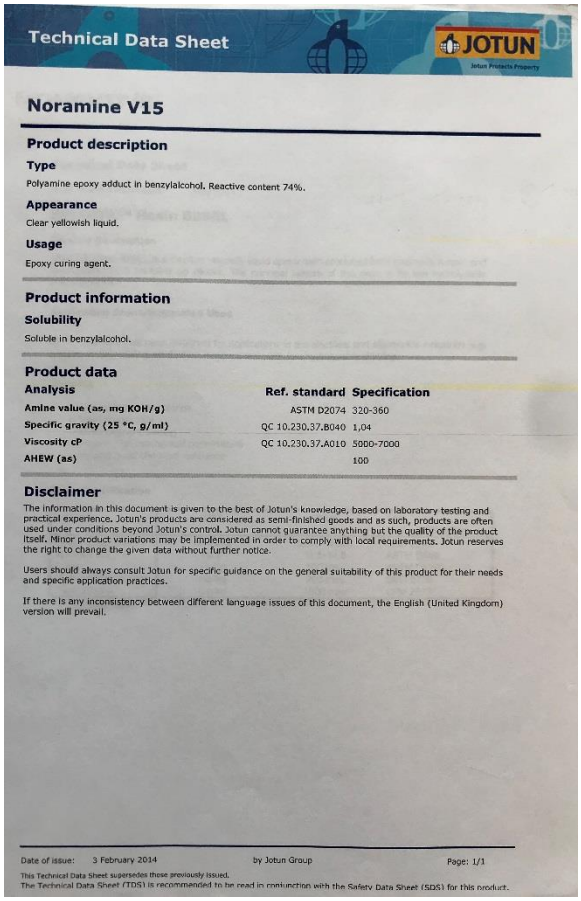

Technical Data Sheet

JOTUN

Jotun Protects Property

Noramine V15

Product description

Type

Polyamine epoxy adduct in benzylalcohol. Reactive content 74%.

Appearance

Clear yellowish liquid.

Usage

Epoxy curing agent.

Product information

Solubility

Soluble in benzylalcohol.

Product data

Analysis	Ref. standard	Specification
Amine value (as, mg KOH/g)	ASTM D2074	320-360
Specific gravity (25 °C, g/ml)	QC 10.230.37.B040	1,04
Viscosity cP	QC 10.230.37.A010	5000-7000
AHEW (as)		100

Disclaimer

The information in this document is given to the best of Jotun's knowledge, based on laboratory testing and practical experience. Jotun's products are considered as semi-finished goods and as such, products are often used under conditions beyond Jotun's control. Jotun cannot guarantee anything but the quality of the product itself. Minor product variations may be implemented in order to comply with local requirements. Jotun reserves the right to change the given data without further notice.

Users should always consult Jotun for specific guidance on the general suitability of this product for their needs and specific application practices.

If there is any inconsistency between different language issues of this document, the English (United Kingdom) version will prevail.

Date of issue: 3 February 2014 by Jotun Group Page: 1/1

This Technical Data Sheet supersedes those previously issued.
The Technical Data Sheet (TDS) is recommended to be read in conjunction with the Safety Data Sheet (SDS) for this product.

Figure B.2: Technical data sheet for the curing agent, Noramin V15 used in this work.

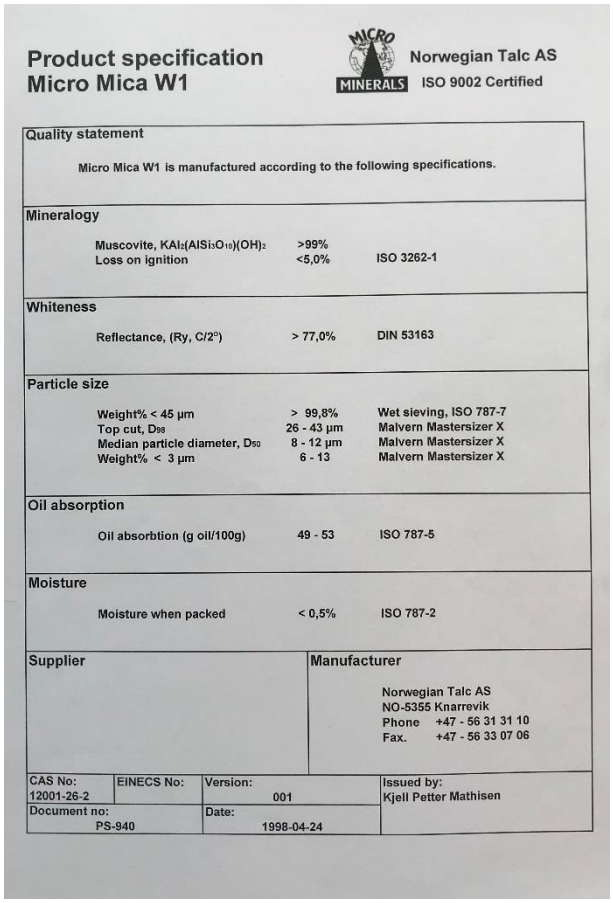

Product specification
Micro Mica W1

MICRO MINERALS

Norwegian Talc AS
ISO 9002 Certified

Quality statement

Micro Mica W1 is manufactured according to the following specifications.

Mineralogy		
Muscovite, $KAl_2(AlSi_3O_{10})(OH)_2$	>99%	
Loss on ignition	<5,0%	ISO 3262-1
Whiteness		
Reflectance, (Ry, C/2°)	> 77,0%	DIN 53163
Particle size		
Weight% < 45 µm	> 99,8%	Wet sieving, ISO 787-7
Top cut, D_{98}	26 - 43 µm	Malvern Mastersizer X
Median particle diameter, D_{50}	8 - 12 µm	Malvern Mastersizer X
Weight% < 3 µm	6 - 13	Malvern Mastersizer X
Oil absorption		
Oil absorbtion (g oil/100g)	49 - 53	ISO 787-5
Moisture		
Moisture when packed	< 0,5%	ISO 787-2

Supplier	Manufacturer
	Norwegian Talc AS NO-5355 Knarrevik Phone +47 - 56 31 31 10 Fax. +47 - 56 33 07 06

CAS No:	EINECS No:	Version:	Issued by:
12001-26-2		001	Kjell Petter Mathisen
Document no: PS-940		Date: 1998-04-24	

Figure B.3: Technical data sheet for the mica powder used in this work.

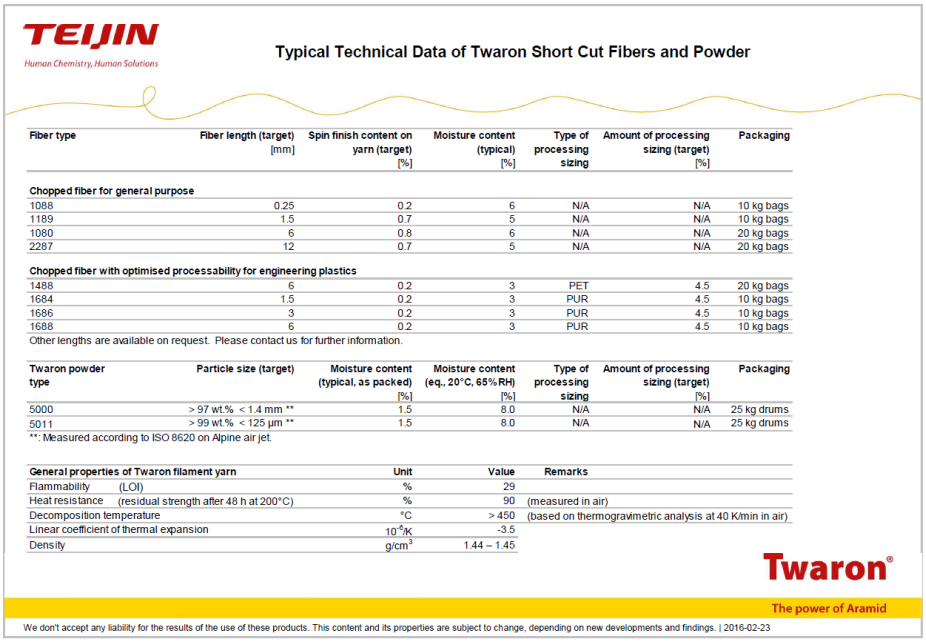

TEIJIN

Human Chemistry, Human Solutions

Typical Technical Data of Twaron Short Cut Fibers and Powder

Fiber type	Fiber length (target) [mm]	Spin finish content on yarn (target) [%]	Moisture content (typical) [%]	Type of processing sizing	Amount of processing sizing (target) [%]	Packaging
Chopped fiber for general purpose						
1088	0.25	0.2	6	N/A	N/A	10 kg bags
1189	1.5	0.7	5	N/A	N/A	10 kg bags
1080	6	0.8	6	N/A	N/A	20 kg bags
2287	12	0.7	5	N/A	N/A	20 kg bags
Chopped fiber with optimised processability for engineering plastics						
1488	6	0.2	3	PET	4.5	20 kg bags
1684	1.5	0.2	3	PUR	4.5	10 kg bags
1686	3	0.2	3	PUR	4.5	10 kg bags
1688	6	0.2	3	PUR	4.5	10 kg bags

Other lengths are available on request. Please contact us for further information.

Twaron powder type	Particle size (target)	Moisture content (typical, as packed) [%]	Moisture content (eq., 20°C, 65%RH) [%]	Type of processing sizing	Amount of processing sizing (target) [%]	Packaging
5000	> 97 wt.% < 1.4 mm **	1.5	8.0	N/A	N/A	25 kg drums
5011	> 99 wt.% < 125 µm **	1.5	8.0	N/A	N/A	25 kg drums

**: Measured according to ISO 8620 on Alpine air jet.

General properties of Twaron filament yarn		Unit	Value	Remarks
Flammability	(LOI)	%	29	
Heat resistance	(residual strength after 48 h at 200°C)	%	90	(measured in air)
Decomposition temperature		°C	> 450	(based on thermogravimetric analysis at 40 K/min in air)
Linear coefficient of thermal expansion		10^{-6}/K	-3.5	
Density		g/cm^3	1.44 – 1.45	

Twaron®

The power of Aramid

We don't accept any liability for the results of the use of these products. This content and its properties are subject to change, depending on new developments and findings. | 2016-02-23

Figure B.4: The technical data sheet for the aramid fibers used in this work. The fiber type used in this work were Twaron powder type, number 5011.

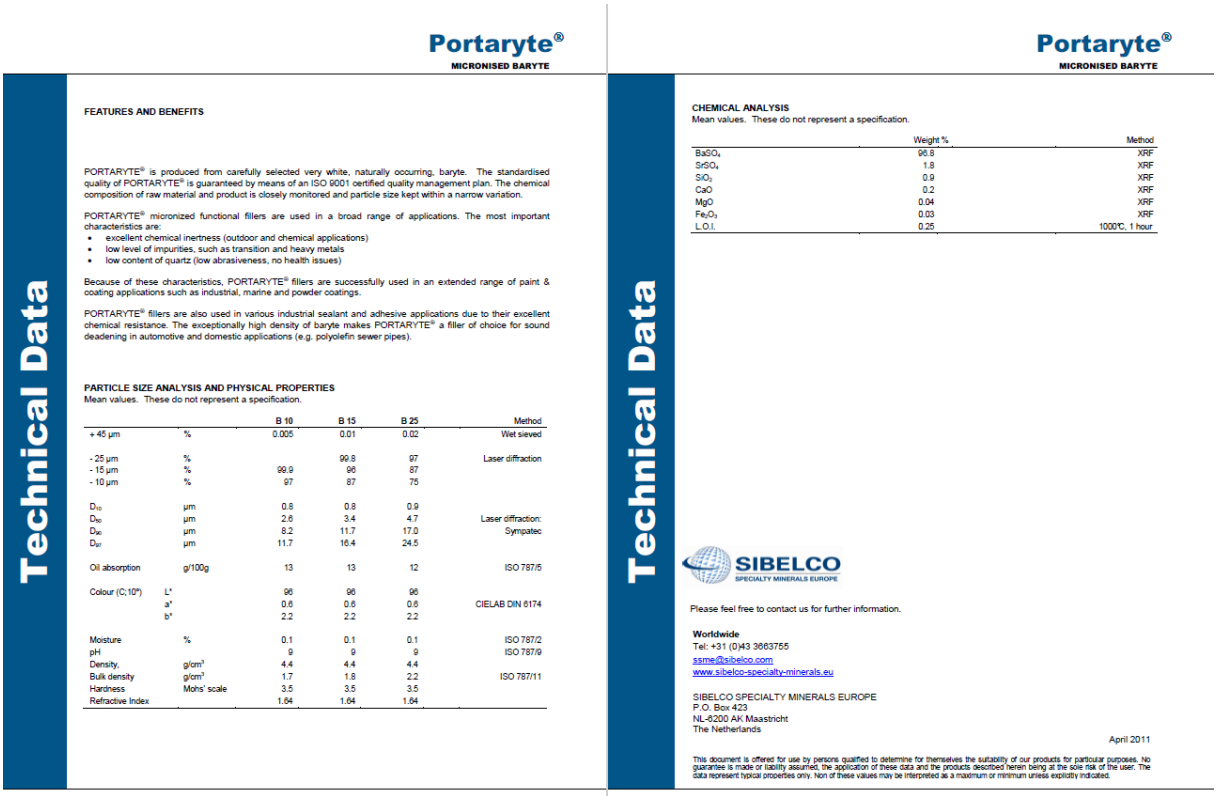

Portaryte®
MICRONISED BARYTE

Technical Data

FEATURES AND BENEFITS

PORTARYTE® is produced from carefully selected very white, naturally occurring, baryte. The standardised quality of PORTARYTE® is guaranteed by means of an ISO 9001 certified quality management plan. The chemical composition of raw material and product is closely monitored and particle size kept within a narrow variation.

PORTARYTE® micronized functional fillers are used in a broad range of applications. The most important characteristics are:

- excellent chemical inertness (outdoor and chemical applications)
- low level of impurities, such as transition and heavy metals
- low content of quartz (low abrasiveness, no health issues)

Because of these characteristics, PORTARYTE® fillers are successfully used in an extended range of paint & coating applications such as industrial, marine and powder coatings.

PORTARYTE® fillers are also used in various industrial sealant and adhesive applications due to their excellent chemical resistance. The exceptionally high density of baryte makes PORTARYTE® a filler of choice for sound deadening in automotive and domestic applications (e.g. polyolefin sewer pipes).

PARTICLE SIZE ANALYSIS AND PHYSICAL PROPERTIES
Mean values. These do not represent a specification.

		B 10	B 15	B 25	Method
+ 45 µm	%	0.005	0.01	0.02	Wet sieved
- 25 µm	%		99.8	97	Laser diffraction
- 15 µm	%	99.9	96	87	
- 10 µm	%	97	87	75	
D_{10}	µm	0.8	0.8	0.9	
D_{50}	µm	2.6	3.4	4.7	Laser diffraction:
D_{90}	µm	8.2	11.7	17.0	Sympatec
D_{97}	µm	11.7	16.4	24.5	
Oil absorption	g/100g	13	13	12	ISO 787/5
Colour (C;10°)	L*	96	96	96	
	a*	0.6	0.6	0.6	CIELAB DIN 6174
	b*	2.2	2.2	2.2	
Moisture	%	0.1	0.1	0.1	ISO 787/2
pH		9	9	9	ISO 787/9
Density,	g/cm³	4.4	4.4	4.4	
Bulk density	g/cm³	1.7	1.8	2.2	ISO 787/11
Hardness	Mohs' scale	3.5	3.5	3.5	
Refractive Index		1.64	1.64	1.64	

Portaryte®
MICRONISED BARYTE

Technical Data

CHEMICAL ANALYSIS
Mean values. These do not represent a specification.

	Weight %	Method
$BaSO_4$	98.8	XRF
$SrSO_4$	1.8	XRF
SiO_2	0.9	XRF
CaO	0.2	XRF
MgO	0.04	XRF
Fe_2O_3	0.03	XRF
L.O.I.	0.25	1000°C, 1 hour

SIBELCO
SPECIALTY MINERALS EUROPE

Please feel free to contact us for further information.

Worldwide
Tel: +31 (0)43 3663755
ssme@sibelco.com
www.sibelco-specialty-minerals.eu

SIBELCO SPECIALTY MINERALS EUROPE
P.O. Box 423
NL-6200 AK Maastricht
The Netherlands

April 2011

Figure B.5: The technical data sheet for the $BaSO_4$ powder (type B15) used in this work.

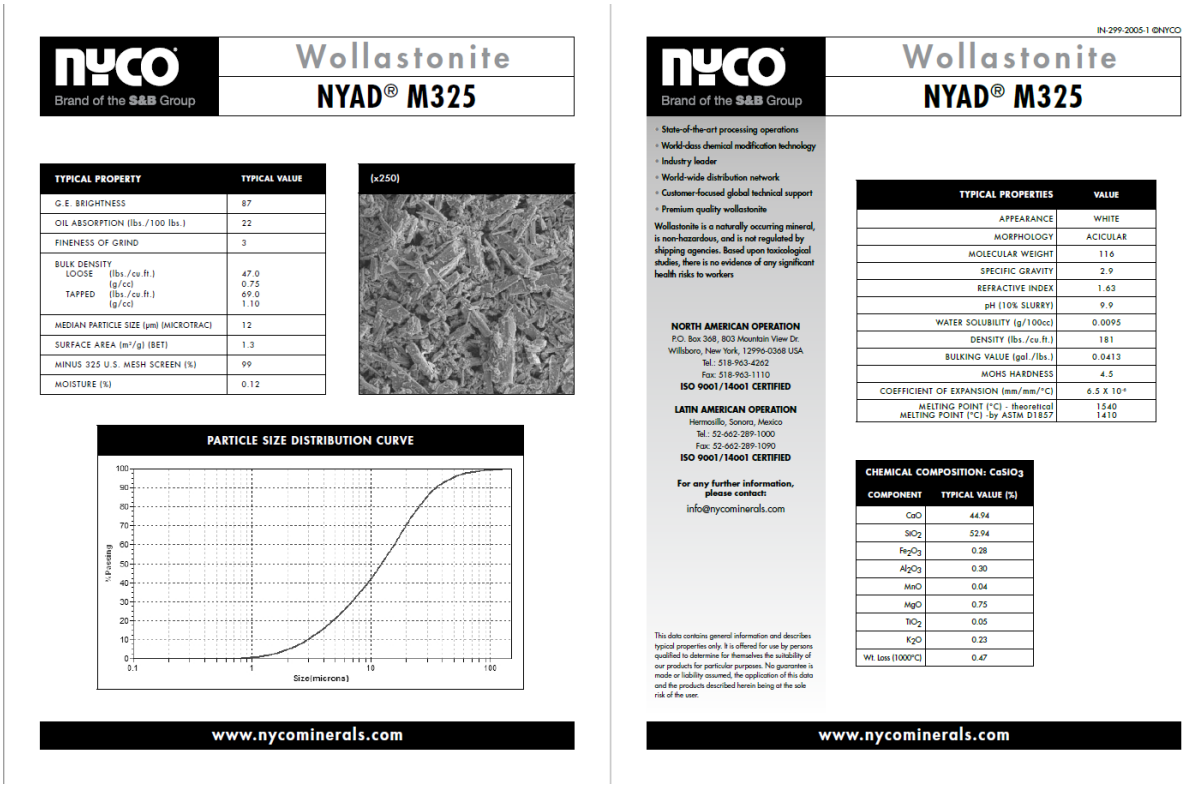

nyco
Brand of the S&B Group

Wollastonite
NYAD® M325

TYPICAL PROPERTY	TYPICAL VALUE
G.E. BRIGHTNESS	87
OIL ABSORPTION (lbs./100 lbs.)	22
FINENESS OF GRIND	3
BULK DENSITY LOOSE (lbs./cu.ft.) (g/cc) TAPPED (lbs./cu.ft.) (g/cc)	 47.0 0.75 69.0 1.10
MEDIAN PARTICLE SIZE (µm) (MICROTRAC)	12
SURFACE AREA (m^2/g) (BET)	1.3
MINUS 325 U.S. MESH SCREEN (%)	99
MOISTURE (%)	0.12

(x250)

PARTICLE SIZE DISTRIBUTION CURVE

www.nycominerals.com

IN-299-2005-1 ©NYCO

nyco
Brand of the S&B Group

Wollastonite
NYAD® M325

- State-of-the-art processing operations
- World-class chemical modification technology
- Industry leader
- World-wide distribution network
- Customer-focused global technical support
- Premium quality wollastonite

Wollastonite is a naturally occurring mineral, is non-hazardous, and is not regulated by shipping agencies. Based upon toxicological studies, there is no evidence of any significant health risks to workers

NORTH AMERICAN OPERATION
P.O. Box 368, 803 Mountain View Dr.
Willsboro, New York, 12996-0368 USA
Tel.: 518-963-4262
Fax: 518-963-1110
ISO 9001/14001 CERTIFIED

LATIN AMERICAN OPERATION
Hermosillo, Sonora, Mexico
Tel.: 52-662-289-1000
Fax: 52-662-289-1090
ISO 9001/14001 CERTIFIED

For any further information, please contact:
info@nycominerals.com

TYPICAL PROPERTIES	VALUE
APPEARANCE	WHITE
MORPHOLOGY	ACICULAR
MOLECULAR WEIGHT	116
SPECIFIC GRAVITY	2.9
REFRACTIVE INDEX	1.63
pH (10% SLURRY)	9.9
WATER SOLUBILITY (g/100cc)	0.0095
DENSITY (lbs./cu.ft.)	181
BULKING VALUE (gal./lbs.)	0.0413
MOHS HARDNESS	4.5
COEFFICIENT OF EXPANSION (mm/mm/°C)	6.5 X 10⁻⁶
MELTING POINT (°C) - theoretical MELTING POINT (°C) -by ASTM D1857	1540 1410

CHEMICAL COMPOSITION: $CaSiO_3$

COMPONENT	TYPICAL VALUE (%)
CaO	44.94
SiO_2	52.94
Fe_2O_3	0.28
Al_2O_3	0.30
MnO	0.04
MgO	0.75
TiO_2	0.05
K_2O	0.23
Wt. Loss (1000°C)	0.47

www.nycominerals.com

Figure B.6: The technical data sheet for the wollastonite powder used in this work.

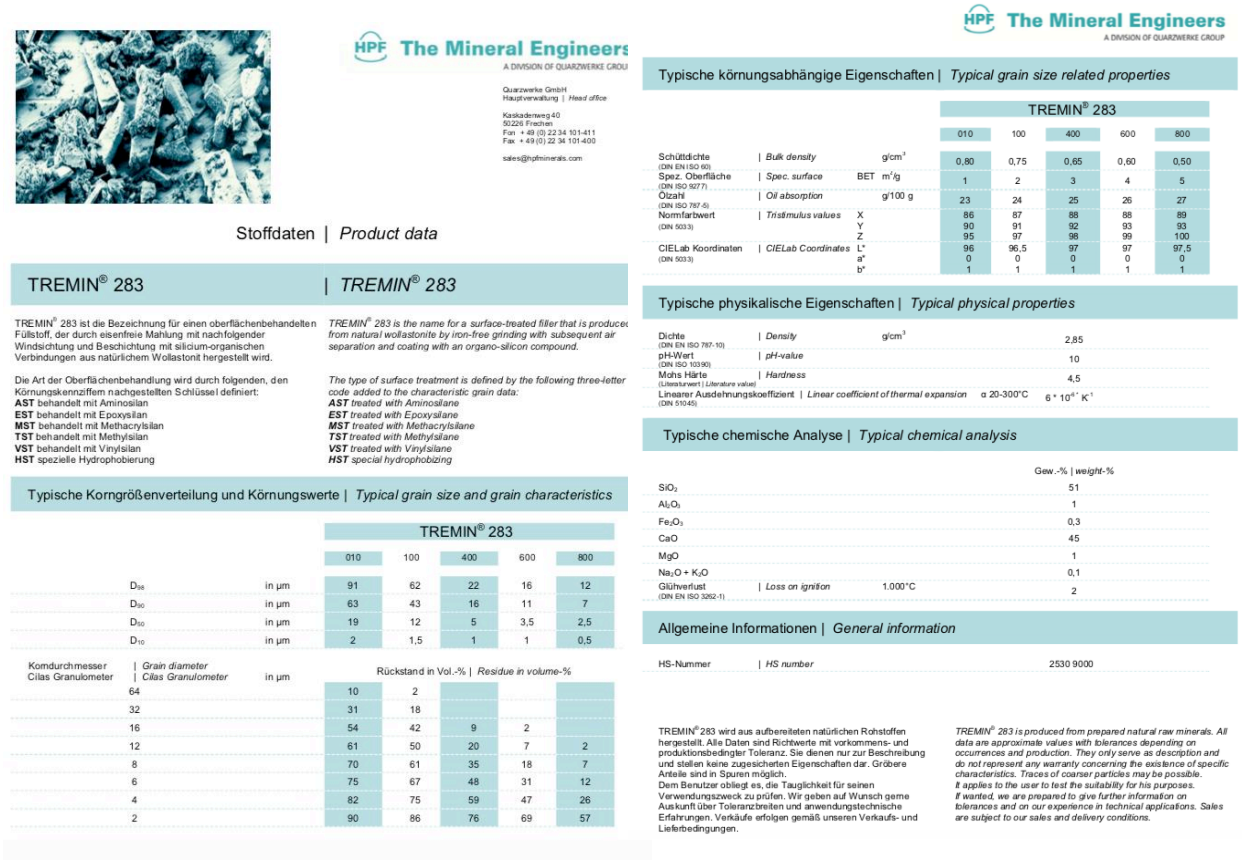

HPF The Mineral Engineers
A DIVISION OF QUARZWERKE GROUP

Quarzwerke GmbH
Hauptverwaltung | *Head office*
Kaskadenweg 40
50226 Frechen
Fon + 49 (0) 22 34 101-411
Fax + 49 (0) 22 34 101-400
sales@hpfminerals.com

Stoffdaten | *Product data*

TREMIN® 283 | *TREMIN® 283*

TREMIN® 283 ist die Bezeichnung für einen oberflächenbehandelten Füllstoff, der durch eisenfreie Mahlung mit nachfolgender Windsichtung und Beschichtung mit silicium-organischen Verbindungen aus natürlichem Wollastonit hergestellt wird.

Die Art der Oberflächenbehandlung wird durch folgenden, den Körnungskennziffern nachgestellten Schlüssel definiert:
AST behandelt mit Aminosilan
EST behandelt mit Epoxysilan
MST behandelt mit Methacrylsilan
TST behandelt mit Methylsilan
VST behandelt mit Vinylsilan
HST spezielle Hydrophobierung

TREMIN® 283 is the name for a surface-treated filler that is produced from natural wollastonite by iron-free grinding with subsequent air separation and coating with an organo-silicon compound.

The type of surface treatment is defined by the following three-letter code added to the characteristic grain data:
***AST** treated with Aminosilane*
***EST** treated with Epoxysilane*
***MST** treated with Methacrylsilane*
***TST** treated with Methylsilane*
***VST** treated with Vinylsilane*
***HST** special hydrophobizing*

Typische Korngrößenverteilung und Körnungswerte | *Typical grain size and grain characteristics*

			TREMIN® 283				
			010	100	400	600	800
D_{98}		in µm	91	62	22	16	12
D_{90}		in µm	63	43	16	11	7
D_{50}		in µm	19	12	5	3,5	2,5
D_{10}		in µm	2	1,5	1	1	0,5
Korndurchmesser Cilas Granulometer	*Grain diameter* | *Cilas Granulometer*	in µm	Rückstand in Vol.-% | *Residue in volume-%*				
	64		10	2			
	32		31	18			
	16		54	42	9	2	
	12		61	50	20	7	2
	8		70	61	35	18	7
	6		75	67	48	31	12
	4		82	75	59	47	26
	2		90	86	76	69	57

HPF The Mineral Engineers
A DIVISION OF QUARZWERKE GROUP

Typische körnungsabhängige Eigenschaften | *Typical grain size related properties*

				TREMIN® 283				
				010	100	400	600	800
Schüttdichte (DIN EN ISO 60)	*Bulk density*		g/cm³	0,80	0,75	0,65	0,60	0,50
Spez. Oberfläche (DIN ISO 9277)	*Spec. surface*	BET	m²/g	1	2	3	4	5
Ölzahl (DIN ISO 787-5)	*Oil absorption*		g/100 g	23	24	25	26	27
Normfarbwert (DIN 5033)	*Tristimulus values*	X		86	87	88	88	89
		Y		90	91	92	93	93
		Z		95	97	98	99	100
CIELab Koordinaten (DIN 5033)	*CIELab Coordinates*	L*		96	96,5	97	97	97,5
		a*		0	0	0	0	0
		b*		1	1	1	1	1

Typische physikalische Eigenschaften | *Typical physical properties*

Dichte (DIN EN ISO 787-10)	*Density*	g/cm³	2,85
pH-Wert (DIN ISO 10390)	*pH-value*		10
Mohs Härte (Literaturwert | *Literature value*)	*Hardness*		4,5
Linearer Ausdehnungskoeffizient (DIN 51045)	*Linear coefficient of thermal expansion*	α 20-300°C	$6 * 10^{-6}$ · K^{-1}

Typische chemische Analyse | *Typical chemical analysis*

	Gew.-% | *weight-%*
SiO_2	51
Al_2O_3	1
Fe_2O_3	0,3
CaO	45
MgO	1
$Na_2O + K_2O$	0,1
Glühverlust (DIN EN ISO 3262-1) *Loss on ignition* 1.000°C	2

Allgemeine Informationen | *General information*

HS-Nummer	*HS number*	2530 9000

TREMIN® 283 wird aus aufbereiteten natürlichen Rohstoffen hergestellt. Alle Daten sind Richtwerte mit vorkommens- und produktionsbedingter Toleranz. Sie dienen nur zur Beschreibung und stellen keine zugesicherten Eigenschaften dar. Gröbere Anteile sind in Spuren möglich.
Dem Benutzer obliegt es, die Tauglichkeit für seinen Verwendungszweck zu prüfen. Wir geben auf Wunsch gerne Auskunft über Toleranzbreiten und anwendungstechnische Erfahrungen. Verkäufe erfolgen gemäß unseren Verkaufs- und Lieferbedingungen.

TREMIN® 283 is produced from prepared natural raw minerals. All data are approximate values with tolerances depending on occurrences and production. They only serve as description and do not represent any warranty concerning the existence of specific characteristics. Traces of coarser particles may be possible.
It applies to the user to test the suitability for his purposes.
If wanted, we are prepared to give further information on tolerances and on our experience in technical applications. Sales are subject to our sales and delivery conditions.

Figure B.7: The technical data sheet for the pretreated wollastonite powder from the Quarzwerke group.

Appendix C. Oil absorption values with liquid epoxy resin

The standard reported oil absorption values are found from absorption of linseed oil. These oil absorption values might not indicate the exact oil absorption the fillers experience with the liquid epoxy used in this work. Oil abs. values were collected experimentally with help from a Jotun employee, Ivar Thinghaugen. 1-5 grams of filler powder was weight out and placed on a glass plate. Liquid epoxy resin was added to the filler/glass plate by a pipette while the liquid epoxy was thoroughly mixed into the powder. The oil absorption value was set when all filler particles were wetted by the epoxy. This was determined to be when the filler and epoxy made a continuous and compact mass. Amount of filler and liquid epoxy needed for each filler is presented in Table C.1. The oil abs. values from the epoxy test differed with a factor of approximately 2 from the linseed oil-abs. values, resulting in lower CPVC values if the epoxy oil-abs. values were used, as shown in Table C.2.

Table C.1: Oil absorption values found experimentally, and the amount of filler and liquid epoxy used in the measurement.

Filler	Weight filler (g)	mL liquid epoxy	Spesific gravity liquid epoxy	g liquid epoxy pr 100g filler
Aramid fibers	1	2.99	1.16	346.840
Mica	5	3.93	1.16	91.176
Wollastonite	5	2.32	1.16	53.824
Barium sulfat	5	1.1	1.16	25.520

Table C.2: Critical pigment volume concentration for the four fillers used in this work calculated with the linseed oil abs. values and the liquid epoxy abs. values. The CPVC formula is given in the table with OA=oil absorption value and ρ=density.

Filler	CPVC, linseed oil (vol.%)	CPVC , liquid epoxy (vol.%)	
Barium Sulfate	61.9	50.4	$CPVC = \frac{1}{1 + \frac{OA * \rho_{filler}}{\rho_{oil}}}$
Mica	39.3	31.1	
Aramid fibers	15.0	18.8	
Wollastonite	59.8	42.6	

Appendix D. Development of curing and mixing procedure

The curing and mixing procedure were tested in the beginning of the work. The mixing procedure for the liquid epoxy/filler mixture and curing agent were tested in order to find a procedure that resulted in paint films that had a good binding system mixture. The liquid epoxy and filler particles were mixed with the use of a speedmixer from the beginning of the work. The curing procedure were tested in order to find a curing method that gave fully cured films. The mixing procedure were established in this work, and the curing procedure were developed by Jotun AS (and not by the work in this thesis). The various adjustments to the mixing method and curing procedure are listed below.

1. Curing procedure: 3 weeks on bench

Mixing method: Hand mixed

The liquid epoxy and curing agent were mixed by hand and left to cure 3 weeks on bench in room temperature. The storage modulus from the DMA experiments indicated additional cross-linking occurring when the measurement temperature was above 100°C (Figure D.1). As expected, the storage modulus decreased at elevated temperature, and passed through a minimum before the curve stabilized, due to the epoxy binding system being cross-linked. The increase in the storage modulus after the minimum (rubbery region) for the room temperature cured samples indicated that the samples cured under these conditions not were fully cured. When the wet paint film underwent curing, the liquid epoxy and curing agent molecules were more and more constrained by the formed cross-links, and some epoxide and amine groups do not collide, and remains uncured. As the temperature increases though the DMA-experiment, the mobility of the molecules in the paint film increases and the cross-linking continues, resulting in an increase in the storage modulus.

2. Curing procedure: 3 weeks on bench + 24 hours in 50°C

Mixing method: Hand mixed

The films from *step 1* were post cured 24 hours in 50°C to complete the curing process, and tested with DMA to check for any additional curing over 100°C. The storage modulus did not increase as much in the high temp. region after the films were post cured, still there was a tiny increase in the high temp region for the post cured films, indicating that the curing process

still not was fully complete (Figure D.2). The experimental results showed little reproducibility, which was thought to be explained by an unequal distribution of curing agent through the film that gave difference in local cross-link density (or defects like air bubbles).

3. Curing procedure: 3 weeks on bench
Mixing method: Speed mixed

Mixing the liquid epoxy and curing agent by a speedmixer should have resulted in less defects/air bubbles and an even distribution of the curing agent, resulting in a more even cross-link density in the films. The results still did not show any better reproducibility for the modulus values at low temperature, but showed better reproducibility for the T_g, probably due to a more even structure/segment size. The paint films were highly brittle, and the bad reproducibility could have been caused by small cracks/destructions during the sample preparation for the DMA tests.

4. Curing procedure: Jotuns procedure (1 day bench, 5 days in 60°C, 1 day bench
Mixing method: Speed mixed
+ New sample preparation method

Jotun has developed a curing procedure (1 day bench, 5 days in 60°C, 1 day bench) which shall give fully cured films for the liquid epoxy and curing agent system used in this work. This procedure was used through the rest of the work as the DMA results did not show any additional curing at high temperature with this procedure. The liquid epoxy and curing agent was speedmixed to obtain a homogeneous film. To avoid cracks/destructions during the DMA sample preparation, the samples were carefully cut and sand paper were used to adjust the sides of the samples. This sample preparation gave results with slightly better reproducibility and was regarded as the best possible precision of the results.

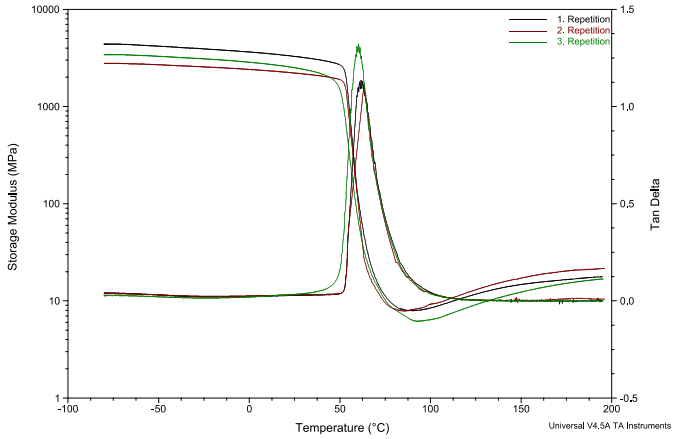

Figure D.1: Storage modulus and tan delta curve for three different neat epoxy samples cured in 3 weeks at room temperature

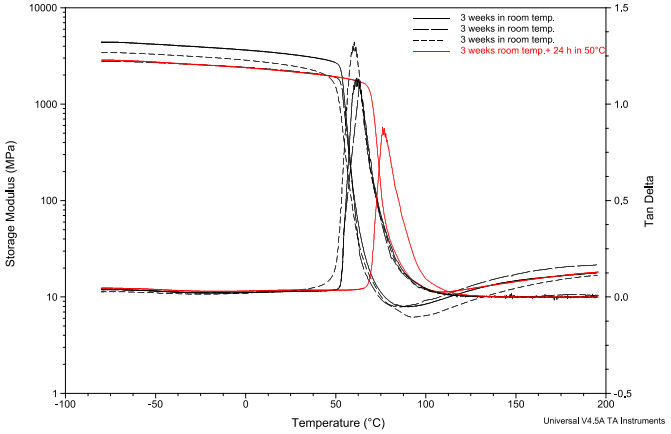

Figure D.2: Storage modulus and tan delta curve for neat epoxy sampled cured 3 weeks in room temperature and postcured 24 hours in 50ºC

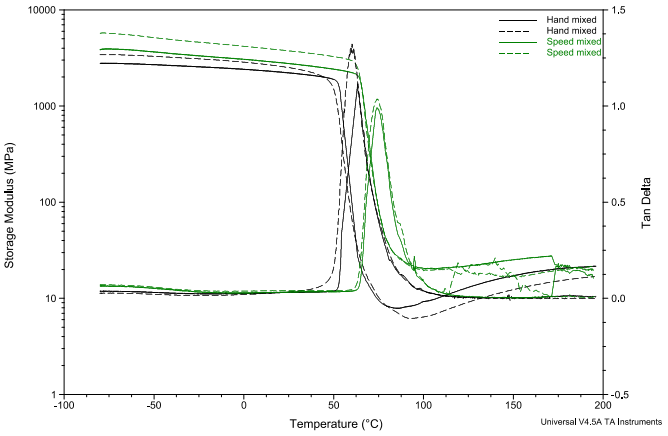

Figure D.3: Storage modulus and tan delta curve for neat epoxy samples cured 3 weeks in room temperature with different mixing method for liquid epoxy and curing agent. The irregularities seen at high temperature were due to problematic sample mounting.

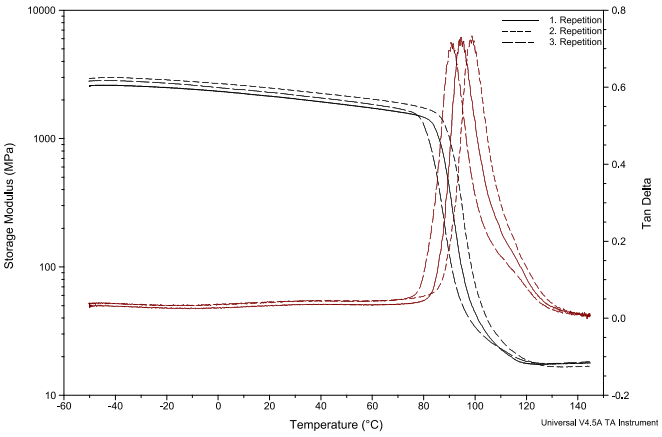

Figure D.4: Three reference neat epoxy samples cured 1 day at bench, 5 days in 60°C and 1 day bench. Amplitude of 5 μm and frequency of 1 Hz, 5°C/min.

Appendix E. XPS spectra

E.1 Survey spectra – Epoxy/filler

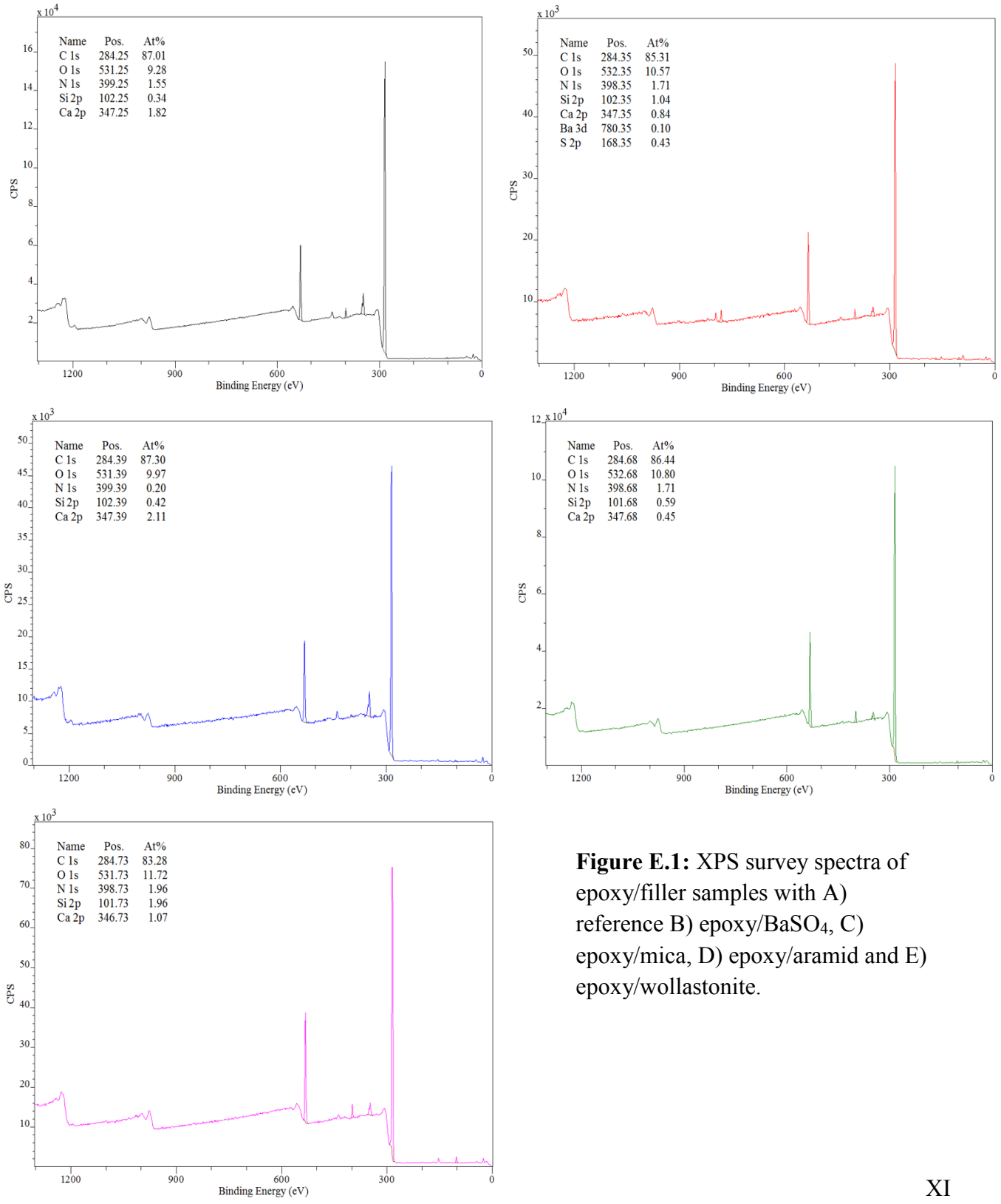

Figure E.1: XPS survey spectra of epoxy/filler samples with A) reference B) epoxy/$BaSO_4$, C) epoxy/mica, D) epoxy/aramid and E) epoxy/wollastonite.

E.1.1 High-resolution spectra – Epoxy/filler

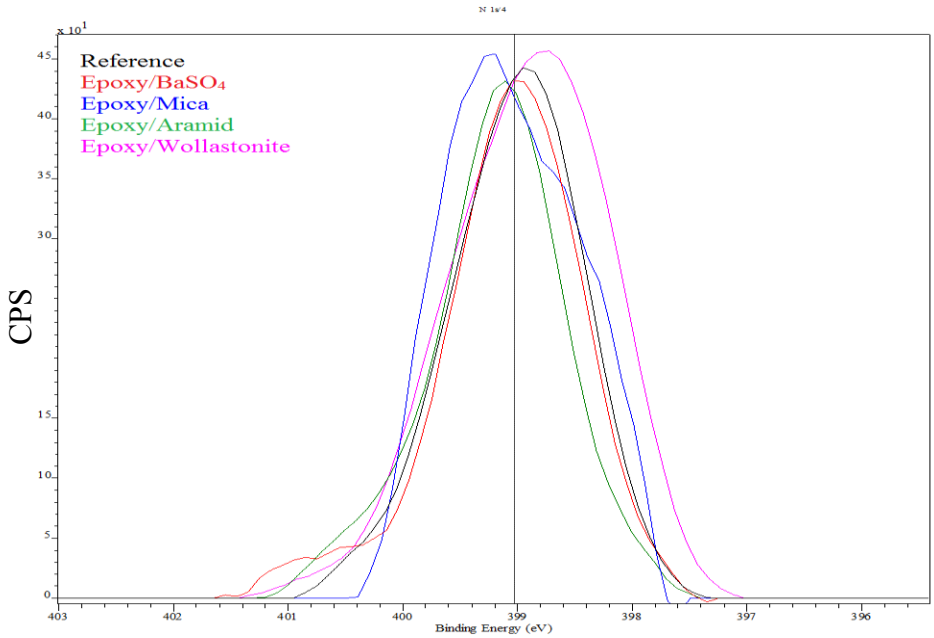

Figure E.2: High-resolution O1s spectra of all the epoxy/filler samples. The spectra have been normalized at the value given by the vertical line.

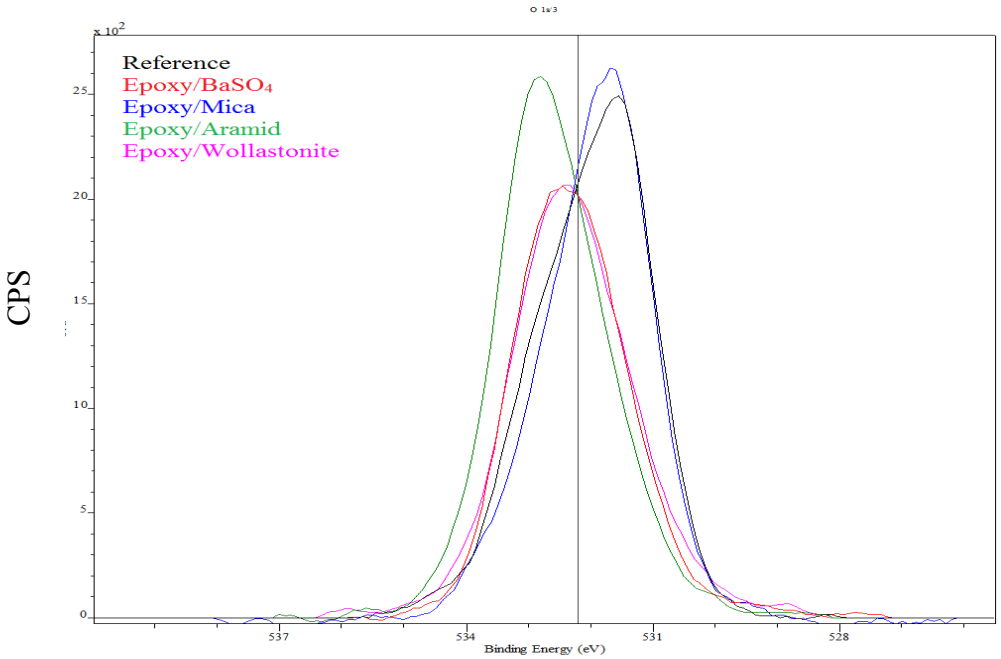

Figure E.3: High-resolution N1s spectra of all the epoxy/filler samples. The spectra have been normalized at the value given by the vertical line.

E.2 Filler elements chemical state as unmodified and modified powders and in the epoxy matrix

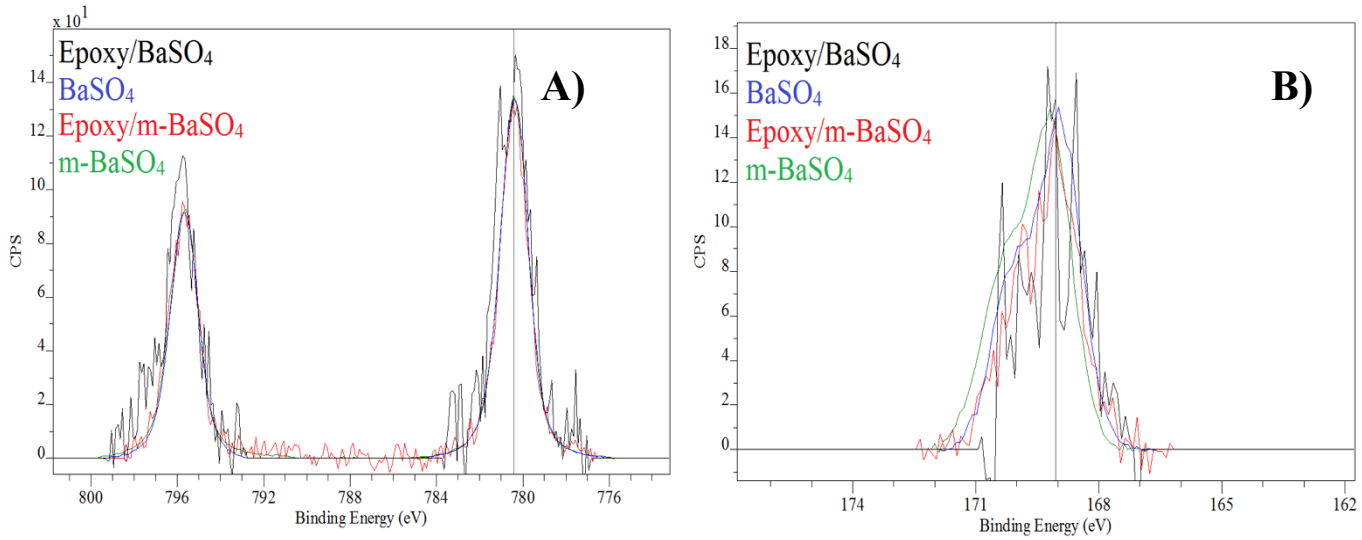

Figure E.4: High-resolution Ba3d (image A) and S2p spectra (image B) of the epoxy/$BaSO_4$ sample, unmodified $BaSO_4$, epoxy/m- $BaSO_4$ sample and modified $BaSO_4$. Normalization given by the horizontal line.

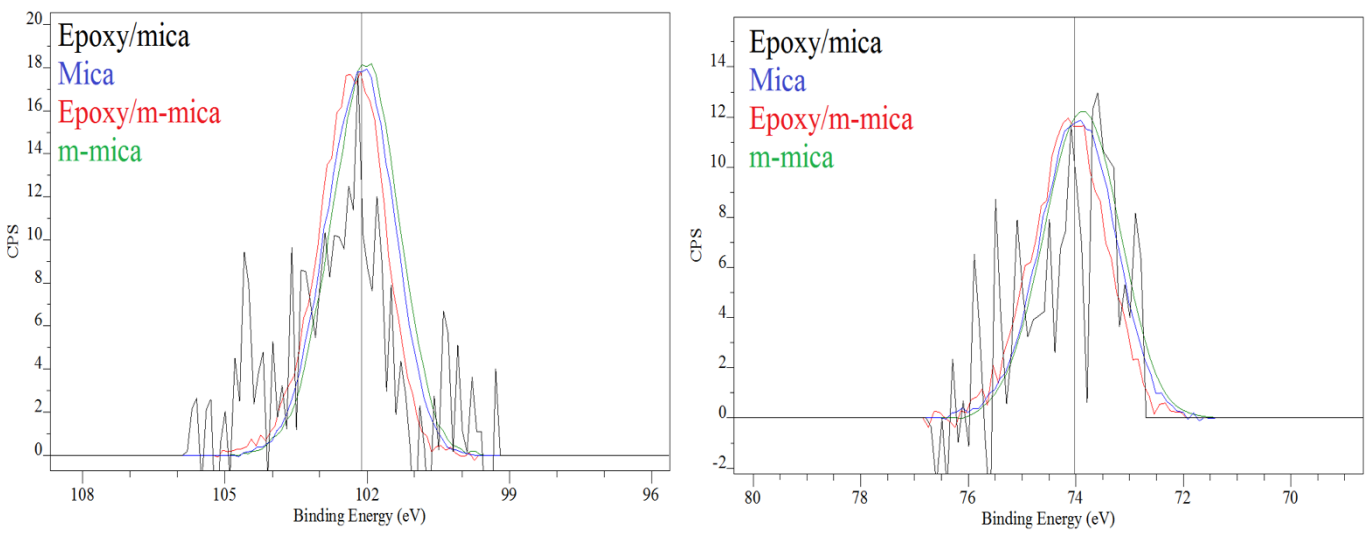

Figure E.5: High-resolution Si2p (image A) and Al 2p (image B) spectra of the epoxy/mica sample, unmodified mica, epoxy/m-mica sample and modified mica. The K 2p signal were too weak in the epoxy/(m-)filler films to be compared to the K 2p signal from the filler powders. The spectra have been normalized at the value given by the vertical line.

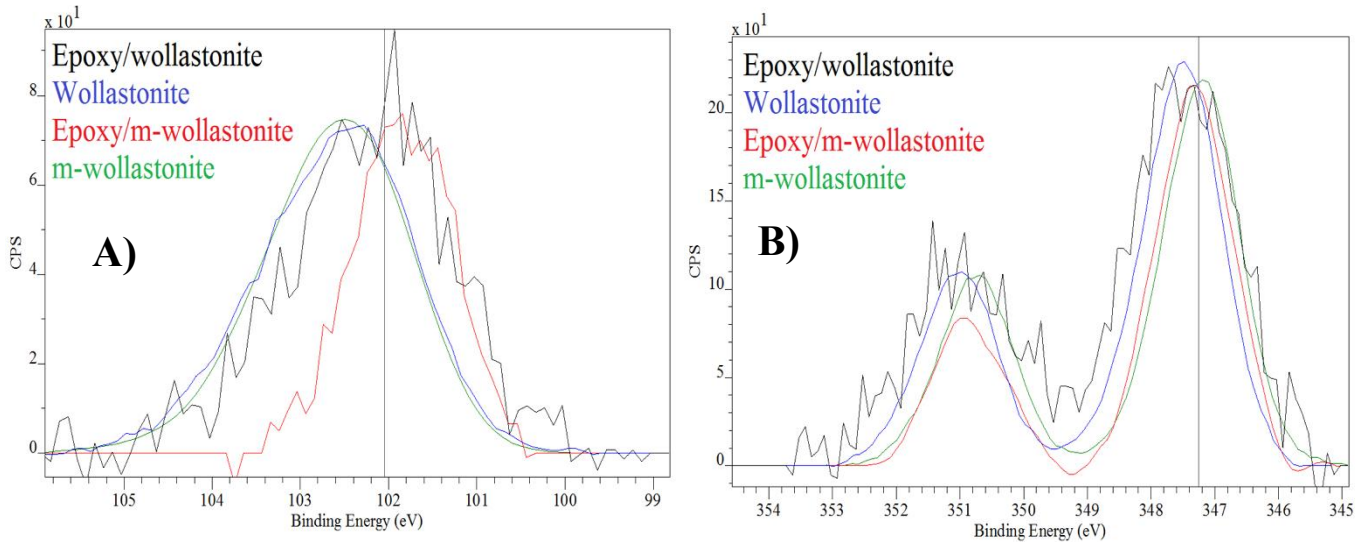

Figure E.6: High-resolution Ca2p (image A) and Si2p (image B) spectra of the epoxy/wollastonite sample, unmodified wollastonite, epoxy/m-wolla sample and modified wollastonite. The spectra have been normalized at the value given by the vertical line.

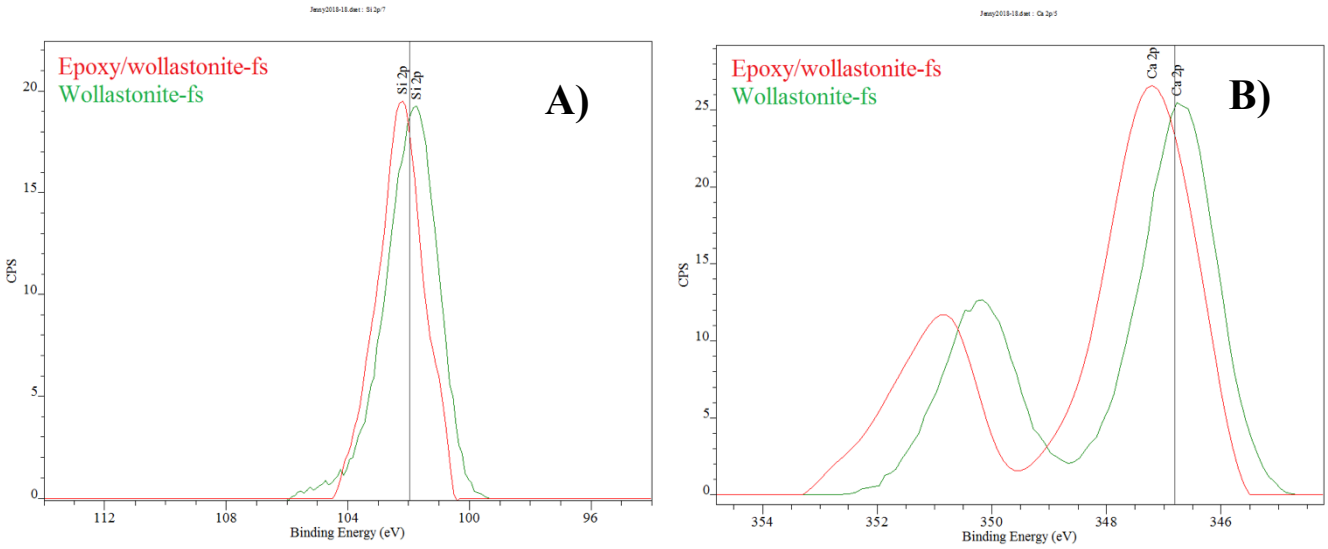

Figure E.7: High-resolution Ca2p (image A) and Si2p (image B) spectra of the epoxy/wollas-fs sample and wolla-fs powder. The spectra have been normalized at the value given by the vertical line.

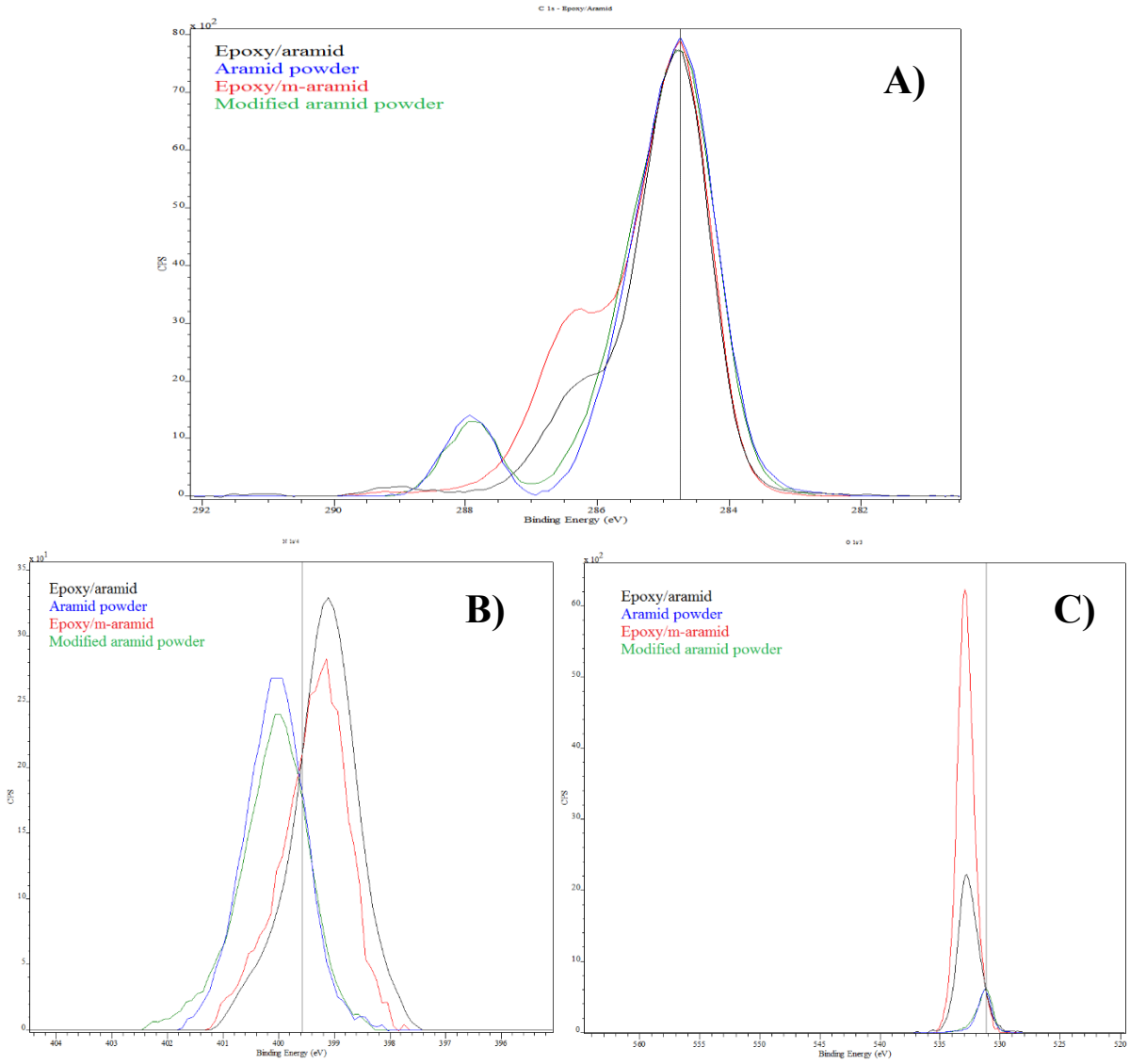

Figure E.8: High-resolution spectra of the epoxy/aramid, unmodified aramid powder, epoxy/m-aramid and modified aramid powder. A) C1s spectra, B) N1s spectra and C) O1s spectra. The chemical state of the aramid fillers as powder and in the epoxy matrix were difficult as the both the aramid fibers and the epoxy matrix consisted of the same elements (carbon, nitrogen and oxygen). There were not observed any new peaks.

E.3 Unmodified and modified filler surfaces

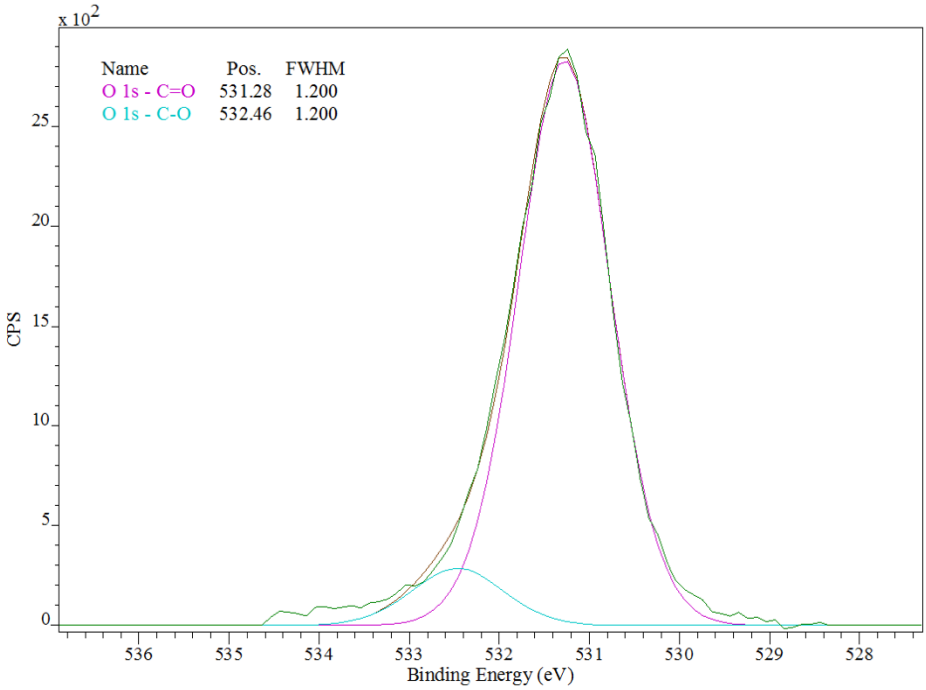

Figure E.9: High-resolution O1s spectrum of the aramid fibers.

Table E.1: Theoretical bulk composition and measured surface composition of the $BaSO_4$ powder, measured in percentage atomic concentration (at.%).

Element	Theoretical	Analysis
Ba	17	8.5
S	17	18.7
O	67	58.8
C	0	13.8
Sr	0	0.3

Table E.2: Theoretical bulk composition and measured surface composition of the mica powder, measured in percentage atomic concentration (at.%).Hydrogen are not detected by XPS and not included.

Element	Theoretical	Analysis
Si	14.3	21.9
Al	14.3	14.4
O	57.1	53.9
K	4.8	5.5
Na	0	0.3
Y	0	0.8
C	0	3.3

Table E.3: Theoretical bulk composition and measured surface composition of the aramid pulp, measured in percentage atomic concentration (at.%).

Element	Theoretical	Analysis
C	78	78.5
O	11	10.7
N	11	10.7

Table E.4: Theoretical bulk composition and measured surface composition of the wollastonite powder, measured in percentage atomic concentration (at.%).

Element	Theoretical	Analysis
Ca	20	13.72
Si	20	24.32
O	60	53.05
C	0	8.68
Y	0	0.24

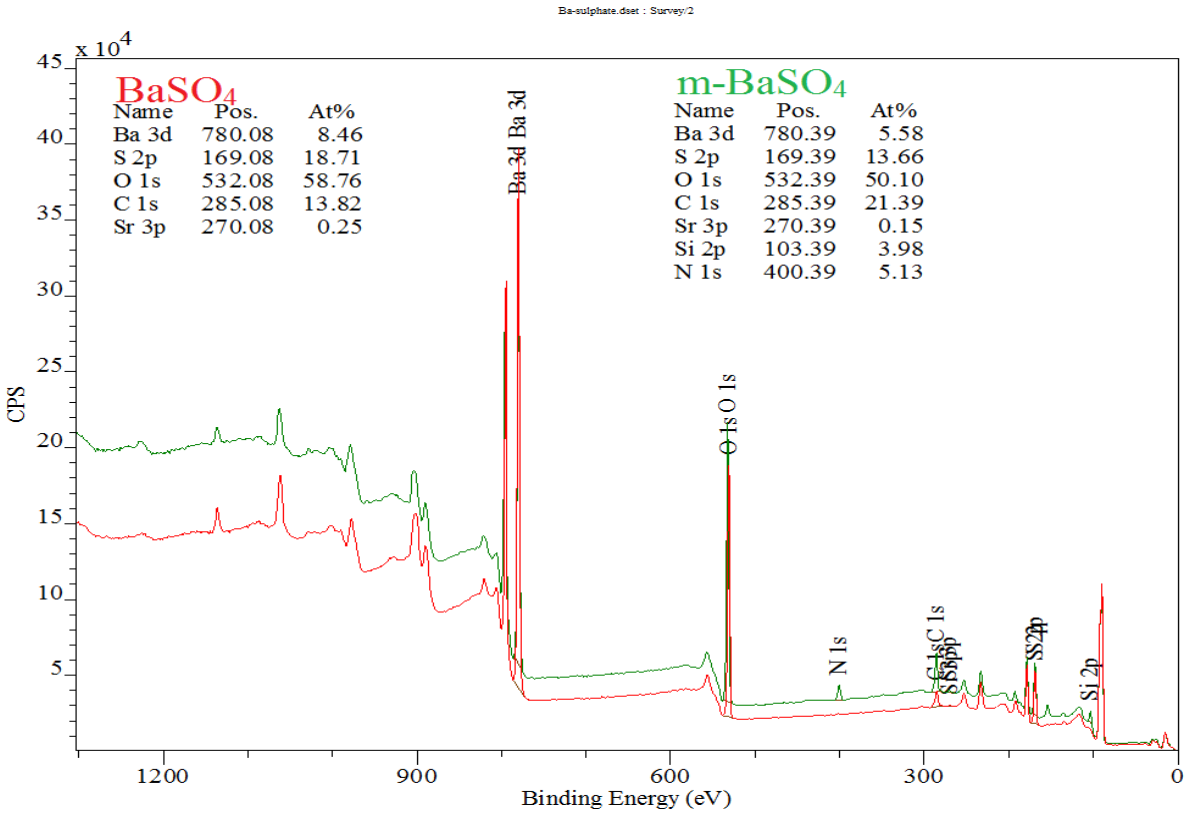

Figure E.10: XPS survey spectra of unmodified and modified $BaSO_4$ powder.

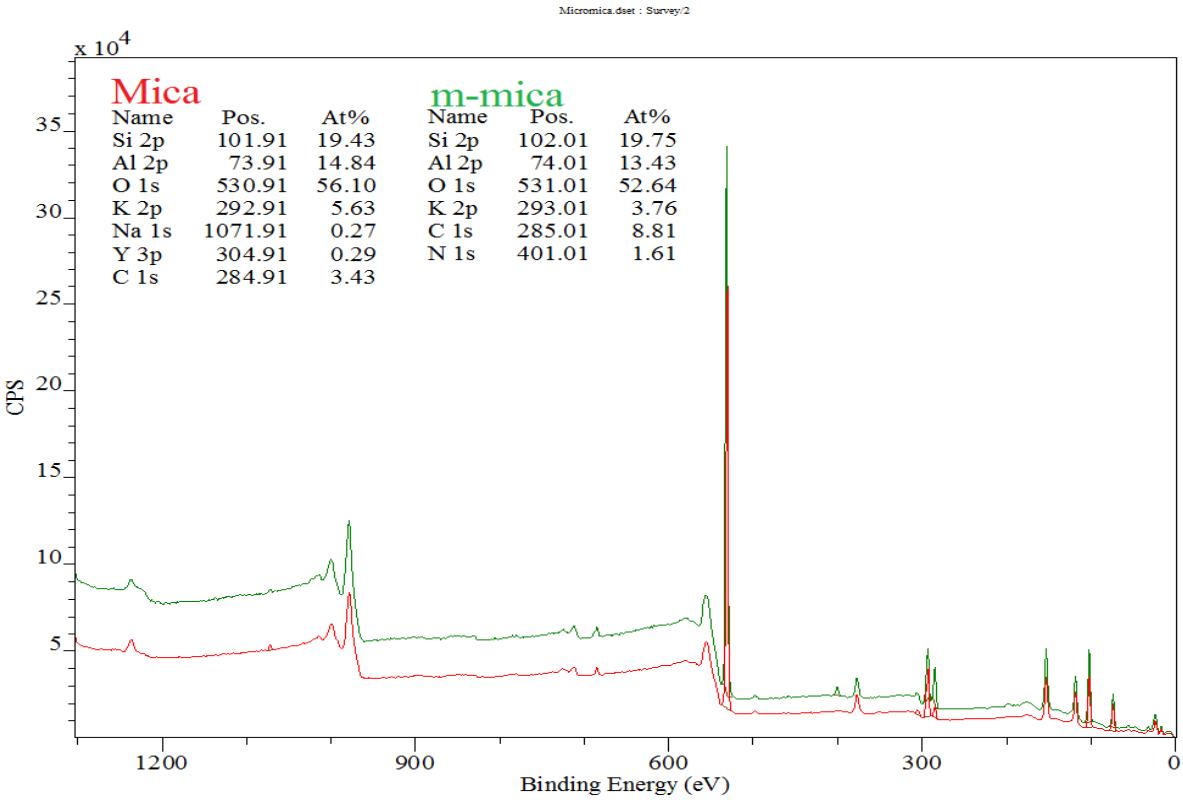

Figure E.11: XPS survey spectra of unmodified and modified mica powder.

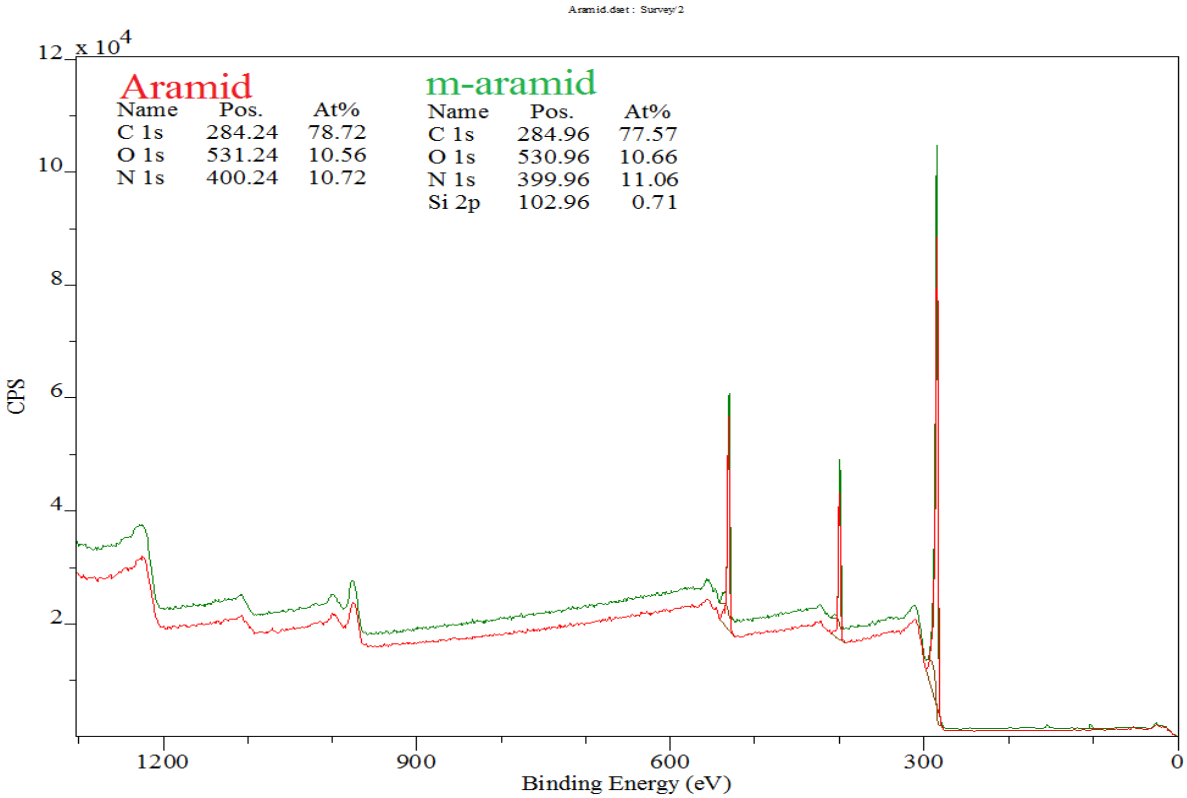

Figure E.12: XPS survey spectra of unmodified and modified aramid powder.

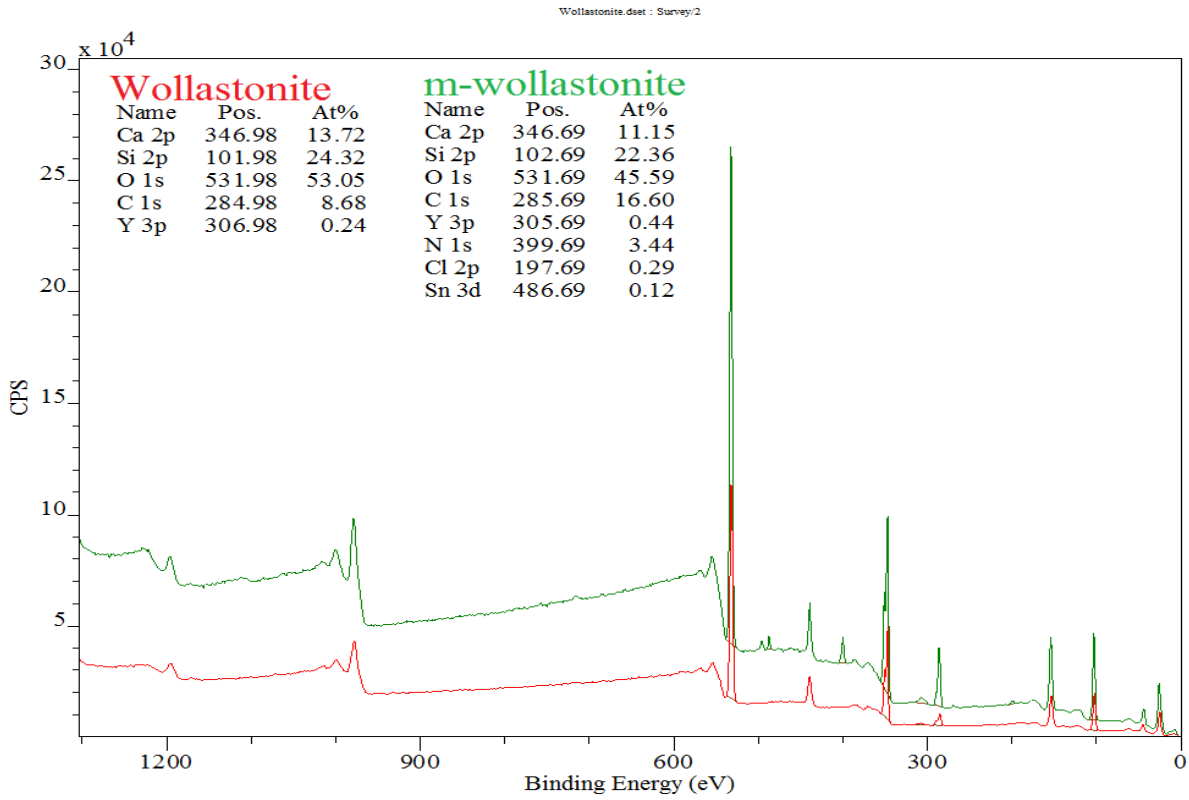

Figure E.13: XPS survey spectra of unmodified and modified wollastonite powder.

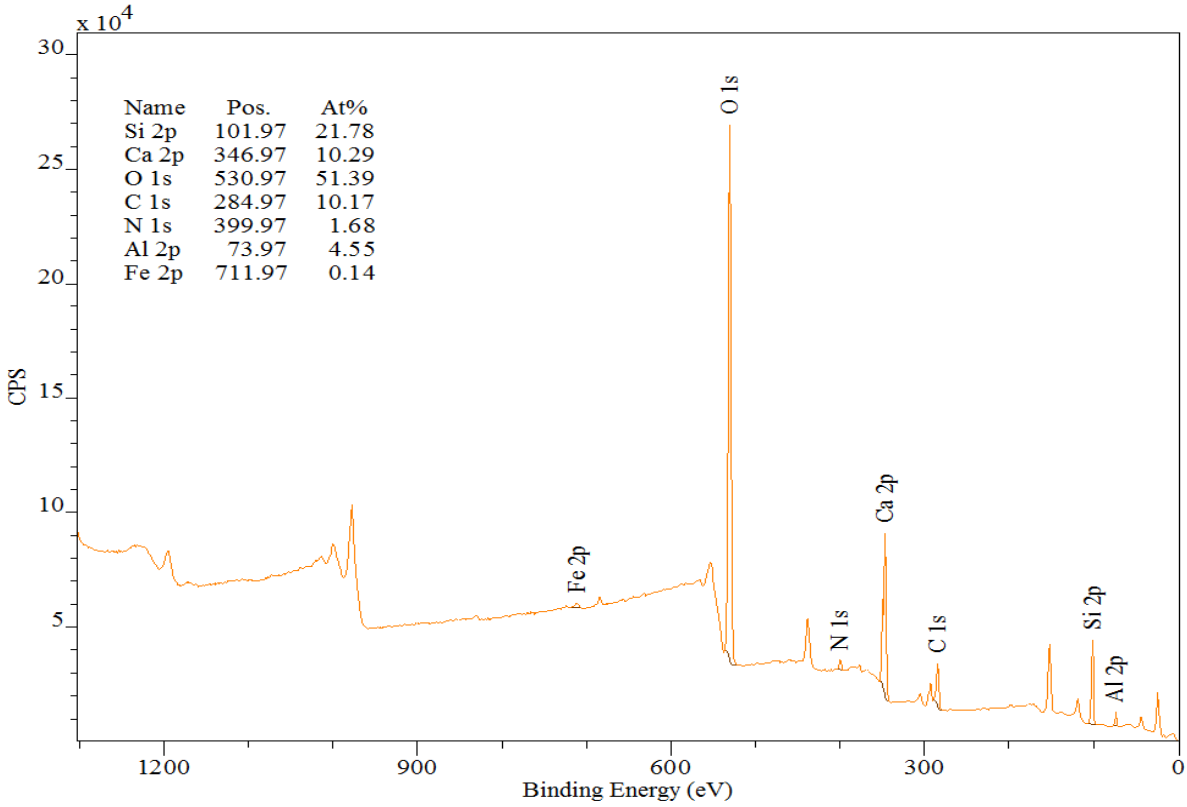

Figure E.14: XPS survey spectra of the pretreated wolla-fs powder.

E.4 Survey spectra – Epoxy/m-filler

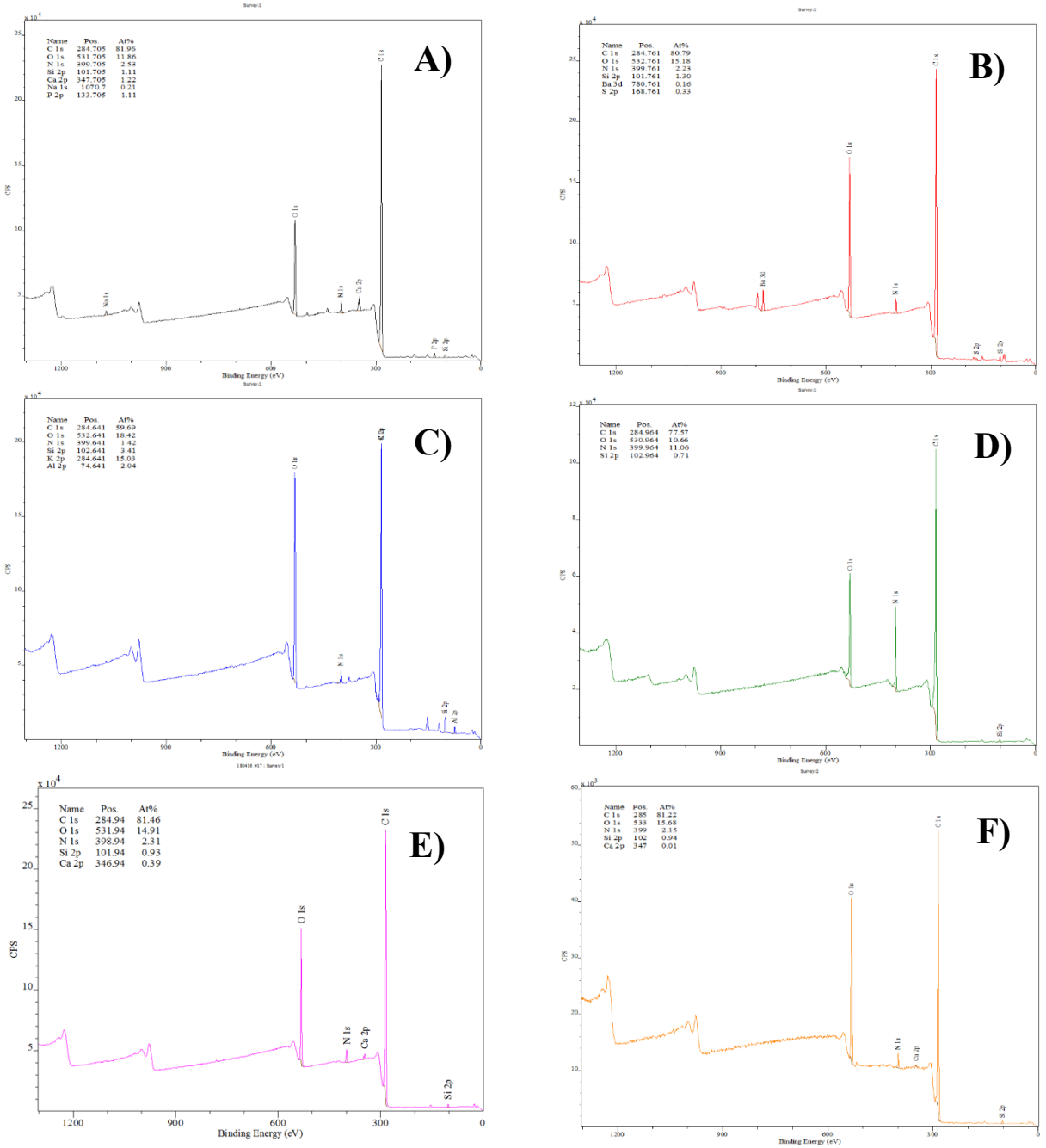

Figure E.15: Survey spectra of fracture surface samples used for XPS analysis of A) reference, B) epoxy/m-$BaSO_4$, C) epoxy/m-mica, D) epoxy/m-aramid, E) epoxy/m-wolla and F) epoxy/wolla-fs.

Appendix F. Fourier transform infrared spectroscopy results

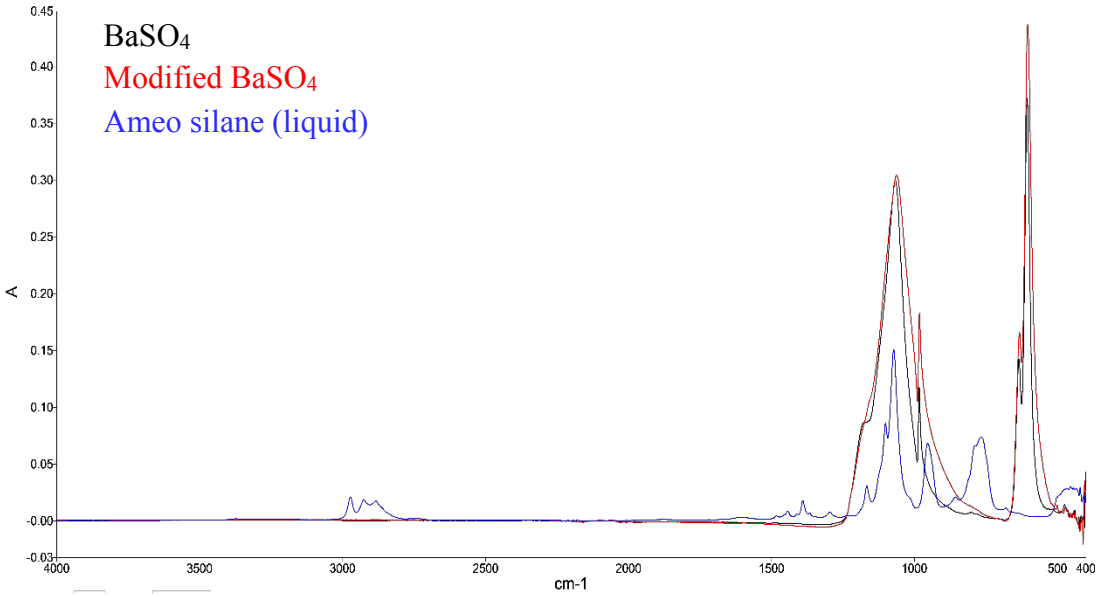

Figure F.1: FT-IR spectra of $BaSO_4$ powder (black), modified $BaSO_4$ powder (red) and ameo silane in liquid form (blue). The spectra were collected with 12 scans and a resolution of 4 cm^{-1} at room temperature.

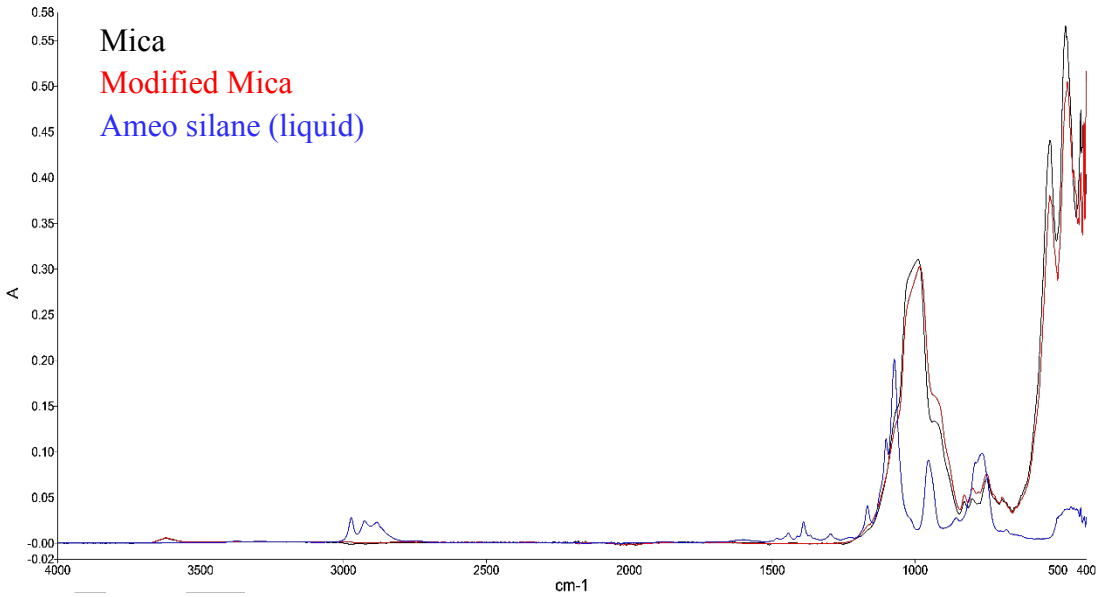

Figure F.2: FT-IR spectra of mica powder (black), modified mica powder (red) and ameo silane in liquid form (blue). The spectra were collected with 12 scans and a resolution of 4 cm^{-1} at room temperature.

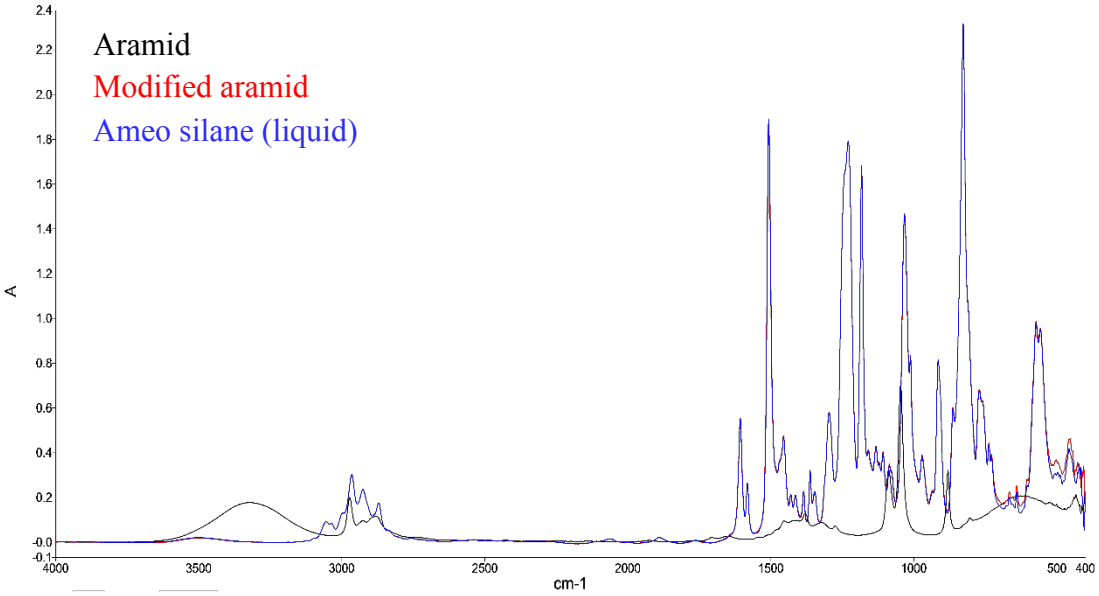

Figure F.3: FT-IR spectra of aramid powder (black), modified aramid powder (red) and ameo silane in liquid form (blue). The spectra were collected with 12 scans and a resolution of 4 cm^{-1} at room temperature.

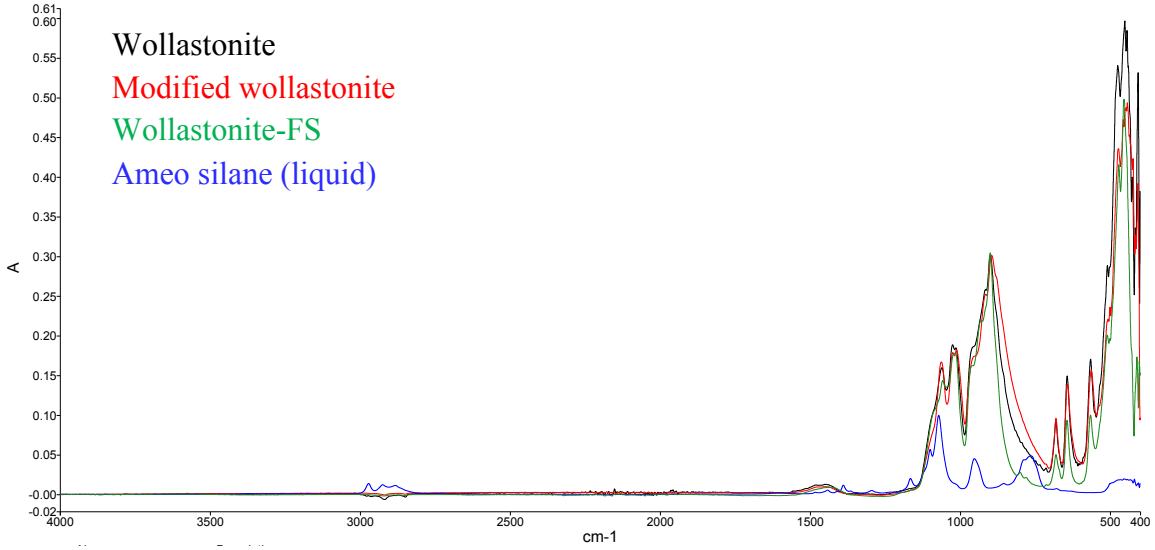

Figure F.4: FT-IR spectra of wollastonite powder (black), modified wollastonite powder (red), the wollastonite-fs powder (green) and the ameo silane in liquid form (blue). The spectra were collected with 12 scans and a resolution of 4 cm^{-1} at room temperature.

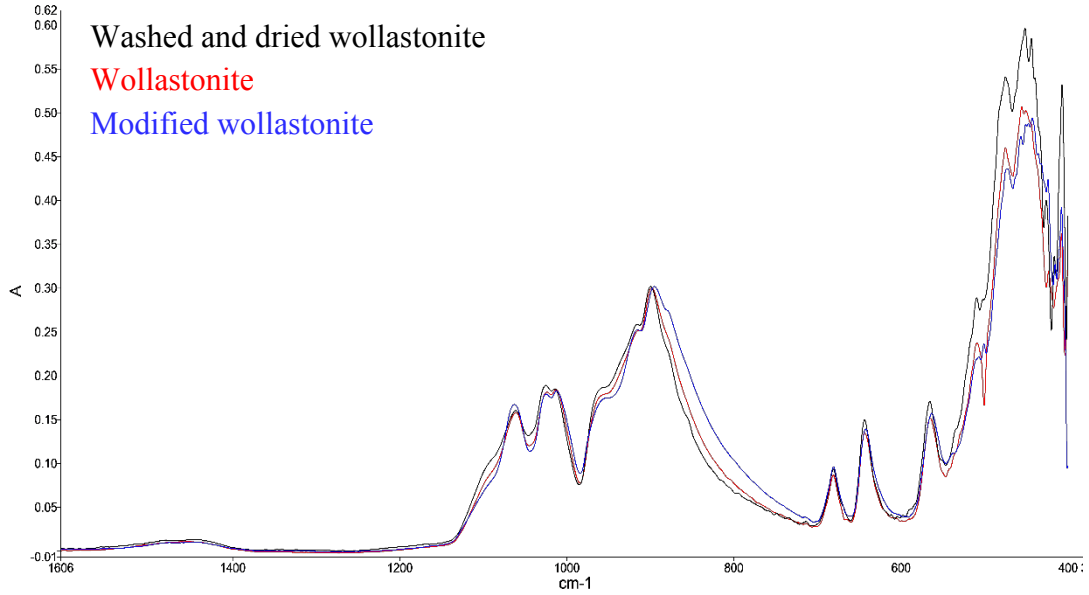

Figure F.5: FT-IR spectra of washed and dired wollastonite powder (black), unmodified mica powder (red) and modified wollastonite powder (blue). The spectra were collected with 12 scans and a resolution of 4 cm^{-1} at room temperature.

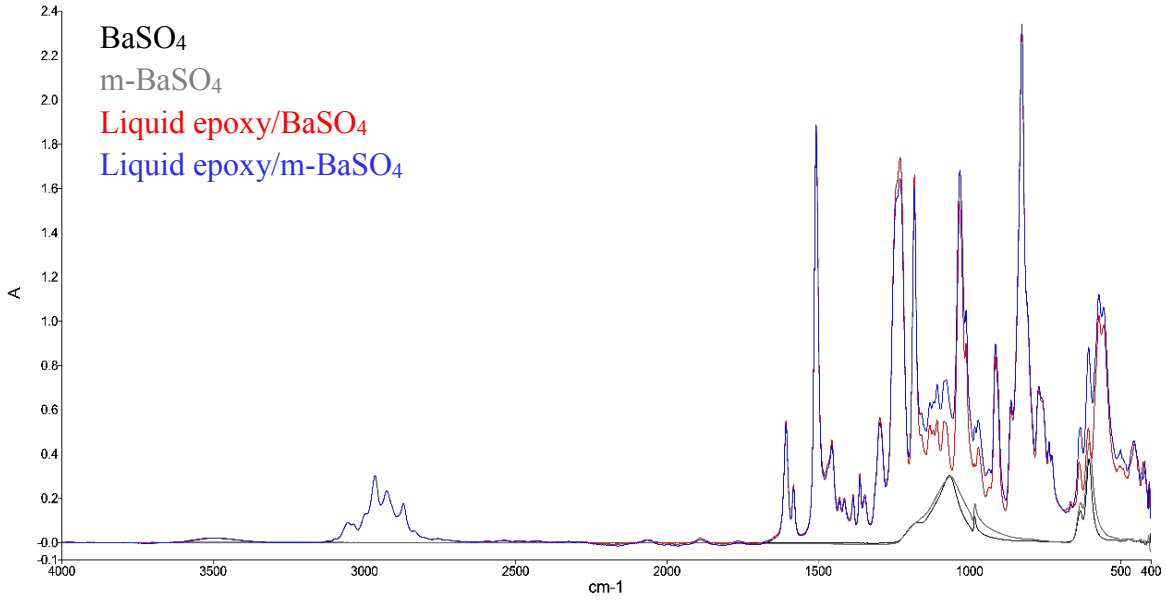

Figure F.6: FT-IR spectra of unmodified $BaSO_4$ powder (black), modified $BaSO_4$ powder (grey), a liquid epoxy/$BaSO_4$ mixture (red) and a liquid epoxy/m-$BaSO_4$ mixture (blue). The spectra were collected by 12 scans, with a resolution of 4 cm^{-1} at room temperature.

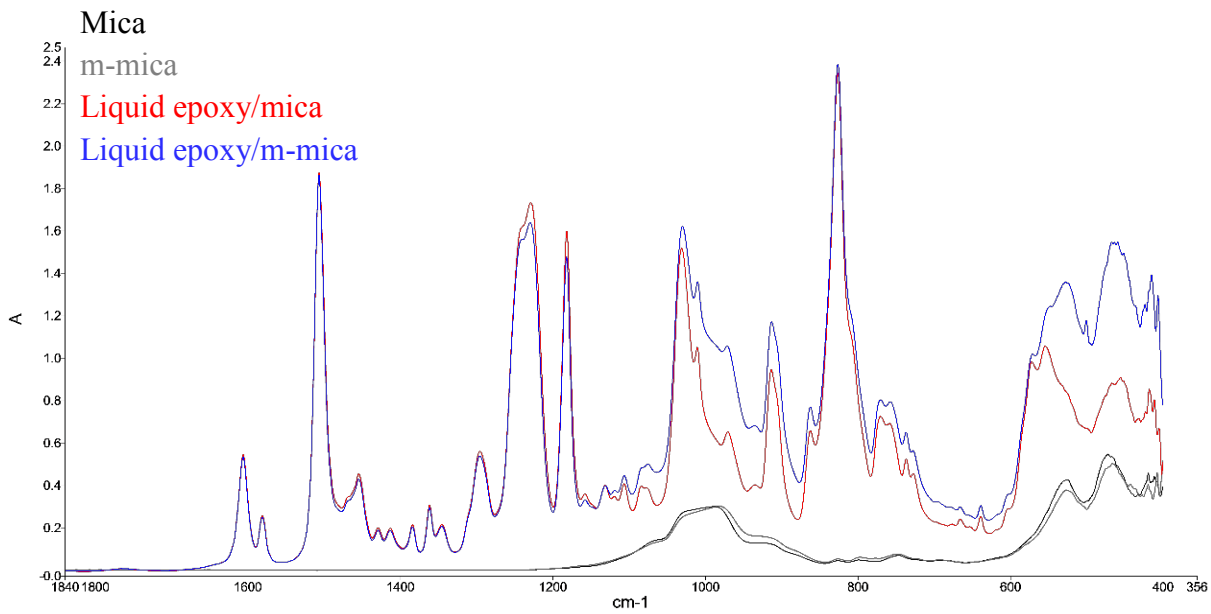

Figure F.7: FT-IR spectra of unmodified mica powder (black), modified mica powder (grey), a liquid epoxy/mica mixture (red) and a liquid epoxy/m-mica mixture (blue). The spectra were collected by 12 scans, with a resolution of 4 cm^{-1} at room temperature.

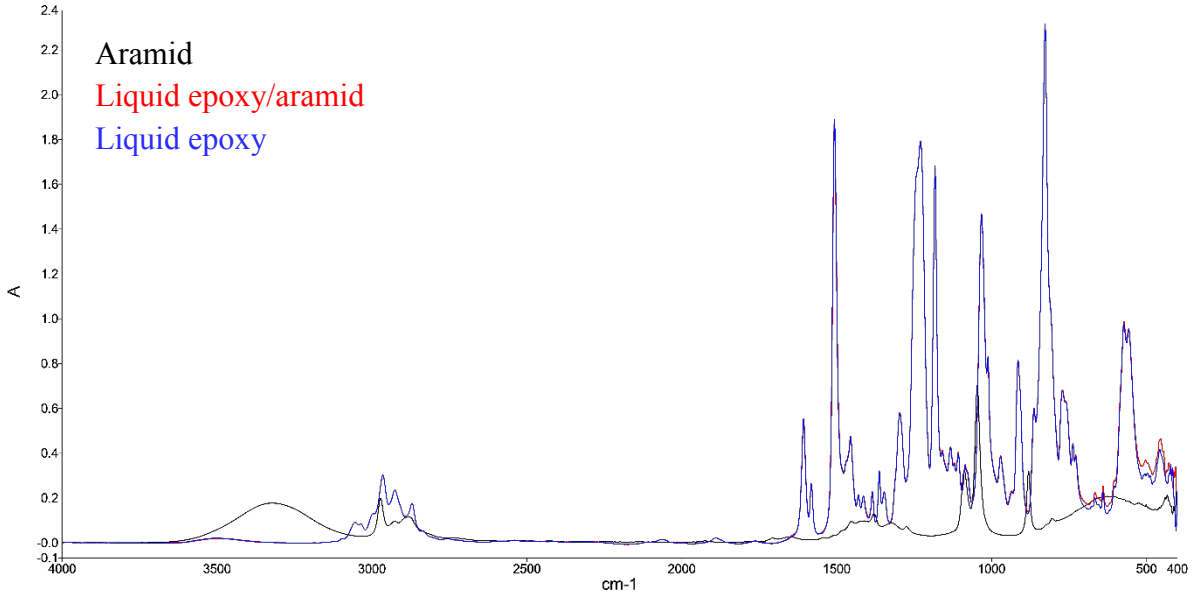

Figure F.8: FT-IR spectra of unmodified aramid powder (black), a liquid epoxy/aramid mixture (red) and pure liquid epoxy (blue). The spectra were collected by 12 scans, with a resolution of 4 cm^{-1} at room temperature.

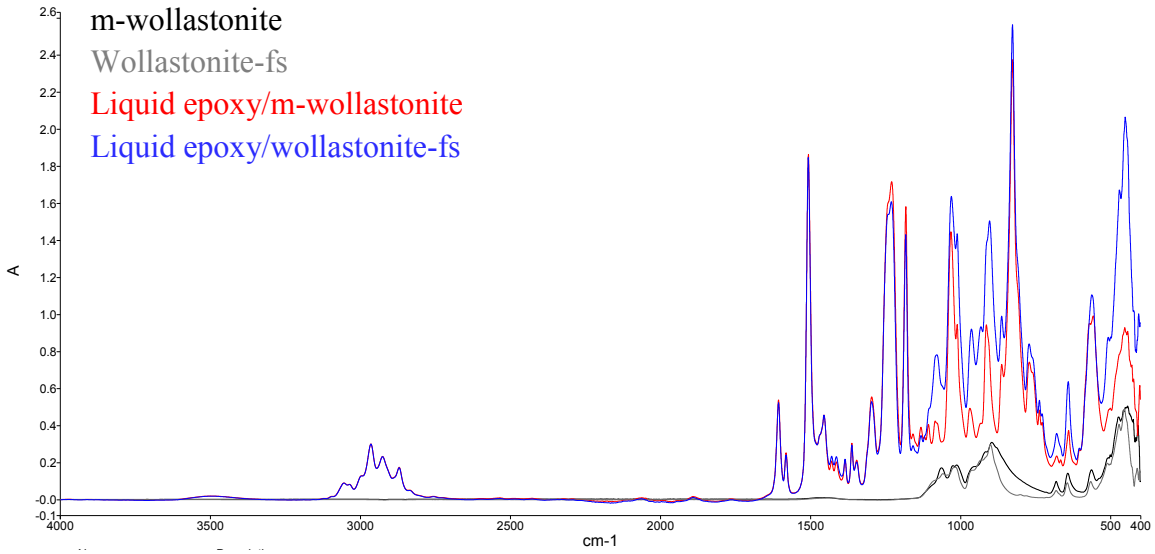

Figure F.9: FT-IR spectra of modified wollastonite powder (black), wollastonite-fs powder (grey), a liquid epoxy/m-wollastonite mixture (red) and a liquid epoxy/wollastonite-fs mixture (blue). The spectra were collected by 12 scans, with a resolution of 4 cm^{-1} at room temperature.

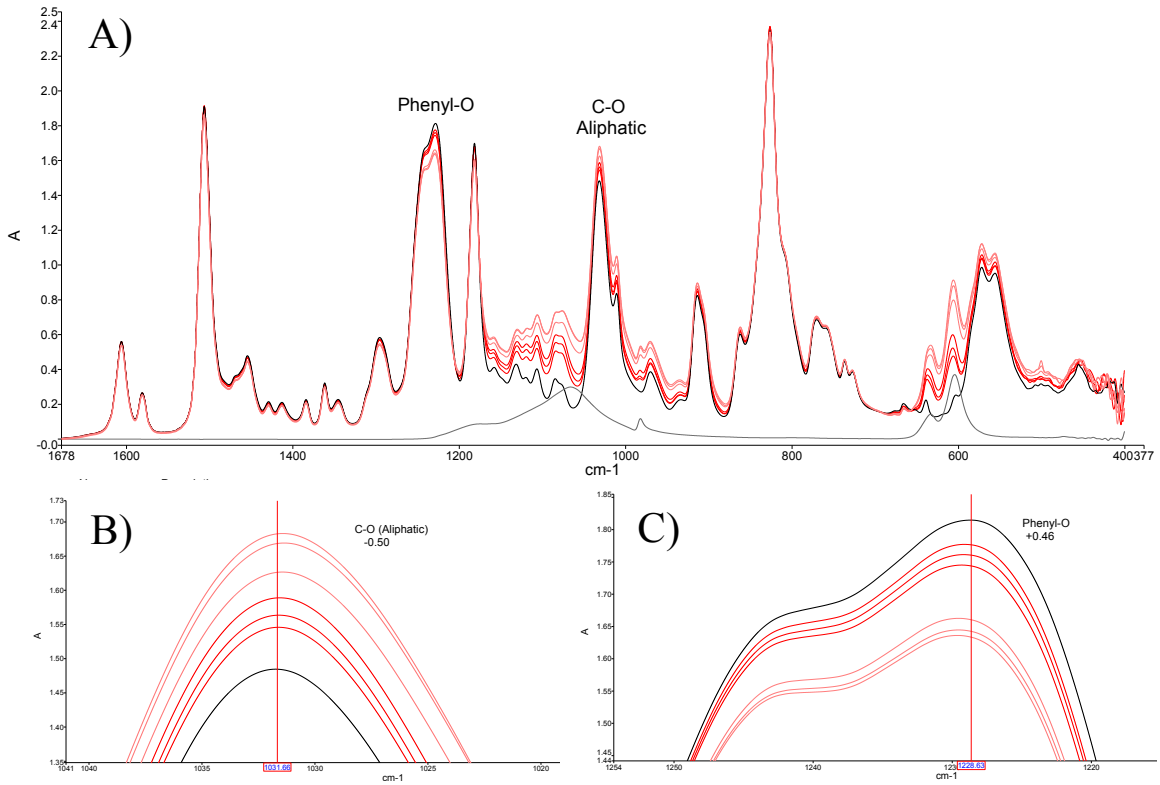

Figure F.10: The FT-IR spectra of pure liquid epoxy (black line), liquid epoxy/$BaSO_4$ mixture (red line, three repetitions), liquid epoxy/m-$BaSO_4$ mixture (light red lines, three repetitions) and unmodified $BaSO_4$ powder (grey line). A) show the spectra with some signals specified to chemical groups, B) close-up image of the C-O signal and C) close-up image of the C-O signal.

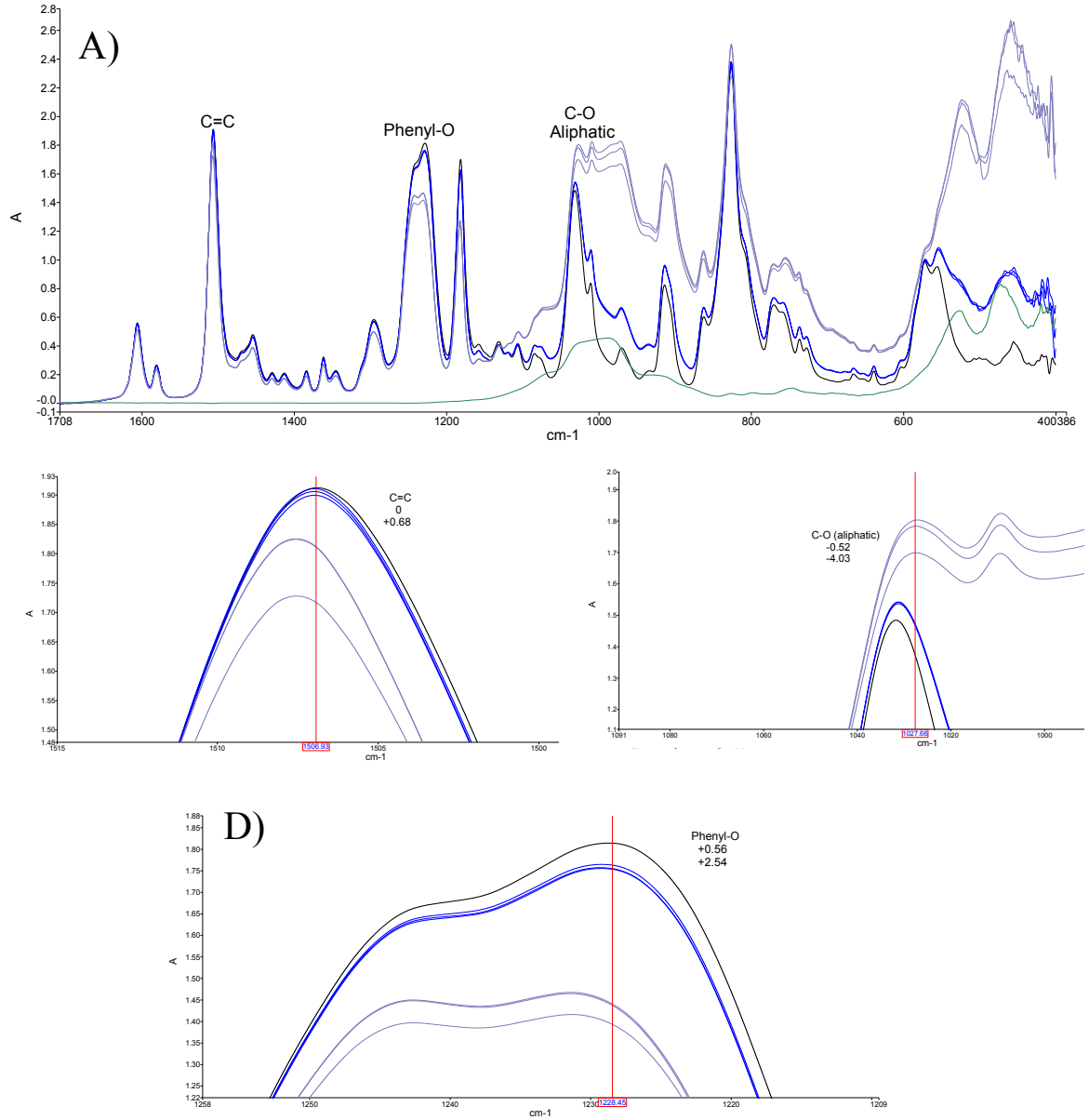

Figure F.11: The FT-IR spectra of pure liquid epoxy (black line), liquid epoxy/mica mixture (blue lines, three repetitions), liquid epoxy/m-mica mixture (light blue, three repetitions) and unmodified mica powder (green line). A) show the spectra with some signals specified to chemical groups, B) close-up image of the C=C signal and C) close-up image of the C-O signal and D) close-up image of the Phenyl-O signal.

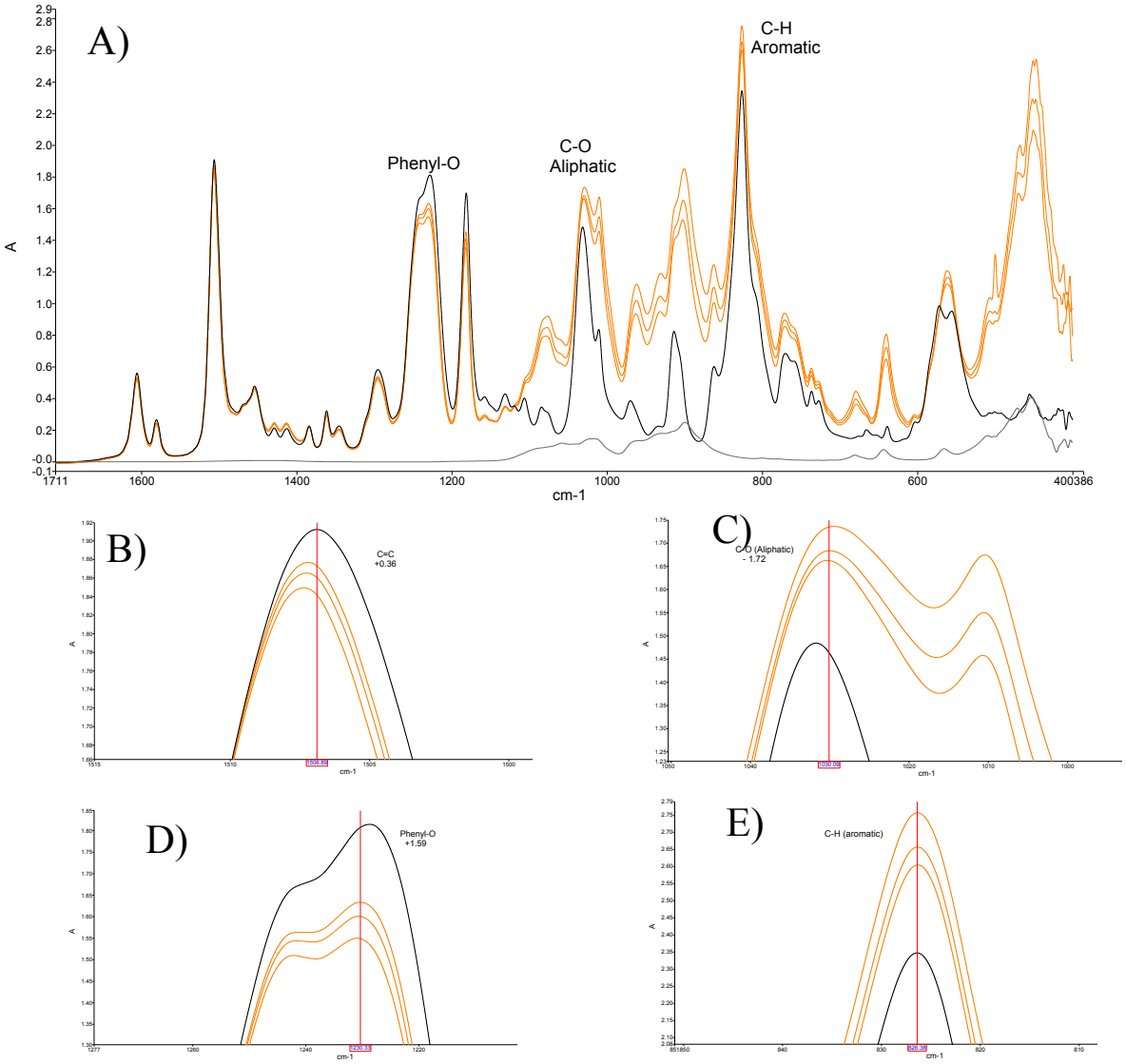

Figure F.12: The FT-IR spectra of pure liquid epoxy (black line), liquid epoxy/wolla-fs mixture (orange lines, three repetitions) and the wolla-fs powder (grey line). A) show the spectra with some signals specified to chemical groups, B) close-up image of the C=C signal and C) close-up image of the C-O signal and D) close-up image of the Phenyl-O signal and E) close-up image of the C-H (aromatic) signal.

Appendix G. Orientation and distribution of filler particles

G.1 Orientation of filler particles in the epoxy/mica and epoxy/wollastonite films

Table G.1: Orientation observed in horizontal and vertical cross-section in the paint films with applied thickness of 200-1200μm. Presented as ratio between number of particles aligned horizontal versus vertical.

Applied wet thickness (μm)	**Epoxy/mica Ratio, horiz./verti.**		**Epoxy/wollastonite Ratio, horiz./verti.**	
	Horizontal	*Vertical*	*Horizontal*	*Vertical*
200	3.7 ± 0.4	6.2 ± 1.5	1.7 ± 0.4	4.7 ± 1.6
400	2.7 ± 0.8	2.1 ± 0.1	5.1 ± 1.1	3.8 ± 0.7
600	2.7 ± 0.2	4.5 ± 2.5	2.3 ± 0.1	3.2 ± 0.7
800	2.8 ± 0.5	2.8 ± 0.7	3.6 ± 0.4	7.7 ± 1.6
1000	2.1 ± 0.4	3.9 ± 1.0	2.2 ± 0.5	3.2 ± 0.9
1200	3.1 ± 1.4	2.6 ± 1.1	3.2 ± 0.2	2.5 ± 0.1
Average	**2.9 ± 0.5**	**3.7 ± 1.5**	**3.4 ± 1.2**	**4.2 ± 1.9**

G.2 Epoxy/m-filler

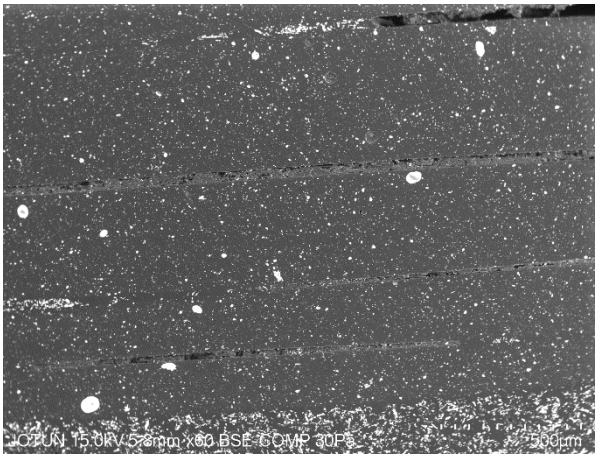

Figure G.1: Cross-section of epoxy/m-$BaSO_4$ films of applied thickness from 200-1000 µm.

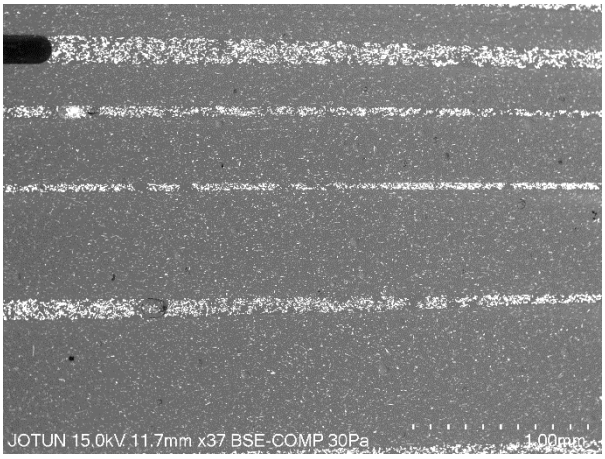

Figure G.2: Cross-section of epoxy/m-mica films of applied thickness from 200-1200 µm.

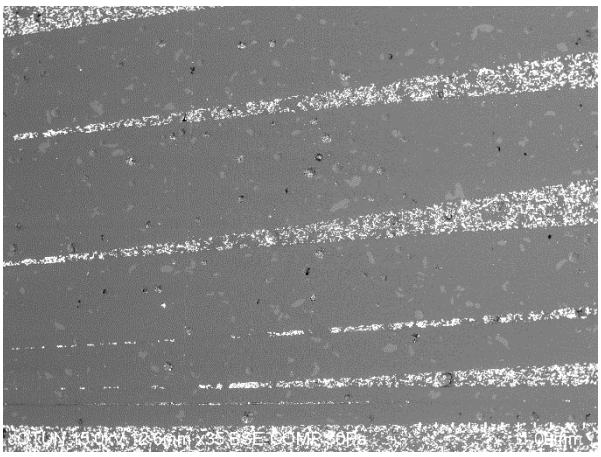

Figure G.3: Cross-section of epoxy/m-aramid films of applied thickness from 200-1200 µm.

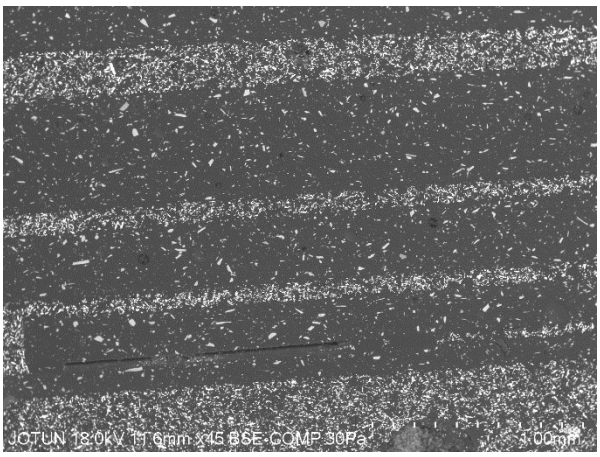

Figure G.4: Cross-section of epoxy/m-wolla films of applied thickness from 200-800 µm.

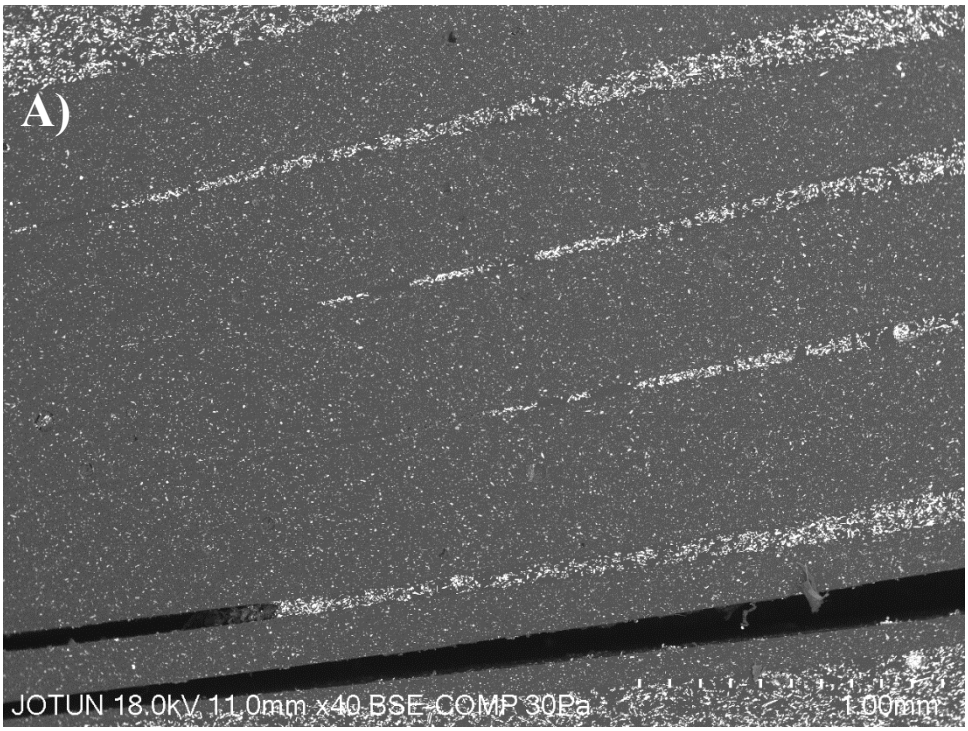

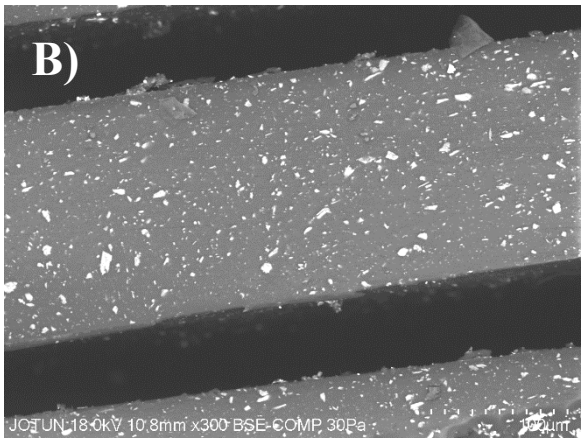

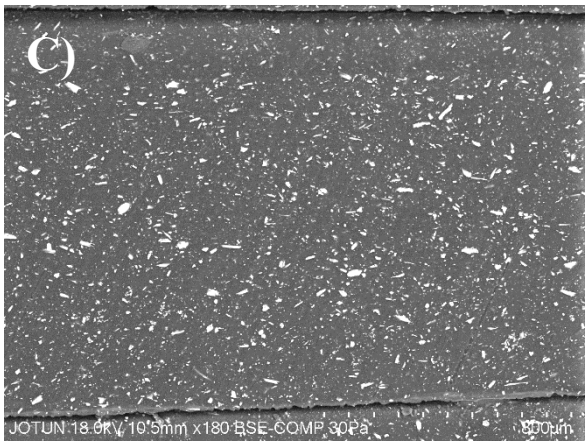

Figure G.5: A) Cross-section of epoxy/wolla-fs films of applied thickness from 200-1200 µm, B) horizontal cross-section of an epoxy/wolla-fs film with applied thickness of 400 µm and C) vertical cross-section of an epoxy/wolla-fs film with applied thickness of 400 µm.

Appendix H. Dynamical mechanical analysis

H.1 Linear viscoelastic region

In order to test the films dynamical mechanical properties, the films were tested with a DMA with an amplitude inside the linear viscoelastic region (LVR) of the samples. The linear viscoelastic region of the samples was found by observing the stress-strain curve of a pure epoxy film. As seen by Figure H.1, the epoxy film had a linear stress-strain curve until ~ 1.2 % in strain.

The samples in a DMA test were kept around 10 mm long, and a strain of 1.2 % would then correspond to a stretch of 120 µm. The amplitude of all DMA experiments was set to 5 µm, a value well inside of the LVR of the pure epoxy sample.

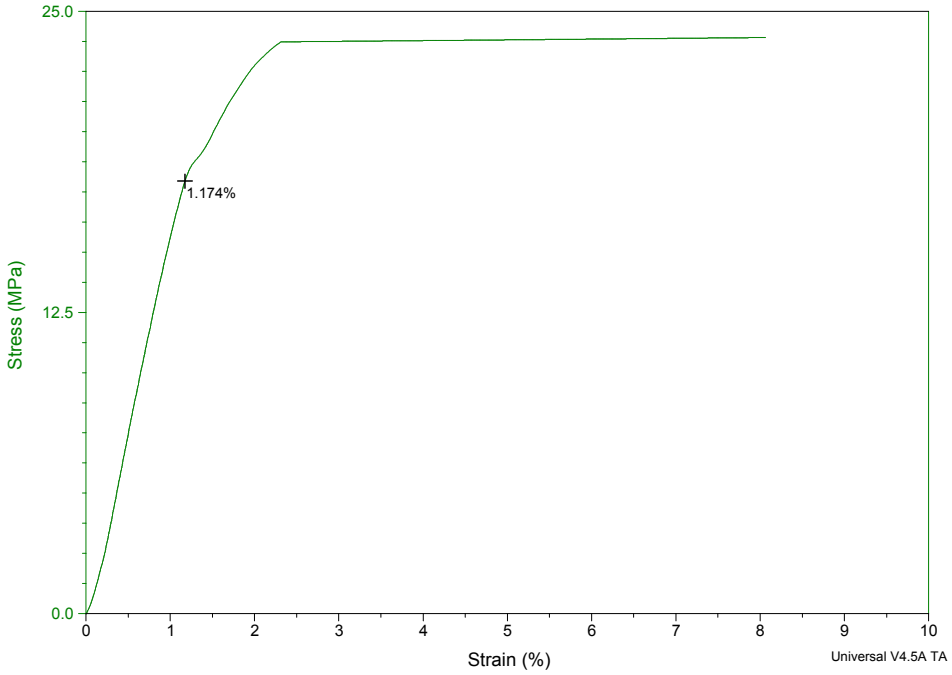

Figure H.1: Stress-strain test with DMA of a pure epoxy film cured 3 weeks in room temperature

H.2 Heating rate, 2°C/min versus 5°C/min

The heating rate in the DMA measurements was set to 5°C/min, but one epoxy/aramid sample was also tested with 2°C/min in order to see if there were any additional transitions at the slower heating rate. Articles with reported values from DMA measurements on epoxy systems have used 2°C/min, 3°C/min and 5°C/min as heating rates [2,3,4], respectively, and as no additional transitions were observed for the epoxy/aramid sample at 2°C/min (see Figure H.2), 5°C/min was chosen as heating rate. The irregularity for the epoxy/aramid sample tested at 5°C/min appeared due to the not fully cured state of the sample and/or problematic sample mounting.

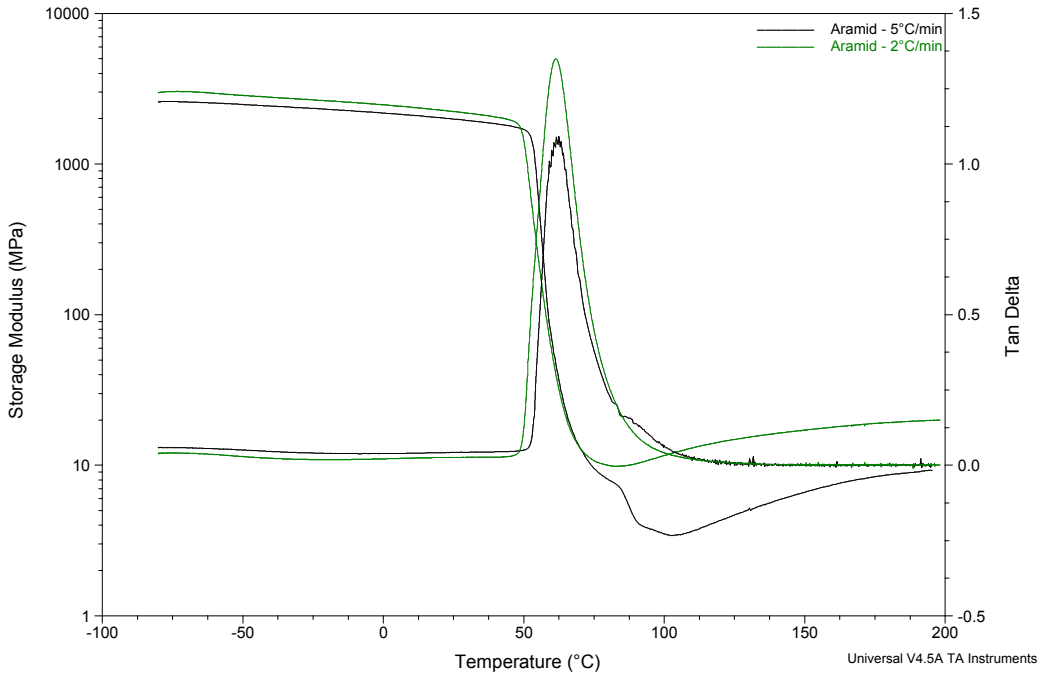

Figure H.2: Storage modulus and tan delta curves for two epoxy/aramid samples tested at 5°C/min (black curves) and 2°C/min (green lines). All other experimental setup was identical (amplitude of 5 μm and frequency of 1 Hz).

[2] D. Olmos, J. Baselga, I. Mondragon, J. Gonzáles-Benito. "The effect of surface modification of silica microfillers in an epoxy matrix on the thermo-mechanical properties – *Journa of adhesion science and technology, 22,* **2008**, 1443-1459

[3] M. Sudheer. "Thermomechanical properties of epoxy/PTW composites" – *Journal of mechanical engineering and automation, 6,* **2016**, 18-21

[4] Z. Yuan, J. Yu, B. Rao, H. Bai, N. Jiang, J. Gao, S. Lu. "Enhanced thermal properties of epoxy composites by using hyperbranched aromatic polyamide grafter silicon whiskers" – *Macromolecular research, 22(4),* **2014**, 405-411

H.3 Tan δ curves

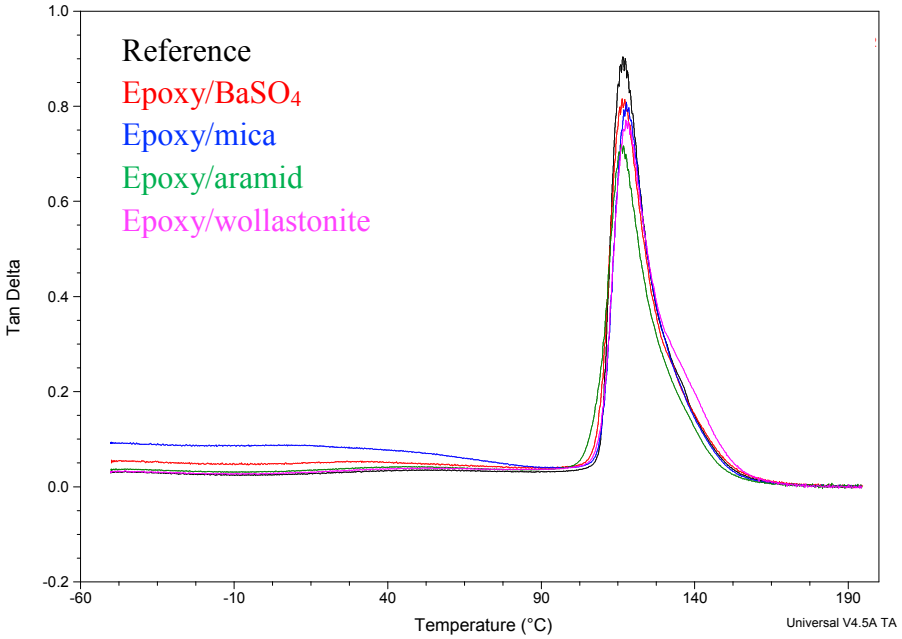

Figure H.3: Tan δ curves which do not show the shoulder on the right side.

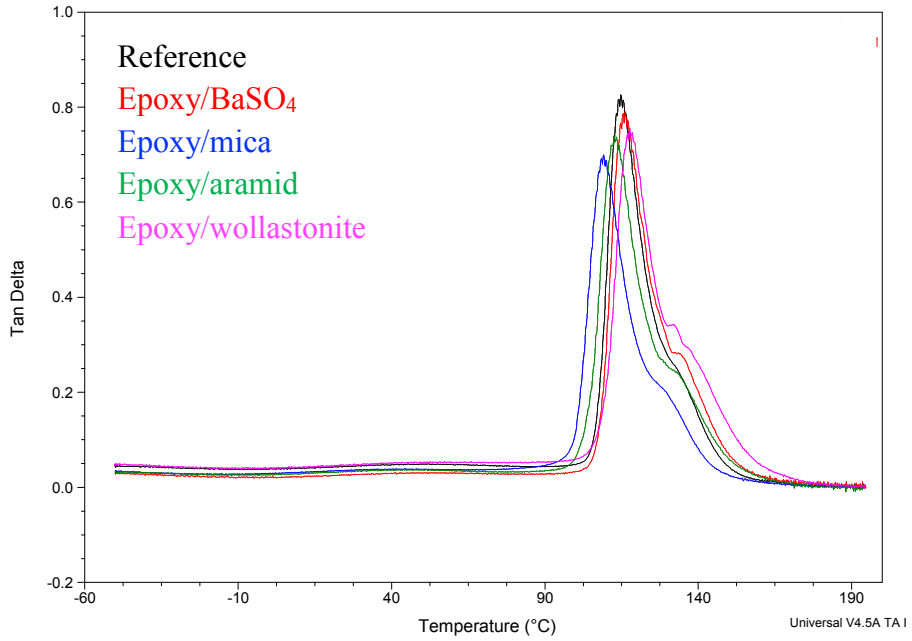

Figure H.4: Tan δ curves which show the shoulder on the right side.

H.4 Directional dependence of mechanical properties

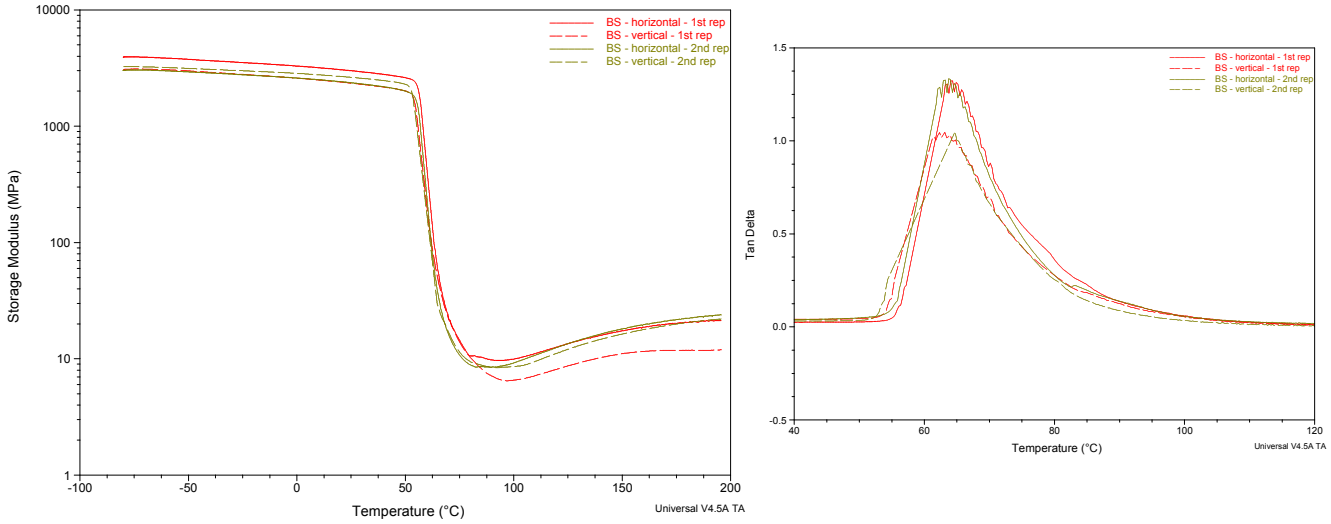

Figure H.5: Storage modulus (left) and tan delta curves (right) horizontal and vertical cut epoxy/$BaSO_4$ samples, cured in room temperature for 2.5-3 weeks. The curves are a result of two repetitions from two batches and are collected with an amplitude of 5 µm and a frequency of 1 Hz. The observed difference can be explained by difference curing accomplishment.

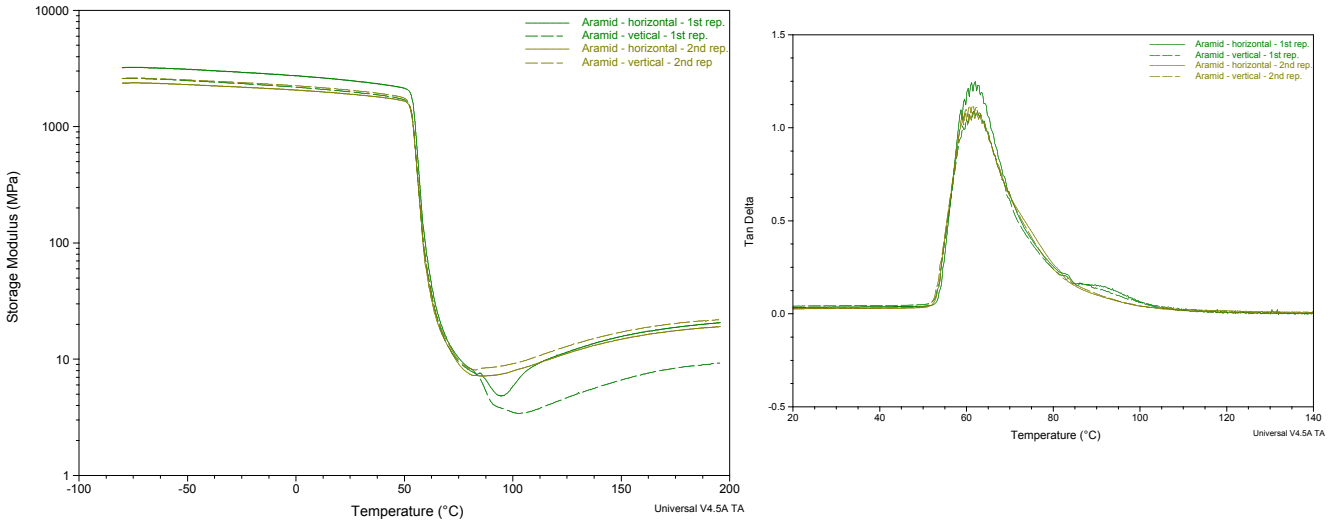

Figure H.6: Storage modulus (left) and tan delta curve (right) for horizontal and vertical cut epoxy/aramid samples, cured in room temperature for 2.5-3 weeks. The curves are a result of two repetitions from two batches and are collected with an amplitude of 5 µm and a frequency of 1 Hz. The observed difference can be explained by difference curing accomplishment or bad sample preparation.

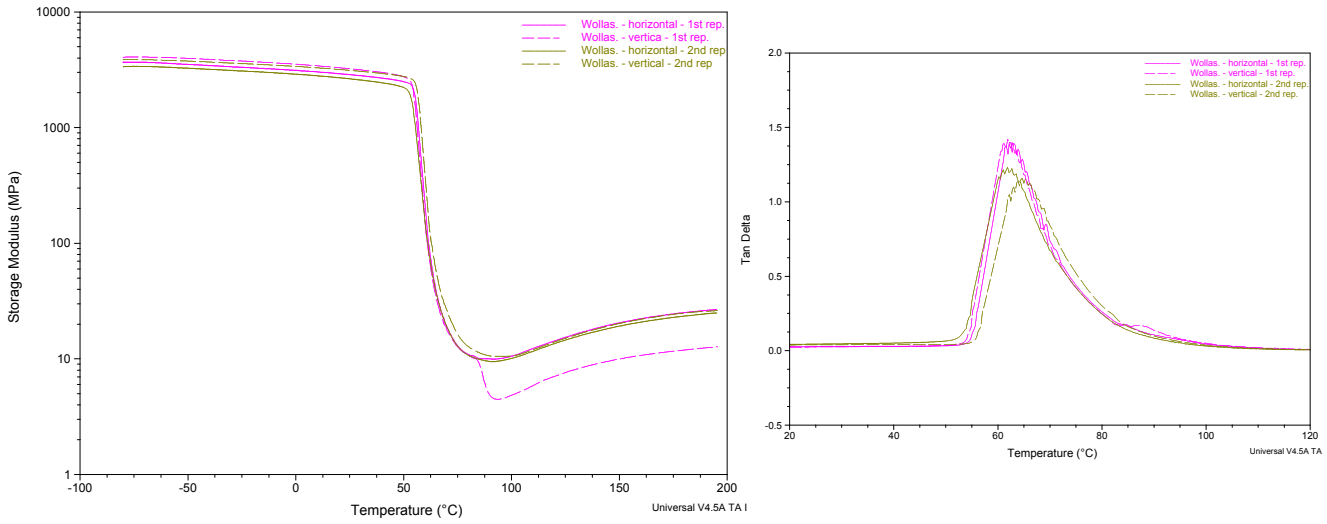

Figure H.7: Storage modulus (left) and tan delta curve (right) for horizontal and vertical cut epoxy/wollastonite samples, cured in room temperature for 2.5-3 weeks. The curves are a result of two repetitions from two batches and are collected with an amplitude of 5 μm and a frequency of 1 Hz. The observed difference can be explained by bad sample preparation.

Appendix I. Plasma treatment of aramid fibers

Plasma treatment of aramid fibers has shown an enhanced effect on the mechanical properties and physical properties of polymer/aramid composites [5,6,7], and were therefore also tested in this work. The aramid fibers were plasma treated with a HDT-400 Hydrophilic treatment device from Jeol Datum. The plasma chamber was operated at grid mode, with a power equal to 200 Watt. The fibers were treated for 1 minute and 10 minutes to observe any difference in treatment time.

Figure I.1 A-C) show the survey spectra and high-resolution spectra of C1s and O1s for the unmodified and plasma treated aramid fibers. The survey spectra show a small increase in oxygen content on the surface after plasma treatment on account of a small decrease in carbon content on the surface. From the C1s and O1s spectra, it is visible that the amount of single bonded oxygen increases, visible as the greater C-O peak at ~286.0 eV in the C1s spectra and the increase in signal at higher binding energy in the O1s spectra. The same results were observed in the work of Lang and Akker [5], and these changes in the fiber surfaces were attributed to the increased adhesion between aramid fibers and epoxy matrix due to epoxy-aramid interactions. Su *et al.*[6] and Hwang *et al.*[8] also observed new signal from –COO- and C=O (not amide) in the C1s spectra after plasma treatment, which indicated that new functional groups had occurred due to the plasma treatment. The interlaminar shear strength and water resistance were enhanced for bismaleimide/aramid composites in the work of Su *et al*., and the interfacial shear strength of epoxy/aramid composites were enhanced in the work of Hwang *et al.*. Samples with epoxy and plasma treated aramid fibers (treated 1 minute) were in this work only tested with DMA and UTM, and the results are presented in Figure I.2-I.5 The T_g, modulus and strength of the epoxy/plasma-aramid samples were approximately the same as for the epoxy/aramid samples, indicating that the plasma treatment did not result in significantly stronger interactions between the epoxy and the aramid fibers.

---

[5] P. J. de Lange, P. G. Akker. "Adhesion activation of twaron aramid fibers for application in rubber: Plasma versus chemical treatment" – *Journal of adhesion science and technology, 26,* **2012**, 827-839

[6] M. Su, A. Gu, G. Liang, L. Yuan. "The effect of oxygen-plasma treatment on Kevlar fibers and the properties of Kevlar fibers/bismaleimide composites" – *Applied surface science, 257,* **2011**, 3158-3167

[7] S.R. Wu, G.S.Sheu, S.S. Shyu. "Kevlar fiber-Epoxy Adhesion and its effect on composite mechanical and fracture properties by plasma and chemical treatment" – *Journal of applied polymer science, 62,* **1996**, 1347-1360

[8] Y. J. Hwang, Y. Qiu, C. Zhang, B. Jarrard, R. Stedeford, J. Tsai, Y. C. Park, M. McCord. «Effects of atmospheric pressure helium/air plasma treatment on adhesion and mechanical properties of aramid fibers" – *Journal of adhesion science and technology, 17(6),* **2003**, 847-860

The exact working condition of the plasma chamber was not known, due to the age of the chamber, but it is believed that air is leaked into the chamber during the plasma treatment as the treatment gas. Not being able to control the gas inlet during treatment and the exact working condition of the chamber is considered as a shortcoming of this procedure. Due to the lack of new chemical groups like C=O (not amide) or –COO- and approximately no change in properties of the epoxy/(plasma-)aramid film, the plasma treatment in this work was believed to not work as desired.

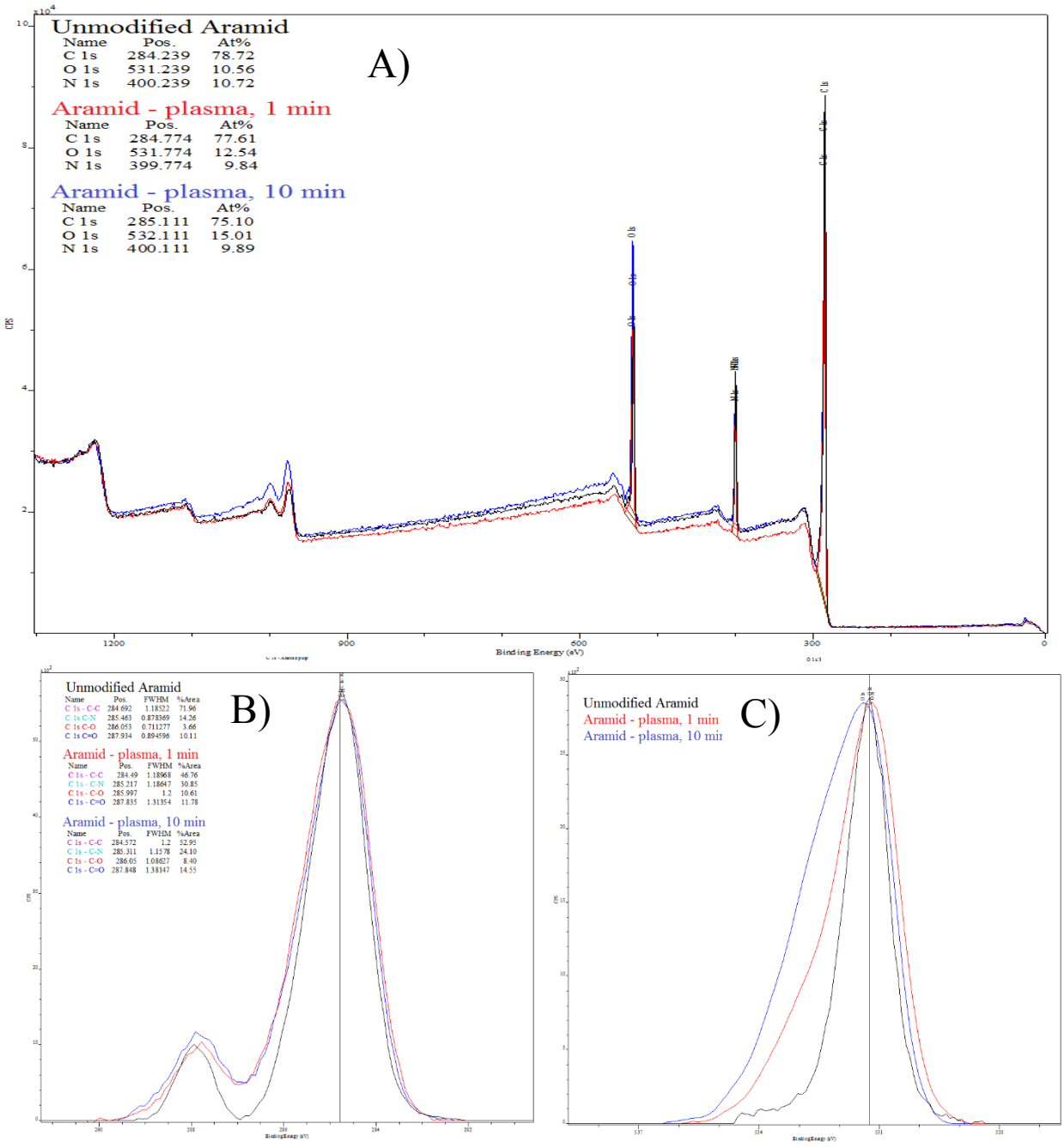

Figure I.1: Spectra of unmodified aramid fibers (black line), and plasma treated aramid fibers for 1 minute (red lines) and 10 mintues (blue lines). A) Survey spectra, B) high-resolution C1s spectra and C) high-resolution O1s spectra.

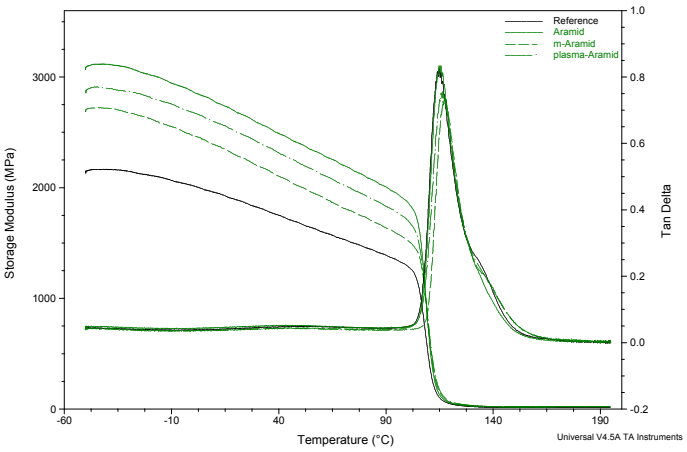

Figure I.2: DMA-results for epoxy/aramid, epoxy/m-aramid and epoxy/plasma-aramid.

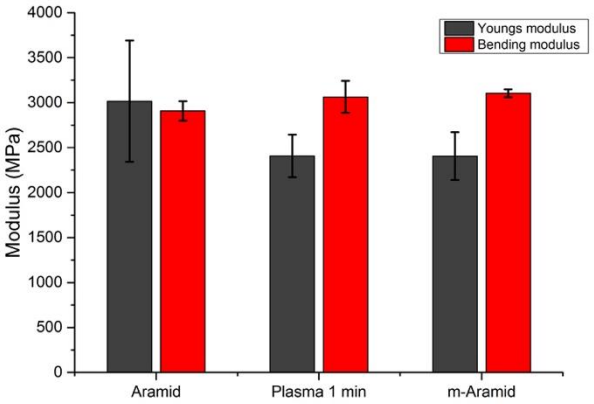

Figure I.3: Youngs and bending modulus for epoxy/aramid, epoxy/m-aramid and epoxy/plasma-aramid at room temperature.

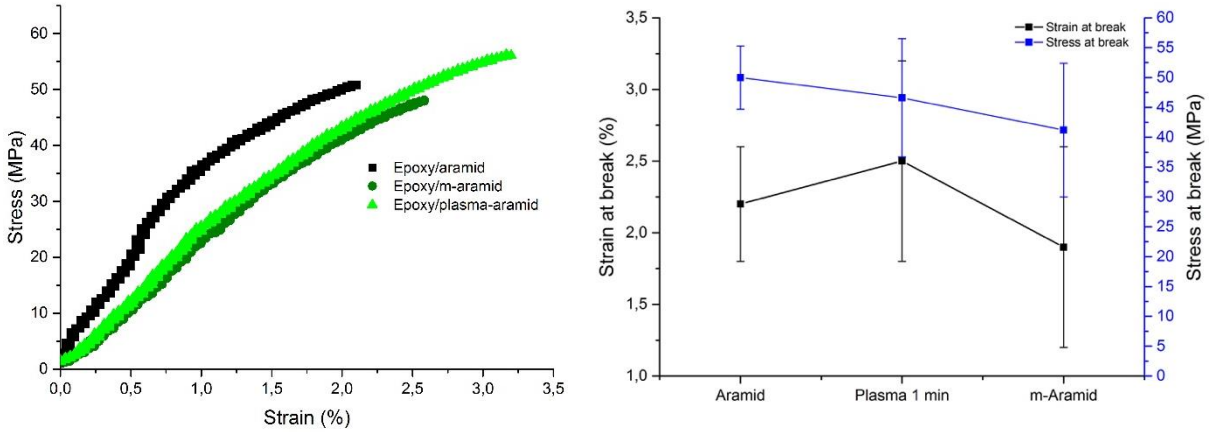

Figure I.4: Tensile test cruve and strain/stress at break for for epoxy/aramid, epoxy/m-aramid and epoxy/plasma-aramid, tested at room temperature.

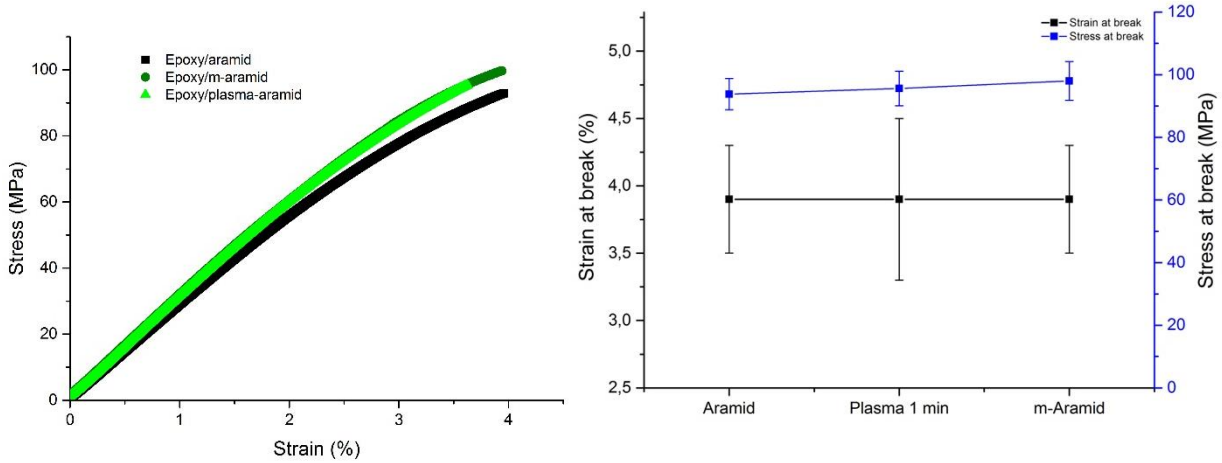

Figure I.5: Flexural test cruve and strain/stress at break for for epoxy/aramid, epoxy/m-aramid and epoxy/plasma-aramid, tested at room temperature